Ecology and Development Series No. 22, 2004

Philip Gbenro Oguntunde

Evapotranspiration and complimentarity relations in the water balance of the Volta Basin: Field measurements and GIS-based regional estimates

Cuvillier Verlag Göttingen

To Victoria (wife), Mercy and David (children)

ABSTRACT

Evapotranspiration (ET) plays a crucial role in the water balance of the Volta River Basin in West Africa. Information regarding biosphere-atmosphere interactions is important in the study of the hydrological cycle. However, there is a need for evapotranspiration models that incorporate the complex feedback mechanisms existing in the soil-plant-atmosphere system. This study was carried out to characterize surface albedo and tree water use at the field level, and model ET at the basin level using standard meteorological parameters.

The surface albedo is a key regulatory factor in atmospheric circulation and plays an important role in mechanistic accounting of many ecological processes, such as ET. In the Kotokosu watershed, a hotspot of land use/land-cover change in the Basin, studies were carried out to determine the effect of roughness and wetness on measured bare-soil albedo; and to examine the influence of phenological stages (emergence, vegetative, flowering and maturity) of cropfields (maize and cowpea) on albedo. Measurements of sap flow, using the temperature difference method, and the related environmental variables, were made in a *Anacardium occidentale* L plantation between October 2001 and January 2003. The relations and interactions of tree water flux with the environmental variables were examined. Ecosystem ET was measured during a wet-to-dry transition period using the eddy correlation system. Cross-correlation analysis and simple calculus were used to estimate the time lags between sap flow and ET, and with solar radiation and vapor pressure deficit. The complementary relationship hypothesis was tested in the Volta Basin using the Advection-Aridity (AA) model. This model is based on conceptual symmetry between actual (ETa) and potential (ETp) evapotranspiration over a large area of regional extent. The AA model was reformulated to make it suitably applicable in the Volta Basin.

Bare-soil albedo generally increases with an increase in solar zenith angle but decreases with an increase in surface roughness and soil wetness. Linear relationships between albedo and surface roughness on the one hand, and mean albedo and soil moisture on the other, indicate that albedo is more sensitive to surface roughness for dry soil. Both roughness and wetness account for about 92% of the variations in bare-soil albedo in the Basin. The range of surface roughness commonly found in the Basin is likely to cause a change between 20 and 25% in surface albedo for wet condition, and less than 12% for dry soil surface. The results further show that seasonal cropfield albedo significantly depends on crop phenology (leaf area index, crop height, etc.). A semi-empirical albedo model that predicts albedo as a function of leaf area index, percent cover, zenith angle, and background soil albedo was developed.

Tree water use shows clear relations with the environmental variables: solar radiation, clearness index, clouds and rains. The coupling of tree canopy to the atmosphere was moderate and a plateau-type response to high evaporative demand was observed. The variation in the time lag showed that trees probably change their water use and water storage strategies in order to cope with changes in available soil moisture. The observed decrease in evaporative fraction from 0.66 to 0.36 suggests an increase in surface resistance, which has implications for boundary layer development, during the wet-to-dry transition period.

Recalibration of wet environment ET (ETw) and reparameterization of wind function yield a marked improvement of the AA model performance. Seasonal surfaces of

ETp and ETw follow the gradients of available energy and moisture, respectively. The monsoon (convective) clouds and harmattan play a significant role in attenuating solar radiation which coupled to seasonal changes in surface albedo influence evapotranspiration processes in the Basin. The good performance of the improved AA model compared to ETa output from a regional circulation model (MM5) indicates the utility of models based on the Bouchet complementary relationship hypothesis in regional/large-scale ET for providing independent estimates of ETa.

Evapotranspiration processes and the related variables investigated in this research provide relevant information that can be integrated with other data for sustainable agricultural water management, eco-hydrological modeling, the study of climate effects of land use/land-cover change and land-surface schemes parameterization.

Evapotranspiration und komplementäre Beziehungen im Wasserhaushalt des Voltabeckens: Feldmessungen und GIS-basierte regionale Schätzungen

KURZFASSUNG

Evapotranspiration (ET) spielt eine wesentliche Rolle in der Wasserbilanz des Voltabeckens in West Afrika. Informationen über die Wechselwirkungen der Biosphäre-Atmosphäre sind wichtig für Studien über die hydrologischen Kreisläufe. Jedoch besteht ein Bedarf nach Evapotranspirationsmodellen, die die komplexen Feedbackmechanismen im System Boden-Pflanze-Atmosphäre berücksichtigen. Ziel dieser Studie ist es, Oberflächenalbedo und Wasserverbrauch der Bäume auf der Feldebene zu charakterisieren und die ET auf der Ebene des Voltabeckens mit standardisierten meteorologischen Parametern zu modellieren.

Der Faktor Oberflächenalbedo reguliert die atmosphärische Zirkulation und spielt eine wichtige Rolle bei der mechanischen Bilanzierung vieler ökologischer Prozesse, wie z.B. ET. Im Einzugsgebiet des *Kotokosu*, ein *hotspot* von Landnutzungs-/Landbedeckungsänderungen im Voltabecken, wurde die Wirkung von Bodenrauhigkeit und -feuchtigkeit auf die gemessene Albedo von freiem Boden untersucht sowie der Einfluss der phänologischen Stadien (Auslaufen, vegetatives Stadium, Blüte und Reife) von landwirtschaftlichen Anbauflächen (Mais und Kuhbohne) auf die gemessene Albedo ermittelt. Messungen des Saftflusses von Bäumen mit der Temperaturunterschiedmethode und der hiermit zusammenhängenden Umweltvariablen wurden in einer Plantage mit *Anacardium occidentale L.* zwischen Oktober 2001 und Januar 2003 durchgeführt und die Beziehungen und Wechselwirkungen des Saftflusses mit den Umweltvariablen untersucht. Ökosystem-ET wurde während einer Übergangsperiode (nass bis trocken) mit der Wirbelkorrelationsmethode ermittelt. Durch Kreuzkorrelationsanalyse und einfachen Berechnungen wurde die zeitliche Verzögerung zwischen Saftfluss und ET bzw. zwischen Solarstrahlung und Dampfdruckdefizit bestimmt. Die komplementäre Beziehungshypothese wurde im Voltabecken mit dem Advektions-Aridităts-(AA)-Model getestet. Dieses Model basiert auf die Symmetrie zwischen aktueller (ET_a) und potentieller (ET_p) Evapotranspiration über ein großes Gebiet in regionalem Maßstab. Das AA-Modell wurde neu formuliert, um einen Einsatz im Voltabecken zu ermöglichen.

Die Albedo von freiem Boden nimmt i.d.R. mit steigendem Sonnenwinkel zu, jedoch mit zunehmender Oberflächenrauhigkeit und -feuchte ab. Lineare Beziehungen zwischen Albedo und Oberflächenrauhigkeit auf der einen Seite bzw. zwischen durchschnittlicher Albedo und Bodenfeuchtigkeit auf der anderen deuten darauf hin, dass die Albedo empfindlicher auf Rauhigkeit bei trockener Oberfläche reagiert. Sowohl Rauhigkeit als auch Feuchtigkeit machen 92% der Variationen in der Albedo des freien Bodens im Voltabecken aus. Das im Voltabecken übliche Maß der Oberflächenrauhigkeit kann zu 20 bis 25% der Veränderungen in der Oberflächenalbedo bei nassen Bedingungen und zu weniger als 12% bei trockenen Oberflächen führen. Die Ergebnisse zeigen weiter, dass die jahreszeitliche Albedo der Anbauflächen signifikant von der Phänologie der angebauten Pflanzen abhängt (Blattflächenindex, Höhe der Pflanzen, usw.). Ein semi-empirisches Albedomodell, das die Albedo als Funktion von Blattflächenindex, prozentualer Bedeckung, Sonnenstandswinkel und Hintergrund-Bodenalbedo bestimmt, wurde entwickelt.

Der Wasserverbrauch der Bäume zeigte bemerkenswerte Beziehungen mit den Umweltvariablen Solarstrahlung, ‚clearness index', Wolken und Regen. Die Koppelung von Kronendach mit der Atmosphäre war mäßig und eine plateauartige Reaktion auf hohe evaporative Nachfrage wurde beobachtet. Die beobachtete Variation der Zeitverzögerung zeigt, dass die Bäume wahrscheinlich ihre Wassernutzungs- und -speicherungsmechanismen verändern, um Veränderungen in der verfügbaren Bodenfeuchte zu bewältigen. Die beobachtete Abnahme des

evaporativen Anteils von 0,66 auf 0,36 deutet auf eine Zunahme des Oberflächenwiderstands hin, was wiederum Folgen für die Entwicklung der Grenzschicht bedeutet.

Die Rekalibrierung der ET unter nassen Bedingungen (ET_w) und die Reparametrisierung der Windfunktion ergaben eine deutliche Verbesserung der Leistung des AA-Modells. Der jahreszeitliche Verlauf von ET_p bzw. ET_w folgen den Gradienten der verfügbaren Energie bzw. Feuchte. Monsunwolken (konvektiv) und Harmattarnwind spielen eine signifikante Rolle bei der Abschwächung der Solarstrahlung, die, gekoppelt mit den jahreszeitlichen Veränderungen der Oberflächenalbedo, die Evapotranspirationsprozesse im Voltabecken beeinflussen. Die gute Leistung des verbesserten AA-Modells verglichen mit der ET_a aus dem regionalen Zirkulationsmodell (MM5) zeigt den Nutzen von Modellen auf der Grundlage der komplementären Beziehungshypothese von Bouchet bei regionalen/großräumigen ET-Untersuchungen für die unabhängige Berechnung der ET_a.

Evapotranspiration und die hier untersuchten abhängigen Variablen liefern relevante Informationen, die mit anderen Daten für nachhaltiges landwirtschaftliches Wassermanagement, Umweltmonitoring, bei der Untersuchung der klimatischen Auswirkungen von Landnutzungs-/Landbedeckungsveränderungen sowie bei der Parametrisierung von Landoberflächensystemen integriert werden können.

TABLE OF CONTENTS

LIST OF SYMBOLS AND ABBREVIATIONS

Symbol	Meaning [unit]
AA	advection-aridity [-]
C_c	cloud cover [tenths]
CH	crop height [m]
CI	clearness index [-]
C_p	specific heat [MJ kg^{-1} $°C^{-1}$]
CRAE	complementary relationship areal evapotranspiration [-]
d	zero plane displacement height [m]
DSS	decision support system [-]
e_a	actual vapor pressure [kPa]
E_c	canopy transpiration [kg m^{-2} s^{-1}]
EC	eddy correlation [-]
e_s	saturation vapor pressure for a given time period [kPa]
e_s - e_a	saturation vapor pressure deficit [kPa]
EF	evaporative fraction [-]
ETa	actual evapotranspiration [mm day^{-1}]
ETp	potential evapotranspiration [mm day^{-1}]
ETw	wet environment evapotranspiration [mm day^{-1}]
f	sap flow density [g cm^{-2} h^{-1}]
f_c	fraction of soil surface covered by vegetation[-]
1 - f_c	exposed soil fraction [-]
G	soil heat flux [MJ m^{-2} day^{-1}]
g_a	aerodynamic conductance [m s^{-1}]
g_c	canopy conductance [m s^{-1}]
GCMs	general circulation models [-]
H	sensible heat flux [MJ m^{-2} day^{-1}]
ITCZ	inter-tropical convergence zone [-]
k	von Karman's constant [0.41] [-]
LAI	leaf area index [m^2 (leaf area) m^{-2} (soil surface)]
LAS	large aperture scintillometer
LE	latent heat flux [MJ m^{-2} day^{-1}]
N	maximum possible sunshine duration in a day [hour]
n	actual duration of sunshine in a day [hour]
n/N	relative sunshine duration [-]

P	rainfall [mm]
Q_t	tree water use [kg h^{-1}]
R	correlation coefficient [-]
Ra	extraterrestrial radiation [MJ m^{-2} day^{-1}]
r_a	aerodynamic resistance [s m^{-1}]
RH	relative humidity [%]
R_n	net radiation [MJ m^{-2} day^{-1}]
Rs	solar or shortwave radiation [MJ m^{-2} day^{-1}]
r_s	surface or canopy resistance [s m^{-1}]
SVAT	soil-vegetation-atmosphere transfer [-]
T	air temperature [°C]
TDR	time domain reflectometry [-]
u_2	wind speed at 2 m above ground surface [m s^{-1}]
u_z	wind speed at z m above ground surface [m s^{-1}]
z	elevation, height above sea level [m]
z_h	height of humidity measurements [m]
z_m	height of wind measurements [m]
z_{oh}	roughness length governing heat and vapor transfer [m]
z_{om}	roughness length governing momentum transfer [m]
a	albedo [-]
a_{PT}	Prestley-Taylor coefficient
g	psychrometric constant [kPa °C^{-1}]
Δ	slope of saturation vapor pressure curve [kPa °C^{-1}]
d	degree of accuracy [-]
q	sun zenith angle [rad]
q_m	soil water content [m^3 (water) m^{-3} (soil)]
l	latent heat of vaporization [MJ kg^{-1}]
r_a	mean air density [kg m^{-3}]
t	time lag [min]
f	latitude [rad]
w	scattering coefficient [-]
Ω	decoupling coefficient [-]

1 GENERAL INTRODUCTION

1.1 Introduction

Sustainable food production and industrial development will depend to a large extent on the judicious use of water resources, as fresh water for human consumption and agriculture is becoming increasingly scarce. An increasing number of countries with limited water and land resources are faced with greater challenges. The dependency on water for future development has become a critical constraint especially in arid and semi-arid regions, where water scarcity is expected by the year 2025 (Smith, 2000). The situation is aggravated by the declining quality of soil and water resources caused, to a large extent, by human activities. There is an urgent need to arrest this human-induced degradation of water and soil resources and reclaim those that have already been degraded in order to meet the present and future needs of mankind. Hence, needs for sustainable use of water resources with respect to different land use patterns and climatic forcing. A good understanding and description of the dynamics of a local/regional/global hydrologic cycle as affected by natural and human activities is the starting point for effective management of water resources of a given basin or region.

Evapotranspiration (ET) is an important component of the water cycle. It is the term used to describe the transfer of water from a variety of surfaces into the atmosphere. Actual evapotranspiration is, through latent heat, responsible for 70% of the lateral global energy transport. ET plays an important role in the redistribution of water on the Earth's surface (Mauser and Schädlich, 1998). Accurate measurement and estimation of evapotranspiration is a basic tool to compute water balances and to estimate water availability and requirements (Pereira et al., 1999). Recently, increased emphasis has been placed on understanding the interaction between regional climate and the hydrological cycle in arid and semi-arid regions (Chehbouni et al., 1997). The water balance of these regions is important for many reasons, including water resource assessment, dry land agriculture, and the possible link between the surface energy balance and climate (Wallace and Holwill, 1997). Advances in hydrological research in the past two decades have been enormous especially in the temperate region while the hydrological knowledge of the tropical zones has advanced much less (van de Giesen et al., 2000). Varied environmental factors exist between the two climatic zones such that

models and approaches developed in one should be locally tested before they are transferred to another zone.

The Volta River Basin in West Africa is a typical example of a semi-arid region in which studies to obtain a better insight into the interactions between soil, vegetation, climate, water and human activities are very important for the overall development of the region. The area is largely characterized by poverty, high population growth and widely varied precipitation, while the main source of livelihood in the sub-region is rain-fed agriculture. The continued pressure on the natural resources in a region like West Africa necessitates a good understanding of catchment hydrology for sustainable water use (Wallace and Batchelor, 1997; van de Giesen et al., 2000). Therefore, effective watershed management is a key to improving agricultural production with significant implications for meeting other water needs.

Several factors such as regional land use/land cover change (LUC) as well as components of the basin water balance should be carefully studied and understood. The development of an effective water management strategy depends on a precise estimate of these components/factors, their interactions and existing feedback mechanisms. Evapotranspiration is one of the most important phenomena in the Volta River Basin; a preliminary study of the annual water balance based on historical data showed that up to 90% of total catchment rainfall is accounted for by ET (Andreini et al., 2000).

The Volta Basin, with a recently observed declining water level in the lake, has undergone numerous environmental changes since the formation of the Akosombo dam about 30 years ago. Studies related to sustainable water use in general, and agricultural water management in particular, is of priority importance in order to increase production without degrading the basin's resources. Changes in land use lead to changes in water use, as evaporation from each component of the land surface is controlled by different factors. These different factors influence both evaporation from the soil and plant transpiration whereby the former is a purely physical process and the latter is also affected by physiological responses (Allen and Grime, 1995).

Any change in actual ET, either through a change in vegetation or climate, directly affects the available water resources and runoff. Changes in vegetal cover through human influence are taking place, both on the field scale through the introduction of new or modified species in agriculture and forestry, and on the regional

scale through deforestation, irrigation and man-induced erosion hazards (Mauser and Schädlich, 1998).

The GLOWA-Volta project (van de Giesen et al., 2002), a research project designed to study "sustainable water use under changing land use, rainfall reliability, and water demands in the Volta Basin" (West Africa), is expected to produce a decision support system (DSS) for sustainable water management in the Volta Basin. Such a DSS package should be based on sound scientific knowledge of regional water cycles amongst other factors. Furthermore, pertinent to our understanding of regional to global change in hydrological cycles is the study of biosphere-atmosphere interactions that consider the effects of climate on ecosystem functions and the potential feedbacks of the land surface to the physical climate system. Studying these interactions require a nested experimental design whereby measurements of fluxes are taken using a variety of methods at different time and space scales (Margolis and Ryan, 1997).

This research (sub-project) seeks to provide field level data needed to validate and/or test land-surface sub-models in the regional circulation models as well as to compute independent estimates of regional evapotranspiration that by-pass the need for soil and vegetation parameters and the complex feedback within the land-atmosphere continuum. The specific objectives are:

1. To measure *in situ* and model surface albedo;
2. To measure tree water use and its dynamic interaction with the ambient environment; and
3. To model the spatial distribution of actual regional evapotranspiration using the complementary relationship hypothesis.

1.2 Research justification

In problems of regional hydrology and global climatology, a knowledge of the large-scale behavior of processes defining fluxes of sensible and latent heat is of paramount importance in understanding the climate, weather, biochemical cycles and ecosystem dynamics. Recent research on improving the representation of land surface-atmosphere interactions within general circulation models (GCMs) has led to the investigation of a wide variety of different soil-vegetation-atmosphere transfer (SVAT) schemes. The project for the Intercomparison of Land Surface Parameterisation Schemes (PILPS) and

the Gediz Basin project are good examples of this effort. Forty-four different SVAT models were identified and investigated by Moehrlen et al. (1998). No clearly defined patterns have emerged from these analyses and no particular model could be adjudged most accurate (Pitman and Henderson-Sellers, 1998; Kite and Droogers, 2000). Accounting for the feedback mechanism in land-surface interactions seems to be the bottleneck of these schemes. Pertinent to our understanding of regional and global change in the hydrological cycle is the knowledge of biosphere-atmosphere interactions that include the effects of climate on ecosystem functions and the potential feedbacks of the land surface to the physical climate system. Studying these interactions requires a nested experimental design whereby measurements of fluxes are taken using a variety of methods, at different time and space scales (Margolis and Ryan 1997). Furthermore, land use effects that may be captured by its surface albedo property and individual components of ET (soil evaporation and transpiration) should be properly understood. To avoid the above complexities, there is therefore a need for models of regional evapotranspiration that incorporate complex feedback mechanisms existing in the soil-plant-atmosphere system. Models based on Bouchet's complementary hypothesis (Bouchet 1963) are examples of such models. The main advantage of these kind of models is that they do not require data on surface resistance, soil moisture content, or other land surface measures of aridity (Brutsaert and Stricker, 1979).

1.3 Thesis outline

This report is divided into six chapters. Chapter 2 reviews the recent developments in evapotranspiration research: basic definitions and concepts, the available paradigms in ET studies, the measurement techniques, and the estimation models. Chapter 3 gives the description of the study area for the whole Volta Basin at large and the Ejura sub-basin where the actual field level measurements took place. Chapter 4 deals with the research methods and analytical procedures. Experimental procedures, modeling techniques, and a complementarity relationship model based on the Advection-Aridity approach are presented. In Chapter 5 and 6, research results and pertinent discussions are presented, while Chapter 7 is the summary and conclusion of the major research findings.

2 RECENT DEVELOPMENTS

2.1 Introduction

Evapotranspiration (ET) is used to describe two processes of water loss from surfaces-evaporation and transpiration. Globally, ET returns about 60% of precipitation to the atmosphere (Brutsaert, 1982), and close to 90% of the water flowing through a river basin may be used in evapotranspiration processes in the tropics (Jensen, 1990). Although ET is one of the most important components of the hydrological cycle, it probably remains, the most poorly understood. The basic definitions and brief description of the ET processes and the influencing factors presented here are based largely on FAO 56 (Allen et al., 1998)

2.1.1 Basic definitions

Evaporation

Evaporation is the process whereby liquid water is converted to water vapor and removed from the evaporating surface. Where the evaporating surface is the soil surface, the degree of shading of the plant canopy and the amount of water available at the evaporating surface are other factors that affect the evaporation process.

Transpiration

Transpiration consists of the vaporization of liquid water contained in plant tissues and the vapor removal to the atmosphere. Plants predominately lose their water through stomata. These are small openings on the plant leaf through which gases and water vapor pass.

Evapotranspiration

Evaporation and transpiration occur simultaneously and there is no easy way of distinguishing between the two processes. When the plant is small, water is predominately lost by soil evaporation, but once the crop is well developed and completely covers the soil, transpiration becomes the main process. The following definition relevant to this study can be given as:

Potential *Evapotranspiration:* The evapotranspiration rate of a short green crop, completely shading the ground, of uniform height and never short of water (Penman, 1948)

***Reference evapotranspiration*:** The rate of evapotranspiration from a hypothetical reference crop with an assumed crop height of 0.12 m, a fixed canopy resistance of 70 s/m and an albedo of 0.23, closely resembling the evapotranspiration from an extensive surface of green grass of uniform height, actively growing, completely shading the ground and not short of water (Pereira et al., 1999).

2.1.2 Factors affecting evapotranspiration

Weather parameters: The principal weather parameters affecting evapotranspiration are radiation, air temperature, humidity and wind speed. Several procedures have been developed to assess the evaporation rate from these parameters.

Crop factors: The crop type, variety and development stage should be considered when assessing evapotranspiration from crops grown in large, well-managed fields.

Management and environmental conditions: Factors such as soil salinity; fertility, diseases, pests and poor soil management may limit crop development and reduce evapotranspiration. Other factors are ground cover, plant density and the soil water content.

Over the past five decades, an enormous amount of research has been conducted on the advances in evapotranspiration of natural and cultivated surfaces (Itier and Brunet, 1996). This has led to considerable progress in our understanding of the physical and biological processes that determine the ET rate. This has also significantly improved measurement techniques, and has provided a large range of simulation or prediction models, as well as numerous user-oriented applications (Itier and Brunet, 1996; Pereira et al., 1999). Furthermore, these major advances have had a tremendous impact on quality, availability and costs of collecting ET data for different applications, because the use of eddy correlation systems, Bowen ratio energy balance systems, sap flow systems to actually measure plant transpiration, and time domain reflectometry (TDR) to accurately determine the soil water balance, have all become commercially available and reliable in recent times (Howell, 1996). In the following pages, the "*state-of-the-*

art" in ET measurement techniques and trends in estimation and modeling are briefly presented.

2.2 Measurement techniques

Different measurement techniques for ET include: lysimeter (water balance), eddy correlation, Bowen ratio, scintillometry, sap flow, humidity variance, airborne flux measurements and remote sensing or thermography (Itier and Brunet, 1996). Four of these methods employed in Glowa-Volta project are briefly described in this section.

2.2.1 Eddy correlation

For about 20 years now eddy correlation (EC) has become the standard measurement technique for evaporation at canopy scale. The main advantage is that it provides direct flux measurements, with no particular assumption on turbulent diffusivities, the shape of the wind profile or the influence of buoyancy forces. The disadvantages of EC include sensitivity to fetch and high cost of maintenance (Brotzge and Crawford, 2003). The flux density is expressed as the covariance between fluctuations in vertical velocity and vapor concentration over a certain period of time. This technique requires sensors with a response time of the order of a fraction of a second. The sonic anemometer is the sensor required for wind velocity measurement, while a hygrometer is used to measure humidity concentrations (Elbers, 2002).

The principle of the eddy correlation system is to sense the contribution of the turbulent signals at a high enough rate and averaging the covariances over a long enough period (typically 15-30 minutes). Both time scales must be determined from spectral considerations (Kaimal and Finnigan, 1994). It is important to note that the time series must be stationary at the scale of the averaging period, which may require some kind of detrending of the original turbulent signals. Other important aspects to be considered are: density correction (Webb et al., 1980); orientation of the wind velocity sensor, flow distortion effects, and geometry of the system. The EC method has been applied in a variety of ways in order to understand the relative importance and functioning of key ecosystem components through the provision of information about the partitioning of the total ecosystem fluxes between sources and sinks (Granier et al., 1990, 2000; Köstner et al., 1992; Scott et al., 2003).

2.2.2 Sap flow

Since the mid - 1930s, different methods, such as weighing lysimeters, large-tree porometers, ventilated chambers, profile micro-meteorological measurements, injection of indicator substances, e.g. isotopes, and recently, the heat-balance and temperature difference methods have been used to estimate tree water use (Tuzet et al., 1997; Wullschleger et al., 1998; Schaeffer et al., 2000). During the 1980s, sap flow gauges, which use a temperature difference principle, were developed by Granier (1985, 1987) and have been successfully used by different researchers since then (Phillips et al., 1997). This method provides a simple, relatively inexpensive but robust means of continuous measurement of whole-plant sap flow and helps to measure transpiration from different species or a single component of mixed vegetation (Granier et al., 1996).

In field conditions the stem heat balance method presently appears as the most interesting technique (Itier and Brunet, 1996). For a stem diameter less than 0.1 m, it consists of setting up a heated ribbon around the stem and properly insulating it from the environment (Sakuratani, 1981). For bigger diameters, a line heat source is installed in the xylem sapwood, and the sap flow can be deduced from changes in sap flow conductivity (Granier 1985, 1987). A problem with this approach is that sap flow lags somewhat behind transpiration because of the capacitance of the trunk and branches (Granier and Loustau, 1994; Phillips et al., 1997). But on a daily basis, sap flow through the stem is equivalent to transpiration. Other physiological problems, such as trunk constriction, could result from the use of sap flow gauges.

The Sap flow technique has been used successfully in different large-scale experiments such as HAPEX-MOBILHY (Granier et al., 1990), HAPEX-SAHEL (Allen and Grime, 1995), BOREAS (Margolis and Ryan, 1997), and EUROFLUX (Granier et al., 2000). In the present study, the sap flow method for tree water-use determination was used during the 2001/2002 seasons and also in conjunction with the EC method during a wet-to-dry transition period (2002/2003). This method was used because of its simplicity, robustness and low cost.

2.2.3 Scintillometry

The use of large aperture scintillometer (LAS) also provides a means of indirectly estimating ET. According to the Monin-Obhukhov similarity theory, the temperature

structure parameter C_T^2 is a universal function of the dimensionless height enabling an estimate of the sensible heat flux. This estimate can be used to determine the latent heat flux, and hence the evapotranspiration, through the surface energy balance. During the unstable conditions during the day, this parameter can be easily related to the refractive index structure parameter (de Bruin et al., 1995). This equipment consists of a transmitter and a receiver properly aligned with a separating path length between 20 m and 5000m. The method has been successfully tested over homogeneous and heterogeneous terrains.

2.2.4 Remote sensing

In recent times, efforts have been made to determine the spatial distribution and temporal variability of actual evapotranspiration (ETa) both through measurements and modeling approaches (Ford, 1994; White, 1994; 1991; Bastiaanssen et al., 1998). Progress in both remote sensing and GIS-based techniques facilitated this. The remote sensing method uses surface reflectance and radiometric surface temperature in combination with ground-based meteorological data to solve the energy balance equation and estimate ET at different scales. Remote sensing information has been used in different ways to determine ET. One approach is to determine the surface-air temperature difference and use this as an input to simple ET models (Seguin, 1993; Ottle, 1994). Other methods are either physically based analytical approaches or numerical models. The accuracy of the remote sensing approach to determine ET at the particular overpass time of the satellite is restricted to cases with no cloud cover. For most mid-latitude climates, especially the tropical regions, these limitations make this approach rather academic. There is an added need to correct the satellite data for atmospheric interference using atmospheric properties such as temperature, humidity and wind speed at the satellite overpass time. Remote sensing data can also be used to determine the spatial distributions and temporal development of the parameters that are needed as input for ET models (Mauser and Schädlich, 1998).

2.3 Trends in evapotranspiration modeling

Our ability to measure ET directly in the natural environment is still limited, because the processes and feedback mechanisms that control the phenomenon are not well

understood. Also, actual field measurement is characterized by numerous constraints such as cost, time and other logistics. In the disciplines where ET is a critical variable, there is, therefore, the need to estimate or model ET using easily observed meteorological parameters.

2.3.1 Main concepts

Theoretical approaches to surface evaporation from the energy balance equation combined with sensible heat and latent heat exchange expressions give the following definition for actual evapotranspiration (Perrier 1977):

$$ET = \frac{\Delta}{\Delta + g}\left[(R_n - G) + \frac{r c_p}{\Delta} H(u)(D_a - D_s)\right] \qquad (2.1)$$

where R_n - G =available energy (MJ/m^2) for the canopy, comprised of net radiation, R_n and the soil heat flux, G; H(u) =exchange coefficient (m/s)between the surface level and a reference level above the canopy but taken inside the conservative boundary sub-layer; D_s and D_a (kPa) =vapor pressure deficits (VPD) for the surface level and the reference level, respectively; r =atmospheric density (kg/m^3); c_p =specific heat of moist air (J/kg°C); Δ =slope of the vapor pressure curve (Pa/°C); and g =psychometric constant (Pa/°C). Equation 2.1 is viewed as a definition for ET rather than a predictor of ET, since it cannot produce estimates for reasons given below (Pereira et al., 1999). The main requirements for the validity of (1) are the following:

1 No local advection occurs over the surface, thus the flux between the two levels is only vertical. Therefore, the conditions at the reference level z_M (solar radiation, wind speed, and VPD) can be considered to be the same as those over a large surrounding area.

2. Turbulent exchange coefficients, H(u), are the same for sensible and latent heat and include the corrections for instability or stability.

3. The surface level is at the height of the crop, h_c, or, for a very low crop or a bare soil, the roughness height for momentum, z_{oM}.

4. The fraction of the energy absorbed by the canopy as heat that is transformed into dry matter can be neglected.

To obtain evapotranspiration with equation 2.1, the most difficult term to estimate is D_s, representing the vapor pressure deficit at the evaporative surface. The bulk of literature on the estimation and measurement of ET over different land covers and climatic conditions have demonstrated the large variation in complexity of the evapotranspiration process. Hence, models ranging from the simple to the physically based have been formulated that describe the processes involved at various levels of complexity with different forms of assumptions to negotiate through the points listed above (Shuttleworth, 1985; Raupach, 1995). The most widely applied of these models was developed by Penman and modified by Monteith (1965). It combines the energy balance of the land surface with the concept of a species dependent surface resistance for water vapor release.

2.3.2 Evapotranspiration paradigms

Brutsaert and Stricker (1979) traced the two general modeling patterns in the literature. The first involves the relationship between potential evapotranspiration (ETp) and large-scale advection, and the second involves symmetry between potential and actual evapotranspiration.

Potential evapotranspiration and large-scale advection

Potential evapotranspiration refers to the rate of evaporation from a large area covered completely and uniformly by actively growing vegetation with water at its disposal as needed. A widely used standard for potential evapotranspiration is based on the approximate solution of equation 2.1 as given by Penman (1948). Because some researchers felt that Penman's equation was derived by combining bulk mass transfer and energy budget considerations, this and all related methods are often referred to as the combination approach. The two-term structure of equation 2.1 as solved by Penman has been interpreted to represent the equilibrium evaporation and the effects of regional or large-scale advection. The concept has been widely investigated, discussed, applied and extended in the past decades. One of such extensions is the outstanding work of Monteith in 1965, which led to the Penman-Monteith equation. The Penman-Monteith (PM) method has been recommended as a better method for estimating daily or longer

periods of ET over a wide range of climate conditions (Jensen et al., 1990). The method requires determination of values of the aerodynamic resistance and canopy resistance. Errors in canopy resistance lead to larger ET errors than do errors in aerodynamic resistance, as canopy resistance is an order of magnitude larger than aerodynamic resistance for a vegetated surface (Hall et al., 1992). While algorithms have been developed to compute canopy resistance from leaf area index (LAI), normalized difference vegetation index (NDVI), and leaf assimilation rate (Jensen et al., 1990; Liang et al., 1994), determination of appropriate values for canopy resistance remains challenging, as derivation of NDVI and LAI from satellite data requires atmospheric, topographic, and radiometric corrections of satellite imagery (Hall et al., 1992).

Recently, the Penman-Monteith method has been standardized and adopted by FAO to compute reference ET that can later be converted to actual ET by the use of appropriate crop coefficients (Allen et al., 1998). Generally, this concept is the most popular and traditional way in which ET is being computed in hydrology and other related disciplines. Consequently, our ability to estimate actual regional evapotranspiration (ETa) is often constrained by models that treat potential evapotranspiration (ETp) as an independent climatic forcing process, often an empirical function of pan evaporation observed at nearby weather stations, or by models that tend to rely on gross assumptions as to the nature of moisture dynamics in each of the components of the land surface–atmosphere interface and of the interactions between them (Hobbins et al., 2001a, 2001b).

Symmetry between potential and actual evapotranspiration

Another method for estimating ET is the complementarity relationship (CR) concept, first proposed by Bouchet (1963). The CR concept states that under the condition of constant energy input to a land surface-atmosphere system, water availability becomes limited, then actual areal ET falls below its potential, and an excess amount of energy becomes available. The excess is in the form of sensible heat and/or long-wave back radiation that increases the temperature and humidity gradients of the over-passing air and leads to an increase in potential ET (ETp) equal in magnitude to the decrease in ET. If water availability is increased, the reverse occurs, and ET increases as ETp decreases. Thus, ETp can no longer be regarded as an independent causal factor. Instead it is

predicated upon the prevailing conditions of moisture availability (Hobbins et al., 2001a, 2001b). Morton (1983) further refined the CR concept and developed a Complementary Relationship Areal Evapotranspiration (CRAE) model that considers the feedback effects of vapor pressure deficit and advection. The CRAE model relies solely on routine climatological observations, uses only globally tuned coefficients, and provides reliable, independent estimates of ET from environmentally significant areas in most parts of the world (Morton, 1983). Brutsaert and Stricker (1979) developed an Advection-Aridity (AA) model based on the CR concept. Hobbins et al. (2001a, 2001b) apply the CRAE and AA models to the conterminous US for estimating regional monthly ET. An important feature of CR models is that they bypass the complex and poorly understood soil-plant-atmosphere processes and do not require data on soil moisture, stomata resistance of the vegetation, or any other aridity measures. A more detailed formulation of AA model is briefly outlined in Chapter four (section 4.3).

3 STUDY AREA

3.1 Volta River Basin

The Volta River Basin is an international catchment shared by six riparian countries: Ghana, Burkina Faso, Togo, Cote d'Ivoire, Benin and Mali. It lies between latitudes 3°N and 11°N and longitudes 0°30'E to 3° W. It covers a huge area of land of the order of 400,000 km^2. About 15 million people, with per capital income of $6.50 /year live in the Volta basin. The largest portions of the basin are found in Ghana and Burkina Faso, and about three quarters of Ghana and two thirds of Burkina Faso are drained by the Volta River. In addition, The River drains a large part of Togo and small portions of Cote d´Ivoire, Benin and Mali (Andreini et al., 2000). The coverage of the Volta basin is shown in Figure 3.1.

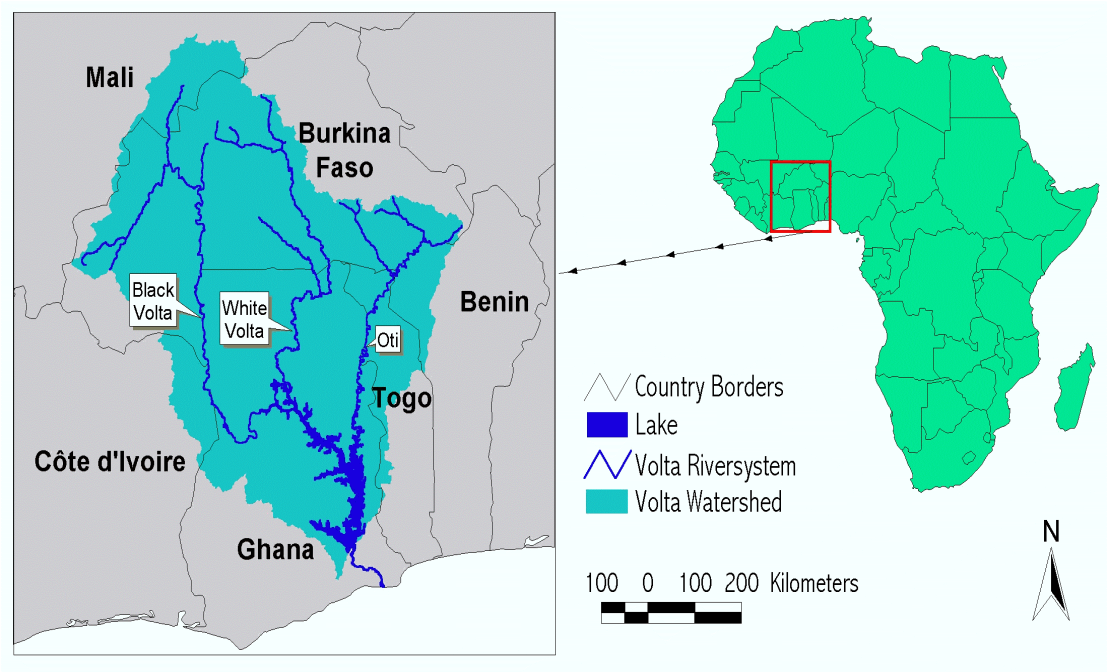

Figure 3.1: The Volta River Basin of West Africa

This study focuses on the Volta River Basin of Ghana (although a small portion of the work was on the entire basin); further discussions shall refer to the basin in Ghana and the "hot spot" watershed at Ejura. The basin can be subdivided into four sub-basins, namely: the White Volta, the Black Volta, the Main Volta, the Oti. The White

Volta is located to the north of Ghana, extending southwards to about latitude 8^0 30' N. The Black Volta extends narrowly from the northwest of Ghana southward across the middle belt up to about 7^0 45' N and 10^0 W as its eastern most spatial extension. It covers parts of the Upper West, Northern and Brong Ahafo Regions. The Main Volta sub-basin is the largest of the sub-basins of the Volta River, stretching over a greater part of Central and Eastern Ghana. The Oti sub-basin is found along the eastern fringes of the Northern Region and flows below the western slopes of the Buem Ranges before joining the Volta (Andreini et al., 2000).

The population of Ghana is about 18 million people with about 38% living within the Volta Basin. The country covers 238,539 km^2 and is the third largest exporter of cocoa. Mineral resources of value include: diamond, gold, manganese, bauxite and iron ore. This area is characterized by increasing population growth, poverty, and unemployment.

3.2 Climate and Weather

The climatic pattern and circulation over Ghana is governed by the southwesterly monsoon winds and the northeasterly trade winds. The moisture-laden monsoon winds blow from the ocean whereas the trade winds, also called harmattan winds, blow from the Sahara desert and are generally dry and dusty. The belt into which the two air masses flow is known as the inter-tropical convergence zone (ITCZ). Weather and climatic circulation in the tropics are closely connected to ITCZ (Walker, 1962). The movements of ITCZ vary by the day and hence the onset and cessation of dry and rainy seasons are subject to considerable variations.

Rainfall varies from year to year and in its distribution during the year. In the Volta basin, unimodal and bimodal rainfall patterns can be recognized. The northern part of the Basin lies within the geographical area with a single maximum rainfall regime. Areas within this rainfall regime experience only one rainy season from about May to August, followed by a long dry season. Mean annual rainfall is 1150 mm. The southern part of the basin, however, experiences a double maximum rainfall regime, with major and minor wet seasons. The two wet periods occur from May to August and from September to October, with a long-term mean annual rainfall of 1400 mm. A

typical monthly rainfall regime in the 'hot spot' watershed near Ejura in the year 2002 is shown in Figure 3.2.

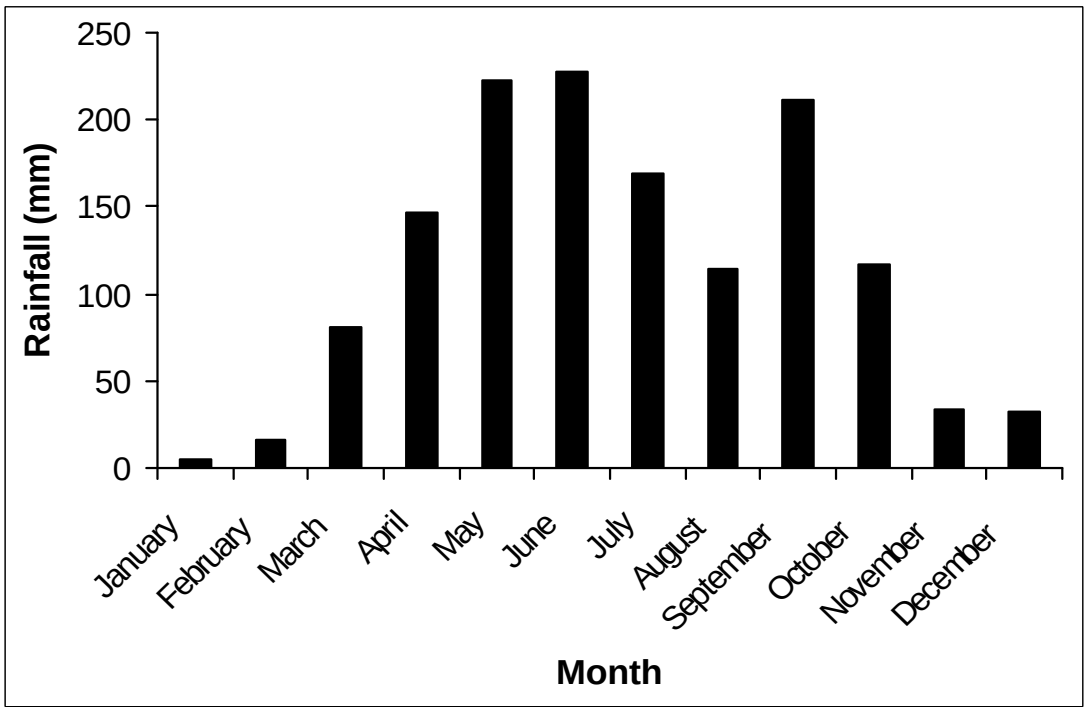

Figure 3.2: Monthly rainfall regime in the year 2002 at Ejura, Ghana

The annual range of mean temperature increases from south to north and the variation is not as pronounced as in the rainfall regimes (Walker, 1962). Across the northern area, the mean monthly temperatures vary from about 36^0 C in March to about 27^0 C in August, whereas in the south, the mean monthly temperatures are lower, ranging from about 30^0 C in March to about 24^0 C in August. On the other hand, relative humidity slightly decreases from south to north. In the north between April to October, night relative humidity can reach 95 % on the average, falling to about 70 % during the day. High values are experienced during the rainy seasons, but these fall to as low as 20% during the dry season. In the Ejura area, relative humidity is higher, varying from about 90% to 95% in the rainy seasons. Across the country, wind speed is generally low and its direction depends on the position of the ITCZ. The ratio of the wind speeds in the harmattan season to that of the other season increases northwards.

3.3 Geology, soils and topography

The main geological formations are Paleozoic formations of bedded sandstones, shales, mudstones and pebbly conglomerate beds (Windmeijer and Andriesse, 1993). The formations are characterized by a layer of ironstone at a shallow depth (Bates, 1962). The rocks are thought to be of the lower paleozoic age, the weathered products of which constitute the parent materials from which the soils have been formed (Bates, 1962). These materials are gently dipping or flat-bedded and are easily eroded (Dickson and Benneh, 1995). Northward of the basin, the groups of soils found include the reddish well-drained upland sandy loams, the yellowish imperfectly drained sandy loams close to the valley bottom, and in-situ alluvial soils of the valley floors (Overseas Development Institute, 1999). The soils are light textured, shallow and gravelly with plinthite and ironstone. In the southern part (Ejura area), Lixisols of dark brown to brown, fine sandy loam top soil overlying, reddish brown to reddish yellow, fine sandy loam to fine sandy clay loam can be found. They are moderately well supplied with organic matter and nutrients. Moisture holding capacity is moderately good. Furthermore, patches of plinthosols are found with poor humus fine sandy loam topsoil. The soils are poorly drained; medium to light textured and subject to seasonal water logging or flooding for varying periods, but generally become thoroughly dry during the dry seasons.

Ghana is generally classified as a lowland country because it mostly lies below 300 m (Walker, 1962). The Voltian escarpment (Mampong scarp) is the most singular topographical feature. The Ejura area is generally characterized by gently dipping or flat-bedded sandstones, shales, and mudstones, which are easily eroded. This has resulted in an almost flat and extensive plain, which is between 60 and 300 m above sea level. A detailed elevation map of the Volta Basin extending a little beyond its boundaries is presented in Figure 3.3.

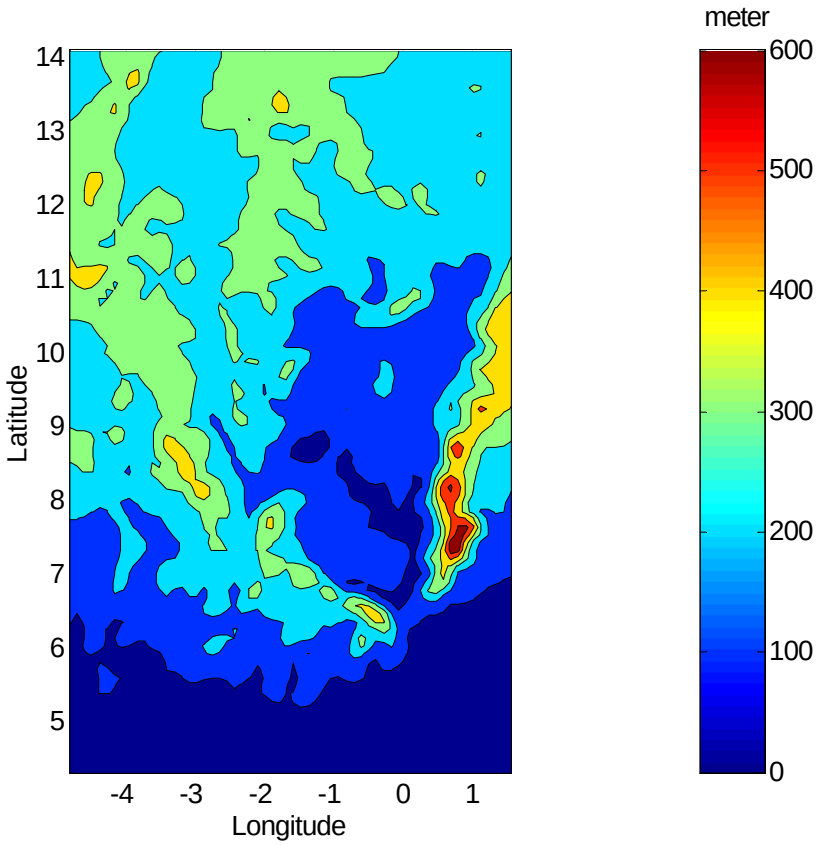

Figure 3.3: Digital elevation model of the study area, West Africa

3.4 Vegetation and agricultural land use

Vegetation changes with increasing latitude in Ghana. The grade is from equatorial evergreen forest in the southwest, to semi-deciduous tropical forest in the north of the forest zone, and through forest savanna transition to Guinea savanna. Sudan vegetation is found in the northeast of the country. Agriculture contributes about 60% of the export earnings and employs about 70% of the population. Crops cultivated in Ghana include maize, millet, sorghum, cowpea, yam, cassava, rice, cotton, water melon, tomatoes, cocoa, cashew, orange, mango, etc.

The natural vegetation in the Ejura area (southern part of the Volta Basin) can be described as wet savannah and is composed of short-branching trees, many less than 15 m high, which do not usually form a closed canopy and are often widely scattered. The ground flora consists of continuous layers of grass, some species reaching a height of about 4 m. The highest cultivated tree crop is cashew with a tree density estimated at 175 trees per hectare.

4 RESEARCH METHODS

4.1 Introduction

This Chapter presents the materials, procedures and techniques used for field measurements and the modeling approach for the large-scale ET.

Installation of equipment for the present research started in the later part of 2001. Data were collected to study the component of evapotranspiration in the water balance of the Kotokosu watershed in Ejura in the southern part of the Volta Basin. Data on soil moisture to 1-m depth were collected twice weekly. Total catchment runoff was measured from the weir close to the outlet, and water potential measurement commenced in the middle of 2002 at two locations in the watershed. Measurements of rainfall and other environmental variables (humidity, temperature, solar radiation, wind run) were made from totaling rain gauges and the weather station located within the study area. Vegetation parameters such as height, Leaf Area Index (LAI), stem diameters and canopy girth were measured together with additional variables such as surface albedo using an albedometer, and surface temperature using an infrared thermometer. The water use pattern of some tree crops was measured using the Granier sap flow system.

Furthermore, the complementarity hypothesis proposed by Bouchet (1963) was tested over the Volta Basin. The advection-aridity model of Brutsaert and Stricker (1979) was implemented using the Climate Research Unit (CRU) high-resolution data set and the output of the MM5 regional circulation model. In addition, the measurement procedures for vegetation biometric, soil moisture and water potential, surface albedo and tree water use are briefly described. Details of meteorological station installations and data acquisition including procedures used in generating the hindcasting data are documented elsewhere (www.glowa-volta.de).

4.2 In-situ measurements

4.2.1 Soil moisture and tension monitoring

Soil water content (q) was routinely measured twice weekly from November 2001 to December 2002 except during periods of sensor failure (July and August, 2002). A profile probe type PR1 (Delta-T Devices, Cambridge, England) was used in three access

tubes located within the watershed. Four sensors were arranged at 10 cm depth intervals down to 40 cm, while a further two were placed at 60 cm and at 100 cm, respectively. Two access tubes were installed in 2001, and the number increased to eight from January to May 2002; and thereafter an additional eight were installed along a well defined transect across the experimental watershed. Two probes 'type ML2x' were used to measure surface (0-5 cm) soil moisture at the tube locations and for special experiments as reported later. The calibrated conversion formulae for mineral soils, supplied by the manufacturer, were used to obtain volumetric q from the millivolt data recorded by the two types of sensors. Tensiometers were used to monitor the soil tension at depths of 30 cm, 60 cm and 100 cm. Profile tension was measured only at two access tube locations with the simultaneous measurement of soil moisture. Tensiometer data were converted using the calibration equation supplied by the manufacturer.

4.2.2 Measurement of surface albedo

Incoming and reflected solar radiation (Rs) was measured with a simple albedometer constructed from two pyranometers horizontally positioned about 1.5 m above the surface. Surface albedo was measured on a monthly basis on different land covers present within the small watershed. These land covers include: farm roads, water body, rocks, cultivated crops, trees and burnt fields. Measurement of catchment elements was taken every month to investigate the seasonal course of surface albedo. The land cover types bare soil and crop fields were further studied in detail.

Bare-soil albedo experiment

Effects of four tillage systems on the albedo of tropical loamy sand were studied under dry and moist surface conditions. The aim was to determine whether tillage-induced roughness and wetness significantly affect measured soil albedo. Land preparation was done in early October 2002. The study site was located within the southern catchment of the Volta Basin (07° 23´ N, 01° 21´W; elevation ≈ 230 m). During the previous three years (1999 – 2001), cowpea and maize had been grown on the field used for this study. Selected physio-chemical properties of the soil are presented in Table 1. The soil is loamy sand, moderately acidic (pH=5.02) with low organic matter content (0.45%). CEC was 4.53 cmol kg^{-1} and bulk density prior to cultivation was 1.63 g cm^{-3}. The four

tillage treatments studied are: Moldboard Plowing (MP), Manual Ridging (MR), Conventional Tillage (CT) and Hand Hoeing (HH). Four plots of land (5 m x 10 m each) on a relatively gentle to near flat slope (< 2%) were used for the respective tillage systems.

Table 4.1: Selected physio-chemical properties of the experimental soil

Parameter	Value/Description
Sand	85.4%
Silt	12.8%
Clay	1.8%
Textural class	Loamy sand
Bulk density	1.63 g cm^{-3}
PH	5.02
Organic matter	0.45%
CEC(Ag+)	4.53 cmol Kg^{-1}
Munsell color (dry)	7.5 YR 4/4
Descriptive color (dry)	Brown
Munsell color (moist)	7.5 YR 4/6
Descriptive color (moist)	Pinkish grey
Average soil moisture (dry)	0.045 m^3 m^{-3}
Average soil moisture (moist)	0.171 m^3 m^{-3}

A three-bladed moldboard implement was attached to a medium-sized tractor for moldboard plowing. A disc plow with an effective width of about 1.2 m and a disc harrow were used to prepare the conventionally tilled soil. Manual ridging and hand hoeing treatments were prepared with the local tillage implements (hoes and cutlasses). Tillage was generally east-west oriented. The smooth reference plot was prepared by applying a sieved (< 2 mm) fraction to cover about 9 m^2 areas to a depth of 5 cm in a 3 m x 3 m x 0.1 m wooden frame. The frame was pre-treated against termite attack and buried to near horizontal level (using a spirit level gage) within a tilled soil. The soil was smoothed using a straightedge. The experimental plot was manually slashed and the plant material removed with a hand rake prior to tillage operations. All the plots were

sprayed with a round-up herbicide to keep the soil surface bare throughout the experimental period. The surface soil water content of the 0-5 cm topsoil was measured with a Delta-T Theta probe type ML2x (Delta-T Devices, U.K.) Surface roughness on each treatment plot was measured with a 100-cm long, 100-pin roughness meter (Cutis and Cole, 1972; Matthias et al., 2000). Following Ogilvy (1991) and Matthias et al. (2000), the roughness parameter was computed as the root mean square deviation (rmsd) of the heights (m) of the pins with respect to a smooth reference surface (Equation 4.1).

$$rmsd\ ,d\ = \left(\frac{1}{n} \sum_{i=1}^{n} h_i^{\ 2} \right)^{\frac{1}{2}} \tag{4.1}$$

where h_i is the *ith* height difference of the pins relative to a flat reference surface, n is number of pins (n = 100). Water content and roughness were measured concurrently with the surface albedo.

The bare-soil surface albedos were measured at five solar zenith angles of 15°, 30°, 45°, 60° and 75° between the months of October and November 2002. The observations of 10 generally cloudless morning hours were used. Shortwave albedo was measured using inverted and upright pyranometers (models: CM 3 and SP LITE, Kipp & Zonen, Delft, Netherlands). The properties of the two pyranometer models used for albedo comparison are presented in Table 4.2. The CM 3 is a broadband thermopile type sensor that integrates solar energy between 0.305 to 2.8 μm while SP LITE is a silicon photovoltaic type sensor with bandwidth from 0.4 to 1.1 μm. The response time for model CM 3 is about 18 seconds and SP LITE less than 1 second. The sensors were placed close enough to the soil surface to ascertain that reflected radiation from the desired soil area was measured. Based on the view factor theory (Reifsnyder, 1967), the fraction f of the total reflected radiation from a square soil area below the albedometer that is received by the sensor is given by Siegel and Howell (1972) as:

$$f = \frac{4}{p} \left[\frac{x}{\sqrt{1+x^2}} \tan^{-1} \left(\frac{x}{\sqrt{1+x^2}} \right) \right] \tag{4.2}$$

where $x = w/h_s$, w is the one-half width (m) of the square area and h_s is the sensor height above the surface.

According to equation 4.2, for the 5 m wide by 10 m long field plots of each treatment, $h_s \approx 0.60$ m and $w = 2.5$ m, about 95.5% of the reflected shortwave radiation originated from a 5 m x 5 m area below the sensor. The rest of the reflected radiation (4.5%) received by the sensor came from the same plot but outside the 25-m^2 areas, while a very small portion may have originated from outside the plot (Matthias et al., 2000).

Table 4.2: Albedometer sensor type, properties and specifications

Specifications	Pyranometer type	
	CM 3	SP LITE
Sensor type	Thermopile	Silicon photovoltaic
Field of view	180°	180°
Response time	18 sec	<1 sec
Sensitivity (calibrated)	20.6 μV/W/m^2	77.0 μV/W/m^2
Tilt response	< ± 2%	No error
Non linearity	< ± 2.5%	< ±1%
Nominal signal range	0 - 50mV	0 - 0.2V
Spectral band range	0.305 – 2.8 μm	0.4 - 1.1 μm
Operating temperature	-40 to +80 °C	-30 to+70 °C
Sensitivity to temperature	6%/°C	0.15%/°C

Source: Adapted from Kipp & Zonen pyranometers instruction manuals (www.kippzonen.com)

Albedo values of different treatments were compared to the albedo of a smooth reference surface by computing the percentage difference as:

$$\%Difference = \frac{a_s - a_t}{a_s} x100\% \qquad (4.3)$$

where a_t *is* mean value of treatment albedo, a_s is mean albedo of the reference smooth surface. A simple linear multiple regression model was fitted to investigate the

combined effects of wetness and roughness on surface albedo. Values of albedo measured with CM 3 were compared with SP LITE to ascertain the differences in their performances.

Cropland albedo experiment

The albedo (α) of vegetated land surfaces is a key regulatory factor in atmospheric circulation and plays an important role in the mechanistic accounting of many ecological processes. This experiment aimed to examine the influence of the phenological stages of maize (*Zea mays*) and cowpea (*Vigna unguiculata*) field, on observed albedo at a tropical site in Ghana. The crops were studied for the first and second cropping seasons in the year 2002. One plot per crop, measuring 10m by 10 m, was demarcated on farmers' fields. The four phenological stages distinguished were (1) emergence or seedling, (2) vegetative, (3) flowering and (4) maturity (physiological maturity). Incoming and reflected solar radiations were measured with a simple albedometer constructed from two pyranometers as earlier mentioned. The leaf area index was measured with a canopy analysis system (LAI-2000, LiCor. Lincoln, NE). During each sampling period, six plants were randomly sampled in the field for non-destructive measurements. Crop height (CH), defined as the average of the heights from the ground to the top of the raised leaves of each plant, was measured with a long ruler with a resolution of 1 mm. Albedo measured from two surfaces, i.e., short grass and bare soil, were used as references to study the relative difference in surface albedo over time (between planting and physiological maturity). The short grass was maintained at a height < 15 cm, while the bare soil was ploughed and harrowed (conventional tillage), which is typical for land preparation by large-scale commercial farmers in this area. Surface albedo was measured at sun angles of 15°, 30°, 45°, 60°, and 75°; and the data used were generally for clear sky days. The crops were studied for first (early) and second (late) cropping seasons in the year 2002. Crop management was similar in both seasons, and measurements were taken between 6:00 am and 11:30 am each day of measurement. Soil samples were also collected for textural classification.

4.2.3 Modeling of surface albedo

An existing model of albedo and selected empirical equations existing in the literature were assembled to simulate the crop fields' surface albedo at different phenological stages. Jensen and Rahman (1987) utilised the albedo model suggested by Uchijima (1976) in which the surface albedo (a), is given as:

$$a = a_c - (a_c - a_u)\exp(-kL) \tag{4.4}$$

where a_c is the reflection coefficient of a fully developed crop canopy, a_u is the reflection coefficient of the underlying soil surface, k is the extinction coefficient and L is the leaf area index. This model was developed for daily average albedo values and cannot be used to account for diurnal variations in the present form. Therefore, the parameters in this equation were estimated from other documented empirical relationships (Ross 1975; Monteith and Unsworth, 1990; Song, 1998) in order to account for the diurnal dynamics of the overall surface albedo. Canopy albedo a_c is given as:

$$a_c = f_c a_{cq} + f_l a_l \tag{4.5}$$

where a_l is the single leaf albedo, a_{cq} represents the albedo of a semi-infinite canopy, f_c and f_l are weighting factors for canopy and single leaf, which are also dependent on leaf area index and solar zenith angle as follows:

$$f_c = 1 - f_l \tag{4.6}$$

$$f_l = \exp(-bL) \tag{4.7}$$

where b =0.5/cos$q$ is the shadow area cast by a unit area of leaf that depends on zenith angle (q). a_{cq} is computed with two equations to account for the direct and the diffuse components of radiation. For the direct component, a_{cq1} is computed as:

$$a_{cq1} = \frac{bw}{(m+b)(1+m)} \quad (4.8)$$

where w is the scattering coefficient and $\mu=(1-w)^{1/2}$. The diffuse component a_{cq2} is computed by substituting ß =1 in Equation 4.8 (Song 1998). a_{cq1} and a_{cq2} are substituted in Equation 4.5 in turn and the average a_c is used for the overall albedo computation (Equation 4.4).

The underlying soil albedo is also a variable parameter and is calculated as a function of soil wetness and the zenith angle of the sun, according to

$$a_u = a_{uw} + a_{uq} \quad (4.9)$$

where a_{uw} represent the effects of soil wetness and a_{cq} is a correction factor for albedo dependence on sun zenith angle (q) and is defined as (Song, 1998):

$$a_{uq} = 0.001\left[\exp\left(0.00358q^{1.5}\right)-1\right] \quad (4.10)$$

The above set of equations was used to compute surface albedo at different sun angles and crop phenological stages. Mean value of scattering coefficient (w) is 0.5, and k ranges from 0.3 to 1.5 (Ross, 1975), the higher values correspond to large horizontal leaves and the lower values to vertical ones. An initial value of k = 0.45 was used for the simulation and thereafter k was optimized by minimizing the sum of squares of the residuals using the first season data. Modeled albedo values, using the optimized parameter, were compared to observed albedo values with an independent second season data set. The goodness-of-fit statistics used in comparing the observed and the predicted values are correlation coefficient(R) and mean bias error (MBE). MBE, which quantifies the bias of the prediction, was computed as:

$$MBE = \frac{1}{n}\sum_{i=1}^{n}(a_i^* - a_i) \quad (4.11)$$

where a_i^* is the predicted value and a_i is the measured value. MBE quantifies the bias of the prediction and should be close to zero for unbiased predictions, while the square of R explains the variations in observed albedo values captured by the simulation.

4.2.4 Whole-tree water use

Part of the data needed to test and validate land surface models is whole-tree water use, which will help hydrologists to resolve issues of water resource management, and to evaluate the role of tree transpiration in catchment hydrology. Furthermore, this measurement was done so as to understand the role of trees in this ecosystem during the dry, wet, and transition seasons as well as the relations and dynamic interactions with climatic factors.

Tree sap flow with Granier system

Sap flow density in the trees was measured using the temperature difference (TD) method developed by Granier (1985, 1987). The method uses heated and unheated thermocouple pairs. The set-up consists of a pair of fine-wire copper-constantan thermocouples connected such that voltage measured across the copper leads represents the temperature difference between the thermocouples. Two cylindrical probes, about 2 mm in diameter, were implanted in the sapwood of the tree trunk with previously installed aluminum tubes, vertically 12-15 cm apart at breast height (about 1.3 m was used in this study). Each of the probes contained a 2 cm long copper-constantan thermo-element with copper heating wiring. The tubes were filled with a heat conductive paste in order to obtain good thermal contact with the probes. The probes were installed on the north side of the tree to minimize direct heating from the sunshine and then shielded with aluminum foils against rainfall. The sensors were connected to the power source and a data logger following the manufacturer's prescriptions (UPGmbH 2001). The upper heating coil dissipates heat into the sapwood and the sap flow surrounding the probe while the lower is unheated. During conditions of zero sap flow density, such as during the night, the temperature difference between the lower and the upper probes represents the steady state temperature difference caused by the dissipation of heat into non-transporting sapwood. This maximum TD value serves as the baseline from which

any increase in sap flow causes a decrease in TD. The following equation was used to compute the sap flow density (*f*, ml cm^{-2} min^{-1}):

$$f = 0.714\left[\left(TD_m / TD\right) - 1\right]^{1.231} \qquad (4.12)$$

where TD_m is the baseline (maximum) temperature difference for the data set or the day. Sap flow data were sampled at 30s interval and averaged and recorded every 30 minutes.

Three trees with about the mean of the diameter size distribution were selected for sap flow measurements. A non-linear regression analysis was used to fit a relationship between water use (kg h^{-1}) and the incoming solar radiation using the Levenberg-Marquardt non-linear minimization procedure to optimize the parameters (Marquardt, 1963). Whole-tree sap flow and canopy transpiration were calculated using sapwood area and tree density. The dry season experiment was between November 2001 and March 2002 while the rainy season measurements were from May to October 2002. A special experiment was conducted between November and January during the 2002/2003-transition period to compare sap flow and eddy correlation measurement systems.

Tree biometric measurements

Fifteen trees were randomly selected within the 0.5 ha sampling plot. Stem diameter at breast height (1.3 m) was measured with a diameter tape. Tree height was measured with a Spiegel relaskop (Relaskop-Technik, Austria), while bark thickness was determined with a small ruler using a chiseled out piece. Sapwood thickness was manually measured with a core sampler, exploiting color differences between sapwood and heartwood resulting from differences in water content. The tree sapwood area was estimated from stem diameter, sapwood thickness and bark thickness. For the rainy season, monthly changes in stem diameter and sapwood area were incorporated in the analysis by assuming a linear increment in stem diameter during the growing season (Table 4.3). Leaf area index (LAI) was measured with a canopy analysis system (LAI-

2000, LiCor, Lincoln, NE) at eight points under the canopy of the individual selected trees. The mean value was computed by averaging all LAI estimates.

Table 4.3: Diameter at breast height (DBH), basal area (BA), and sapwood area (SWA) of the gauged trees before and after the experiment

Tree	March (15-03-02)			November (17-11-02)			$^{\#}\Delta$ DBH
no	DBH (cm)	BA (cm^2)	SWA (cm^2)	DBH (cm)	BA (cm^2)	SWA (cm^2)	(cm)
1	15.91	198.78	134.96	21.00	346.36	221.18	5.09
2	16.88	223.65	149.88	24.30	463.77	286.76	7.43
3	13.80	149.60	104.81	17.50	240.53	159.90	3.70
Mean	15.53	189.39	129.88	20.93	344.16	222.61	5.40

$^{\#}$ Increase in tree DBH from March to November

4.2.5 Relations with meteorological variables

Both linear and non-linear regression analyses were used to fit relationships between transpiration and the environmental variables. One such variable is the clearness index (*CI*), a measure of sky condition, computed as (Ogunjobi et al., 2002):

$$CI = \frac{Rs}{R_O} \qquad (4.13)$$

where *Rs* is the global radiation and R_o is the daily extraterrestrial radiation. A simple linear model was fitted between sap flux (*f*) and *CI*. The multiple linear regression equation between water use (Q_t, kg h^{-1}) and weather variables is of the form:

$$Q_t = a + b * Rs + c * H + d * T \qquad (4.14)$$

where *Rs* is solar radiation, *H* is relative humidity, *T* is air temperature and *a, b, c, d* are the fitted parameters. The first type of non-linear equation combines a quadratic hyperbolic response to *Rs* and a linear response to *T* and *H*. The equation is of the form:

$$Q_t = a * Rs/(Rs+b) * (c + d * T) * (100 - e * H) \qquad (4.15)$$

where e is a fitted parameter. The second type of non-linear model is a modified Priestly-Taylor formula presented as (Bosveld and Bouten, 2001):

$$lE_c = a_{PT}\left(\frac{\Delta}{\Delta+g}(R_n - G) + b\right) \qquad (4.16)$$

where a_{PT} and b are fitted parameters representing a typical Priestly-Taylor coefficient and a parameter accounting for periods of zero or negative available energy ($A = R_n - G$), respectively. The Levenberg-Marquardt non-linear minimization procedure was used to optimize the parameters (Marquardt, 1963), using 30-minutes time step values of the observed data. A measure of accuracy (d), to compare the relative performance of these different models, was computed as follows:

$$d = \frac{|R_p - R_m|}{R_p} x100\% \qquad (4.17)$$

where R_p and R_m are the predicted and the measured correlation coefficients. Increase in d from one model to the other represents a decrease in performance accuracy.

Stomata conductance and decoupling coefficient

The canopy conductance was estimated by inverting the Penman-Monteith equation (Granier and Loustau, 1994):

$$\frac{1}{g_c} = \left[\frac{\Delta}{g}\left(\frac{A - lE_c}{lE_c}\right) - 1\right]\frac{1}{g_a} + \frac{r_a}{E_c}\frac{C_p}{lg}VPD \qquad (4.18)$$

where g_c (m s^{-1}) is the canopy conductance, Δ (kPa K^{-1}) is the rate of change of vapor pressure with temperature, g (kPa K^{-1}) is the psychrometric constant, r (kg m^{-3}) is the density of the dry air, C_p is the specific heat capacity of the air (J kg^{-1} K^{-1}), *VPD* is the

vapor pressure deficit (kPa), g_a is the boundary layer conductance (m s^{-1}), l is the latent heat of water vaporization (J kg^{-1}), E_c is the canopy transpiration (kg m^{-2} s^{-1}), and A is the available energy at the canopy level (J m^{-2} s^{-1}). Aerodynamic conductance (g_a) was calculated from wind speed using the equation (Granier et al., 2000):

$$g_a = \frac{k^2 u}{\ln[(z-d)/z_0]} \tag{4.19}$$

where u is the wind speed (m s^{-1}) and z is the wind measurement height(m). The zero plane displacement (d) and the roughness length (z_0) were taken as 0.75 and 0.1 of the tree height (= 6.9 m), respectively; k is the von Karman constant (= 0.4). Available energy was estimated according to Granier and Loustau (1994). Half-hourly estimates of g_c were calculated using all the variables specific to those time steps, while daily g_c was based on the daily average of all the variables.

The decoupling coefficient was calculated after Monteith and Unsworth (1990) as:

$$\Omega = \frac{\Delta + g}{\Delta + g\left(1 + g_a / g_c\right)} \tag{4.20}$$

The relative significance of radiative (E_{eq}) and advective (E_{imp}) energy on E_c was estimated using the equations:

$$E_c = \Omega E_{eq} + (1-\Omega) E_{imp} \tag{4.21}$$

$$E_{eq} = \frac{eA}{l(e+1)} \tag{4.22}$$

and

$$E_{imp} = \frac{C_p}{lg} g_c VPD \tag{4.23}$$

where E_{eq} is the “equilibrium” transpiration rate that would be obtained over an extensive surface of uniform wetness and E_{imp} is the atmospheric “imposed”

transpiration rate through the effects of a vapor pressure deficit (VPD). e is given as Δ/g (Javis and McNautghon, 1986; Phillips et al., 1997; Wullschleger et al., 2000).

4.2.6 Eddy fluxes

The eddy correlation system was used to measure latent (*LE*) and sensible heat (*H*) fluxes over the orchard. This device was mounted at a height of 10 m, which was about 4.8 m above the mean tree height, from a tower installed in the middle of the plot. The three axis components of wind speed were measured with a 3-D sonic anemometer (Gill Instruments Ltd., UK) and water flux was measured with a Krypton hygrometer (model KH_2O, Campbell Scientific, UK). A detailed description of the set up and operation of the device is given by Elbers (2002) and data set was provided by Burose et al.(2004). Eddy correlation measurements started on November 9, 2002 and stopped on January 28, 2003. A total of 79 days of reliable data was available over this drying transition period. Two softwares (EC_NCDF and ALTEDDY) were used to process on-line sensible heat and water fluxes after making adequate corrections to the fluxes following the recommendations of Aubinet et al. (2000) and using the time constant of 200 s for the digital filter. The *LE* estimated by the two softwares was compared and the possible implications on energy and water balance are discussed.

4.2.7 Time lag estimation

The dynamic responses of whole-tree sap flow (S_F) and evapotranspiration (ET) to environmental driving forces were assessed using cross-correlation analysis. Time lags (t) were roughly estimated for (1) tree-canopy pairs, i.e., S_F and ET (2) stem and canopy individually with respect to both R_S and VPD. A range of time lags was introduced for each pair of time series and the corresponding range of correlation coefficients (R) was obtained by use of the cross-correlation function (ccf) given as:

$$R = \frac{Cov[X(t), Y(t+t)]}{s_x . s_y} \qquad (4.24)$$

i.e., the covariance of *X* and *Y* time series variables divided by the product of their standard deviations, s_x and s_y, respectively. Where *r* is the correlation between *X* and *Y*, *t* is time and $_t$ is a lag introduced between *X* and *Y*.

The lag that corresponds to maximum *R* is retained as the time lag for that pair. This procedure is commonly used to determine the lag between time series pairs (Phillips et al., 1997, 1999; Post and Jones, 2001; Bond et al., 2002), but its accuracy is mainly affected by the periodicity or the averaging period for the measurements. For example, lag for a time series pair with 20 min time step will be to the nearest 20 min and the one for 5 min will also be to the nearest 5 min. Therefore, to determine time lag ($_t$) more precisely, a quadratic model (the most successful equation with coefficient of determination, $R^2 > 0.99$) was fitted between correlation (*R*) and $_t$:

$$R = at^2 + bt + c \qquad (4.25)$$

where *a, b* and *c* are the constant coefficients of the function and $a \neq 0$. Applying simple differential calculus to Equation 4.25:

$$\frac{dR}{dt} = 2at + b \qquad (4.26)$$

at maximum *R*, Equation 4.26 equals zero and thus, $_t = -b/2a$. This analysis was done for 12 days of available data in November (DOY 323-334), 7 days in December (DOY 359-365) and 3 days in January (DOY 1-3).

4.3 Large-scale evapotranspiration estimates

Bouchet´s hypothesis

The hypothesis of a complementary relationship (Bouchet, 1963) states that over areas of a regional scale and away from any sharp environmental discontinuities, there exists a complementary feedback mechanism between actual (ETa) and potential (ETp) evapotranspiration (Figure 4.1). In this context, ETp is defined as the evapotranspiration that would take place from a moist surface under the prevailing atmospheric conditions, limited only by the amount of available energy. Under conditions where ETa equals ETp, this rate is referred to as the wet environment evapotranspiration (ETw). The

complementary relationship hypothesis is essentially based on empirical observations, supported by a conceptual description of the underlying interactions between evapotranspiring surfaces and the atmospheric boundary layer.

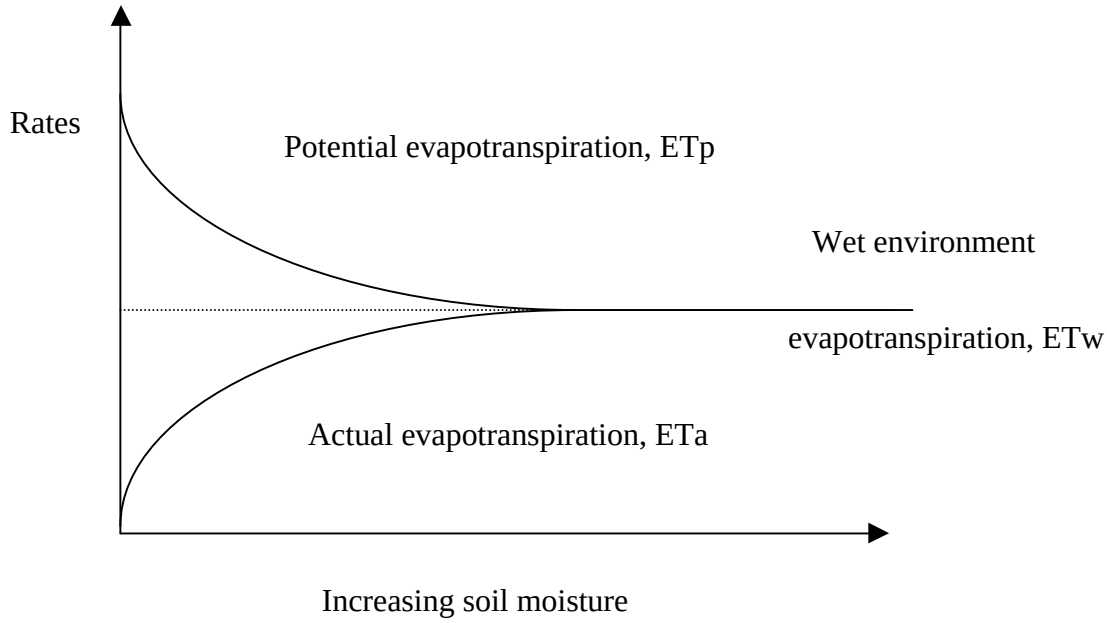

Figure 4.1: Schematic representation of the complementary relationship.

Bouchet (1963) hypothesized that when, under conditions of constant energy input to a given land surface–atmosphere system, water availability becomes limited, ETa falls below its maximum (ETw), and a certain amount of energy (q1) becomes available. This energy excess, in the form of sensible heat and/or long wave back radiation, increases the temperature and humidity gradients of the overpassing air and leads to an increase in ETp equal in magnitude to the decrease in ETa. If water availability is increased, the reverse process occurs, and ETa increases as ETp decreases. Thus ETp ceases to be a climatologically constant forcing function, but depends on the conditions of moisture availability. This may be expressed as:

$$ETa - ETw = -q1 \tag{4.27}$$

$$ETp - ETw = q1 \tag{4.28}$$

Combining Equations 4.27 and 4.28 to give the complementary relationship,

$$ETp + ETa = 2ETw \qquad (4.29)$$

This hypothesis has been tested in different continents but mostly in the USA (Morton, 1983; Parlange and Katul, 1992a; 1992b; Kim and Entehkabi, 1997; Lhomme, 1997, Hobbins et al., 2001a, 2001b; Szilagyi, 2001; Szilagyi et al., 2001). Its validity in West Africa is tested herein.

The Advection-Aridity model

The complimentary relationship Advection-Aridity model proposed by Brutsaert and Stricker (1979) was implemented in this study. The potential evapotranspiration ETp in Equation 4.29, was given by Penman (1948):

$$ETp = \frac{\Delta(R_n - G)}{\Delta + g} + \frac{gE_a}{\Delta + g} \qquad (4.30)$$

The first term of Equation 4.30 represents a lower limit on the evaporation from moist surfaces, as the second term tends towards zero over large, homogeneous surfaces under steady state conditions. The second term represents the effects of large-scale advection. Δ is the slope of the saturated vapor pressure curve at air temperature (Pa/°C), g is the psychrometric constant (Pa/°C), and R_n-G is the available energy at the evaporating surface (W/m^2). E_a is known as the 'drying power' of the air and is a product of a function of the wind speed $f(U_r)$ at height Z_r above the evaporating surface and the vapor pressure deficit (e_a -e_s); e_a and e_s are actual and the saturated vapor pressure, respectively. E_a takes the general form:

$$E_a = f(U_r)(e_s - e_a) \qquad (4.31)$$

The original wind function proposed by Penman (1948) was adopted in the Advection-Aridity model. This is simple, empirically based and of the form:

$$f(u_r) \approx f(u_2) = 0.26(1 + 0.54u_2) \quad (4.32)$$

where u_2 is the wind speed at 2 m in m/s. With this wind function and the vapor pressure deficit in mbars, E_a is computed in mm/day. Two models are used to calculate the wet environment evaporation (ETw): the Priestley and Taylor (1972) empirical equation proposed to estimate partial equilibrium evaporation. This is given by:

$$ETw1 = a_{PT} \frac{\Delta(R_n - G)}{\Delta + g} \quad (4.33)$$

where the value of constant a_{PT} was empirically determined and is given between 1.26 and 1.28. Brutsaert and Stricker (1979) suggested another ETw equation derived from energy balance equation as:

$$ETw2 = \frac{(Rn - G)}{(1 - b_e) + a_e(g / \Delta)} \quad (4.34)$$

where $a_e = 0.63$ and $b_e = 0.15$.

Substituting Equations 4.30, 4.31 and 4.33 in 4.29 yields the expression for regional ETa:

$$ETa1 = (2a_{PT} - 1)\frac{\Delta}{\Delta + g}(R_n - G) - \frac{g}{\Delta + g} f(u_2)(e_s - e_a) \quad (4.35)$$

In formulating this model for use in three-day time-steps, Brutsaert and Stricker (1979) ignore any effect of atmospheric instability in the wind function term. An alternative form is obtained by substituting Equations 4.30, 4.31 and 4.34 in 4.29 leading to:

$$ETa2 = \left[\frac{2\Delta}{(1 - b_e)\Delta + a_e g} - \frac{\Delta}{\Delta + g}\right](Rn - G) - \frac{g}{\Delta + g} \mathrm{f}(u_2)(e_s - e_a) \quad (4.36)$$

The two forms (4.35 and 4.36) are tested in this study

4.3.1 Model data requirements and sources

The major benefit of complementary relationship models is that they require only easily measured meteorological data and do not require local calibration of parameters beyond the ones built into the models. The models require data on average temperature, wind speed, solar radiation, relative humidity, albedo, and elevation and do not require data on soil moisture, stomata resistance properties of the vegetation, or any other aridity measures. Data used to run the CR model are from two sources: (1) Climate Research Unit, University of East Anglia, Norwich, UK (Mitchell et al., 2003) herein referred to as 'CRU data' and hindcasting meteorological data simulated with the MM5 regional circulation model (Kunstmann, 2002).

CRU data treatment

Monthly large-scale evapotranspiration was estimated for West Africa using the Global Gridded Climatology presented at a new high resolution (0.5° latitude/longitude) and made available by the Climate Impacts LINK project, Climate Research Unit, University of East Anglia, Norwich, UK. This data set includes: precipitation, average temperature, cloud cover, and vapor pressure. Other parameters were estimated following the procedures outlined in FAO 56 (Allen et al., 1998).

Radiation was estimated from the published monthly extraterrestrial radiation (Ra) data. A set of polynomial functions of third degree was fitted between Ra and the latitude on a monthly basis (Table 4.4).

Table 4.4: Regression models to estimate extraterrestrial radiation (Ra) as a function of latitude ($_f$). $ß_1$ to $ß_4$ are the model parameters and R^2 is the coefficient of determination.

Month	$R_a = b_0 + b_1 f + b_2 f^2 + b_3 f^3$				R^2
	$ß_1$	$ß_2$	$ß_3$	$ß_4$ (x 10^{-6})	
January	36.203	-0.3883	-0.0048	30	1.000
February	37.514	-0.2640	-0.0060	-50	1.000
March	37.898	-0.0438	-0.0031	8	0.9997
April	36.799	0.1664	-0.0052	-10	0.9971
May	34.706	0.3424	-0.0056	-3	0.9984
June	33.393	0.4257	-0.0075	80	0.9998
July	33.896	0.3652	-0.0046	-8	0.9999
August	35.675	0.2317	-0.0048	-8	0.9988
September	37.236	0.0225	-0.0020	-200	0.9923
October	37.396	-1848	-0.0046	-8	0.9999
November	36.303	-0.3323	-0.0063	60	0.9999
December	35.624	-0.4206	-0.0043	20	0.9999

The cloud cover was converted to the sunshine ratio with a regression model using data from FAO 24 (Table 2, page 5; Doorenbos and Pruitt, 1977). This is given as:

$$\frac{n}{N} = 0.9518 - 0.1145 C_c + 0.00889 C_c^{\,2} - 0.0012 C_c^{\,3} \qquad (4.37)$$

where n is the actual sunshine and N is the maximum possible sunshine, C_c is the cloud cover in tenths. The coefficient of determination, R^2 for the equation is 0.998.

Wind speed data were scarce and monthly wind maps were composed by interpolation from a 3-month average wind data available for West Africa. This was expected to be of better quality than the single value of global average (2 m/s) as suggested by Allen et al. (1998) for places without wind data.

MM5 hindcasting data treatment

Simulations of MM5 generated the meteorological variables for the Volta basin and its immediate environment (between latitude 4.3^0 and 14.2^0 and from longitude -4.8^0 to 1.5^0). The data set is gridded in 12 x 12 km^2; a finer resolution compared to the CRU data. The output is a 3-hourly data, which was aggregated to monthly. The simulation set-up was changed from time to time, either for improvement of one sub-model or for the use of better-input data. Thus, out of three years of available data, two year covering April 2002 to March 2004 were used for this study. During this period, the simulation set-up was consistent with the same input data type. Monthly ET maps were constructed based on the complementary relationship Advection-Aridity model. Seasonal trend of ET and total water-use from respective land-use type was examined.

5 SURFACE ALBEDO AND TREE WATER USE

This chapter gives the results and discussion on surface albedo and tree water use. The chapter is divided into six sections with each section presenting the findings from a uniquely designed field experiment. A short background is first presented for each section to provide the readers with state of knowledge and the specific objectives of the particular field experiment.

5.1 Bare-soil albedo

Background

Bare-soil evaporation plays a key role in the water balance of an ecosystem. Appropriate representation of the soil water balance is critical in ecosystem simulation models, especially in semiarid regions (Wythers et al., 1999). Accurate information on available energy at the soil surface is crucial in the estimation of bare-soil evaporation, and thus, all factors that influence net radiation should be considered important. For a wet bare soil, evaporation occurs at the potential rate and is a large fraction of the net radiation on a daily basis (Priestly and Taylor, 1972). Higher net radiation, on a rough soil surface relative to a smooth soil surface, is partly due to a lower reflection coefficient on a rough soil surface (Coulson and Reynolds, 1971; Idso et al., 1975; Potter et al., 1987). Multiple reflections occurring between soil particles have been suggested as the mechanism that lowers surface reflectance of a rough soil surface (Arnfield, 1975; Twomey et al., 1986).

In addition to tillage-induced surface roughness, wetness also influences soil surface albedo and affects soil-water processes important in crop production and soil conservation (Cresswell et al., 1993). The albedo of a surface, defined as a fraction of reflected shortwave solar radiation (wavelength, ι = 0.3-3.0 μm), is one of the primary factors influencing ecological, biophysical and plant physiological processes as well as local and global climates (Yin, 1998; Tooming, 2002). Soil albedo helps to modify soil temperature, which in turn affects soil biophysical processes, such as seed germination, root growth, plant development and microbial activity (Potter et al., 1987; Matthias et al., 2000). Bare-soil albedo is affected by optical properties of soil surface, solar zenith angle and degree of wetness or dryness of the soil surface (Idso et al., 1975; Jacobs and

van Pul, 1990; Matthias et al., 2000). However, it remains unclear which of the factors, i.e., zenith angle, surface wetness, roughness, or tillage orientation, etc., is the most critical to bare-soil albedo (Cresswell et al., 1993; Matthias et al., 2000). Therefore, efforts to investigate the energy balance at the earth surface are frustrated by significant uncertainties in the estimated magnitude of surface albedo (Iziomon and Mayer, 2002).

Despite the importance of soil albedo data in different land surface processes and hydrological models, there have been very few studies along this direction in sub-saharan Africa. The limited availability of such data motivated this study as part of the larger on-going field campaign of the GLOWA Volta project in West Africa. The main objective of this investigation was to determine the effects of tillage, surface moisture and sensor type on the surface albedo of a bare tropical soil. This in turn will support the energy balance studies at watershed level. The acquired data and insights are also important for improving satellite based-albedo estimates.

Findings and discussion

Soil surface conditions for the period of the experiment are presented in Table 5.1. Average surface roughness for the moist and dry soil as well as soil moisture content for the tillage systems and smooth reference soil are shown. A typical surface configuration (immediately after tillage operation) across a 1-m width of the plots is plotted in Figure 5.1. The four tillage treatments studied are: Moldboard Plowing (MP), Manual Ridging (MR), Conventional Tillage[1] (CT) and Hand Hoeing (HH). MP followed by MR is clearly distinguished while the difference between CT and HH is not clear. Roughness parameter, rmsd (d), increased from 2.1 cm for HH to 6.2 cm for MP for the moist soil following tillage. Few rainfall events, totaling 150.5 mm (14 wet days), during the experiment caused a reduction in surface roughness for all the treatments. The range of soil moisture was from 0.024 m^3 m^{-3} in MR (dry soil) to 0.211 m^3 m^{-3} in HH (moist soil).

[1] Conventional Tillage here refers to a tillage system in which the plowing operation is followed by harrowing. This is the land preparation common with large commercial farmers in the study area.

Table 5.1: Average values of surface roughness and soil water content for the four tillage treatments and the smooth reference surface (standard deviation given in parentheses).

Tillage treatment	Surface roughness (cm)		Soil water content (m^3/m^3)	
	Moist	Dry	Moist	Dry
Moldboard plowing	6.2 (0.86)	3.4 (0.78)	0.162 (0.009)	0.042 (0.003)
Manual ridging	4.1 (0.61)	2.3 (0.54)	0.179 (0.014)	0.024 (0.004)
Conventional tillage	2.2 (0.30)	1.2 (0.27)	0.147 (0.008)	0.043 (0.011)
Hand hoeing	2.1 (0.28)	1.1 (0.24)	0.211 (0.006)	0.053 (0.007)
Smooth surface[#]	0.2 (0.08)	0.2 (0.09)	0.155 (0.015)	0.064 (0.008)

[#] Reference surface

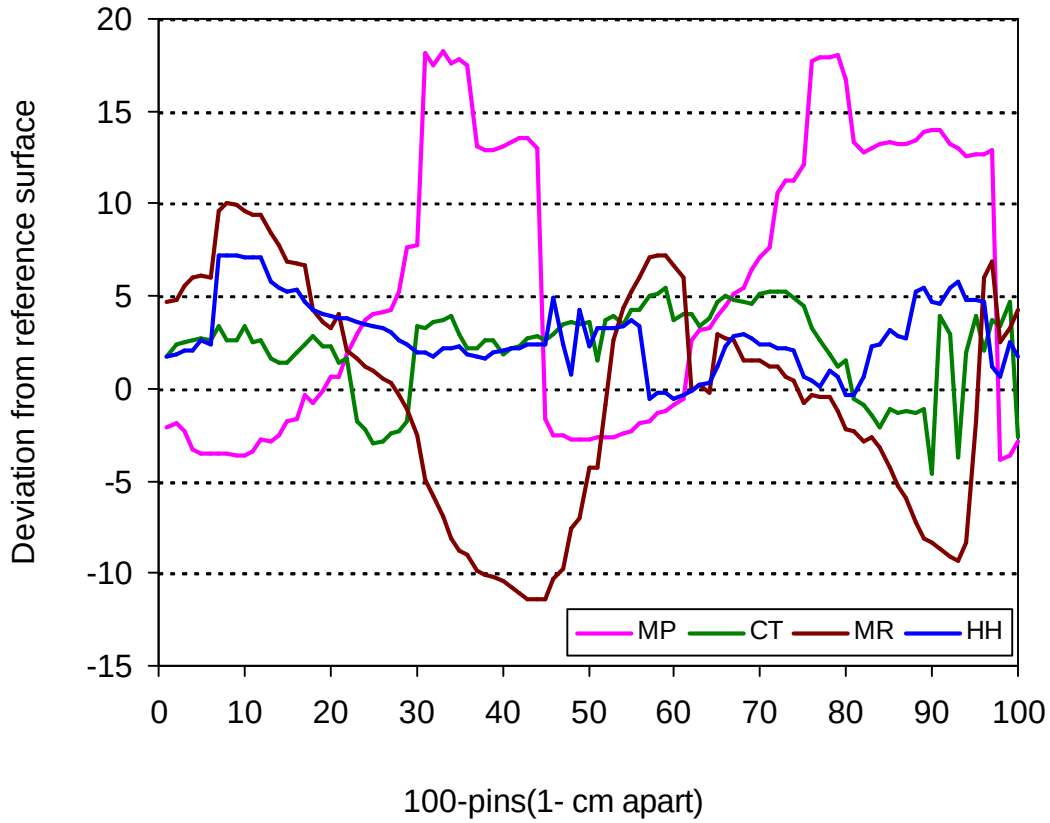

Figure 5.1: Typical surface configuration for the tillage treatments relative to smooth reference surface.

Albedo values at five zenith angles are shown in Figure 5.2 for both sensor types. The graph shows a gradual increase in surface albedo with corresponding increase in zenith angle of the sun. Both sensors showed the same pattern of albedo with

respect to zenith angle, especially for the dry soil surface. A lower value of measured albedo using CM 3 on wet rough soil and at 75° appeared inconsistent with the generally observed patterns. This inconsistency may be due to low sensor sensitivity as compared to SP LITE. The albedo values for the smooth reference surface also increased with the zenith angle. The highest value occurred at zenith angle 75° and the lowest at zenith angle 15°. Although the mechanism of the influence of zenith angle on albedo is not yet properly understood (Cresswell et al., 1993), the results of this study agree with the work of Idso et al. (1975), Matthias et al. (2000) and the wave scattering theory (Ogilvy, 1991). The effects of zenith angle on albedos between dry and wet surfaces can be deduced from Figure 5.2. The rate of increase of albedo with respect to zenith angle is higher on a dry surface as compared to a wet surface. This positively increased gradient was clearly observed with the two sensor types used in this experiment. These results are in contrast to Idso et al. (1975), who detected no differences in the zenith angle effect on albedo between wet and dry surfaces.

Mean albedos for the four tillage treatments studied as measured with CM 3 and SP LITE sensors are presented in Table 5.2. The results indicate that albedo reduced with increasing surface roughness for both wet and dry soil conditions. Means for the treatments and the smooth reference surfaces ranged from 0.109 (wet soil) to 0.287 (dry soil), and 0.147 (wet soil) to 0.275 (dry soil) as measured with CM 3 and SP LITE respectively. The pattern of the roughness effect on the mean albedo appears to be identical for the wet and dry soil surface conditions. To further illustrate the roughness effects on the mean albedo values, the results of Equation 4.3 are presented in columns 5 and 6 of Table 5.2. The maximum percentage decrease of the mean albedos (≈ 38% and 26% for CM 3 and SP LITE) occurred on the roughest surface (MP, wet), while the minimum percentage decrease (≈5% and 6% for CM 3 and SP LITE) occurred on CT and HH. On this soil, the range of surface roughness commonly found in large commercial grain production as well as yam and root crop cropping is likely to cause between 20% and 25% changes in surface albedo for wet conditions and less than 12% for a dry soil surface.

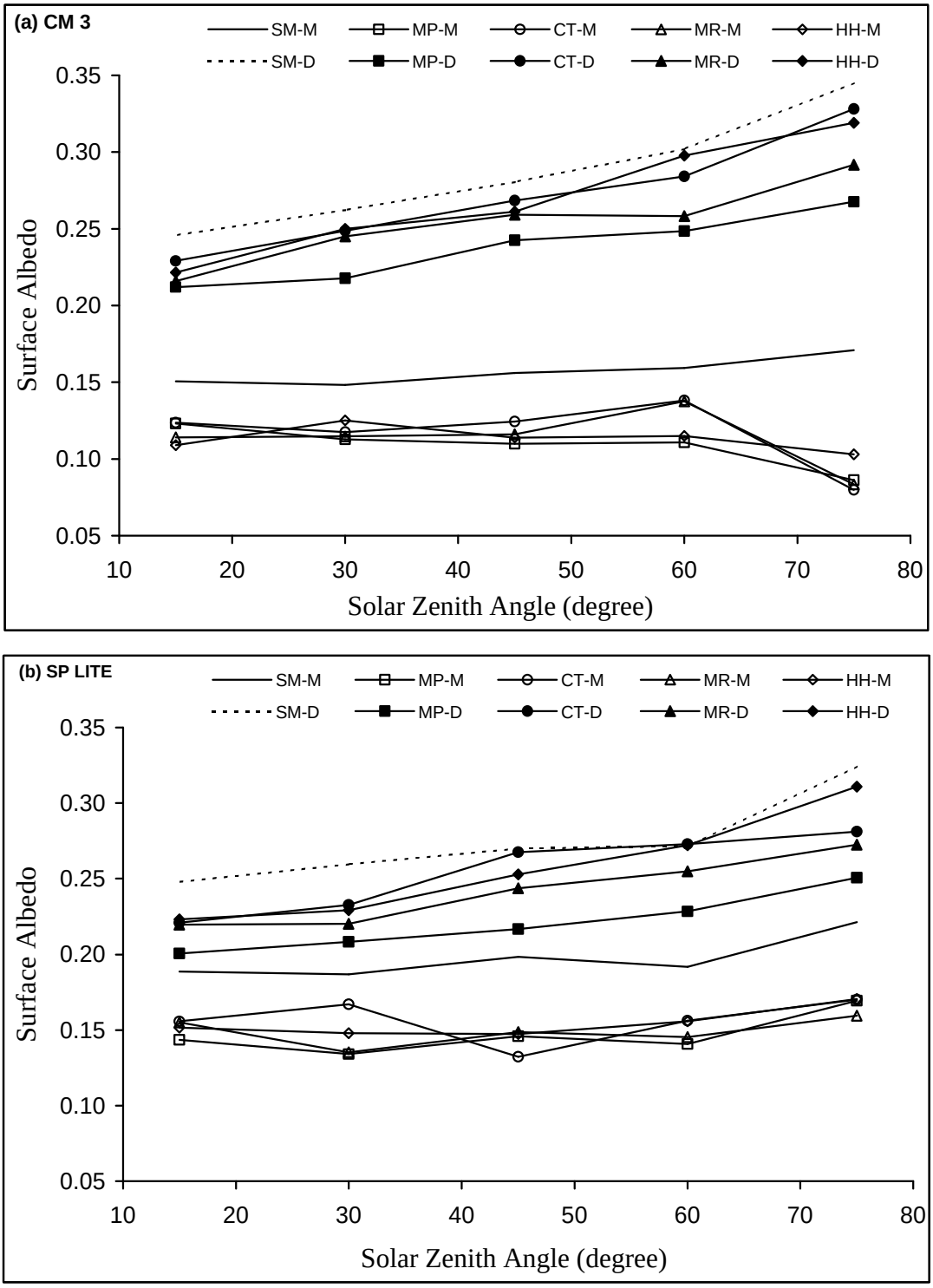

Figure 5.2: Surface albedo at five solar zenith angles for moldboard plowing, conventional tillage, manual ridging, hand hoeing and smooth reference surfaces as measured with (a) CM 3 and (b) SP LITE pyranometers.

Table 5.2: Mean albedo for the four tillage treatments as measured by CM 3 and SP LITE pyranometers (standard deviation given in parentheses).

Surface	Tillage Treatment	Mean albedo		% Decrease[#]	
		CM 3	SP LITE	CM 3	SP LITE
Moist	Moldboard Plowing	0.109 (0.014)	0.147 (0.013)	30.85	25.64
	Manual Ridging	0.113 (0.019)	0.149 (0.009)	27.87	24.63
	Conventional Tillage	0.117 (0.022)	0.156 (0.015)	25.66	20.83
	Hand Hoeing	0.113 (0.008)	0.155 (0.010)	27.82	21.66
	Smooth surface	0.157 (0.089)	0.197 (0.014)	na	na
Dry	Moldboard Plowing	0.238 (0.023)	0.221 (0.020)	17.21	19.55
	Manual Ridging	0.254 (0.027)	0.242 (0.023)	11.53	11.80
	Conventional Tillage	0.272 (0.037)	0.255 (0.027)	5.37	7.10
	Hand Hoeing	0.270 (0.039)	0.258 (0.036)	6.00	6.17
	Smooth surface)	0.287 (0.039)	0.275 (0.029)	na	na

[#] Computed with Equation 4.3; na = not applicable (reference surface)

Shortwave albedo was regressed against the surface roughness (Figure 5.3). The results from this regression analysis show that bare-soil albedo is highly dependent on surface configuration or roughness (R^2= 0.988), especially when the soil surface has become very dry and the effects of wetness are completely eliminated. The rate of albedo decrease with surface roughness is higher for dry soil (-1.62) than for wet soil (-0.73). The difference in slope coefficients and R^2 show that soil moisture also plays a crucial role in bare-soil albedo. This result agrees with Potter et al. (1987), who observed that radiation reflectance decreased with increasing surface roughness on a fine loamy soil. Also, Matthias et al. (2000) obtained a similar result on Gila fine sandy loam and Pima clay loam. The range of tillage-induced roughness here is expected to affect bare-soil evaporation and have implications for the overall conservation of soil water. Reductions in surface albedo caused by surface roughness have been reported to increase available energy on the land surface (Potter et al., 1987). Furthermore, their results showed that soil heat flux was not significantly affected; hence the resulting increase in net radiation on a rougher soil surface would be partitioned between latent heat flux and/or sensible heat flux.

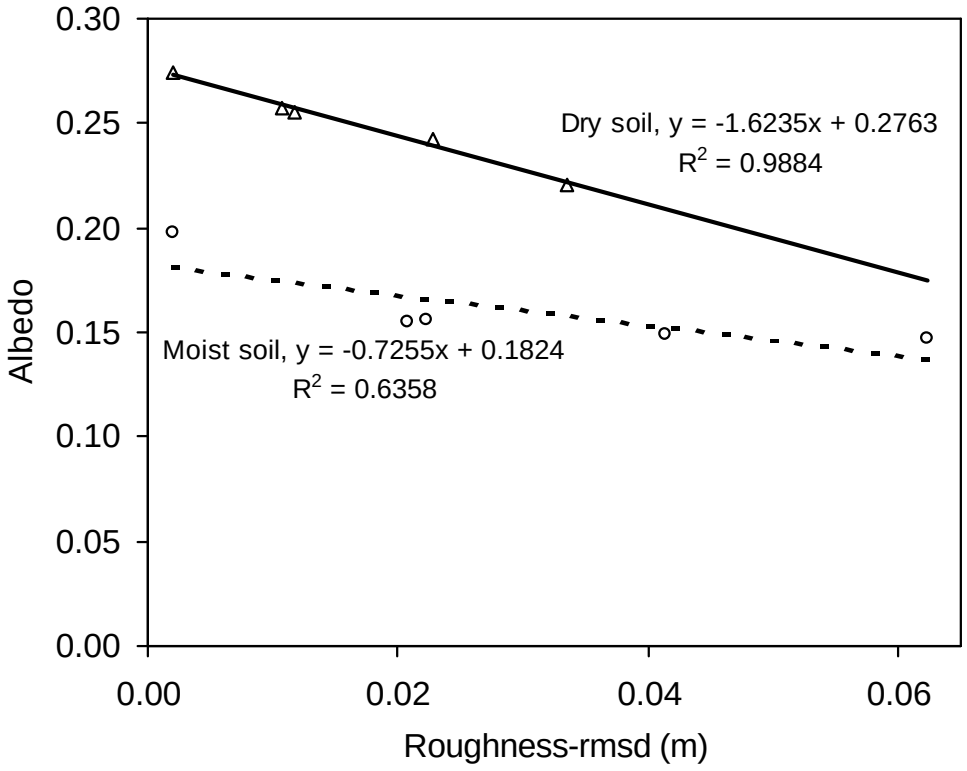

Figure 5.3: Values of albedo regressed against surface roughness for dry and wet soil conditions.

Significant changes in mean albedo with soil wetness were observed ($p<0.01$). The bare-soil surface albedo increased rapidly from wet to dry surface conditions in all the tillage treatments (Figure 5.2 and Table 5.2). About 39% increase in mean shortwave albedo is associated with a decrease in soil water content from 0.155 m^3 m^{-3} to 0.064 m^3 m^{-3}. It should be noted that the moisture content used here was measured from a depth of 0 to 5 cm by the hand held theta probe. Idso et al. (1975) and Cresswell et al. (1993) also observed a decrease in surface albedo with increasing surface moisture. It has been explained that the reduction in wet soil albedo was due to a decrease in the relative refractive index of the medium around the soil particles which further leads to increases in light scattering in the direction of the incident radiation, resulting in absorption of more incident photons and, hence, albedo is decreased (Twomey et al., 1986; Lobell and Asner, 2002).

The combined effect of surface roughness (d) and soil moisture (q_m) on shortwave albedo (a) is fitted in a simple multiple linear regression model. The equation is of the form:

$$a = 0.29 - 1.08d - 0.56q_m \qquad (5.1)$$

The goodness of fit R^2=0.923 and standard error of estimate (SE)= 0.016. The model statistics reveal that the model constant (SE=0.011) and the coefficient of q_m (SE=0.082) are significant at p<0.001, while the coefficient of d (SE=0.302) is significant at p<0.01. Both variables account for about 92% of the variations in surface albedo. From the magnitude of the absolute values of the coefficients, roughness appears to be more important, but the higher value of SE coupled with a relative lower level of significance imply that the relation between d and a is less clear-cut.

The albedometer sensor type produced some degree of bias in the measured values of shortwave albedo as indicated in the results. Figure 5.4 showed the comparison of the measured albedo using the two types of pyranometer models, CM 3 and SP LITE. The slightly higher values measured with SP LITE were consistent with the spectra bandwidth response of silicon type sensors as compared to thermopile type sensors. SP LITE albedometer, relative to CM 3, measured an overall positive bias of about 3.3%. Previous studies have also showed that silicon type sensors always over-estimate solar radiation and albedo (Stroeve et al., 2001; Bugbee et al., 2001). In the present study, it was observed that CM 3 has some practical disadvantages in the field; especially with unstable or transient cloud conditions, because the response time is high and hence the required time for sensor stability before actual reading is high. Furthermore, comparing all the data for CM 3 and SP LITE, significant differences (p<0.001) were found for wet soil albedo values while the data for dry soil were not different for the two pyranometer models. Furthermore, we used the data for only the smooth reference surface in order to eliminate roughness effects from sensor type effects. For the dry soil, the mean comparison between the two sensors was not significantly different, whereas for the wet soil it was only slightly significant (p=0.049).

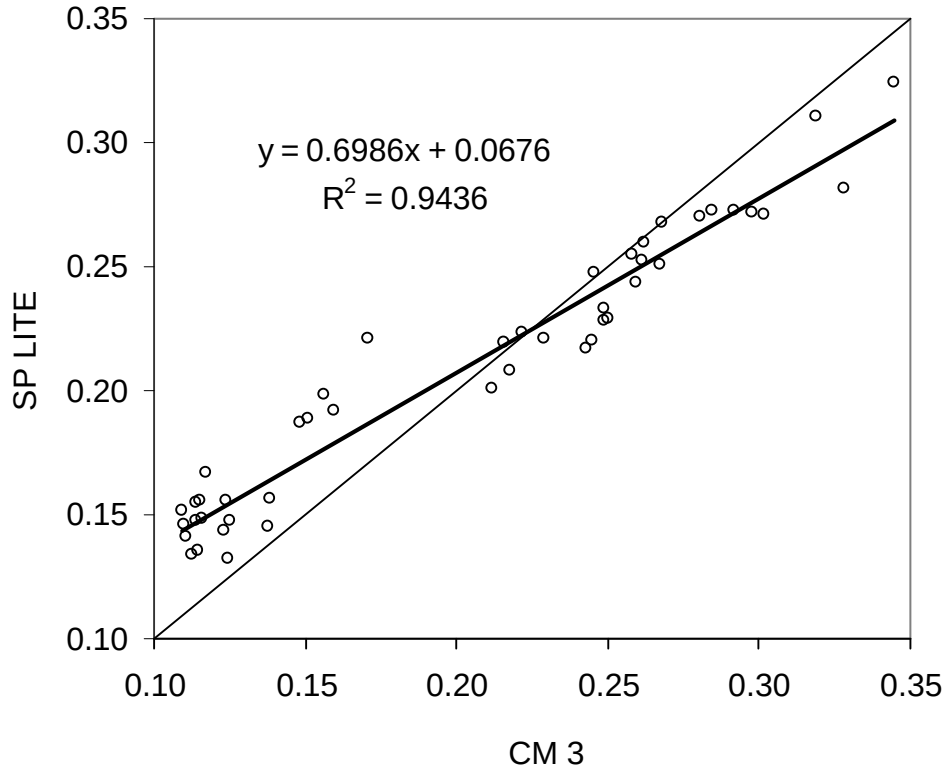

Figure 5.4: Comparison the surface albedo as measured by the two-pyranometer types: CM 3 and SP LITE.

It appears that the two types of sensor compared here are suitable for albedo measurement in this environment. They are still used in many applications because of their very low cost as compared to very expensive but precise ones such as the CM 21 and Eppley pyranometers (Maurer, 2002).

5.2 Crop field albedo

5.2.1 Background

The albedo of vegetated land surfaces is an input parameter in crop growth models, eco-hydrological models such as Soil-Vegetation-Atmosphere-Transfer (SVAT) schemes and in the study of water and energy fluxes of ecosystems. The information on albedo is crucial in accounting for such processes as evapotranspiration, photosynthesis, and surface temperature changes (Giambelluca et al., 1999; Iziomon and Mayer, 2002). Errors in albedo directly lead to uncertainties in computed net radiation, energy fluxes and in simulated global surface temperature (Sellers et al., 1996; Yin, 1998).

A review of the literature revealed that a number of albedo measurements (ground-based, aircraft or satellite) have been undertaken in the recent past (Standhill, 1970; Pinker et al., 1980; McCaughey, 1987; Ben-Gai et al., 1998; Song 1998; 1999; Iziomon and Mayer, 2002). Although the data generated from these measurement procedures are not directly comparable, some general knowledge about surface albedo has emerged. For example, albedo tends to decrease with vegetation height and leaf wetness but increases with leaf area index (Jacobs and van Pul, 1990; Linacre, 1992; Cuf et al., 1995). Furthermore, effects of micrometeorological parameters, such as wind and dew have been reported. Wind speed and direction have been shown to cause canopy re-inclination and hence lead to diurnal asymmetry in surface albedo, while dew can lead to a decrease in early morning albedo values (Minnis et al., 1997, Song, 1998).

The albedo of crop and agricultural fields is not constant, but changes during the growing season (Jacobs and van Pul 1990; Song 1999). After land preparation, the surface albedo is mainly determined by soil surface characteristics including roughness of the soil and moisture content of the topsoil. Close to the end of the cropping season, it is mostly determined by canopy physical conditions, crop height, canopy architecture and leaf area index. The spectral properties of leaves change during the growing season from young to old leaves showing different reflectance responses (Ross 1975). Studies have been carried out on the diurnal and seasonal course of surface albedo especially for grasslands, forestlands, and crop fields (Pinker et al., 1980; McCaughey, 1987; Jacobs and van Pul, 1990; Song, 1999). From these studies, it appears that albedo is closely related to leaf area index and sun angle. A generally increasing trend was observed from crop green up to peak green and slightly decreased towards senescence. In the diurnal variations, albedo decreases with solar elevation under clear sky conditions (Iziomon and Mayer, 2002).

This study was carried out to generate requisite albedo data especially at critical crop phenological or developmental stages during the growing season. Changes in albedo values were examined from *in-situ* field measurements from maize and cowpea fields. The effects of crop development and sun angle on albedo were studied. The aim was to evaluate how much albedo of reference bare soils and short grass changes in response to changing land cover by crop growth and development as represented by four phenological stages: emergence or seedling, vegetative, flowering

and maturity. An additional objective was to compare the simulated and the measured albedo values. These phenological categories are often used in studies related to crop water requirements to isolate the most critical period of water use in crop growth and development (Alatise, 2002, San Jose, 2003). A bare-soil reference surface was used to determine the relative magnitude of differences in albedo of the cropped field over the growing season, while short-grass reference surface was used to quantify the deviation of crop field albedo, from the generally accepted and frequently used grass albedo, which is taken as 0.23 in many eco-hydrological models.

5.2.2 Observed and modeled crop field albedo results

The textural classification analysis carried out on the soil yielded 85% sand fraction, 13% silt and 2% clay contents. Hence, the soil is a loamy sand soil. Average albedo values for five sun angles (on clear days), leaf area index (LAI) and crop heights (CH) are presented in Table 5.3 for different phenological stages of both maize and cowpea fields during the first and second growing season of 2002.

There was an increase in values of albedo from seedling to physiological maturity. Mean LAI and CH increased similarly to albedo. LAI increased from 0.42 to 4.47 in the maize field for both seasons, while it developed from 0.45 to 5.38 in the cowpea field. The values of these three measured parameters were not significantly different ($p>0.05$) for both seasons and for the corresponding phenological status. Maize albedo showed a gradual increase from seedling to maturity, while cowpea albedo increased from emergence to flowering and slightly decreased at maturity stage. Both cropping seasons showed similar trends of the measured parameters. The first and second season data were therefore combined for mean comparison and least significant difference tests. From the ANOVA, albedo values for the maize field showed an overall significance ($p<0.01$) within the phenological groupings and at 5% level of significance for the cowpea field.

Table 5.3: Mean of five albedo values, leaf area index and crop height for maize and cowpea fields during the first (1st) and second (2nd) cropping seasons, 2002.

Crop type	Phenological stage	Mean albedo		Leaf area index		Crop height	
		1st	2nd	1st	2nd	1st	2nd
Maize	Emergence	0.179	0.196	0.48	0.42	0.11	0.09
	Vegetative	0.232	0.242	2.77	2.55	1.00	1.10
	Flowering	0.270	0.254	4.02	3.70	1.81	1.76
	Maturity	0.276	0.256	4.47	4.21	1.82	1.76
Cowpea	Emergence	0.204	0.195	0.57	0.45	0.05	0.05
	Vegetative	0.252	0.242	4.13	3.92	0.51	0.49
	Flowering	0.260	0.261	5.38	5.02	0.63	0.58
	Maturity	0.253	0.245	4.05	4.02	0.71	0.66

This comparison shows a very significant difference especially between seedling and other stages for both crops. Paired comparisons of other groupings were not significant at 5% level (Table 5.4). In the maize field, measured albedo values of vegetative compared with flowering, and vegetative compared with maturity stages were significantly different at 10%, but the difference in albedo values between flowering and maturity was not significant ($p>0.1$). Correlating the albedo values with crop LAI and CH showed the dependence of surface albedo on the crop phenology. The value of the correlation coefficient between a and LAI equals 0.970, between a and CH it equals 0.969 for maize and similarly 0.988 and 0.943, respectively, for cowpea.

Furthermore, in order to study the effect of crop growth and development on the reflection coefficient, two reference surfaces were taken and the observed values were compared with the respective values at different growth stages. Mean values of albedo for the tilled bare-soil reference surface (Table 5.5) were 0.189 and 0.190 for first and second seasons, respectively, while the values were 0.245 and 0.251 correspondingly for the short grass reference surface. The CV ranged between 10% and 13% for the two surfaces.

Table 5.4: Multiple comparisons of mean albedo values at the four phenological stages

Crop	I	J	Md(I-J)	Sig. level	Remark
Maize	1	2	-0.050	0.001	***
	1	3	-0.075	0.000	***
	1	4	-0.078	0.000	***
	2	3	-0.025	0.098	*
	2	4	-0.028	0.058	*
	3	4	-0.004	0.801	ns
Cowpea	1	2	-0.040	0.026	**
	1	3	-0.054	0.004	***
	1	4	-0.048	0.009	***
	2	3	-0.014	0.438	ns
	2	4	-0.007	0.681	ns
	3	4	0.006	0.713	ns

Md(I-J) is mean difference for I and J; I, J are phenological stages (1=seedling, 2=vegetative, 3=flowering, and 4=maturity); * significant at 0.10 level; ** significant at 0.05 level; and *** significant at 0.01 level.

Table 5.5: Albedo values (measured at five sun angles) for the first and second season reference short grass and bare tilled soil

	Solar angle (degree)							
Surface	15°	30°	45°	60°	75°	Mean	SD	CV (%)
Short grass (1^{st})	0.273	0.269	0.246	0.239	0.199	0.2450	0.030	12.11
Short grass (2^{nd})	0.290	0.275	0.243	0.235	0.223	0.2511	0.033	12.92
Bare soil* (1^{st})	0.224	0.188	0.182	0.178	0.177	0.1898	0.020	10.33
Bare soil (2^{nd})	0.230	0.195	0.188	0.174	0.166	0.1904	0.025	12.94

1^{st} is first season; 2^{nd} is second season; * conventionally tilled; SD is standard deviation; and CV is coefficient of variation.

The mean reference albedo values were used to calculate a percentage difference between the crop field mean albedo (a) and the reference surface (a_r) albedo using:

$$\%Difference = \frac{a - a_r}{a_r} x100\% \qquad (5.2)$$

The results of the Equation 5.2 were plotted in Figure 5.5. Positive values indicate an increase in a with growth and development stage, and negative values indicate a reduction in a as compared to the particular reference values of albedo. The percent change in albedo ranged from –6 % to 45 % in the maize field (bare-soil reference) and 2 % to 37 % in the cowpea field. Similarly, for the short-grass reference surface, percent change ranged from about –27 % to 13 % in the maize field and –22 % to 6 % in the cowpea field.

There was an observed increase in percent change of albedo for both crops and seasons with respect to the tilled bare soil reference surface. A more rapid increase took place from the seedling to vegetative stage, followed by a gradual increase from the vegetative to maturity stage especially in maize. There was a slight reduction from flowering to physiological maturity in cowpea. A reduction was observed at the seedling stage of the first season maize (Figure 5.5a); this was probably due to a difference in topsoil wetness of the crop fields and tilled bare soil.

This pattern of change is explained by the LAI and CH (Table 5.3). High correlations ($R>0.94$) indicate association of albedo to LAI and CH. The albedo of the crop fields changed considerably during the growing season. In the emergence stage, it is mainly influenced by soil optical properties and other soil surface conditions. As the season progresses, the effects of the physical condition of leaves and crop structures become more significant. This agrees with the findings of Ross (1975), Jacobs and van Pul (1990) and Song (1998). In Figure 5.5b, percent change with respect to the short-grass reference surface is presented. The results show a mixed picture of reduction during seedling and vegetative stages, while a slight increase occurred from flowering to maturity.

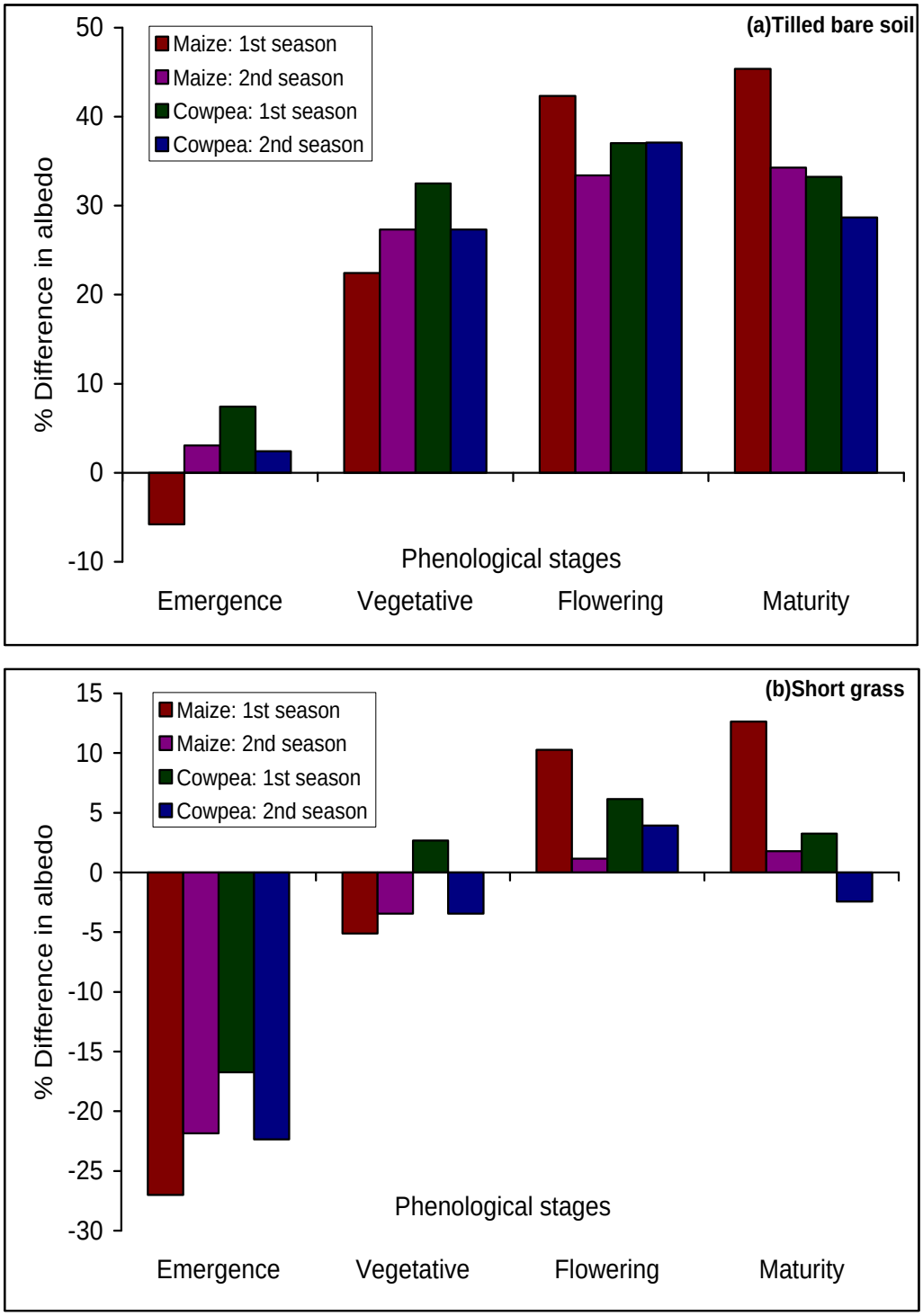

Figure.5.5: Mean percentage change in albedo relative to the corresponding reference albedo at different phenological stages (a) bare tilled soil as reference surface and (b) short grass as reference surface.

The observed difference ranged from about –27 % to 13 % in the maize field and –22 % to 6 % in the cowpea field. This indicates that during the growing seasons, a crop field could probably show the same reflection behavior as a short grass field. It would be very interesting to know if there is a certain period during the growing season, and in plant communities, when some or all the vegetation responds or reflects radiation almost equally. From the present results, there appears to be an equality of average albedo somewhere between the vegetative and flowering stages (Figure 5.5b).

Figure 5.6 shows values of albedo measured and simulated for both maize and cowpea fields. Albedo was measured at five different sun positions during the morning hours of generally clear sky days. The albedo values were generally highest at the 15° sun angle and decreased with increasing solar elevation. The pattern of modeled and measured albedos is similar (Figure 5.6). The optimized model parameter (*k*) was 0.77 and 1.13 for maize and cowpea, respectively. However, the model underpredicts the actual values especially at lower sun angles. The rate of change of albedo with respect to sun angle is similar for both crops and seasons. For the maize field, the albedo values increased from emergence (LAI<1.0) to maturity (LAI>4.2), but a slight difference in simulated values of albedo during flowering and maturity is apparent. This is similarly true for the cowpea, except that the difference between the vegetative and maturity is not apparent at all (Figure 5.6).

Two goodness of fit statistics, correlation coefficient (R) and mean bias error (MBE), are presented in Table 5.6, where of model estimates and observed albedo values (first season data only) are compared. R varies between 0.977 for flowering to 0.996 at maturity for maize and MBE ranges from –0.0153 to 0.0042. The model seems to be more accurate for cowpea, with R ranging from 0.910 at seedling to 0.999 in the vegetative period. The MBE also varies between –0.0084 and 0.0027. The negative sign indicates underprediction and the positive shows overprediction. When the data are combined (maize and cowpea), the model shows a generally good agreement with measured data (Table 5.6). The independent data set used to plot a 1:1 line between the predicted and observed albedo values for both crops is shown in Figure 5.7. The solid 1:1 line represents a situation of perfect prediction. Data points falling below the 1:1 line are the underestimated values while those above the line are overestimated.

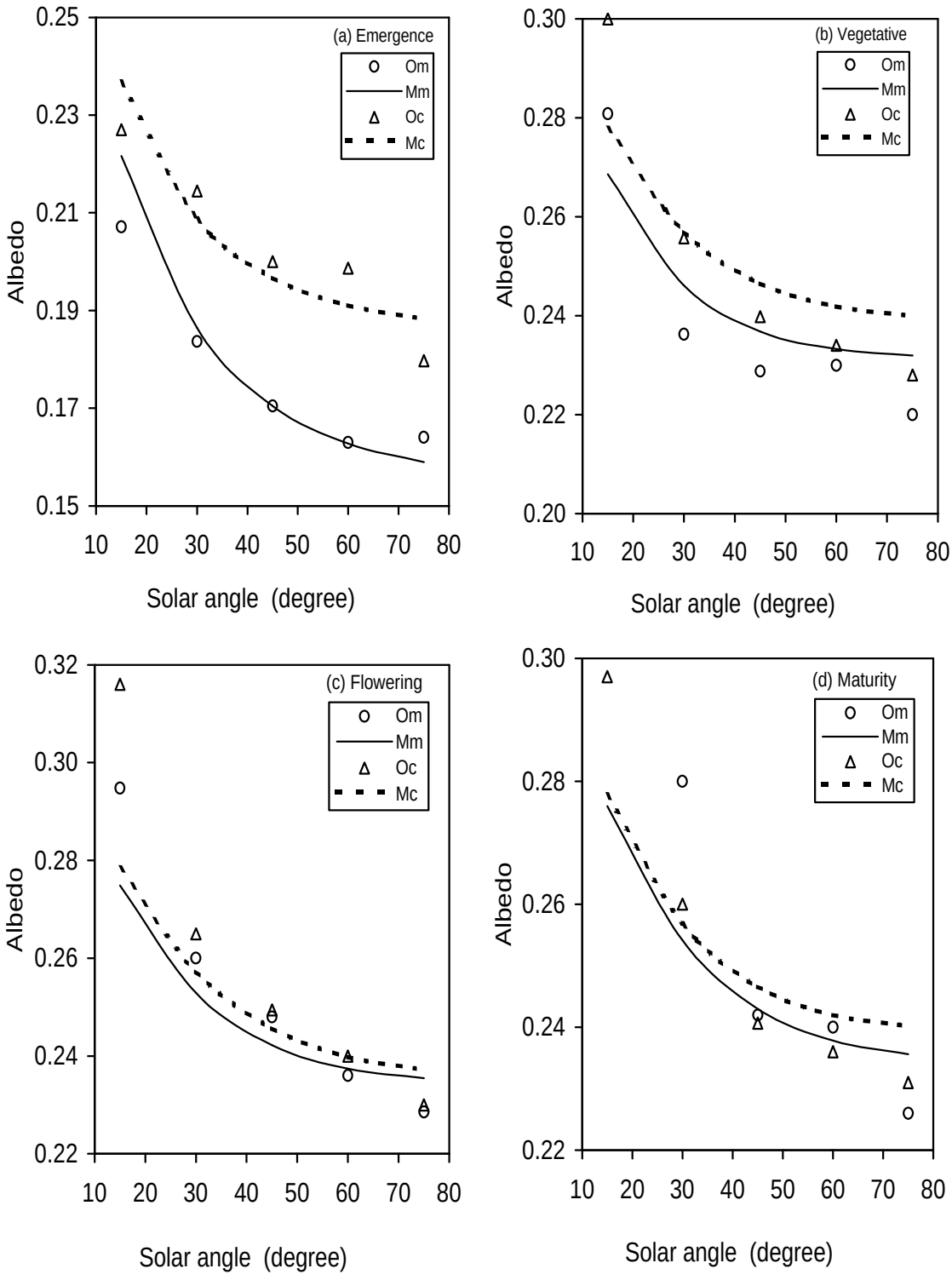

Figure 5.6: Variations in observed and simulated albedo with sun angle in the stages (a) emergence (b) vegetative, (c) flowering, and (d) maturity. O=observed, M=modeled, m=maize, c=cowpea.

Table 5.6: Correlation coefficients (R) and the mean bias error (MBE) to compare the simulated and the measured albedo values (first season data)

Phenological	Maize		Cowpea		Combined	
stage	R	MBE	R	MBE	R	MBE
Emergence	0.996	0.0024	0.910	0.0003	0.958	0.0014
Vegetative	0.977	0.0042	0.997	0.0011	0.983	0.0027
Flowering	0.993	-0.0049	0.994	-0.0084	0.987	-0.0067
Maturity	0.995	-0.0153	0.999	-0.0002	0.933	-0.0078
Overall mean	0.990	-0.0034	0.975	-0.0018	0.965	-0.0026

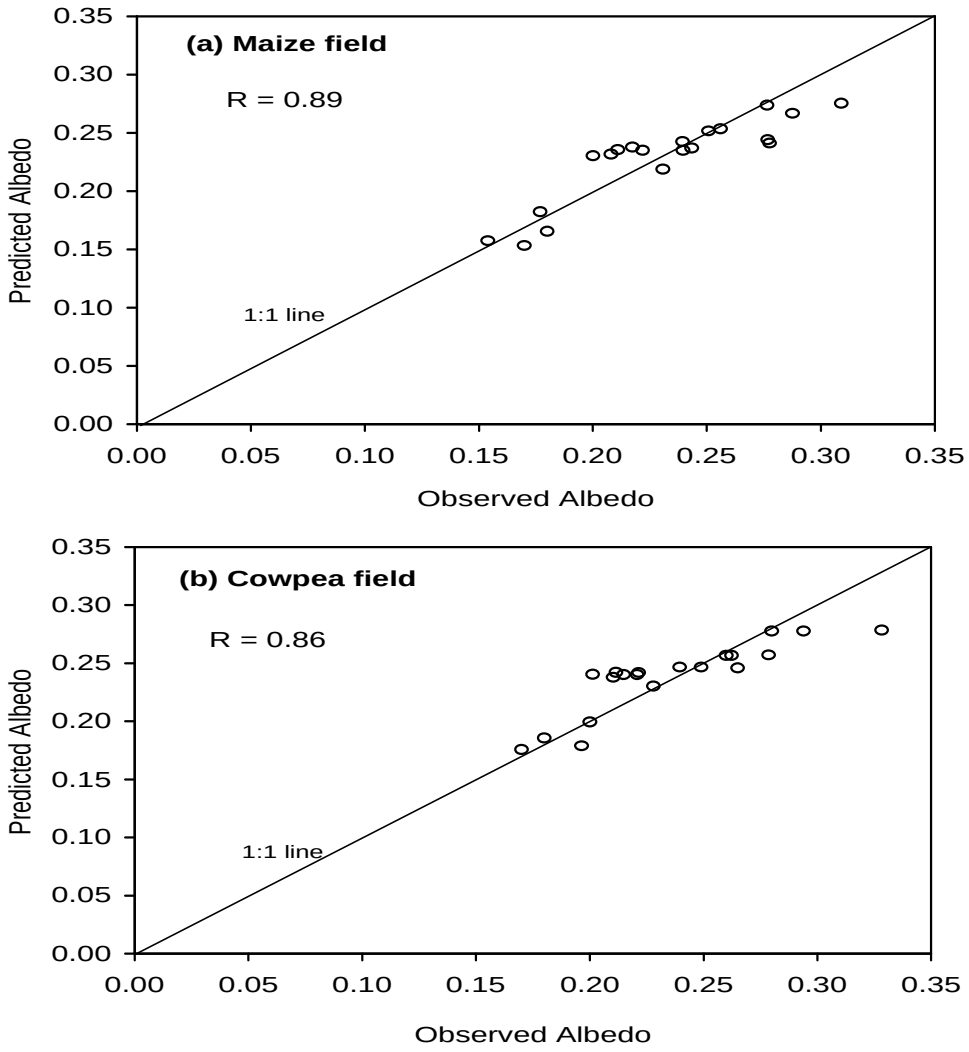

Figure 5.7: Graph of 1:1 line comparing predicted and observed albedo values (second season data only) in (a) maize field and (b) cowpea field. The line represents perfect prediction.

5.3 Seasonal variation in albedo from different watershed elements

5.3.1 Background

Surface albedo is a fundamental parameter, to set up a surface energy balance, as it describes the ratio of the light reflected to the light received by a body. Values for albedo range from 0 (pitch black) to 1 (perfect reflector). Surface albedo is often calculated for clear-sky conditions. It is one of the most important parameters influencing the earth's climate and radiation budget. Surface albedo is prone to seasonal changes and inter-annual variability (Jacobs and van Pul, 1990, Grant et al., 2000). Site-specific surface albedo data have been obtained from in situ observations and often have a high temporal resolution. In recent time, space-borne measurements by means of remote-sensing techniques are becoming more and more important (Li and Garand, 1994). Nevertheless, these measurements should be calibrated by in situ observations. The main aim of this measurement was to study the trend in surface albedo from different surfaces during a typical year. The albedo data so generated are expected to be used to correct the remote sensing algorithms used in extracting surface albedo.

Observed seasonal variations

The ranges of observed albedo values, mean and standard deviations, for January, April, July and October 2002 are presented in Table 5.7. The mean is shown for January to October in a line graph in Figure 5.8. Expectedly, the lowest albedo values (0.046-0.069) were recorded on the 'burnt field' in January with a gradual increase as the charred matter is replaced (Figure 5.8). There is an observed decline on 'pond water' albedo during February and March, probably because charred particulate matter from bush fires settled in the pond and darkened the water, thereby reducing the surface reflectance. However, immediately after the onset of rain, the pond water increased in volume and became clearer, and coupled with growth of vegetation in the pond, the measured albedo increased. The tree albedo was relatively stable throughout the year. The relative lower values during the months of January to April are likely the result of plant stress as shown by yellowing of the leaves during this dry period. Generally, higher albedo values, for most of the surfaces, were recorded between June and September (the peak of green-up during the rainy season). 'Farm road' showed a slight decrease over the season apparently due to changing surface moisture. Changes in

vegetal characteristics during the season have distinct effects on the variations observed in these watershed elements reflectance responses. It should be noted that the names given for each surface at the beginning of the experiment were retained throughout the season for simplicity. For example, 'burnt field' will only be applicable between January and March when there were profuse bush fires within and around the catchment. Similarly, 'rice stubble' was used for an old rice field, which changed from the onset of rain with grasses and eventually became water-logged towards the end of the rainy season. The noticeable changes, which actually affected all the surfaces to different degrees, may be responsible for the observed seasonal variation in surface albedo.

Table 5.7: Range, mean and standard deviation (in parenthesis) of albedo during the year 2002

Nature of	January		April	
surface	Range	Mean	Range	Mean
Pond water	0.179-0.259	0.211(0.033)	0.144-0.172	0.161(0.009)
Green grass	0.179-0.329	0.251(0.051)	0.191-0.236	0.215(0.016)
Rock	0.289-0.338	0.313(0.018)	0.146-0.170	0.155(0.009)
Burnt field	0.046-0.069	0.052(0.007)	0.186-0.219	0.205(0.010)
Trees	0.206-0.310	0.253(0.037)	0.194-0.271	0.235(0.025)
Farm road	0.187-0.218	0.206(0.013)	0.180-0.201	0.189(0.007)
Rice stubble	0.190-0.226	0.209(0.016)	0.189-0.201	0.196(0.004)
	July		October	
	Range	Mean	Range	Mean
Pond Water	0.221-0.234	0.225(0.004)	0.116-0.224	0.170(0.034)
Green grass	0.207-0.299	0.253(0.033)	0.105-0.296	0.163(0.024)
Rock	0.165-0.192	0.179(0.011)	0.143-0.190	0.180(0.008)
Burnt Field	0.218-0.279	0.251(0.023)	0.168-0.241	0.171(0.018)
Trees	0.227-0.281	0.261(0.018)	0.257-0.302	0.196(0.023)
Farm road	0.186-0.205	0.198(0.007)	0.134-0.212	0.277(0.014)
Rice stubble	0.213-0.255	0.232(0.018)	0.220-0.293	0.260(0.024)

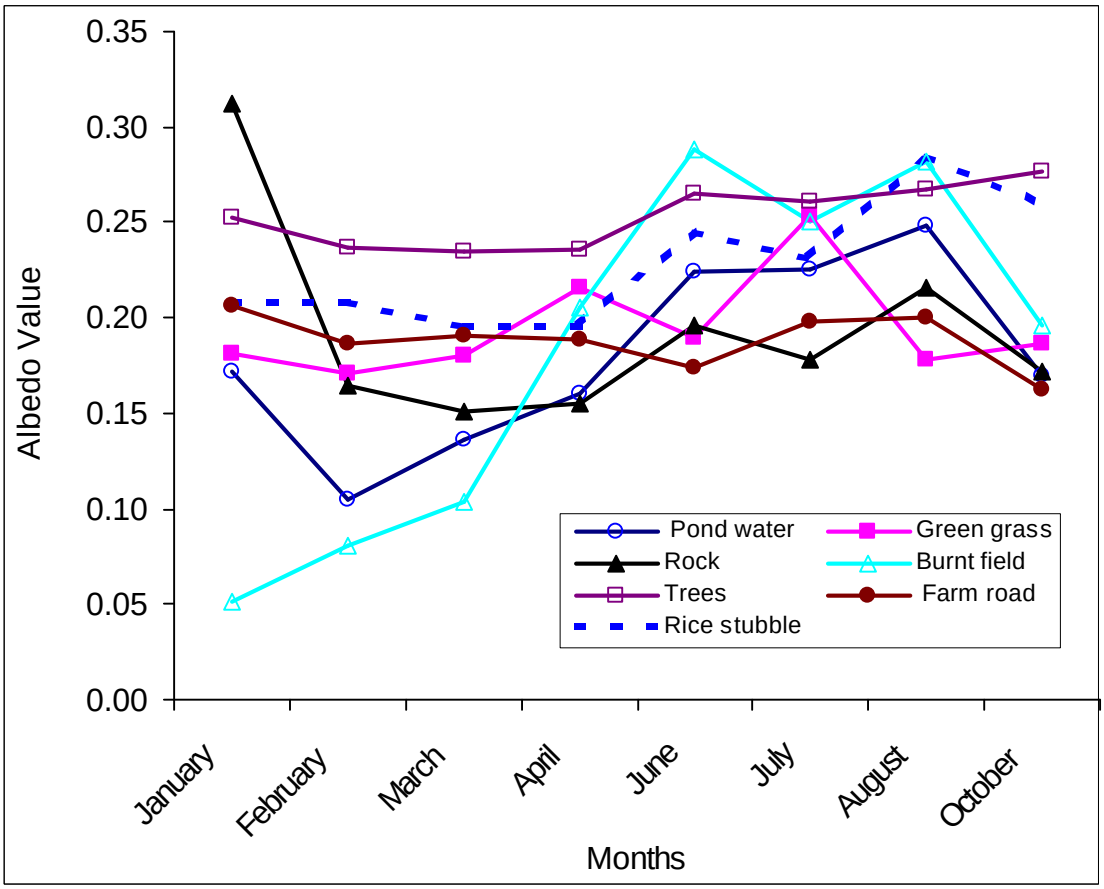

Figure 5.8: Mean seasonal variation in albedo from different watershed elements

5.4 Tree water-use and canopy processes during the dry season

5.4.1 Background

In semi-arid regions characterized by water scarcity and unreliable rainfall, proper water management strategies for optimum production for agriculture and other water needs are important. The Volta Basin in West Africa is such a region, characterized by rural poverty and increased population pressure (Andreini et al., 2000). Studies related to sustainable water use in general, and agricultural water management in particular, are of priority importance in order to increase production without degrading the basin's resources. Change in land use leads to changes in water use, as evaporation from each component of the land surface is controlled by different factors. These different factors influence both evaporation from the soil and plant transpiration, whereby the former is a purely physical process, the latter is also affected by physiological responses (Allen and Grime, 1995). Available models, well validated with measured independent data, are needed for efficient management of land and water resources and as sub-models for general or regional circulation models (Stannard, 1993; Dolman et al., 1993). Part of the data needed is whole-tree water use, which will help hydrologists to resolve issues of water resource management, to evaluate the role of transpiration in forest and woodland hydrology and to quantify the water requirements of short-rotation forests (Cienciala and Lindroth, 1995; Loustau et al., 1996; Barrett et al., 1996; Wullschleger et al., 1998).

Measured sap flows have successfully been used to derive canopy conductance by inversion of the Penman-Monteith equation (Phillips et al., 1997; Cienciala et al., 2000; Wullschleger et al., 2000; Lagergren and Lindroth 2002). Equations to compute the decoupling factor (Ω), using canopy conductance (g_c), aerodynamic conductance (g_a) and other thermodynamic factors have been formulated (Javis and McNaughton, 1986; Monteith and Unsworth, 1990). The closer the value of Ω to unity, the lower the influence of stomata control and the more the transpiration will depend on radiation whereas, as Ω gets closer to zero, the humidity deficit of the air plays a crucial role and the canopy is said to be aerodynamically well-coupled to the atmosphere (Javis and McNaughton, 1986). Studies have generally shown that the smoother and denser the canopy is, the more poorly it is coupled to the atmosphere. Also, needle-leaved canopies are generally better coupled than broad-leaved species.

In the 2001/2002 dry season, sap flow measurements were taken in Ejura, Ghana (West Africa), in the southern part of the Volta Basin, with the objective of obtaining direct and independent estimates of transpiration from the woody component of the vegetation on the pilot site. The specific objectives of this study include: examination of the day-to-day and diurnal patterns of whole-tree water use, canopy transpiration, canopy conductance, and the level of coupling of the cashew tree canopies to the atmosphere, thereby allowing better understanding of these canopy processes in relation to the climatic variables.

Observed patterns and Climatic dependence

Climatic variables

Daily mean meteorological parameters for the period between mid December and end of March are shown in Figure 5.9. Average air temperature was fairly constant throughout the period, and the precipitation quite scanty, which is typical of a dry season in West Africa. Temperatures ranged from 20-27 °C, with the lowest value during the harmattan[2] period in January 2002. Total rainfall recorded at the weather station was 19.5 mm. The highest mean daytime solar radiation was observed in March (505 Wm^{-2}) and the lowest in January (170 W m^{-2}), when the atmosphere is dry and dusty as a result of harmattan. Low humidity values were observed during the months of January and February, while the highest daily value of vapor pressure deficit (VPD = 2.95 kPa) was recorded on Julian day 40. Wind speed showed a generally progressive slight increase (Figure 5.9d), with the highest value (2.37 m s^{-1}) recorded in March. Mean diurnal patterns for these variables are presented in Figure 5.10. Solar radiation peaked around mid day (12:30 h) while the maximum diurnal VPD was observed about 2 hours later (14:30 h). Air temperature (Figure 5.10) showed a similar trend to VPD, while humidity showed an inverse pattern to temperature. On a typical day, the maximum wind speed is recorded two to three hours before midday.

[2] Harmattan refers to dry, dust laden north easterly wind occurring around November to January in the study area (West Africa)

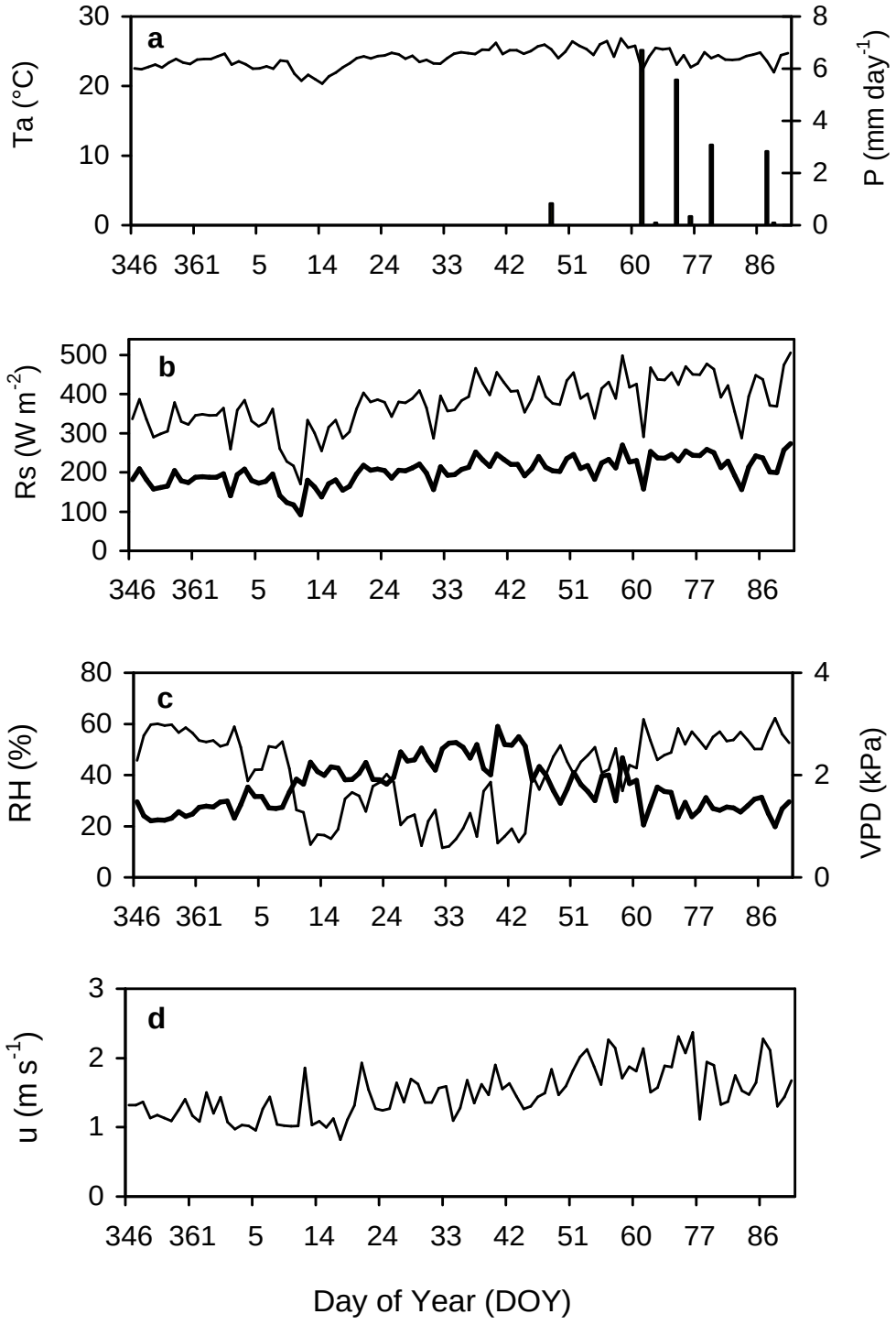

Figure 5.9: Average daily measured (a) air temperature and precipitation, (b) solar radiation (thick line for daytime average), (c) vapor pressure deficit (thick line) and humidity (normal line), and wind speed from December 2001 to March 2002.

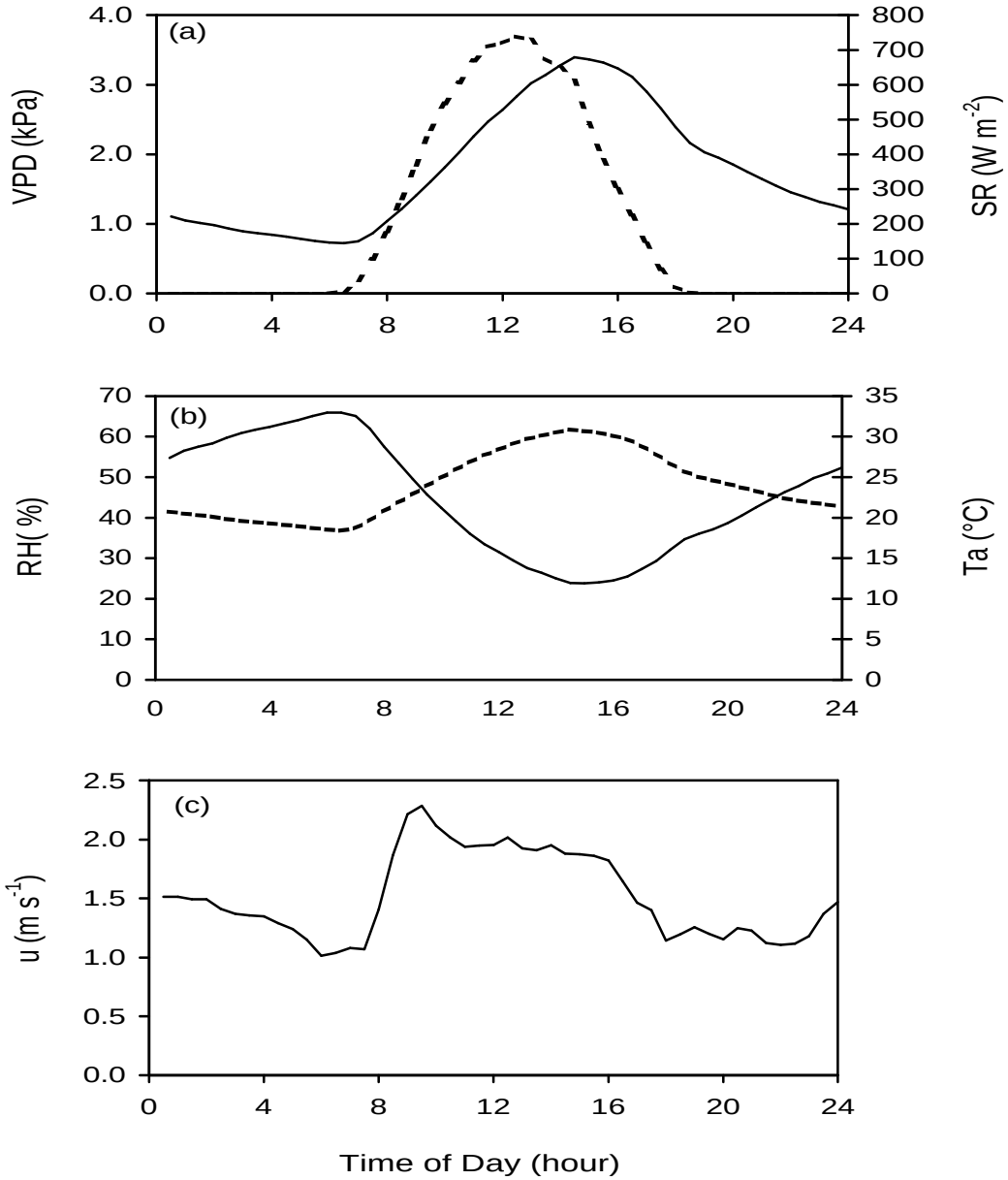

Figure 5.10: Average diurnal pattern of (a) vapour pressure deficit (solid line) and solar radiation (dashed line), (b) humidity (solid line) and temperature (dashed line), and wind speed.

Tree characteristics and biometric relations

Stem diameter at breast height for the 15 sampled trees ranged from 10.8 to 20.0 cm, with an average of 14.55 cm. Trees no. 3, 7 and 11 (Table 5.8) were selected for sap flow measurement as they represent the average diameters of the sampled trees. Tree height varied between 5.9 and 8.3 m, basal area between 91.6 and 314.2 cm^2, and sapwood area between 71.9 and 225.2 cm^2.

Table 5.8: Allometric characteristics of the 15 selected cashew trees (sap flow gauges were implanted on trees no. 3, 7, and 11)

Tree no.	DBH (cm)	Height (m)	Sapwood thickness (cm)	Bark thickness (cm)	Basal area (cm^2)	Sapwood area (cm^2)
1	16.8	7.4	5.1	0.9	221.7	158.6
2	17.0	7.3	5.1	1.0	227.0	160.2
3	**14.6**	**7.2**	**4.1**	**0.8**	**168.4**	**116.5**
4	16.8	7.8	4.5	1.1	221.7	141.9
5	13.9	6.3	4.6	0.8	151.7	111.3
6	14.8	6.6	3.9	0.7	172.0	116.4
7	15.3	6.8	4.6	1.0	183.3	125.4
8	13.5	6.9	5.4	0.9	143.1	106.9
9	12.5	5.7	4.4	0.8	122.7	89.8
10	14.5	6.5	4.9	1.1	165.1	113.9
11	**14.2**	**6.9**	**4.0**	**0.7**	**158.3**	**110.5**
12	11.9	6.8	4.7	1.0	111.2	76.8
13	11.6	6.7	4.3	0.6	105.7	79.7
14	20.0	8.3	5.6	1.2	314.2	225.2
15	10.8	5.9	4.4	0.5	91.6	71.9
Mean	14.55	6.87	4.64	0.87	170.52	120.34

A power relationship was fitted for the 15 trees and a relationship between sapwood area (SA) and stem diameter at breast height (DBH) is presented in Figure 5.11a. The coefficient of determination, R^2=0.981, for the relationship was highly significant. Similarly, a linear relationship was observed between sapwood area and basal area (BA). The regression line (Figure 5.11b) has a slope of 0.68, intercept of 4.92 and R^2 of 0.982. The clear trend between SA and BA does not cross zero, possibly because the relationship keeps changing as the tree develops heartwood. Teskey and Sheriff (1996) observed a similar relation between SA and BA in *Pinus radiata* trees.

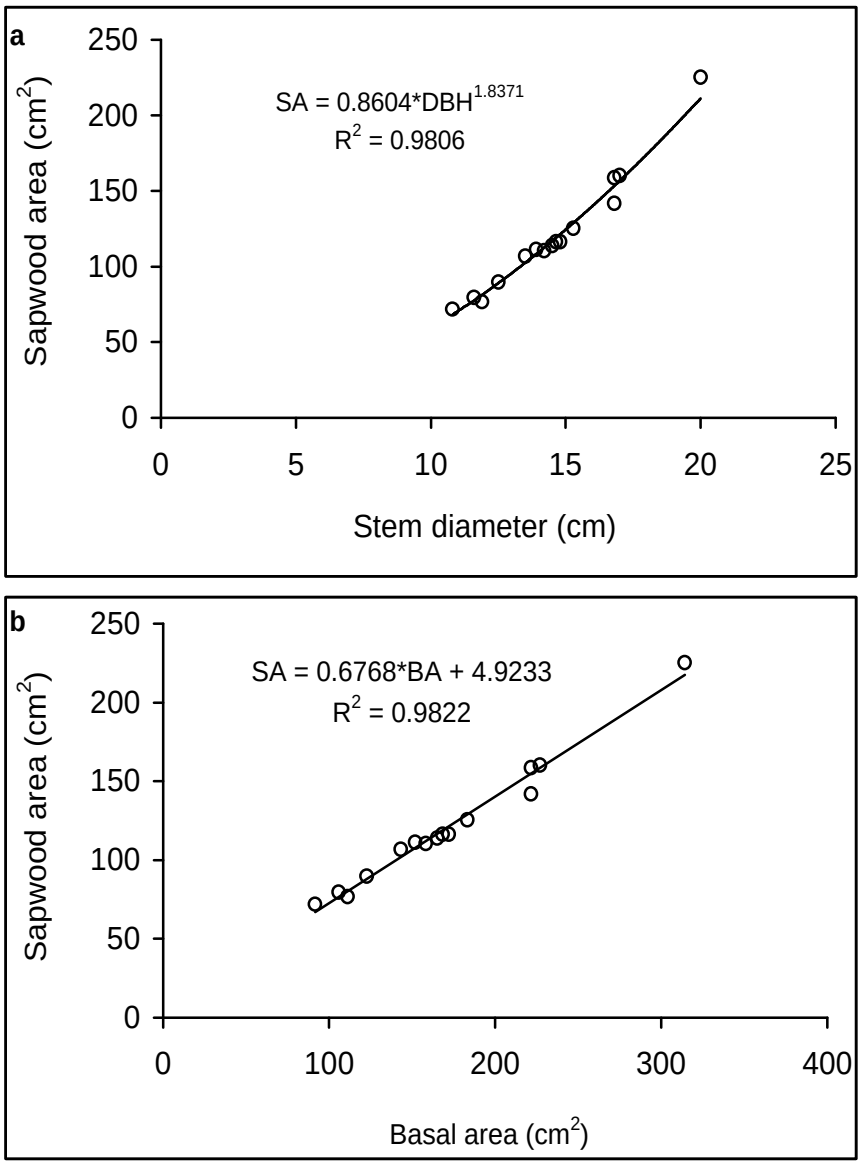

Figure 5.11: Relationship between sapwood area (SA) and (a) stem diameter (DBH), and (b) basal area (BA) of the fifteen trees sampled.

Whole-tree sap flux and canopy transpiration

Average sap flow density on sapwood area basis for the gauged trees is illustrated in Figure 5.12.

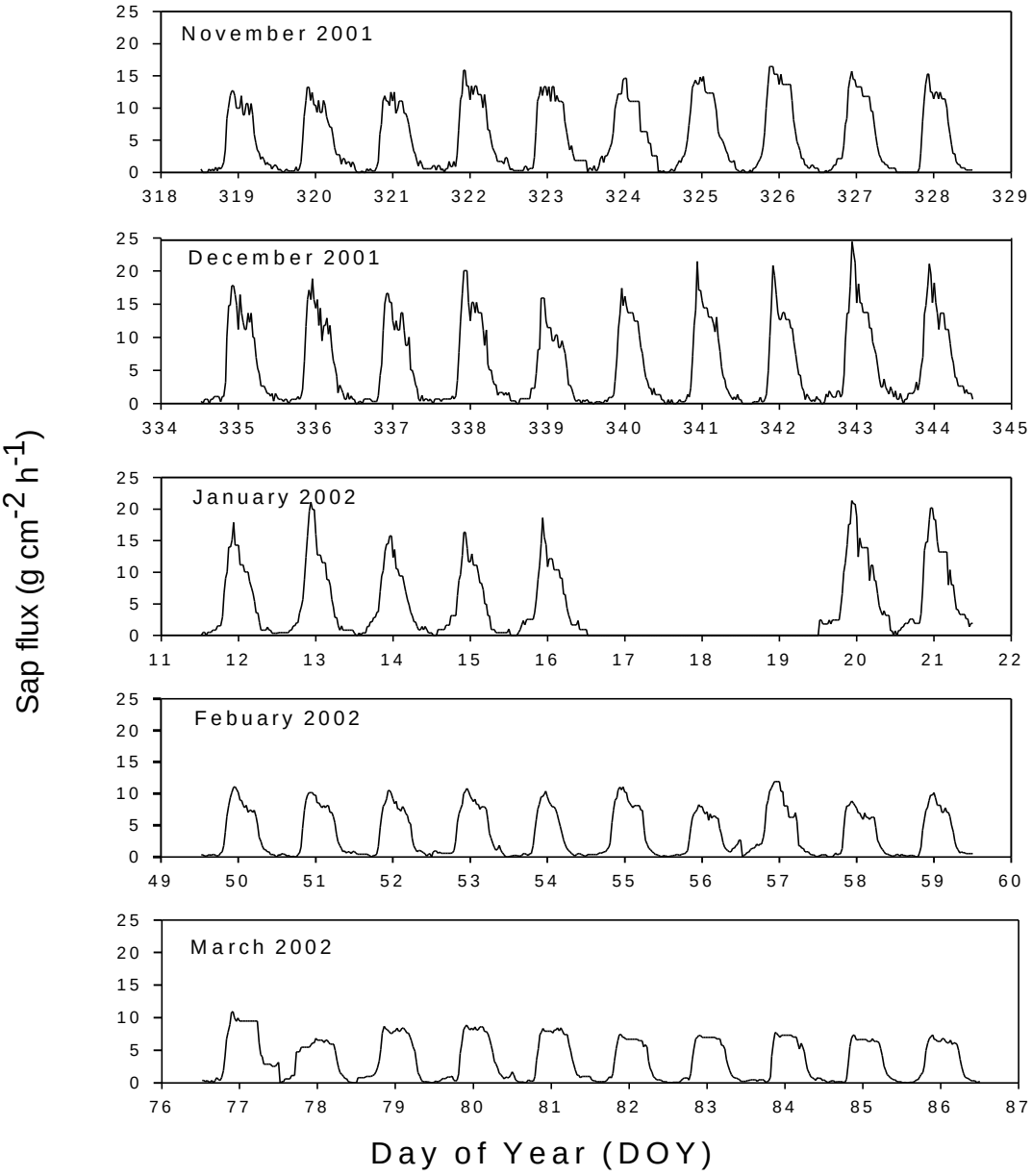

Figure 5.12: Mean sap flow density on sapwood area basis from November 2001 to March 2002 showing a total of 47-day measurements during the dry season.

At the onset of the dry season in November 2001 (DOY 319-328), the maximum half-hourly sap flux ranged from 12.4 to 16.4 g cm^{-2} h^{-1}. In December (DOY 335-344), the observed maximum sap flux increased and varied between 15.9 and 24.4 g cm^{-2} h^{-1}. This range slightly decreased (15.7-21.4 g cm^{-2} h^{-1}) in January 2002 (DOY 12-21),

partly because of changing environmental variables due to harmattan conditions prevailing during this period. Consistently low values were observed during the peak of the dry season in February (DOY 50-59) and March (DOY 77-86). The values ranged from 8.3 to 11.9 g cm^{-2} h^{-1}, and 6.9 to 10.9 g cm^{-2} h^{-1} for the two months, respectively. Mean diurnal data for the 47-day measurement period and standard deviation are shown in Figure 5.13.

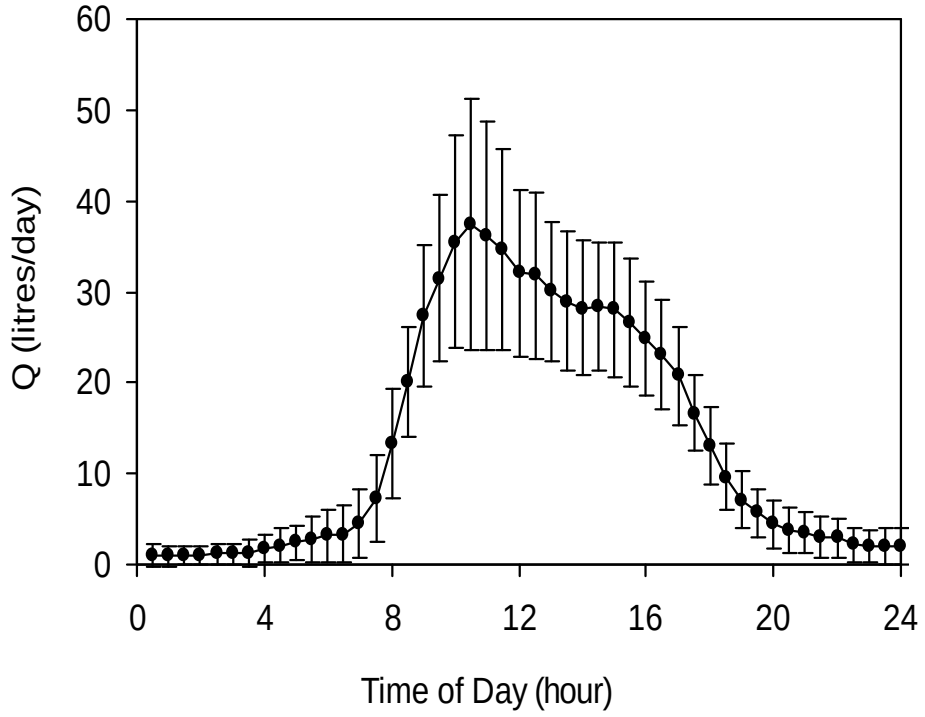

Figure 5.13: Overall mean diurnal water use (litres day^{-1}) pattern of *Anacardium occidentale L* over a typical dry season (vertical bars represent ± standard deviation).

The overall mean diurnal water use varied between 0.94 liter day^{-1}, at mid-night, and 37.3 liters day^{-1}, shortly before the mid-day (between 10-11:00). The water-use pattern shows a rapid rise in sap flow from sunrise to the peak and thereafter steeps out to near zero flow after sunset. The vertical bar showing the standard deviation indicates that sap flow varied more during the daytime and especially during peak water use periods. Tree transpiration was estimated from sap flow using sapwood area and tree density. Daily average canopy transpiration (mm/day) for the entire study period is

presented in Figure 5.14. Observed daily transpiration ranged from 0.37 to 0.93 mm day^{-1} with an overall mean of 0.58 ± 0.15 mm day^{-1}.

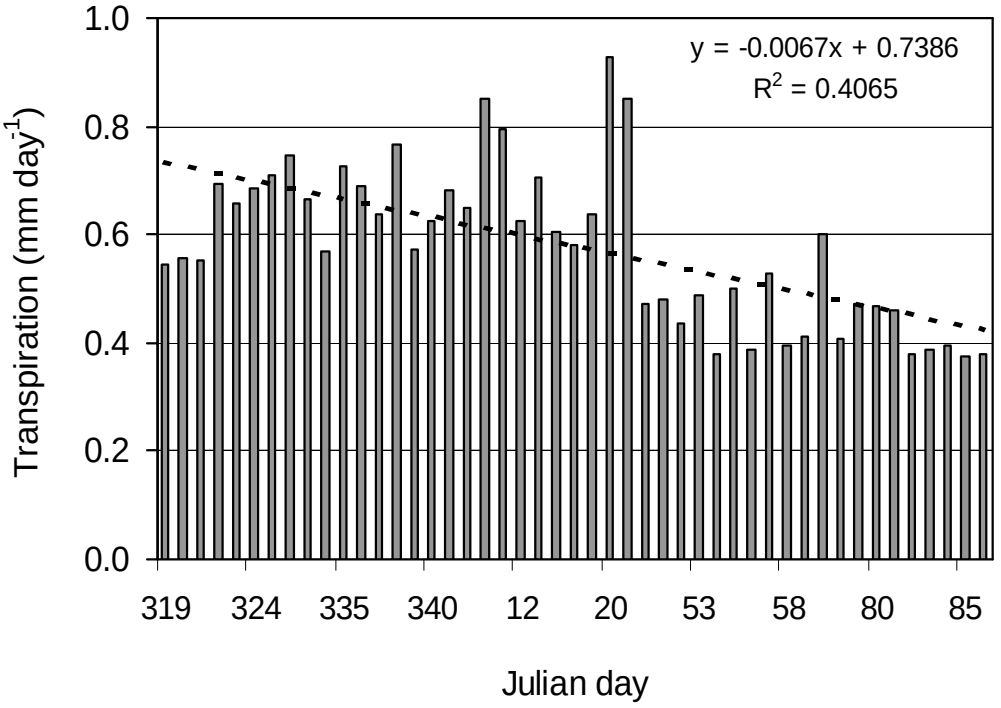

Figure 5.14: Daily average canopy transpiration. The trend line shows the declining nature of the transpiration during the dry season.

Two levels of water use are observed. Higher values were observed in December and January and lower values in February/March. Averages in January and December show that more water was transpired than in November, February and March. To ascertain whether there were significant differences within the periods studied, mean differences of the periodic transpiration were compared using the student t test and the LSD post-hoc test. The results of the test are shown in Table 5.9. All the values for November, December and January were significantly different ($p<0.0001$) when paired against February and March. All other pairs were not significantly different ($p>0.05$).

Table 5.9: Mean comparison of canopy transpiration during the measurement period

#Month (I)	Month (J)	md (I-J)	Sig. level	Remark
1	2	-0.061	0.10759	ns
1	3	-0.067	0.11189	ns
1	4	0.191	0.00001	*
1	5	0.205	0.00000	*
2	3	-0.005	0.89586	ns
2	4	0.252	0.00000	*
2	5	0.267	0.00000	*
3	4	0.257	0.00000	*
3	5	0.272	0.00000	*
4	5	0.015	0.69164	ns

#I and J are compared months (1=November, 2=December, 3=January, 4=February, and 5=March)

Generally, transpiration is expected to decline as the soil column becomes drier following the pattern of the trend line shown on Figure 5.14. A slight increase to the third month (January) and thereafter a sharp decrease was observed. This may be the result of the physiological requirements of the crop during flowering and fruit development, which commenced in December and peaked in January. In February and March the soil was very dry, tree water use was restricted, and observed transpiration showed an expected response to water deficit, in spite of high atmospheric demand. Lagergren and Lindroth (2002) also observed a similar response of transpiration to decreasing soil water in pine and spruce in central Sweden.

Sap flow showed a closer relationship with the *Rs* and very little concordance with the vapor pressure deficit of the ambient air. The diurnal averages transpiration, *Rs* and *VPD* were used to show these relationships (Figure 5.15). The time lag between the observed sap flow peak and SR is approximately 2 hours while it was 4 hours (doubled) in the case of *VPD*. In fact, even the pattern is more similar to *Rs* than to *VPD*. Following this observation, a simple equation that relates a parabolic response of tree water use to incoming *Rs* without any time lag considerations was fitted. The equation is of the form:

$$Q_t = \frac{aRs}{b + Rs} \qquad (5.3)$$

where Q_t is sap flow rate (kg h^{-1}), *Rs* is solar radiation (W m^{-2}), *a* and *b* are fitted parameters specific to the tree.

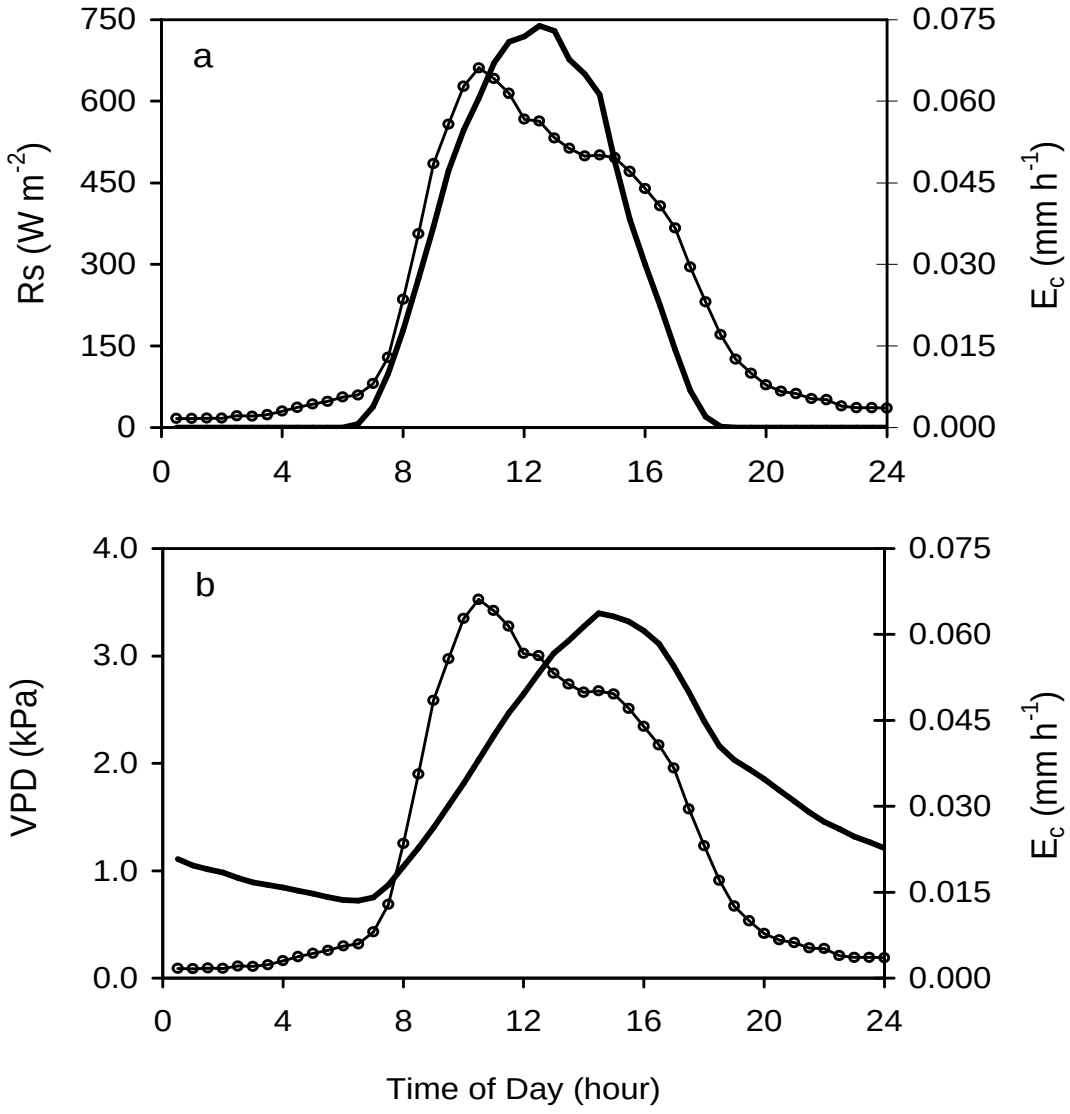

Figure 5.15: Mean diurnal pattern of tree water use (line with circles), solar radiation (*Rs*), and (b) vapor pressure deficit (*VPD*).

Data sets from DOY 50-55 and DOY 77-80 were used to calibrate the non-linear regression model (Equation 5.3), and validation was done with DOY 56-59 and DOY 81-86, respectively. Both the results of the curve fitting and the validation are shown in Figure 5.16. It was observed that changes in sap flow were dependent on changes in solar radiation. The coefficient of determination of the fitted equation was

0.87 and 0.91 when tested with independent data sets. *Rs* were responsible for about 90% of the variations in Q_t.

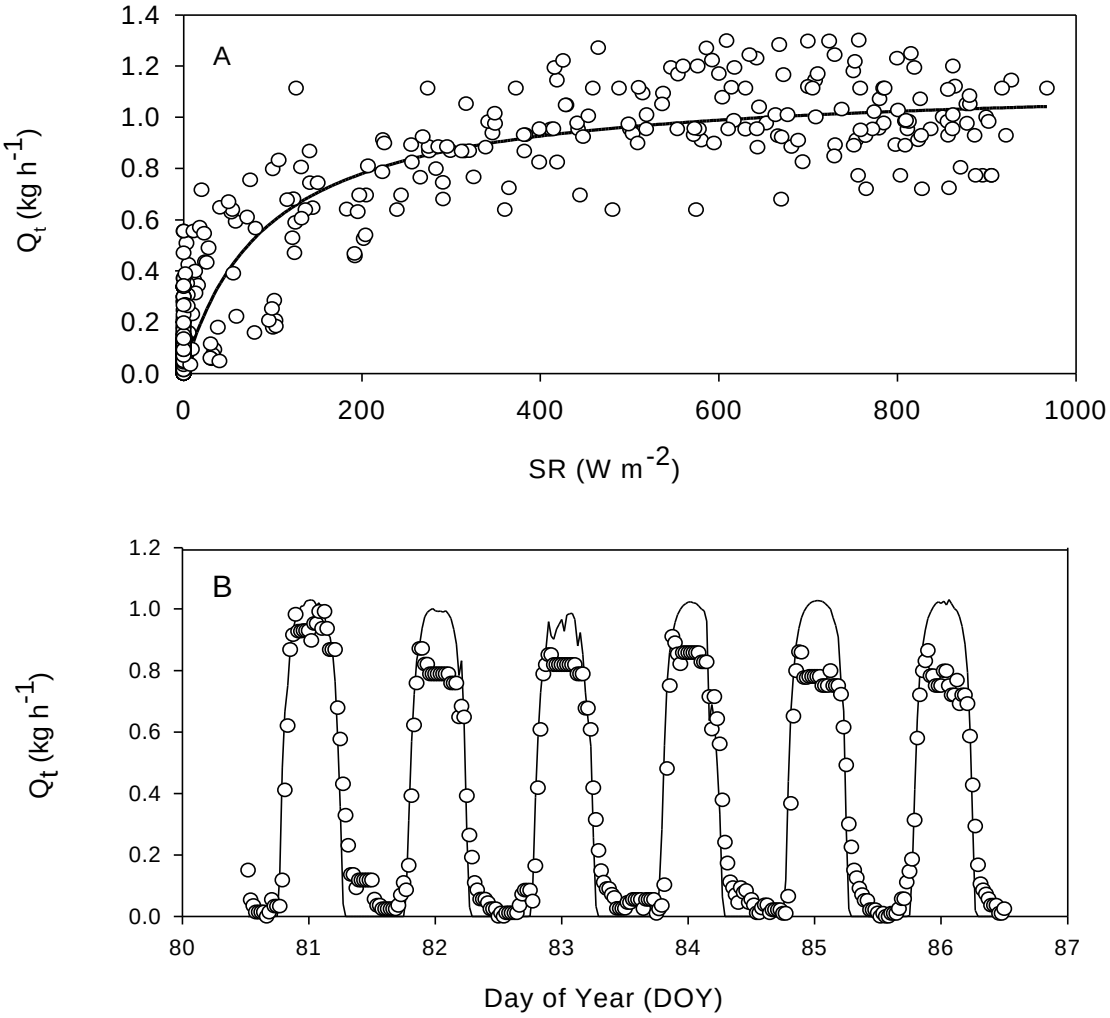

Figure 5.16: Dependence of sap flow on solar radiation: (A) curve fitting results from Equation 5.3, and (B) Example of the measured (circle) and fitted (line) sap flow in half-hourly resolution.

Inclusion of a function of vapor pressure deficit or humidity contributed very insignificantly to the R^2. Parameters "*a*" and "*b*" were found to be 1.14 kg h^{-1} and 92.76 W m^{-2}, respectively. Their units were derived dimensionally. Figure 5.16A also indicates that sap flow responded to radiation almost linearly from sunrise and reached a threshold value at which the rate of change starts to reduce until finally the response to any further changes in radiation becomes insignificant. Others have also found a

significant relationship between Q_t and *Rs*, either with time lag (Hinckley et al., 1994), or without (Köstner et al., 1992; Cienciala et al., 2000).

Tree conductance and decoupling coefficient

Canopy conductance, derived from the Penman-Monteith equation, aerodynamic conductance, and decoupling coefficient showed considerable day-to-day and diurnal variations. The daily course of the computed g_c averaged over the measurement period is shown in Figure 5.17. It increased rapidly between 7:00 and 8:30, at which time maximum g_c occurred, and decreased to the lowest value between 12:00 and 14:00; after that an increase was observed. Computed daily averages of g_c varied from 2.2 to 14.1 mm s^{-1}, while the estimated daytime course of g_c, excluding the wet canopy hours in the morning and evening period, ranged from 4 to 21.6 mm s^{-1} with a diurnal mean of 7.8 ± 5 mm s^{-1}. Variation in g_a is somewhat different as it rises to its peak between 9:00 and 10:00 and was always of higher magnitude as compared to g_c (Figure 5.17b). The order of magnitude ranged from 1.0 to 14 times the g_c value during daytime. The decoupling factor (Ω) followed a similar pattern as g_c (Figure 5.17c). The mean diurnal value of Ω was 0.46, and the values varied between 0.25 and 0.77. The average daily values of Ω, g_c and g_a were correlated against transpiration. The observed transpiration accounted for about 74% variations in both Ω and g_c. This is understandable, since g_c was not measured independently but was derived from the same transpiration data. The decoupling coefficient was highly correlated (R^2= 0.96) to canopy conductance and less correlated (R^2=0.15) to aerodynamic conductance (g_a).

Tree water use declined as g_c and Ω decreased. Readily available soil water led to higher tree conductance and transpiration, while high water deficit led to lower conductance and transpiration despite the prevailing higher atmospheric demand.

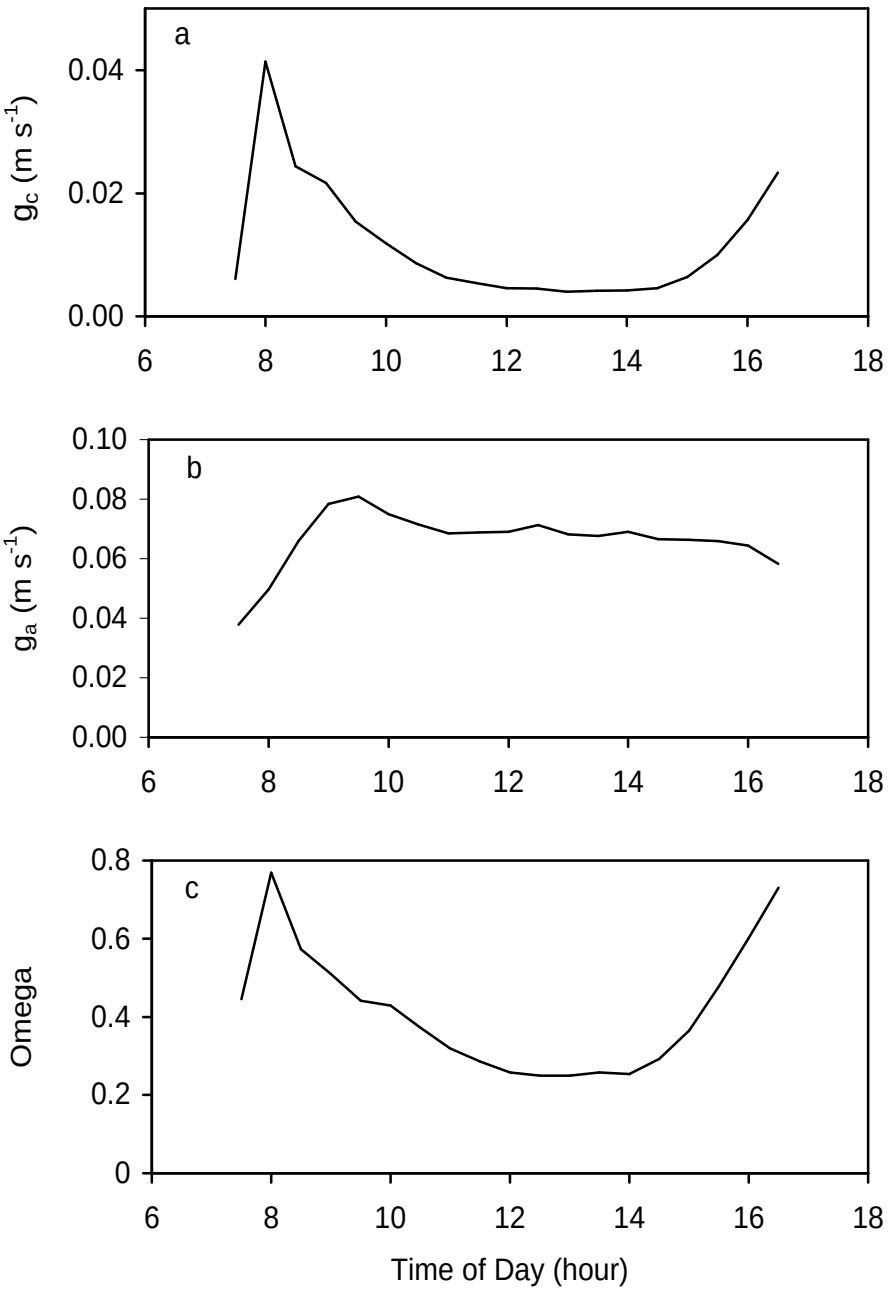

Figure 5.17: Daily course of (a) derived tree conductance, (b) calculated aerodynamics conductance and (c) decoupling coefficient estimated from Equation 4.20.

Regardless of soil water availability, plant resistance may also limit water uptake under high evaporative conditions (Margolis and Ryan, 1997). When this occurs, water uptake becomes uncoupled from the course of atmospheric water demand, leading to higher canopy resistance (Cienciala et al., 2000). According to Machado and Tyree (1994), plant resistance can also be affected by embolism of conductive tissues

particularly during drought. We observed a reduction in transpiration and increasing plant resistance under high evaporative demand and high moisture deficit for *A. occidentale*. The relative importance of stomata in regulating water use and aerodynamic coupling between tree canopy and the atmosphere was measured by the Ω parameter (Javis and McNaughton, 1986, Magnani et al., 1998; Goldberg and Bernhofer, 2001). Generally, smooth, uniform, broadleaf canopies have high Ω values while rough, small-leaf canopies have low values (Javis and McNaughton, 1986; Hinckley et al., 1994). The value of Ω obtained here is in concordance with the fact that the *A. occidentale* species has smooth and medium to broad-leaved canopy, and its canopy processes behave similarly to several other tropical woody species (Hinckley et al., 1994; Kelliher et al., 1995). Our observation showed both day-to-day as well as diurnal variations of Ω. This is in agreement with recently published data, which indicate that Ω is not constant for a given canopy, but varies with changes in environmental factors (Köstner et al., 1992; Hinckley et al., 1994; Magnani et al., 1998). The canopy was more coupled in the afternoon than in the morning as a result of large canopy conductance, and Ω was lower during critical soil water depletion (February/March) with reduced transpiration rates. The average value over the dry season for *A. occidentale* was 0.46, which is lower than the 0.66 obtained for hybrid poplar in Washington (Hinckley et al., 1994). Meinzer et al. (1993) reported a Ω value of 0.5 (similar to our result) during the dry season in *Anacardium excelsum*, a species with large leaves and emergent canopy growing in central Panama.

Furthermore, the impact of Ω in regulating transpiration was explored by estimating "equilibrium" transpiration (E_{eq}) and "imposed" transpiration (E_{imp}) using Equations 4.22 and 4.23. The values obtained were then substituted in Equation 4.21 together with the average Ω (0.43). Our data indicates that *A. occidentale* transpiration was largely dominated by the "equilibrium" rate of transpiration with a contribution of about 92% the total canopy transpiration. This closely agrees with the result of a simple parabolic model fitted in Equation 5.3, where solar radiation was found to explain nearly 90 % of the variations in tree water use.

5.5 Tree water use and prediction during the rainy season

5.5.1 Background

Intensification of tree planting as is currently observed in the West African sub-region is expected to have an impact on regional hydrology and climate circulation. In this study area, cashew (*A. occidentale)* is one of the preferred tree crops for its economic return potentials and environmental benefits. *A. occidentale* is a medium to broadleaved species that grows best in tropical regions with 500-3500 mm rainfall (Rehm and Espig, 1991). It is drought tolerant, and on dry sloping lands is often the only cultivated plant that produces a cash income and serves for erosion control. In areas with high rainfall (>1500 mm), it only thrives on well-drained soils.

A significant expansion of cashew plantations throughout West Africa should be expected in the near future if the current planting rate is sustained over the next decade. In central Ghana, arable cropland, fallow, and marginal lands are continuously being converted into cashew plantations, especially because of its economic importance and ability to thrive well on soils of varied quality (Rehm and Espig, 1991; Yidana, 1996). The water use of this fast growing, newly introduced species is expected to change or modify catchment hydrology. Although the economic factor is the main consideration for this land-use change, it is of importance to assess the environmental aspects of the newly created ecosystems (Bruijnzeel, 1996) as well as the potential hydrological impacts (Allen et al., 1999). A proper understanding of water use limits and controls of this tree crop will help in the application of existing eco-hydrological models and/or development of new ones (Calder, 1998). Adequate knowledge of the interaction between transpiration and the environment is necessary to properly represent, at local, regional and global scales, the exchanges of latent and sensible heat at the base of the planetary boundary layer (Wright et al., 1995; Magnani et al., 1998). If cashew products are to make a significant contribution to the national economy, large areas will need to be planted especially in the forest-savannah transition zone of Ghana. This is expected to have serious implications on aquifer recharge and river flow, especially during dry years. Hence, one aim of this study was to investigate and quantify the water use and discuss the potential hydrological impacts of cashew trees in central Ghana and West Africa.

Transpiration rates were estimated from whole-tree sap flow by Granier System (see Research methods, Chapter 4). These estimates are presented alongside other measured environmental variables and derived plant physiological parameters to assess the influence of these variables on tree water use. One distinct environmental factor reported is the clearness index (*CI*), which gives the transmission factor or a measure of attenuation of the incoming solar radiation by the sky (Ogunjobi et al., 2002). The objectives of this study were to: analyze water flux using the measured sap flow; investigate the dependence of transpiration on environmental variables, and to predict tree water use from easily measured climatic factors. These data are needed to develop, calibrate, and/or validate water-use models (e.g., Grip et al., 1989; Calder, 1992), which are helpful for predicting long-term hydrological effects of plantations.

5.5.2 Observed patterns and environmental control

Weather

Daily weather variables for each month during the rainy season are summarized in Table 5.10. A diurnal minimum temperature of 18.7 °C was observed in August and a maximum of 35.7 °C was recorded in April. August was the most humid month (H = 85.2%), while April had the lowest value of mean daily humidity (74.7 %). Daytime maximum solar radiation ranged from 914 W m^{-2} in July to 1067 W m^{-2} in October. An annual total rainfall of 1380 mm was recorded at the Ejura Observation Station in 2002. The daily pattern of rainfall is illustrated in Figure 5.18a. About 90 % of total annual rainfall was observed between April and October with the highest monthly total of 228 mm occurring in June. However, the highest number of wet days (12 days) occurred in the months of May, July and October. Potential evaporation (Penman, 1948), used as a measure of evaporative demand, and clearness index were calculated over the rainy season (Figure 5.18b and 5.18c). Both parameters showed a similar trend, and *CI* was found to explain about 86 % of the variations of the evaporative demand (R^2= 0.86). Very clear days were found in October followed by April and May relative to other months. No completely overcast day was observed (*CI*<0.05), but lower values exist in the middle of the rainy season mainly because of the presence of convective clouds during this period.

Table 5.10: Minimum, maximum and mean half-hourly weather variables for the rainy months (standard deviation in parenthesis), 2002.

Month	Air temperature (°C)			Relative humidity (%)			Wind speed (m s^{-1})			Solar radiation (W m^{-2})	
	Min	Max	Mean	Min	Max	Mean	Min	Max	Mean	Max	Mean
April	19.9	35.7	27.4 (1.1)	47.3	98.2	74.7 (4.5)	0.00	7.56	1.58 (0.31)	957.3	228.5 (33.0)
May	19.8	34.7	26.4 (1.3)	53.2	98.7	79.8 (4.1)	0.00	6.12	1.31 (0.29)	950.7	213.5 (37.9)
June	19.4	33.8	25.2 (1.1)	40.4	98.9	81.7 (3.7)	0.00	5.68	1.36 (0.25)	966.5	192.4 (46.6)
July	19.3	32.3	24.7 (0.8)	57.2	98.6	85.0 (2.6)	0.00	4.25	1.35 (0.18)	913.5	167.3 (32.4)
August	18.7	31.9	24.0 (0.9)	58.8	99.6	85.2 (3.3)	0.00	3.96	1.38 (0.31)	920.3	154.8 (44.8)
September	19.2	33.1	24.5 (0.9)	53.1	99.4	84.0 (2.6)	0.07	4.03	1.28 (0.20)	997.4	180.5 (33.5)
October	19.5	34.0	25.0 (1.1)	47.4	99.2	83.2 (4.7)	0.01	7.74	1.18 (0.22)	1066.6	220.6 (49.0)

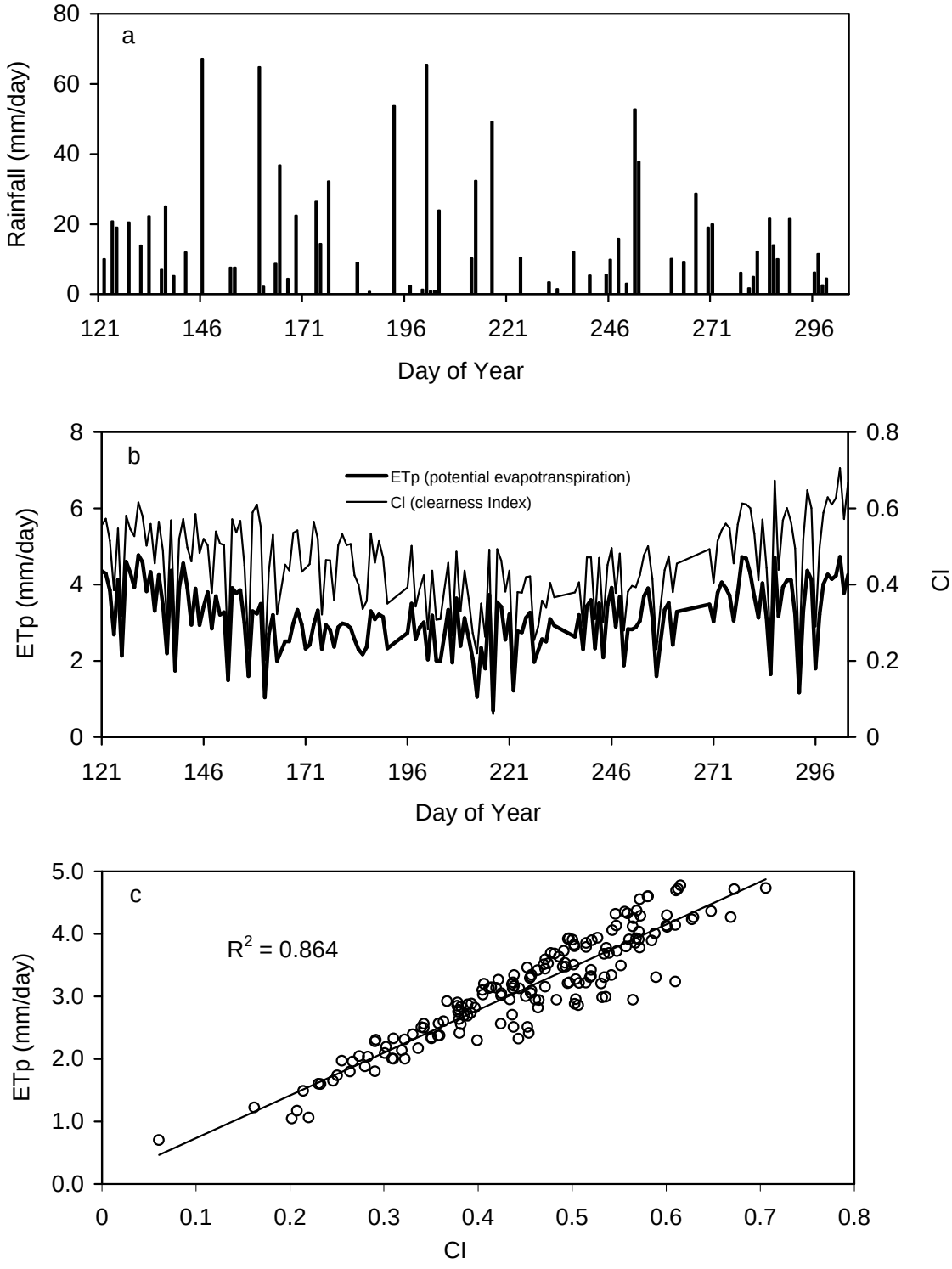

Figure 5.18: (a) Daily precipitation, (b) daily evaporative demand and clearness index, and (c) association between the evaporative demand and clearness index during the rainy season.

Soil water and tree water use

Figure 5.19 shows the variations in the volumetric soil moisture content in the cashew plantation to a soil depth of 1 m. The selected days for each month are typical for that month. Rapid soil water content depletion was noticed from January to March, the peak of the dry season, but the occurrence of the first and second rain on the March 02 and 09, 2002 initiated the soil column refill as shown in Figure 5.19. By May 24 almost all the deficit created during the dry season was already re-filled, but drying out started again in November, the beginning of the dry season. The observed sequence of profile re-fill and drying out observed agrees with previous studies (Calder et al., 1997; Hall et al., 1998; Allen et al., 1999).

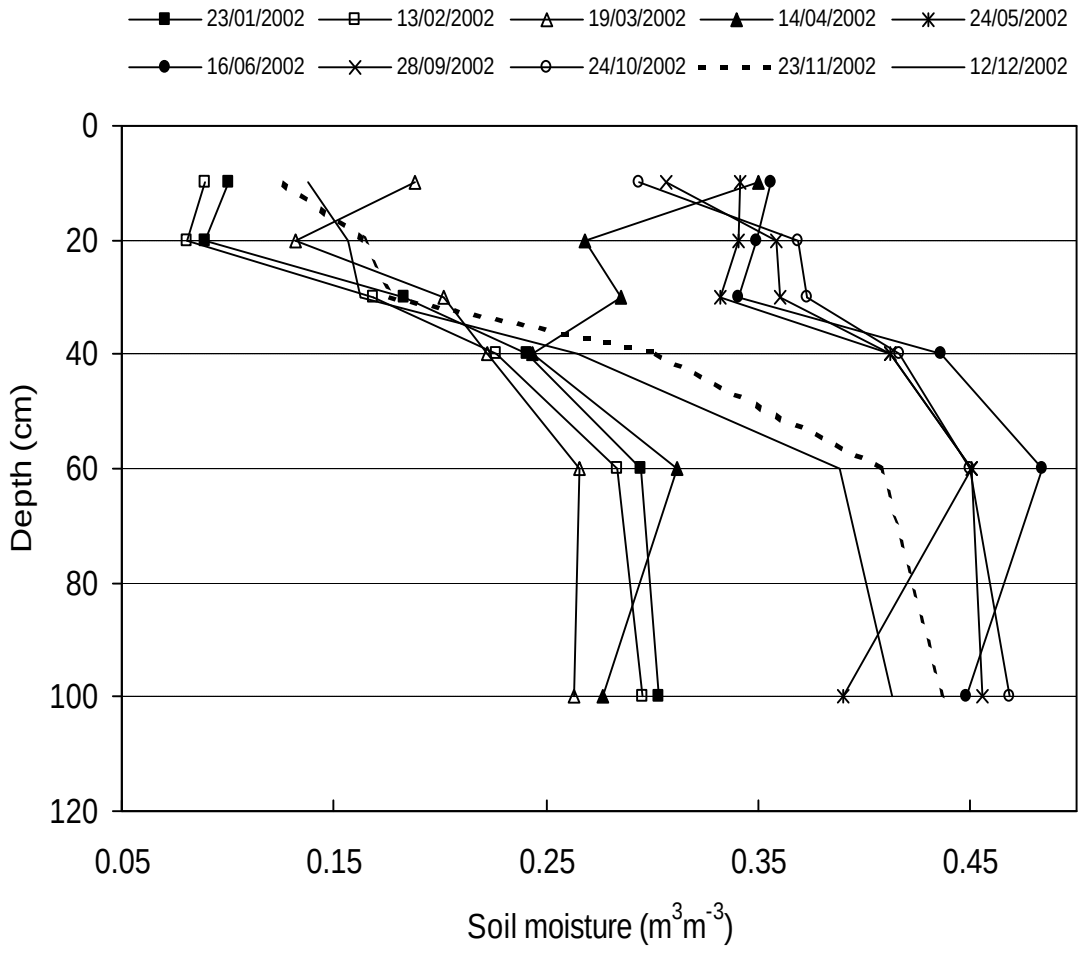

Figure 5.19: Profile soil water regime in the cashew plantation for the year 2002.

Figure 5.20 shows the variation in mean soil water content during the rainy season. The rate of increase in soil water was rapid at the beginning of rains between April and May (i.e., between DOY 91 and 152). The minimum average of 0.23 m^3 m^{-3} in profile soil water was observed on April 3, whereas the maximum average of 0.41 was observed in July. No significant difference was observed in the mean monthly water content between June to October 2002 ($p>0.05$). This suggests that soil water may not be responsible for any observed variations in transpiration during this wet season. A power function fitted between soil water and tension with $R^2 = 0.88$ (data not shown) was used to interpolate soil water for days without soil moisture data. Tree water use was plotted on a daily basis against soil moisture (Figure 5.21). The scatter plot showed no particular trends, suggesting that tree water use during this period was not limited by soil water deficit, since water was readily available. Calder (1998) already noted that raindrop size, plant physiology, and radiation, but not soil water and tree size, are the major factors controlling evaporation in wet tropical climates. Furthermore, Bauerle et al. (2002) indicated that when soil water is extractable, measured and modeled transpiration is mainly controlled by atmospheric demand.

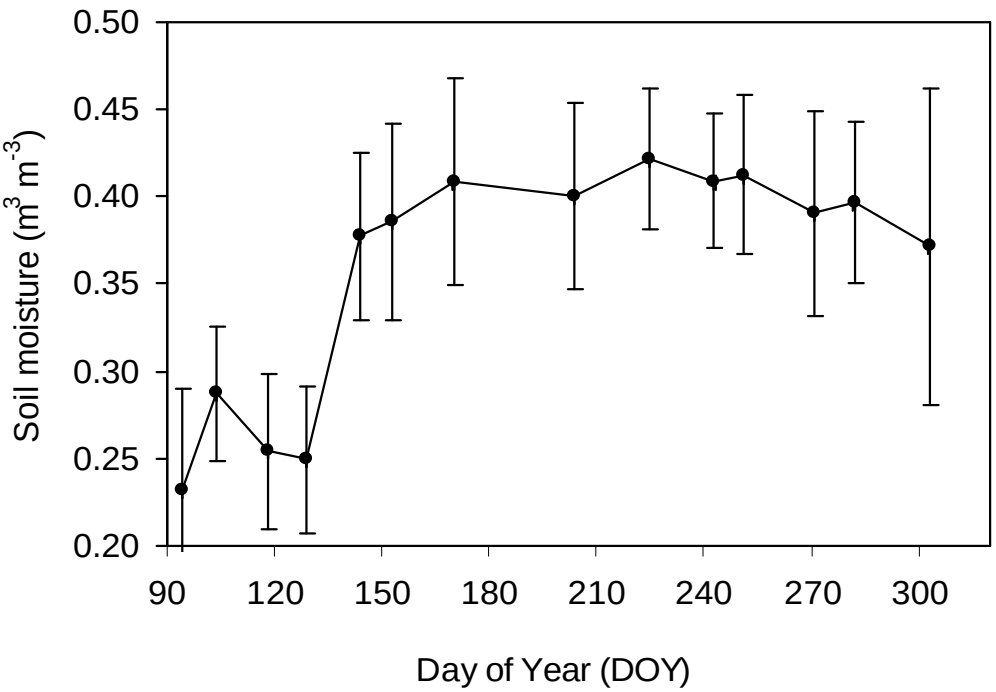

Figure 5.20: Average soil moisture in the 1-m column over the rainy season. The vertical bar is the standard deviation from the mean value.

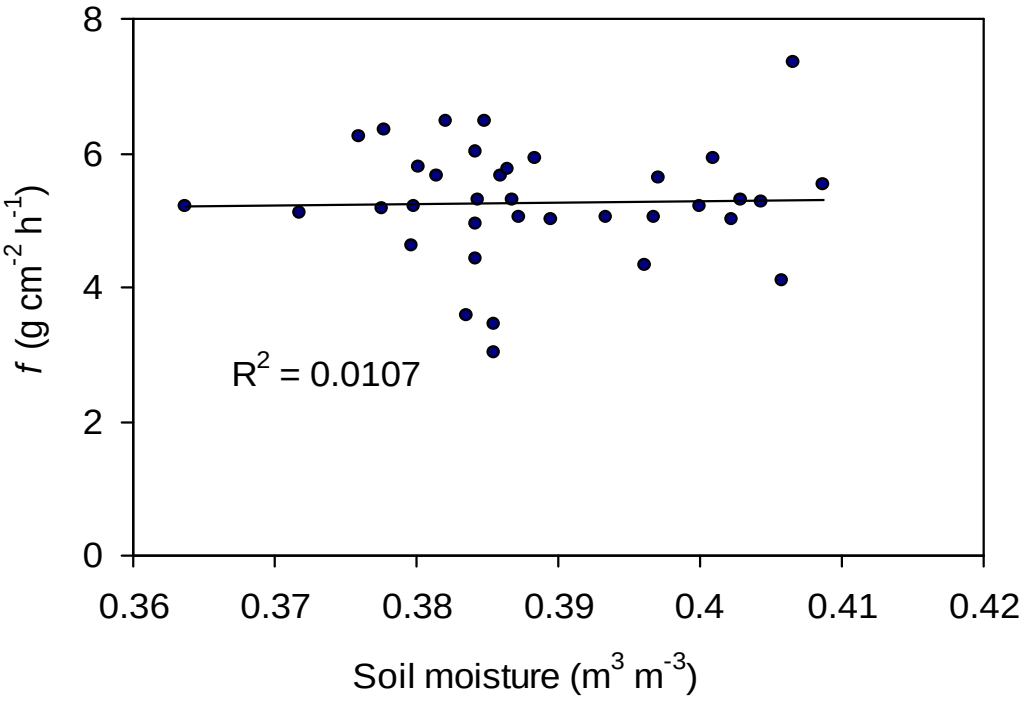

Figure 5.21: Relation between daily mean sap flow density and soil moisture.

Sap flow patterns and sky conditions

The daily course of sap flow density (*f*), solar radiation (*Rs*) and vapor pressure deficit (*VPD*) for three days with different sky conditions are shown in Figure 5.22. The climatic condition on June 06 represents typical partially clouded days; days with daytime precipitation are represented by June 13, while October 31 represents a very bright day (CI = 0.65). On the partly cloudy day, the diurnal patterns of *Rs* and *f* were similar, with the peak values at about mid-morning. The maximum daytime *Rs* was about 400 W m^{-2} and the daily mean value was 97.6 W m^{-2}. Transpiration and VPD were poorly coupled as shown in Figure 5.22 (right). Maximum daytime VPD was below 1.0 kPa with a daily mean of 0.43 kPa. The average transpiration for the day was 3.42 g cm^{-2} h^{-1}. On the rainy day, the pattern was affected by precipitation and interception (June 13, Figure 5). *Rs* and *f* also had a similar daytime course, with a daytime peak occurring after mid-day and the rainfall event taking place between 8.30 and 11.00. Daily mean *Rs* was 134.7 Wm^{-2}, VPD was 0.52 kPa and a low value of *f* (2.13 g cm^{-2} h^{-1}) was recorded.

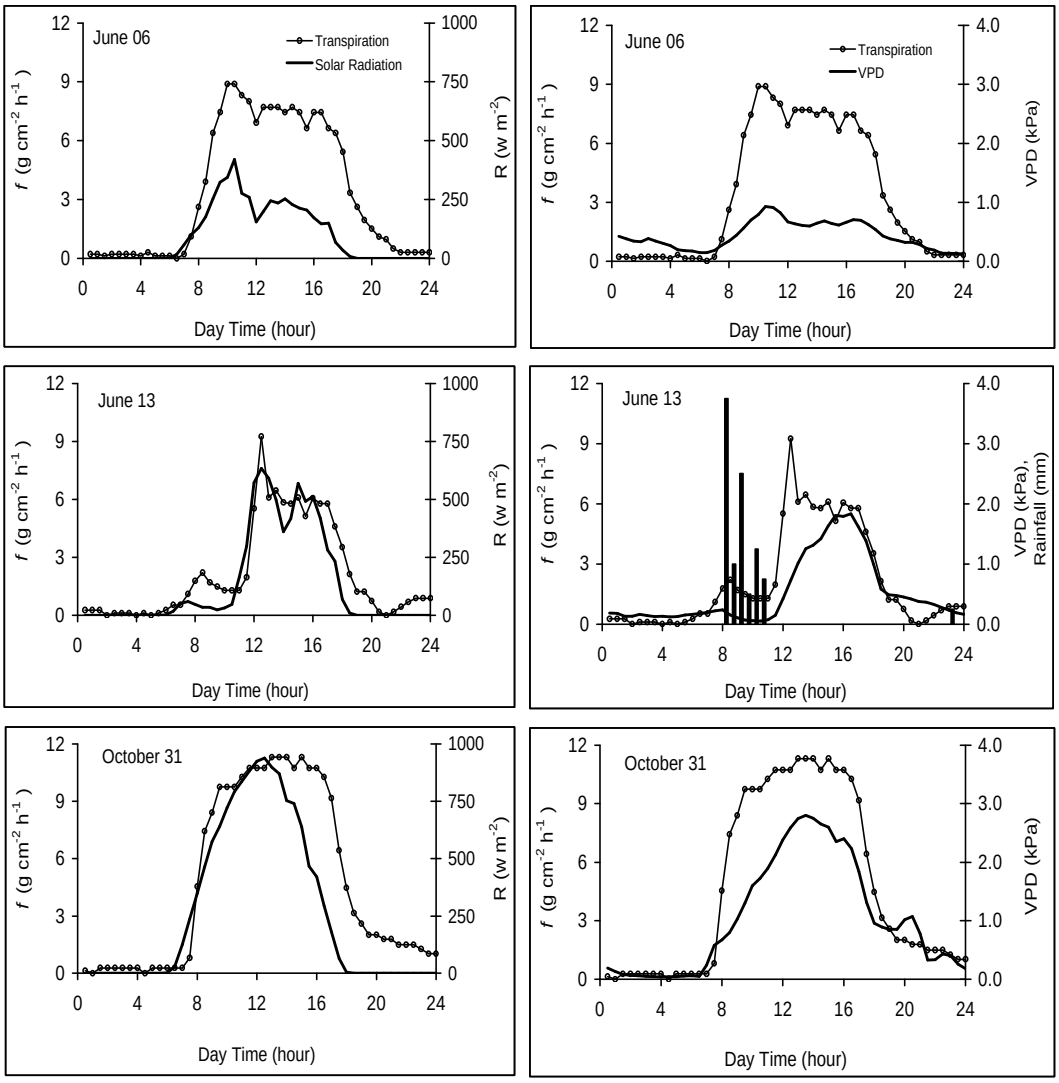

Figure 5.22: Transpiration pattern and sky conditions for three contrasting days (June 06, 13 and October 31, 2002).

On the bright day, both *Rs* and *VPD* were fairly coupled to water flux, with a daily mean *f* of 4.9 g cm^{-2} h^{-1}, *Rs* of 267.8 Wm^{-2} and *VPD* of 1.04 kPa. *Rs* peaked around 12:30 and *VPD* about 13:30. The maximum daytime value was 938.9 W m^{-2} for *Rs*, 2.80 kPa for *VPD* and 11 g cm^{-2} h^{-1} for *f*. In order to determine the relative effects of sky condition or transmission factor on tree water use, the daily time series of *f* and *CI* were plotted for the entire study period (Figure 5.23). The pattern was very similar and their association yielded linear trend ($R^2 = 0.73$) presented in Figure 5.23b.

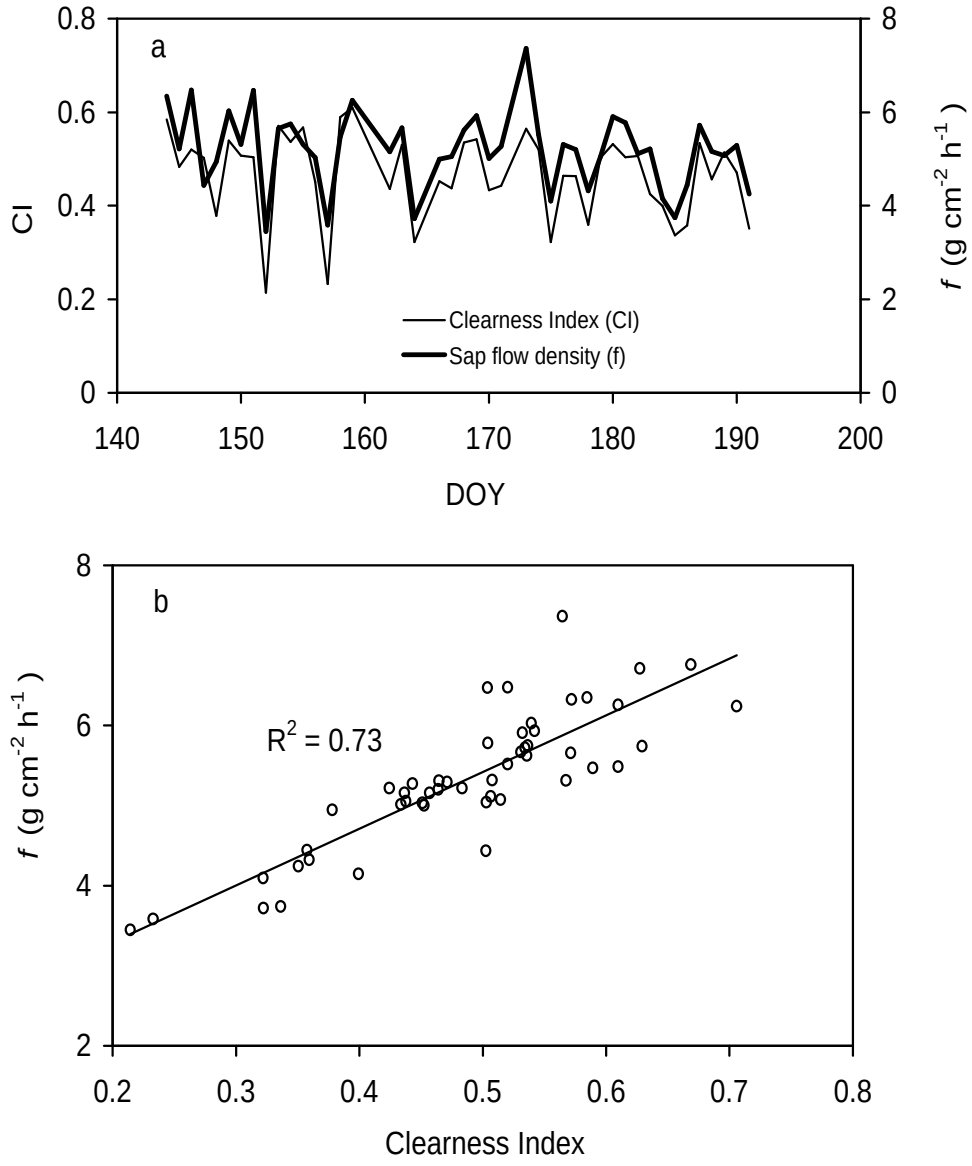

Figure 5.23: (a) Daily pattern of tree water use and clearness index, (b) association between water use and clearness index.

Most studies have focused on the analysis and interpretation of data restricted to periods of 'dry canopies' and de-emphasize water flux during wet canopy, cloudy or overcast days (Köstner et al., 1992; Wullschleger et al. 2000; Sommer et al., 2002). The data in this study show the effects of clear sky, cloudiness and rains on water use pattern in *A. occidentale*. On a typical partially cloudy day (June 6, 2002), cloud systems played an important role both in the pattern and the daily mean water use. The low value of *CI* (0.23) was probably due to the presence of convective clouds occurring within the highly humid atmosphere, which cause a marked attenuation of the incoming

solar radiation during the wet (monsoon) months in West Africa (Jegede, 1997; Ogunjobi et al., 2002). On June 13, occurrence of precipitation shifted the diurnal transpiration pattern forward for the duration of the rainfall, while the combination of cloud and canopy wetness resulting from the rainfall interception reduced *f* below the observed value of June 6 despite higher values of R and CI on June 13. This result is in accordance with Bruijnzeeel (1996) and Dykes (1997) who reported that evaporation in wet tropical climates might be limited by rain events, due to high frequency of rainfall and high interception evaporation. This is possible because intercepted water reduces transpiration, and evaporation of intercepted water consumes part of the energy that would otherwise be used for transpiration. Wullschleger et al. (2000) similarly reported considerable variation in whole-tree and canopy-scale processes in red maple trees as a result of rains, clouds and clear skies between June and August 1997.

Limits, controls and prediction of transpiration

Estimated canopy conductance (g_c) ranged from 4 to 21.2 mm s^{-1} with mean of 8.0 ± 3.3 mm s^{-1}. Poor correlation of g_c to all the environmental variables was observed. Figure 5.24 shows the relationship between g_c, soil moisture, and clearness index. The conductance data was also fitted for equations of different forms. The results show that a dependence of g_c on the combined climatic variables could not be found. Cienciala et al. (2000) also obtained a similar result in *Acacia mangium* plantations. Therefore, the dimensionless decoupling coefficient, Ω (Javis and McNaughton, 1986) was computed so as to generate additional information on the environmental control of transpiration. For the entire period, average daily Ω, based on wind speed measured from the weather station and not directly over the canopy, was 0.40 and ranged from 0.28 to 0.59. This moderate value of Ω and the poor correlation of g_c with climatic variables suggest that the cashew tree canopy was moderately coupled to the atmosphere and hence stomata control of transpiration was small.

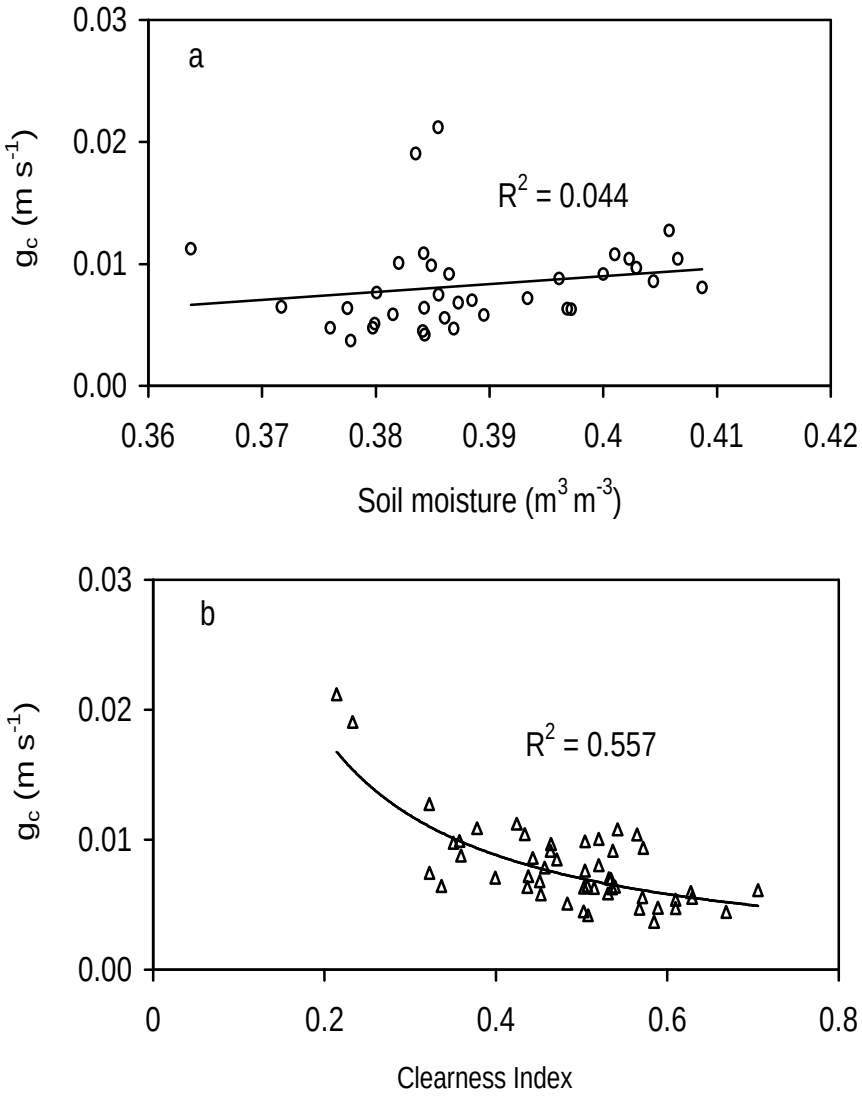

Figure 5.24: Relations between canopy conductance (g_c) and (a) soil moisture, and (b) clearness index.

Transpiration was strongly correlated with the climatic parameters (air temperature, radiation, humidity, vapor pressure deficit) with R^2 ranging from 0.68-0.76 as shown in Figure 5.25 (half-hourly data). A visual examination of the data suggests that at higher values of *VPD* and Rs (*VPD*>1.5 kPa and *Rs*>150 Wm^{-2}), tree sap flow shows a plateau-shaped curve, indicating stomata closure (Figure 5.25b & d). It can be noted that this high evaporative demand resulted in increased canopy resistance, thereby limiting water uptake even under abundant soil water. A similar observation was made by Hogg et al. (1997) and Margolis and Ryan (1997).

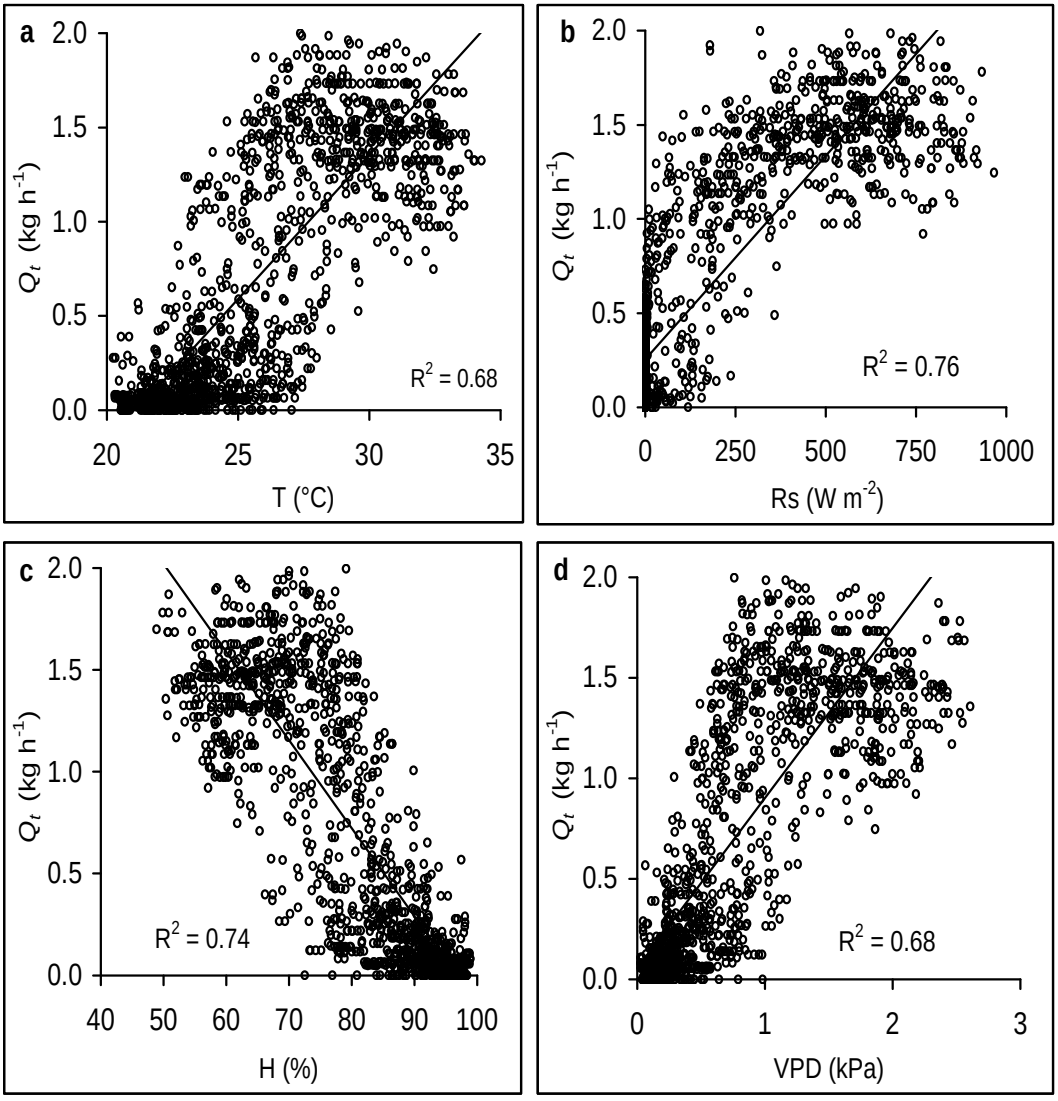

Figure 5.25: The dependence of tree water use on climatic parameters (a) temperature, (b) radiation, (c) humidity and (d) vapor pressure deficit.

The tree water use could be predicted from weather parameters by simple to multiple linear regression models. The results of the fitted models are shown in Table 5.11. Half-hourly variables including night-time observations were used for this analysis. Solar radiation, followed by relative humidity and air temperature, had the most significant contribution to the prediction of water flux. Radiation alone explained about 76 % of the variations in the water uptake by the cashew tree (Equation A4, Table 5.11), whereas the inclusion of humidity and temperature in the model increased the coefficient of determination (R^2) from 0.758 to 0.827. Exclusion of *T* from the analysis

did not significantly affect transpiration predictions, as temperature contributed only about 0.2 % to the explained variance (Table 5.11). Furthermore, a set of non-linear models derived from Equation 4.15 and the modified Priestly-Taylor (Equation 4.16) were fitted with the same data set as above. The results showed a better fit as compared to the linear models, but the difference was not significant. A modified Priestly-Taylor (MPT) had the lowest coefficient of determination ($R^2 = 0.726$), whereas the response of transpiration to the combined function of *Rs*, *H* and *T* produced the highest coefficient of determination ($R^2 = 0.862$).

Table 5.11: Model statistics for calibration and validation of the water use prediction equations

Regression models	Eq.	R^2	SE	r^2	d (%)
$Q_t = a + b*R + c*H + d*T$	**A1**	0.827	0.291	0.817	0.61
$Q_t = a + b*R + c*T$	A2	0.807	0.308	0.794	0.82
$Q_t = a + b*R + d*H$	A3	0.825	0.293	0.814	0.67
$Q_t = a + b*R$	A4	0.758	0.345	0.746	0.80
$Q_t = a*R/(R+b)*(c+d*T)*(100-e*H)$	**A5**	0.862	0.260	0.833	0.53
$Q_t = a*R/(R+b)*(c+d*T)$	A6	0.828	0.291	0.840	0.72
$Q_t = a*R/(R+b)*(100-e*H)$	A7	0.834	0.286	0.841	0.42
$Q_t = a*R/(R+b)$	A8	0.821	0.296	0.832	0.66
$lE_c = a\left(\frac{\Delta}{\Delta+g}(R_n - G) + b\right)$	**A9**	0.730	3.21	0.712	1.26

R^2 for calibration data (n = 1392), r^2 for validation data (n = 588), SE is the standard error of estimate, d is a measure of accuracy and *a, b, c, d* and *e* are fitted model parameters. Equations A1, A5 and A9 are the same as Equations 4.14, 4.15 and 4.16 in the text.

Independent data were used to validate the predictions from these models and their performances were quite good. Comparing the predicted and the observed Q_t, a range of r^2 from 0.712 to 0.841 was found. A measure of accuracy (d) computed (Equation 4.17) shows that the non-linear models, except MPT, performed better than their corresponding linear models. The results suggest that the diurnal pattern of water uptake by *A. occidentate* could be predicted using linear and non-linear regression

models. Figure 5.26 shows a 1:1 plot of observed and predicted transpiration based on Equations 4.14 and 4.15. The linear model and MPT generally over-predicted night-time transpiration, whereas the non-linear models underpredicted transpiration during the night. This is because the parameter "*a*" and "*ß*" in equations 4.14 and 4.16 are indicative of night-time evaporation, but equation 4.15 was based on the assumption that there is no evaporation when R=0 (Bosveld and Bouten, 2001; Lagergren and Lindroth, 2002). The analysis shows that tree water use was highly related to solar radiation as compared to the other weather variables. In fact, the low wind speed recorded in this area do not favor large-scale advection of energy to increase transpiration rates, and hence radiation is likely to exercise more limits and controls on tree evaporation rates.

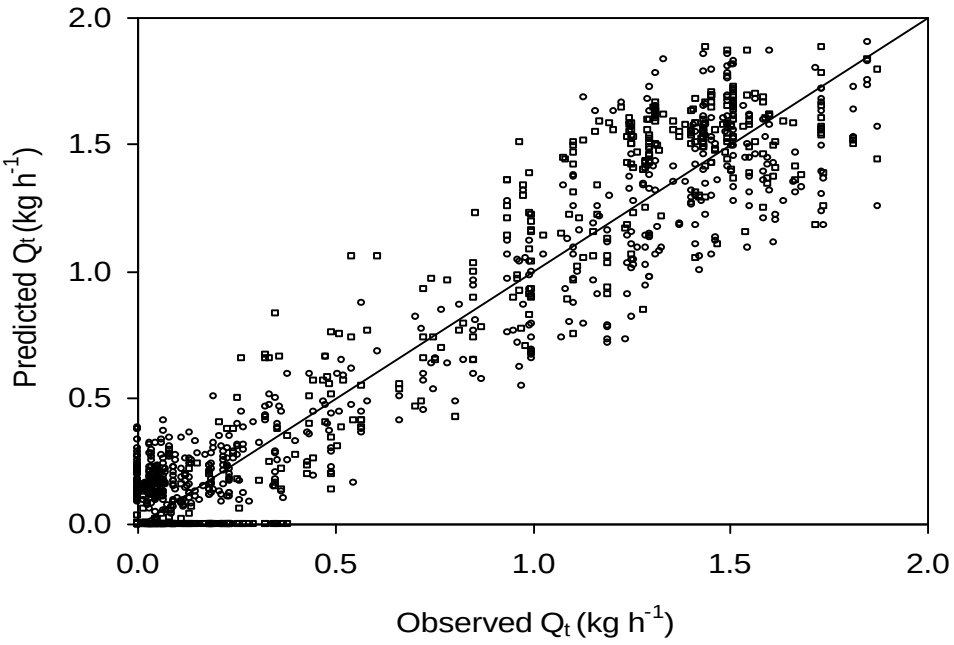

Figure 5.26: Predicted and observed tree water flux using independent data set. Open circle = equation 4.14; rectangle = non-linear Equation 4.15.

5.6 Tree and ecosystem water flux during a wet-to-dry transition period

5.6.1 Introduction

Pertinent to our understanding of regional and global change in the hydrological cycle is the knowledge of biosphere-atmosphere interactions that include the effects of climate on ecosystem functions and the potential feedbacks of the land surface to the physical climate system. Studying these interactions requires a nested experimental design,

whereby measurements of fluxes are taken using a variety of methods, at different time and space scales (Margolis and Ryan, 1997). Forest and woodland ecosystems often include an understory of grasses, forbs, shrubs or smaller woody plants (Scott et al. 2003) that may make significant contributions to the total ecosystem flux depending on stand structure. Generally, in closely spaced stands, trees play a dominant role in total evaporation, whereas in stands with widely spaced trees, evaporation from understory vegetation, litter and soil is a major component of the total ecosystem water loss (Eastman et al. 1988; Kelliher et al., 1990; Scott et al., 2003).

Furthermore, information on temporal patterns and dynamics of water fluxes from soil to canopy is relatively scarce in the moist tropical forest, but may be of importance to climate models (Godstein et al., 1998; Phillips et al., 1999). To understand the temporal dynamics, there is a critical need to measure time lags (t) in water movement through plants for the purpose of estimating canopy transpiration and conductance from xylem sap flow data (Diawara et al., 1991; Granier and Loustau, 1994; Phillips et al., 1997). Time lag for water transport between stems and canopies can be estimated based on lags between stem uptake and canopy eddy flux measurements (Granier and Loustau, 1994; Phillips et al., 1997). Although some studies have neglected the use of lag times (Köstner et al., 1992; Cienciala et al., 2000), errors introduced to the estimate of canopy transpiration if lags were disregarded could be up to 30 % on a stand level (Phillips et al., 1999).

In this study, sap flow, eddy correlation and/or large aperture scintillometry systems were used concurrently to measure field level fluxes. The results reported here cover measurements taken during a dry-down (transition) period between November 2002 and January 2003 near Ejura in the southern part of the Volta Basin. The objectives of this study were (1) to examine the temporal patterns between xylem sap flow and eddy water flux and their interaction with the atmospheric forcing with a view to determine their respective lags; (2) to estimate the relative contribution of trees and understory components of total evaporation in this ecosystem.

5.6.2 Xylem flow – eddy flux diurnal relations

Cross-correlations at different time lags between above-canopy evaporation and stem sap flow are presented in the form of correlograms in Figure 5.27.

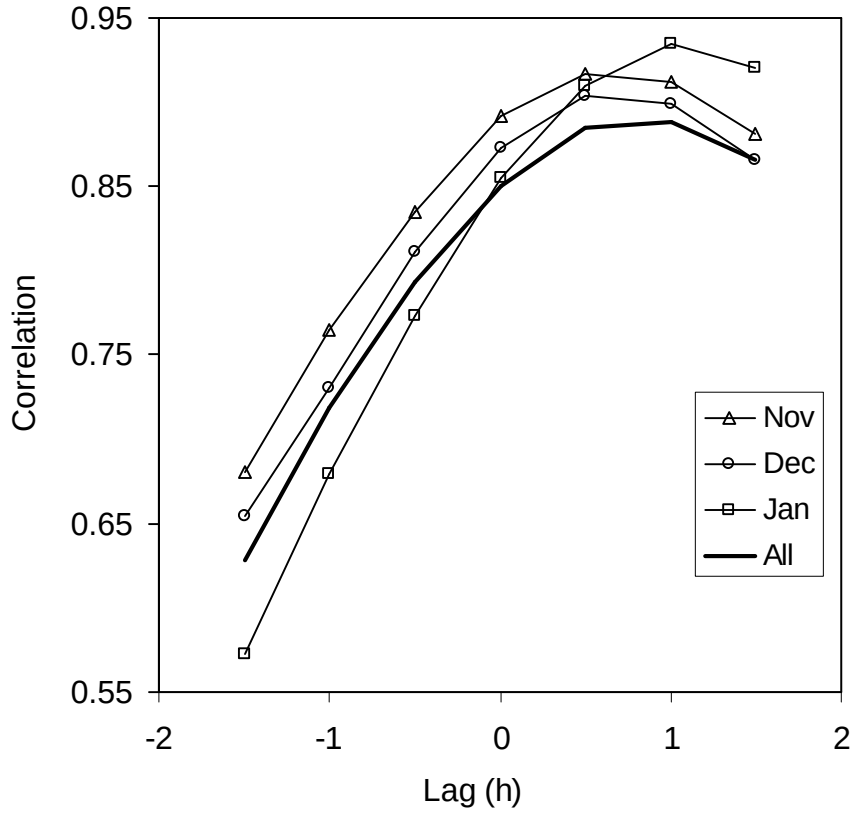

Figure 5.27: Cross-correlation between above-canopy evaporation and stem sap flow (Equation 4.24). Maximum R for each curve corresponds to the time lag for each period.

The patterns of the correlograms for November and December look similar. The observed correlation ranged from 0.68-0.92 in November and from 0.64-0.91 in December. The maximum R being at $_t$ = 30 min for both months. Time lag for the period in January was quite different, with $_t$ between 60 and 90 min, and the maximum correlation at $_t$ = 60 min. Using all the data in one single cross-correlation analysis yielded a slightly different picture. The time lag was between 30 and 60 min, with the maximum r = 0.90 at $_t$ = 60 min. The $_t$ values are obviously to the nearest periodicity or the time series-averaging period, which are just half-hourly in our study. Using Equations 4.25 and 4.26, more exact $_t$ values that are independent of the averaging period were obtained. The R^2 for equation relating R to time lag (Equation 4.25) was very high for each of the periods considered (R^2 > 0.991). Lag was estimated as 43.5 min in November, 46.1 min in December and increased to 75.6 min in January. For the combined data, $_t$ = 53.6 min.

A direct comparison between measurements of sap flow and total evaporation (evapotranspiration) showing diurnal patterns is presented in Figure 5.28. Stand transpiration is per unit ground area, whereas crown transpiration is per unit crown area. The average for each corresponding measurement period was used. Generally, the temporal evolution of sap flow is smoother than the water flux measured by the eddy correlation system. It should be noted that sap flow lagged behind canopy evaporation even with a time lag of 30 min taken into account in plotting Figure 5.28. Stem flow started later and reached a maximum earlier than evaporation. Eddy correlation measurement indicated some negative values during the night and in the early morning, which are not consistent with the near-zero value measured with the sap flow method. In addition, evaporation by eddy correlation was more perturbed by transient daytime atmospheric conditions than sap flow. The patterns of above-canopy water flux were quite similar for the three observation periods, but sap flow changed slightly. In November (DOY 323-359), tree transpiration reached a maximum in the mid-morning and stayed almost constant for the entire afternoon before decreasing in the evening, whereas in December (DOY 359-365) and January (DOY 1-3), tree transpiration reached a maximum in the mid-morning, decreased slowly during the afternoon and showed a sigmoid decrease during the late afternoon to evening.

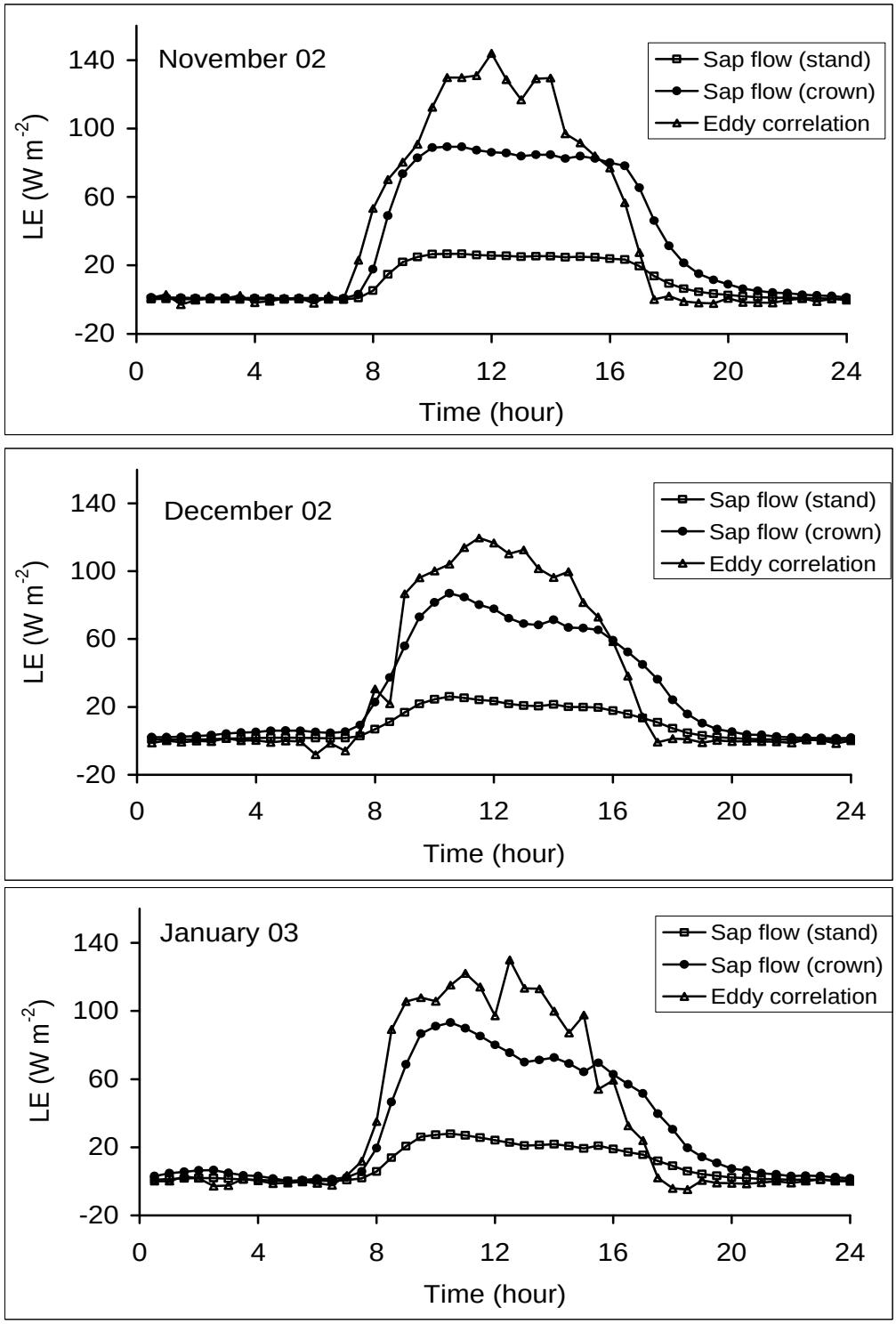

Figure 5.28: Mean diurnal course of latent heat fluxes as measured by eddy correlation and sap flow measurement systems. Sap flow was computed per unit crown area and per unit ground area.

In order to estimate the extents to which the variation of eddy water flux and sap flow are correlated, we regressed tree transpiration (stand and crown) with canopy evaporation (Figure 5.29). The value of R^2 indicated that there is up to 70% agreement in the diurnal patterns of sap flow and eddy flux.

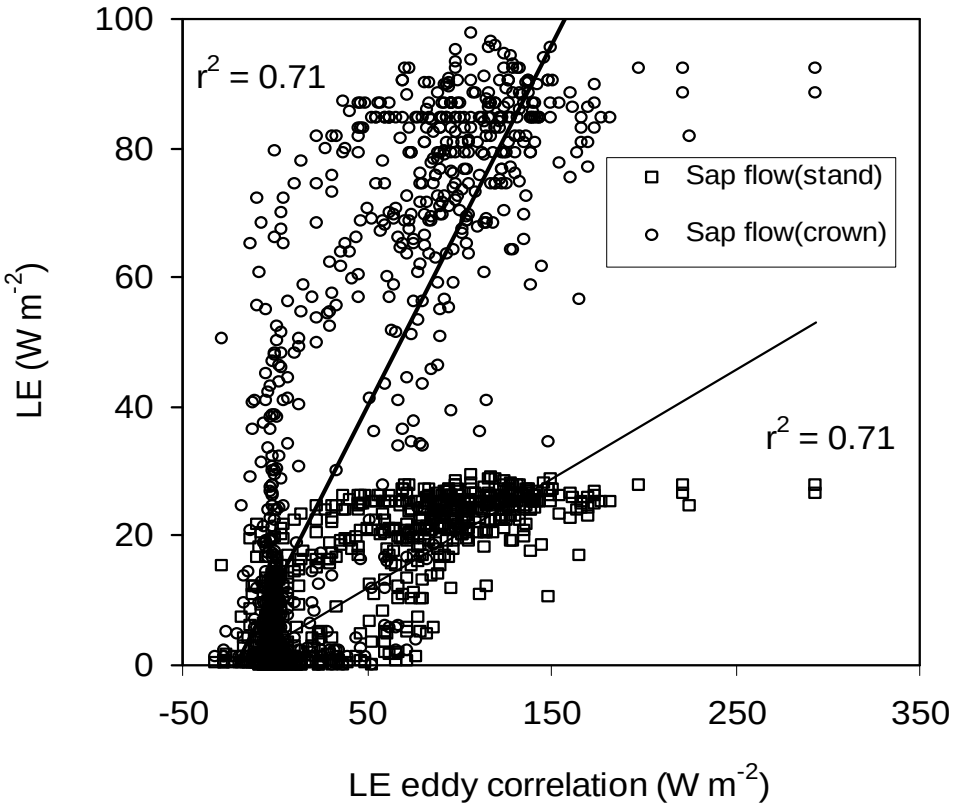

Figure 5.29: Comparison of half-hourly latent heat flux measured by sap flow method and eddy correlation system.

5.6.3 Water flux – climatic forcing temporal dynamics

The diurnal evolution of sap flow (S_F), eddy flux (ET) expressed as latent energy (LE), *Rs* and *VPD* averaged over the measurement period (22 days) are shown in Figure 5.30. It can be seen that: (1) both eddy water flux and sap flow are well correlated to radiation with eddy flux showing a better coupling; (2) the vapor pressure deficit lagged behind both eddy flux and sap flow.

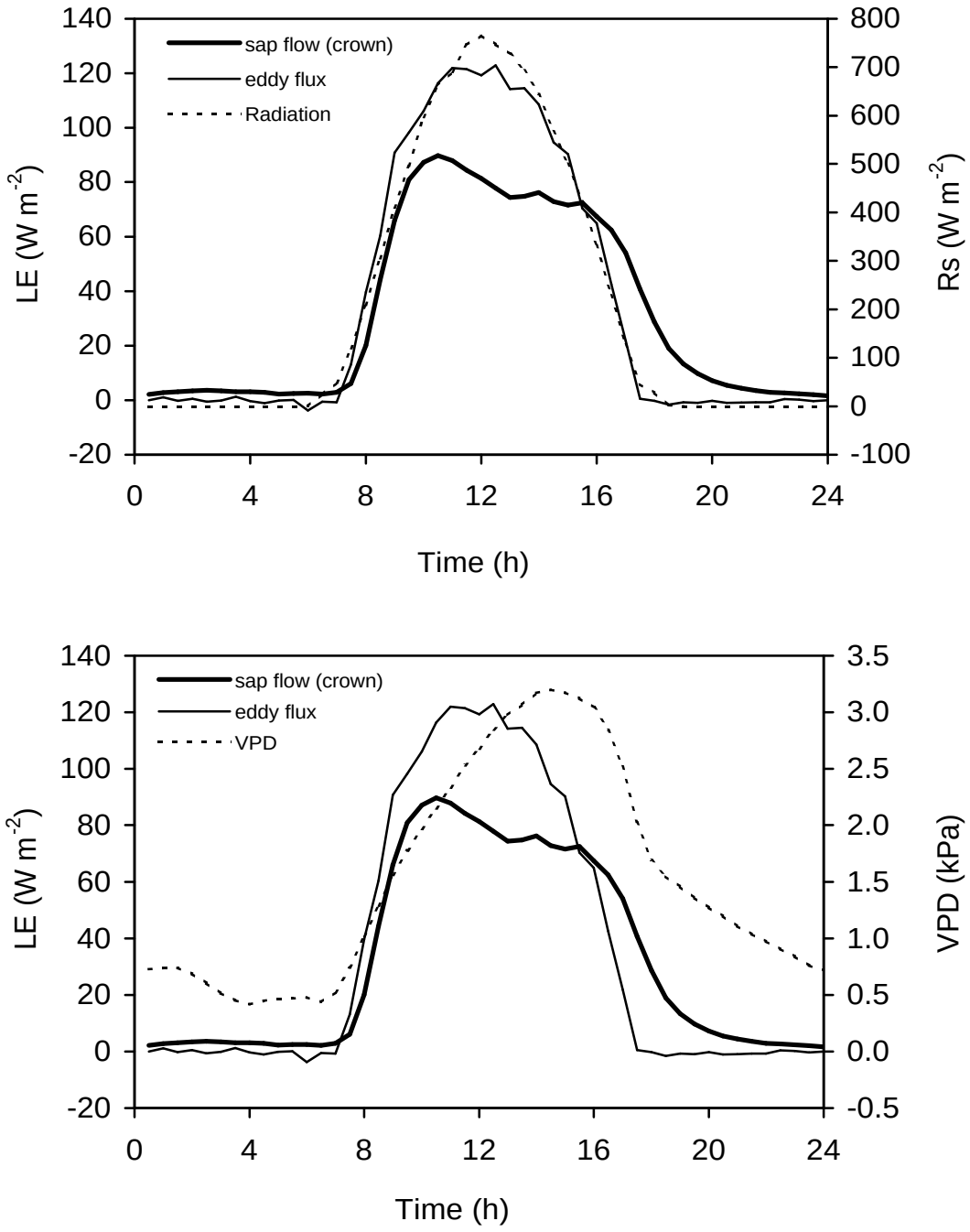

Figure 5.30: Temporal patterns of water fluxes (LE) in relation to (a) solar radiation (R_S) and (b) vapor pressure (D) with time lag of 30 min (average of 22 days).

The time lags between water fluxes and R_S or D were also estimated as earlier described. Combining all the data (n=1056), ET lagged behind R_S by 25 min (R = 0.921), but led *VPD* by up to 165 min (R = 0.821). Similarly, S_F lagged R_S with a slightly longer duration ($_t$ = 32 min; R =0.917), whereas $_t$ with respect to *VPD* was 58 min. Using a 30 min time lag, half-hourly values of sap flow and eddy flux were

linearly related to the incoming global radiation and vapor pressure deficit as shown in Figure 5.31. Water fluxes showed a better correlation with R_S ($r^2 > 0.81$) than with D ($r^2 > 0.38$).

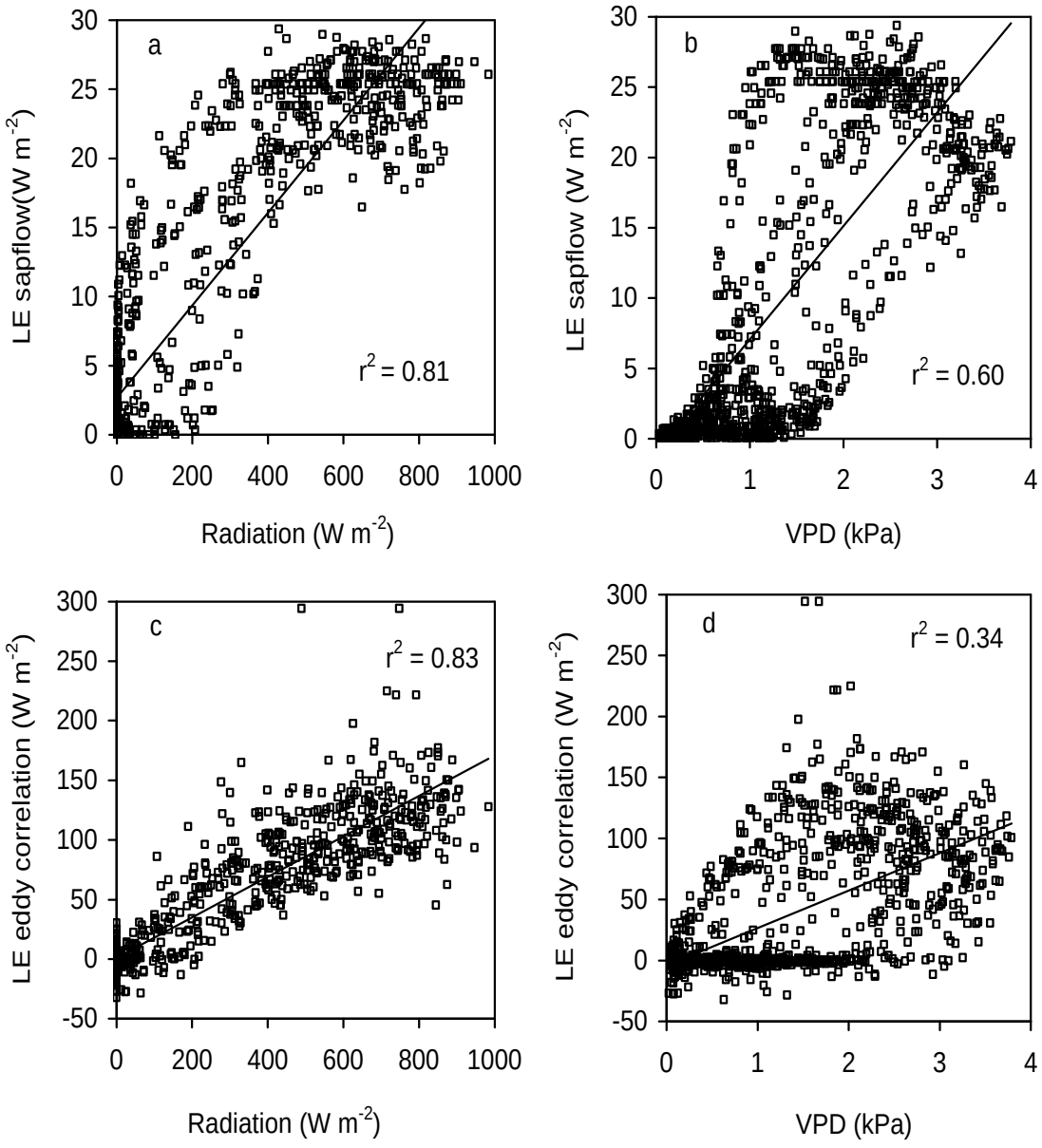

Figure 5.31: Scatter diagram of stand transpiration by sap flow (a and b) and eddy flux (c and d) against solar radiation (R_S) and vapor pressure deficit (VPD).

5.6.4 Daily estimates of sap flow and eddy fluxes

Daily estimates of tree transpiration and above-canopy evaporation were computed as sums between the hours of 7:00 and 16:00. This was to avoid the night-time and early

morning (negative values) evaporation from the eddy correlation measurements. Figure 5.32 shows the daily pattern of the fluxes over the 22 days of concurrent measurements (DOY: 323-359, 359-365 and 1-3). The values for eddy flux ranged from 2.01 to 3.17 mm day^{-1} with a mean value of 2.7 mm day^{-1} and a coefficient of variation of 12 %. Generally, there was a slight decrease in daily values during this drying transition period. Similarly, the observed stand transpiration decreased slightly ($p > 0.05$) over the period. The value ranged from 0.55 to 0.72 mm day^{-1} with a mean of 0.65 mm day^{-1} (CV = 8 %). On average, the contribution from trees was estimated at about 25 % of the total evaporation.

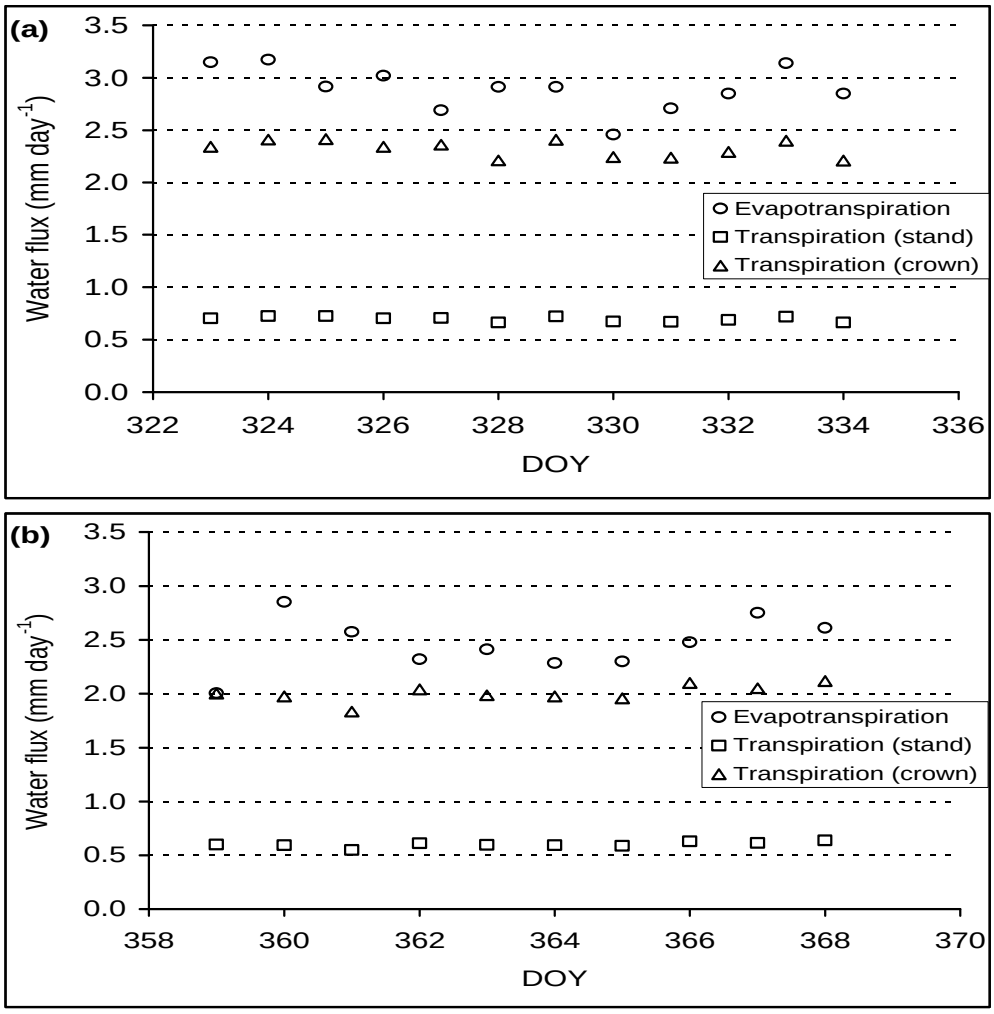

Figure 5.32: Daily values of tree transpiration (crown and stand) and evapotranspiration (averaged between 7:00 and 16:00 GMT) for (a): DOY 323-334 and (b) DOY 359-365, 01-03). DOY 366 = 01 Jan. 2003.

Soil moisture was also measured in a bare patch between the tree rows. The soil moisture profile (Figure 5.33), monitored bi-weekly during the 22 days, was used to estimate the daily contribution from the bare soil. The average daily water loss from a 1-m soil column was computed as 0.3 mm, which translates to about 11% of the total evaporation.

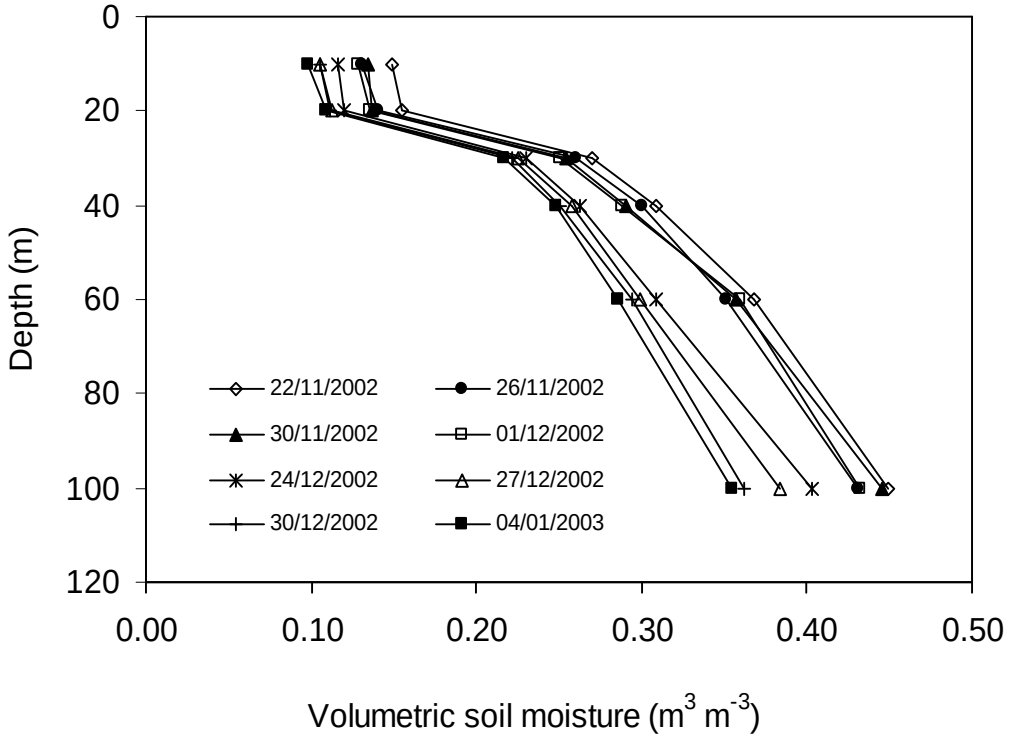

Figure 5.33: Average volumetric soil moisture in 1-m soil column during 22 days of concurrent measurements.

In order to assess the general pattern of evaporation over an extended period during the transition period, the evaporative fraction (*EF*) was computed as the ratio of latent heat (*LE*, W m^{-2}) to available energy:

$$EF = \frac{LE}{LE + H}$$

where *H* (W m^{-2}) is the sensible heat flux. The daily time series (averaged between 7:00 – 16:00) for LE and EF for the 79 days between November 9, 2002 and January 27, 2003 are shown in Figure 5.34. Both LE and EF decreased gradually. Total evaporation

varied from 2.33 to 5.52 mm day^{-1} with a mean of 3.52 mm day^{-1}. The average evaporative fraction was 0.48 and ranged between 0.66 (days following the end of the rainy season) to 0.36 (at the end of transition period).

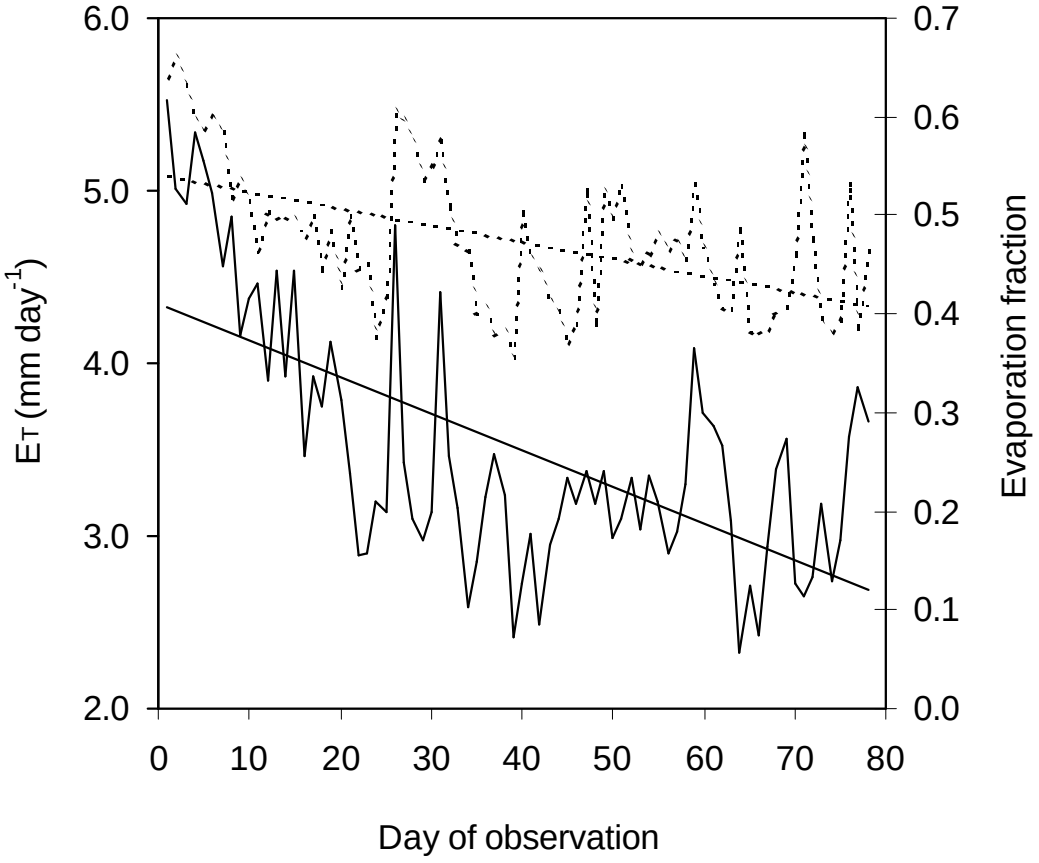

Figure 5.34: Total evaporation (solid line) and evaporative fraction (dashed line) observed for 79 days during the transition period. Day 1 = November 9, 2002 and day 79 = January 27, 2003.

5.6.5 Discussion

Considering the fact that there was a total rainfall of about 13 mm on only one (November 23, 2002) out of the 22 days of concurrent measurements, and that a total of 28 mm was observed between December 03 to 09, 2002, the entire measurement period could be referred to as a "drying-out" or transition period. The estimated time lag between S_F and ET increased gradually as the drying-out period progressed. This result is similar to previous studies that reported a non-constant time lag in maritime pine

(Loustau et al., 1996) and jack pine (Saugier et al., 1997). Although the interpretation of the time lag is complex, changes in water storage along the stem and leaves above the gauging sensors are thought to be partly responsible (Saugier et al., 1997; Phillips et al., 1999). During this period of 22 days, a small and insignificant decrease in transpiration was observed, which suggests that the increase in $_t$ may be a result of lower transpiration rates leading to more time needed to replenish the water stored above the gauging sensors. Furthermore, since this period is mainly used by *A. occidentale* for flowering and fruiting, changes in water uptake, storage and release may be an adaptation strategy for the tree to cope with the impending water deficit.

The observed behavior of stem flow and eddy flux in relation to radiation and vapor pressure deficit slightly differs. Whereas E_T quickly responds to radiation and follows it throughout the day (Figure 5.30), S_F responds a bit later and follows R_S up to late afternoon (16:00), after which VPD becomes influential. Radiation was the main driver for evaporation both from the trees and the understory. It can be seen in Figure 5.31, that sap flow exhibits a parabolic response to solar radiation. The fast responses of water fluxes to R_S coupled with high R^2, is an indication of their aerodynamic decoupling from the atmosphere. The higher time lag (165.3 min) between E_T and VPD as compared to S_F (58.4 min) reveals that the degree of decoupling for tree crowns is less than for the above-canopy evaporation. This suggests that the relative contribution of trees to the total evaporation is small compared to the undergrowth (grasses, crops, short shrubs and bare soil) that covers about 70 % of the plot and understory beneath the trees. The high divergent time lag between E_T and S_F (with VPD) stated above is assumed to be due to the undergrowth contribution to the total evaporation. Many studies have shown that such within-row grasses and understory are almost completely decoupled from the vapor pressure deficit but highly related to the net radiation (Diawara et al., 1991; Scott et al., 2003). Hence the dominating effects on the observed eddy flux.

The lower percentage of evaporation contributed from the cashew orchard was a result of low tree density (about 175 trees per ha). Previous studies have shown that transpiration from trees can account for about 90 % of the total evaporation from closely spaced stands (Kaufmann and Kelliher, 1991), whereas in stands with widely spaced trees, evaporative loss from the understory vegetation, soil and litter can become the

major component, as observed in agroforestry systems (Eastman et al., 1988) and in young stands where the trees have been thinned and pruned (Kelliher et al., 1990). Furthermore, in two *Acacia mangium* plantations, where one stand had a density that was about double that of the other, Cienciala et al. (2000) observed a large difference in their respective stand transpiration rates.

The contribution of understory evaporation was not directly measured in the present study but was treated as the residual of total evaporation, tree transpiration and bare-soil evaporation estimated as earlier stated. However, this understory evaporation quantity is uncertain due to uncertainties associated with: scaling tree to stand transpiration (Granier et al., 1990; Cienciala et al., 2000), estimation of bare-soil evaporation, and total evaporation by eddy correlation (Twine et al., 2000; Brotzge and Crawford, 2003). Similar to Granier et al. (1990), it was observed that between-tree variability of sap flux density was low, probably because the trees were young, even-aged, and of low stem density, which allowed full crown exposure eliminating possible shadowing effects. Instrument error, surface heterogeneity, and the theoretical assumptions behind the eddy correlation method have been used to explain problems of energy budget closure (Brotzge and Crawford, 2003).

Differences in methods or softwares used to process fluxes can also contribute to uncertainties in eddy fluxes. This was shown by comparing water flux estimated with two different programs (ALTEDDY II and EC_NCDF). An independent sample test showed that their mean difference is significant ($p = 0.02$). The region enclosed in the cumulative probability density curves of the two estimates (Figure 5.35) explains the difference. ALTEDDY II estimated slightly higher values of fluxes relatively to EC_NCDF, but one cannot be adjudged as being better than the other, since they were not compared to any standard. The main interest here is to show that uncertainties can stem from techniques of processing eddy correlation raw data. Another source of discrepancies in the value of eddy flux relative to sap flow is the possibility of advected moisture from nearby ponds, swamps, and stream. These surfaces are within 250 to 450 m in a valley meandering around the experimental site and passing through the entire 90 ha plantation. A roughly estimated footprint analysis (ALTEDDY II) showed that average day-time fetch could vary from 200 to 600 m. Hence, there is a likelihood that

vapor flux from these water bodies and rice fields affected the magnitude of the total evaporation observed with the eddy correlation method.

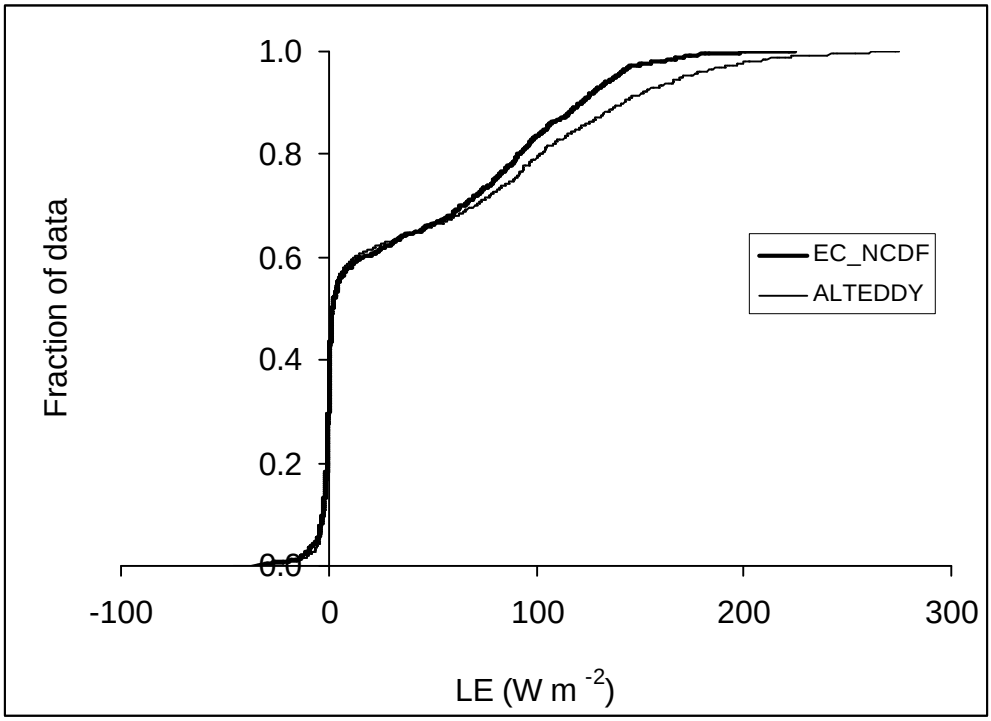

Figure 5.35: Cumulative probability density function for the estimated water flux with ALTEDDY II and EC_NCDF softwares.

Based on the estimated average evaporation fraction, less than 50 % of the available energy was used in actual evapotranspiration during the wet-to-dry transition season studied. The observed decreases in evaporative fraction suggest that there is a change in biosphere-atmosphere interaction (increase in surface resistance) over the studied ecosystem during the transition from rainy to dry season. A high evaporative fraction translates to lower boundary layer depth, whereas a low evaporative fraction results in the development of a deep, dry atmospheric boundary layer (Margolis and Ryan, 1997).

6 REGIONAL EVAPOTRANSPIRATION MODELING

6.1 Background

There is still a significant gap in our understanding of the status of the hydrologic cycle. One of such poorly understood processes includes the mechanisms governing evapotranspiration from land surfaces. Estimation of actual evapotranspiration (ETa) from standard meteorological parameters is an important issue in hydrology, water resources, and climatology. In computing evapotranspiration, the physics of energy and mass transfer at the land surface-atmosphere interface can be adequately modeled at small temporal and spatial scales (Parlange and Katul, 1992a; 1992b), yet the understanding of the processes at monthly, or seasonal, and regional scales required for use in hydrology, water management, and climate modeling is limited.

The most commonly used method of estimating actual evapotranspiration on an annual basis is the water balance equation applied over a watershed. This is given as the difference between precipitation and runoff. The drawback of this method lies in the fact that the underlying assumptions are almost impossible to verify. Such assumptions include (Szilagyi, 2001): (1) changes in water storage between hydrologic years are not significant; (2) no other sources of groundwater in the catchment exist except recharge from precipitation; and (3) the only groundwater sink is via base flow to the stream where runoff is measured. Furthermore, possible significant uncertainties in both precipitation and runoff measurements affect the accuracy of the ETa so computed.

There is therefore a need for models of regional evapotranspiration that incorporate the complex feedback mechanisms existing in the soil-plant-atmosphere system. Models based on Bouchet's complementary hypothesis (Bouchet, 1963) are examples of such models. Bouchet hypothesis states that over areas of regional extent and away from sharp environmental discontinuities, a complementary feedback mechanism exists between actual evapotranspiration (ETa) and potential evapotranspiration (ETp). That is, as moisture availability becomes limited, under conditions of constant energy input, ETa falls below its potential limit, leading to a corresponding increase in ETp. The main advantage of these kinds of models is that they do not require data on surface resistance, soil moisture content, or other land surface measures of aridity (Brutsaert and Stricker, 1979).

The two most widely known models incorporating soil-plant-atmosphere coupling are the Complementary Relationship Areal Evapotranspiration (CRAE) model (Morton, 1983) and the Advection-Aridity (AA) model (Brutsaert and Stricker 1979). Whereas the CRAE model has been tested and applied in different regions, including in a basin in Kenya (Morton, 1983, Hobbins et al. 2001a; 2001b, Szilagyi et al., 2001), the validity and applicability of the AA model in West Africa especially in the Volta Basin, is the subject of this study.

The study reported in this chapter evaluates the complementarity relationship hypothesis in the context of large-scale distributed surfaces and compares the performances of two versions of the AA model as proposed by Brutsaert and Stricker (1979). The specific objectives include: (1) computation and examination of the spatial distribution of the monthly evapotranspiration surfaces; (2) comparing the modeled actual evapotranspiration to the output from the *state-of-the-art* regional circulation model-MM5; (3) reformulating the AA model to make it applicable in West Africa; and (4) validating the reformulated AA model with an independent dataset over the Volta Basin.

6.2 Spatial patterns and the complementarity relationship structure with CRU data

Using a 25-year record (1936-1961) covering the period before the construction of the Akosombo dam, monthly maps of ETp, ETw and ETa were constructed using the input surfaces of average temperature, cloud cover and vapor. The monthly surfaces of ETp, ETw and ETa are presented in Figures 6.1, 6.2 and 6.3, respectively, as annual values with their cumulative density functions (cdfs). Figure 6.1 reveals well-delineated zones of ETp estimates. There is generally a latitudinal trend in the ETp estimates along the entire basin, with ETp ranging from about 1340 mm at the southern part of the basin to 2175 mm at the northeastern part in Burkina Faso. The average value for the whole basin is about 1800 mm, with a standard deviation of 213 mm and a coefficient of variation of about 12%. The cumulative density function for the ETp shows that over 50% of the basin has ETp values higher than 1800 mm. This shows that the atmospheric water demand is generally high, typical of semi-arid and arid tropical regions.

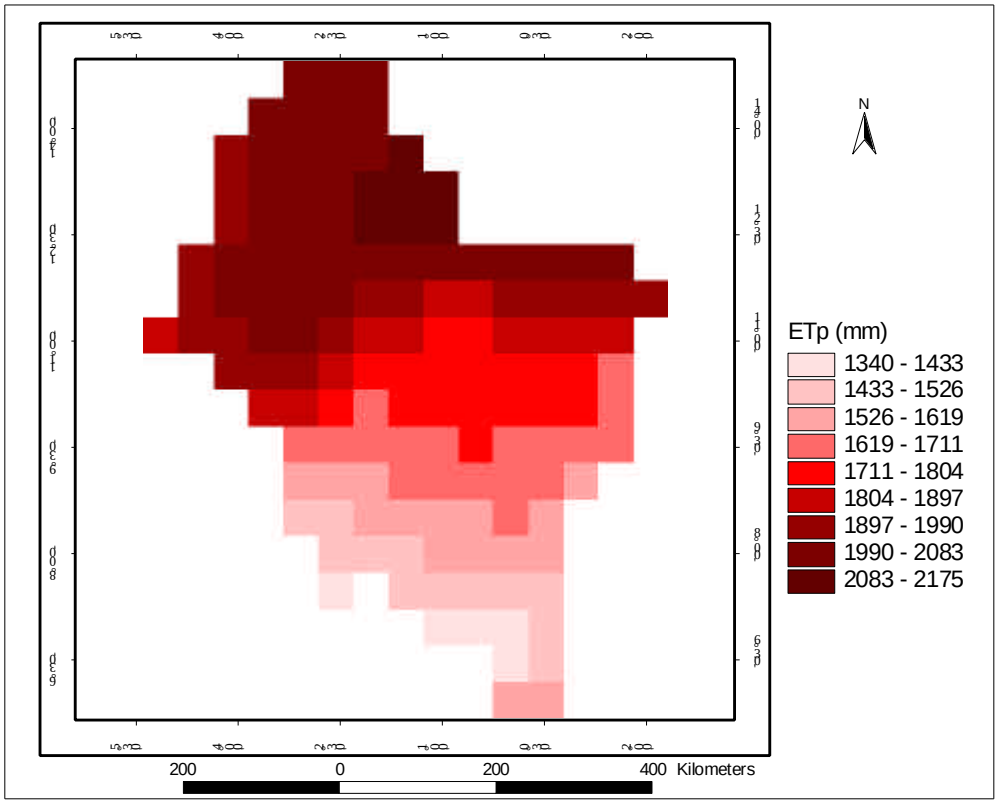

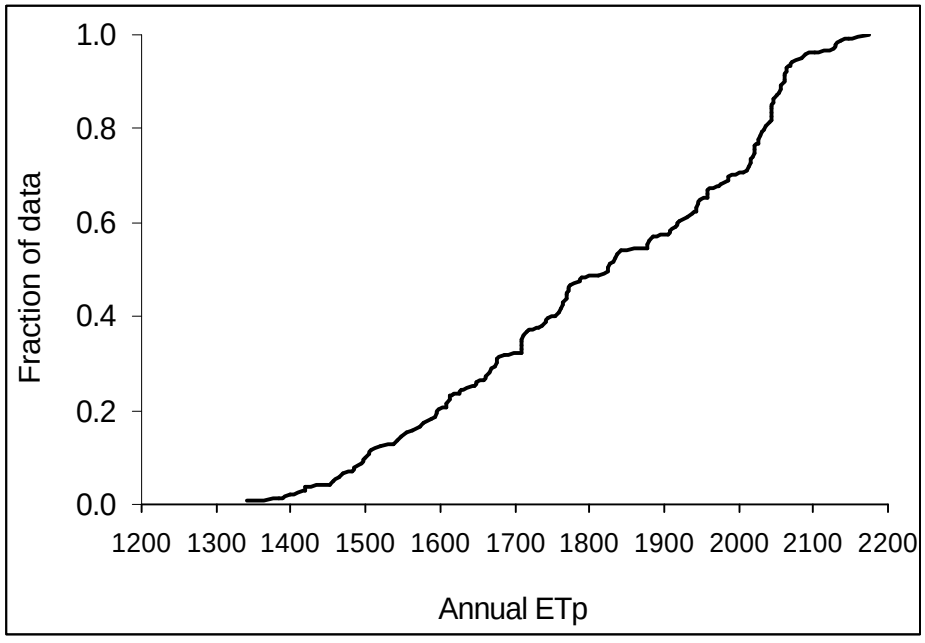

Figure 6.1: Spatial pattern of annual ETp over the Volta basin (1936-1961) and the cumulative distribution function (cdf) of annual Etp

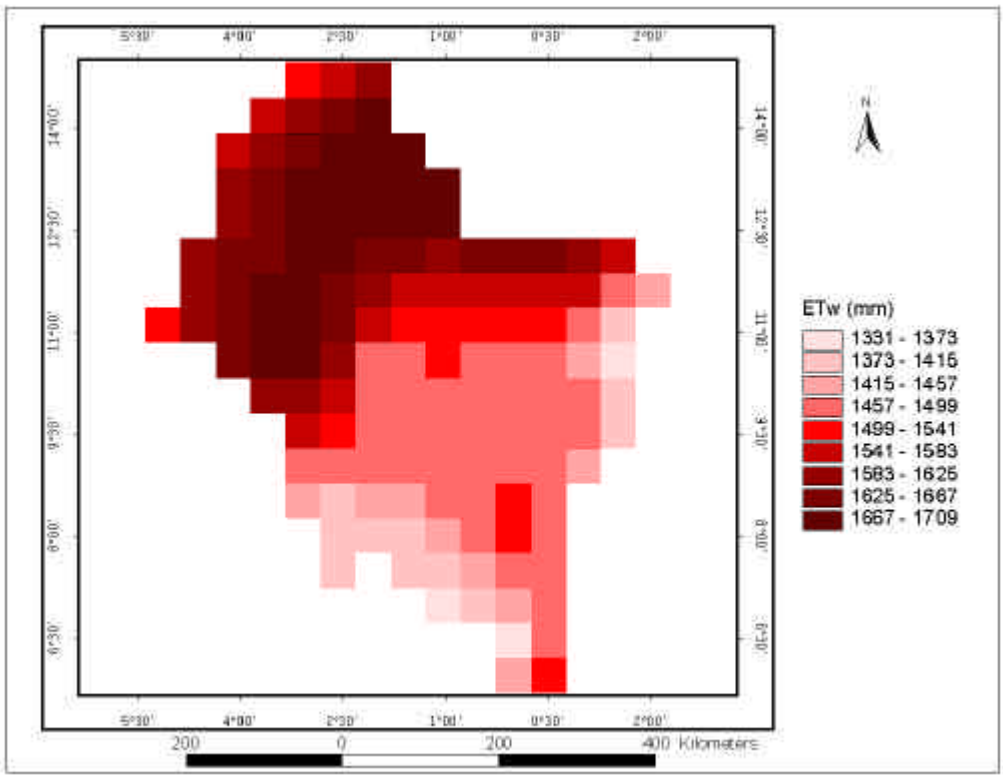

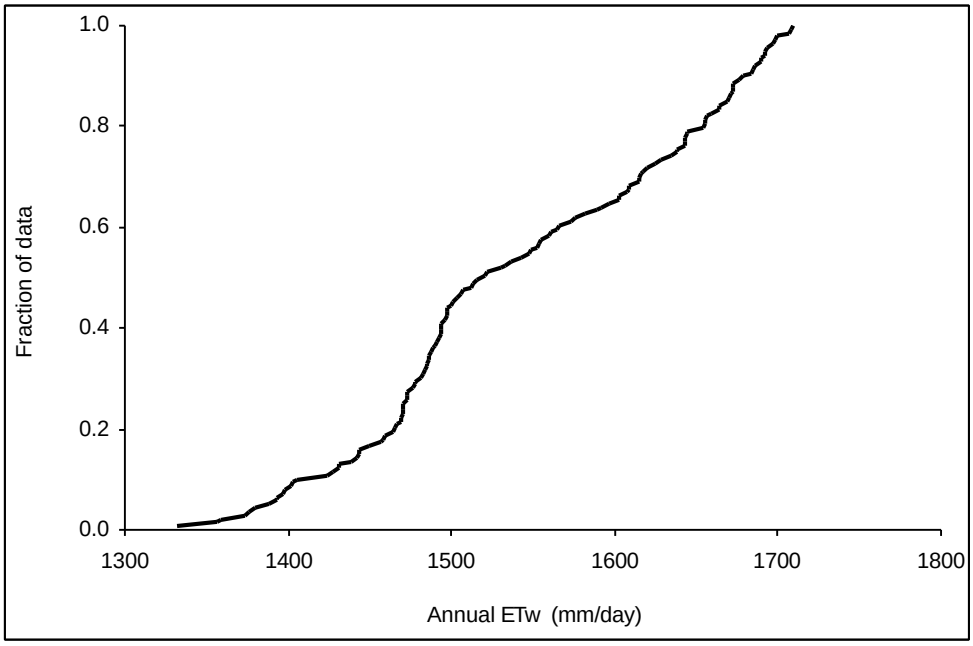

Figure 6.2: Spatial pattern of annual ETw over the Volta basin (1936-1961) and the cumulative distribution function (cdf) of annual ETw

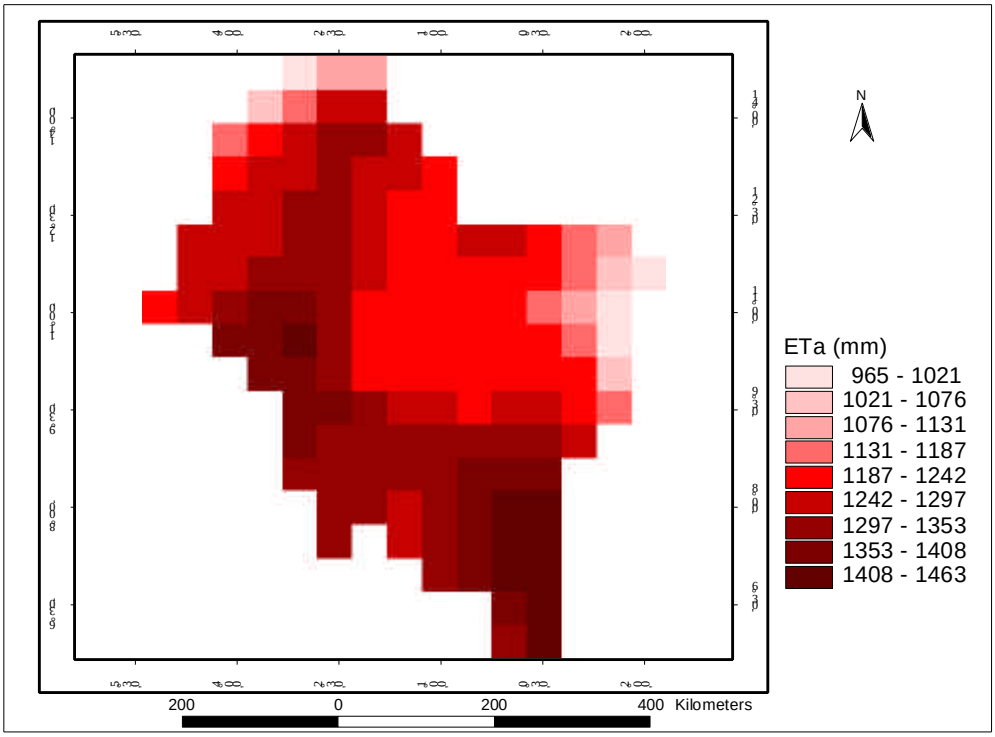

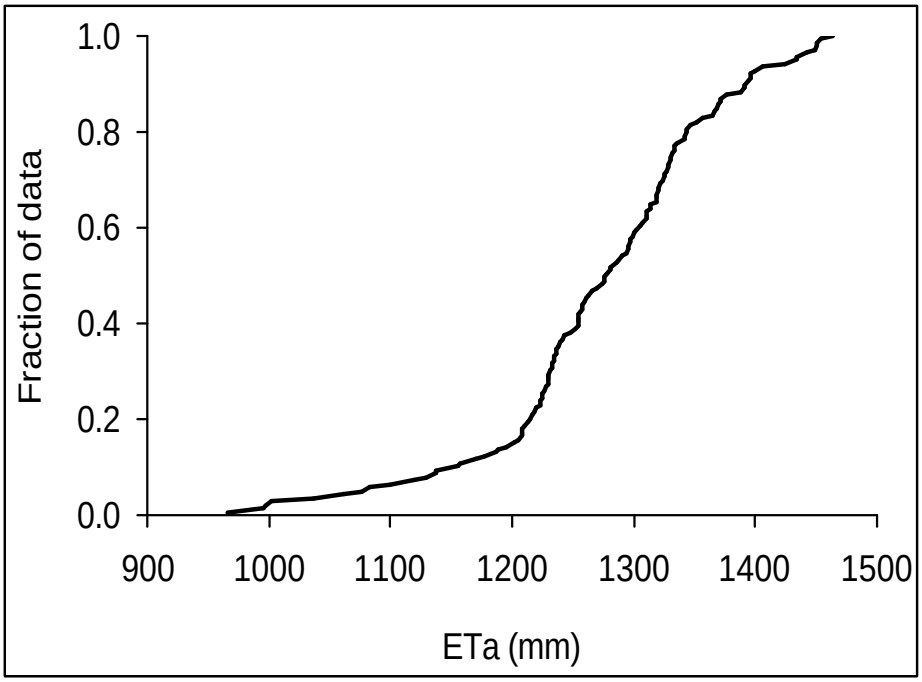

Figure 6.3: Spatial pattern of annual ETa over the Volta basin (1936-1961) and the cumulative distribution function (cdf) of annual ETa

The spatial pattern of ETw (Figure 6.2) is similar to that of ETp. ETw displays an increased value towards the more arid north of the basin. It ranges from about 1300 mm to 1700 mm, with an average of about 1500 mm and a CV of 6%. The cdf shows that 50% of the landscape has an ETw greater than 1500 mm. ETw shows a high correlation with ETp ($R = 0.89$). This may be because both models (Penman and Priestley-Taylor) used in the complementary relationship AA model to estimate ETp and ETw are largely dependent on the available energy.

The AA model predicts the highest values of ETa in the basin south around the Ghanaian town called Ada, which is closely bordered by the Gulf of Guinea. Figure 6.3 shows that ETa decreases north and east away from the Gulf and especially the small portions of Togo, Benin and Mali. The mean annual ETa for the whole basin was estimated as being about 1250 mm with 8% CV and a range of 960 mm to 1460 mm. The ETa cumulative probability distribution function (cdf) shows that about 20% of the basin evaporates close to 1200 mm depth of water per annum. The decreasing gradient up north is similar to the observed decrease in precipitation northwards, due to limited moisture availability. ETa exceeds precipitation in many of the pixels within the basin, indicating overestimation by the AA model, low values of precipitation from the CRU data set, or violations of the water balance assumptions.

A major interest of this study is to examine the existence of the complementary relationship between actual and potential evapotranspiration in the Volta Basin of West Africa. Figure 6.4 shows the relationship between average annual values of standardized ETa, ETp and precipitation. These standardized values were generated as the ratio of ETa, ETp and precipitation to ETw. The standardized precipitation component was used as a measure of moisture availability/ index. Although, a few outliers are present, the complementary structure is evident. The continuous lines relating standardized ET rates to standardized precipitation represent the locus of points that would correspond to strict complementarity.

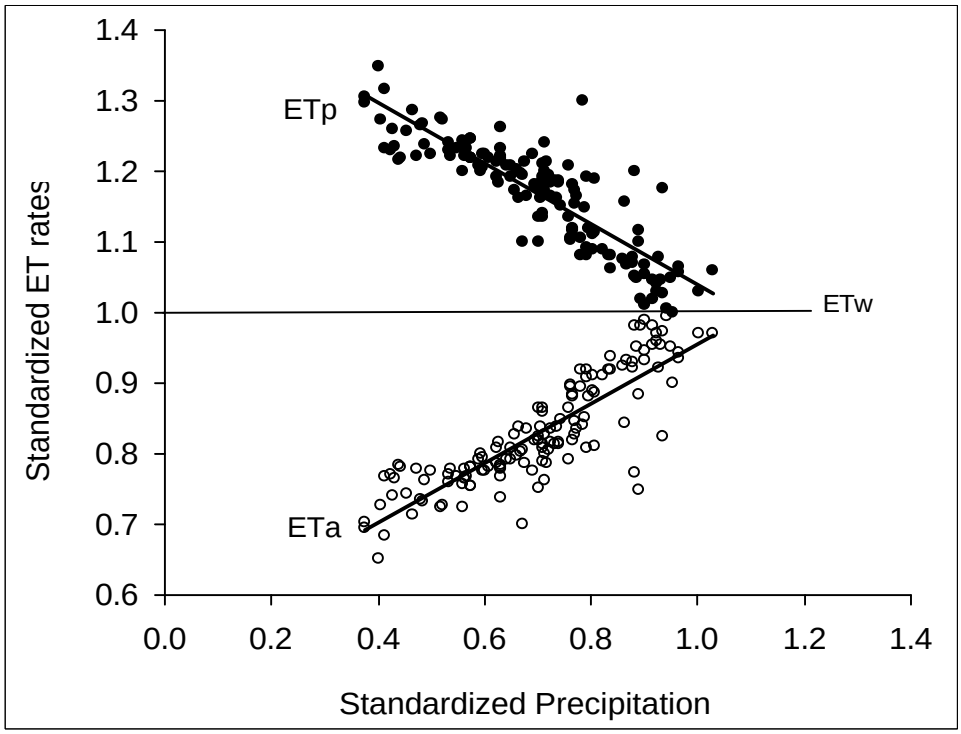

Figure 6.4: Complementarity relationship structure in the Volta Basin, West Africa

Figure 6.4 indicates a generally symmetrical structure between ETa, ETp and precipitation on an annual basis. The clustered points around the horizontal line drawn to represent the ETw were identified as pixels on the water bodies in which the upper limit of ETa was probably reached; otherwise on an annual and regional basis, natural land surfaces will not approach saturation, thereby keeping the ETa below its maximum limit of ETw.

6.3 Monthly patterns of the complementarity relationship components

A finer resolution (12 km x 12 km) gridded data set produced from the hindcasting simulations by a regional climate model, the MM5 community model (Kunstmann, 2002), was used as input to the AA model versions 1 and 2. Version 1 (referred to as AA1) used the Priestley-Taylor formula to compute ETw, whereas version 2 (referred to as AA2) used the ETw derived from the energy balance as proposed by Brutsaert and Stricker (1979). AA2 has, to the best of the author's knowledge, not been tested since

its recommendation. Formulation for AA2 is given in Chapter 4. Hence 1 and 2 herein denotes the ETw and ETa computed by the two versions of AA model, respectively.

The modeled seasonal (monthly) potential evapotranspiration maps are presented in Figure 6.5. Starting from the month of April, the onset of rain for the southern portion of the basin covering the transition zone of Ghana including the Ashanti and Brong Ahafo regions of Ghana, ETp ranges from about 4 mm/day to about 7 mm/day with the values generally increasing with latitude. Large patches in the order of 4.5 mm/day spread along the coastline and around the Volta Lake to the right of the lower side of the study area. In May, apart from pockets of higher value ETp (about 8 mm/day) spread between Latitude 13^0 N and 14^0 N, there are generally three distinct ETp classes showing an almost similar pattern with slightly lower values. There is a clear seasonal trend in the ETp.

During the rainy months, June-October, there is a gradual decrease in ETp values with negative latitudinal trends, whereas, between November and January there is a reversal of the trend. During the dry period between November and January, the ETp is generally lower in absolute values compared to the rainy season. There seems to be a significant attenuation of solar radiation, and hence the available energy, over a large portion of the basin during this period. This may be attributed to (1) the influx of the northeasterly trade wind entering the basin through the northern part (Walker, 1962) and (2) the influence of seasonal changes in surface albedo earlier reported in this study. This wind is hot and highly laden with dust and haze from the Sahara desert and is popularly referred to as the harmattan. This tends to prevent the solar radiation from reaching the soil surface and therefore has implication for energy availability at that surface. The pocket and patches in the complicated pattern may be the result of the terrain complexity and/or the land-use pattern present across the study area.

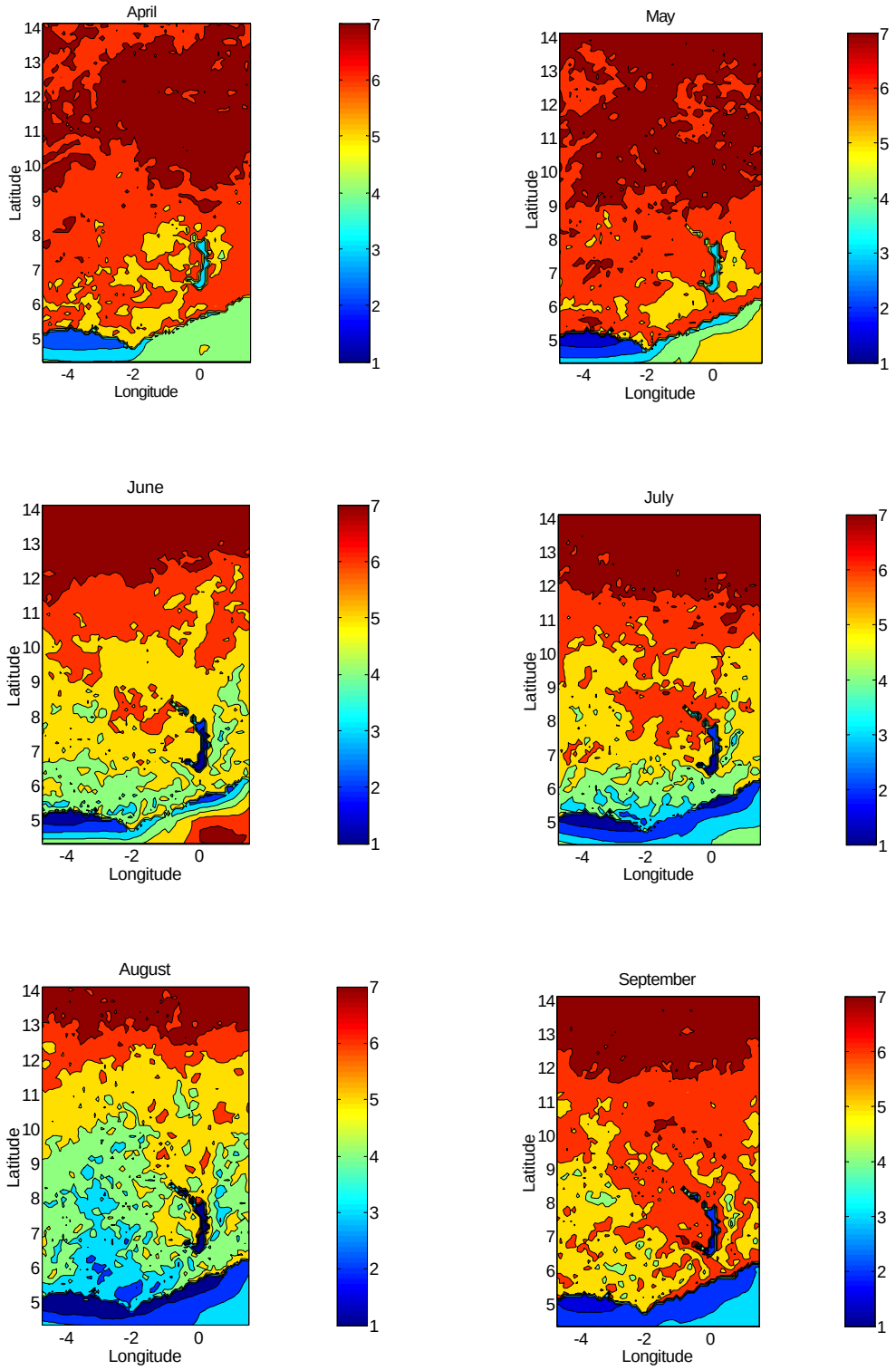

Figure 6.5: Monthly potential evapotranspiration maps showing seasonal variation

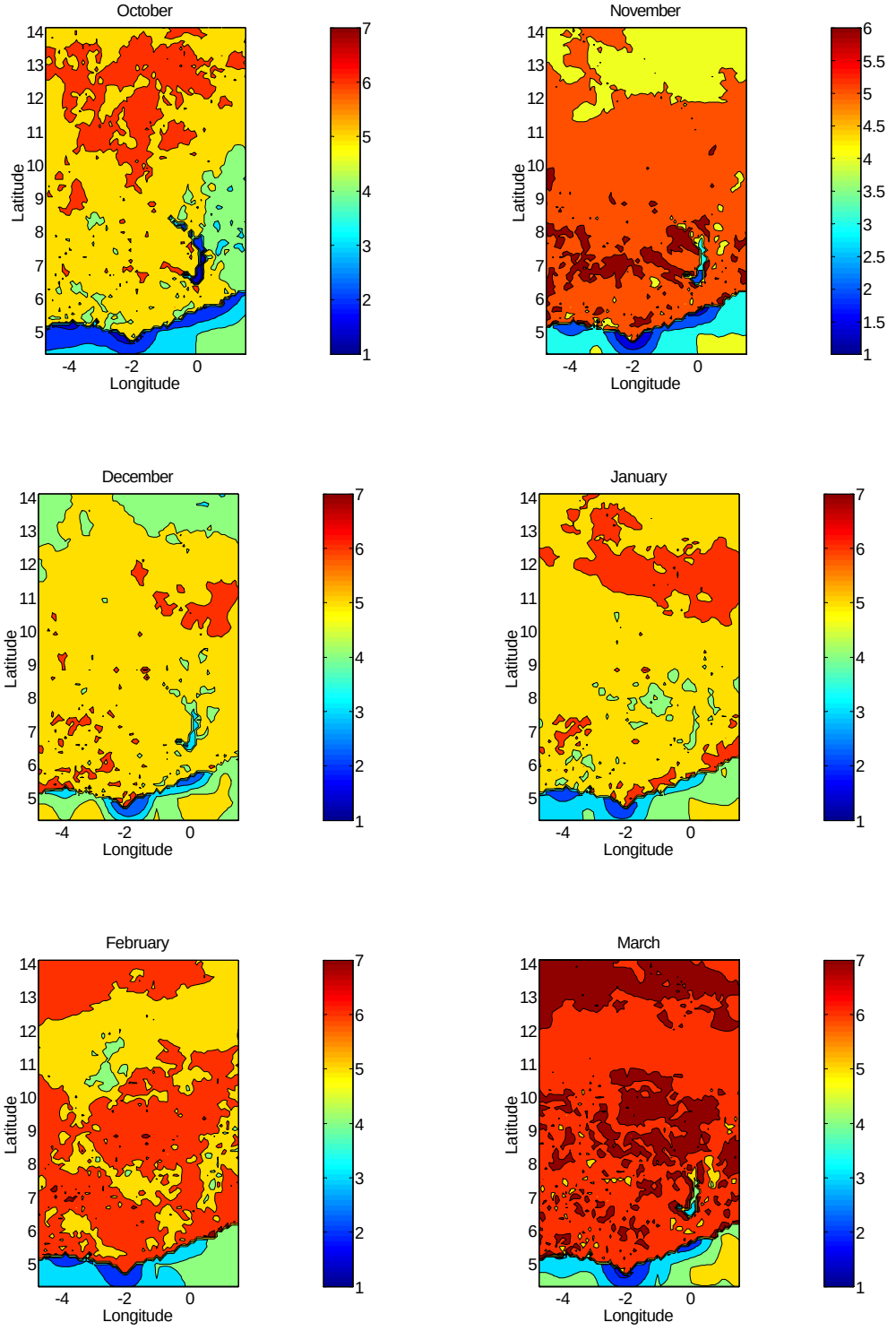

Figure 6.5: Continued

Figures 6.6 (a-n) show the monthly distribution of ETw, ETa and the differences computed with AA1 and AA2. The predicted ETw and ETa appear to be seasonally

influenced. In April and May, which are the onset of rains, over a larger part of the basin both ETw and ETa are negatively correlated with the latitude, showing higher values along the moisture gradient. The ETw1 was consistently higher than the ETw2 in more than 90 % of the landscape, which directly led to higher estimates of ETa1 and produced a range of differences in the order of –0.05 mm/day to 0.3 mm/day. From June onwards, the trends in modeled ETw and ETa start to change in the reverse direction, with higher ETw up north and lower down south of the basin. It then becomes more pronounced as the rainy season progresses until October, when it was observed that the pattern started to change again to the earlier observed trends. Between November and March, the ETw and ETa maps are very distinct in their spatial pattern and also similar to the pattern in April and May. The order of magnitude of differences in ETw for the two models was –0.02 mm/day to 0.16 mm/day yielding a corresponding of ETa –0.05 mm/day to 0.35 mm/day. The spatial pattern clearly indicates that ETa and ETw are generally influenced along the axis of moisture gradient/availability. For example, during the transition and dry months (November to March) the availability of moisture decreased with increasing latitude, and this directly dictates the pattern of the ETw and ETa, thus the available moisture determines the ET rates. But during the rainy season, when almost everywhere in the basin the moisture supply is ample, the available energy, which obviously is higher up north, dominates the ET processes leading to higher absolute values of ETw and ETa. Furthermore, AA1 and AA2 models predicted the lower differences during the dry season. These suggest that the two models predict ETa closely during the dry than the wet months.

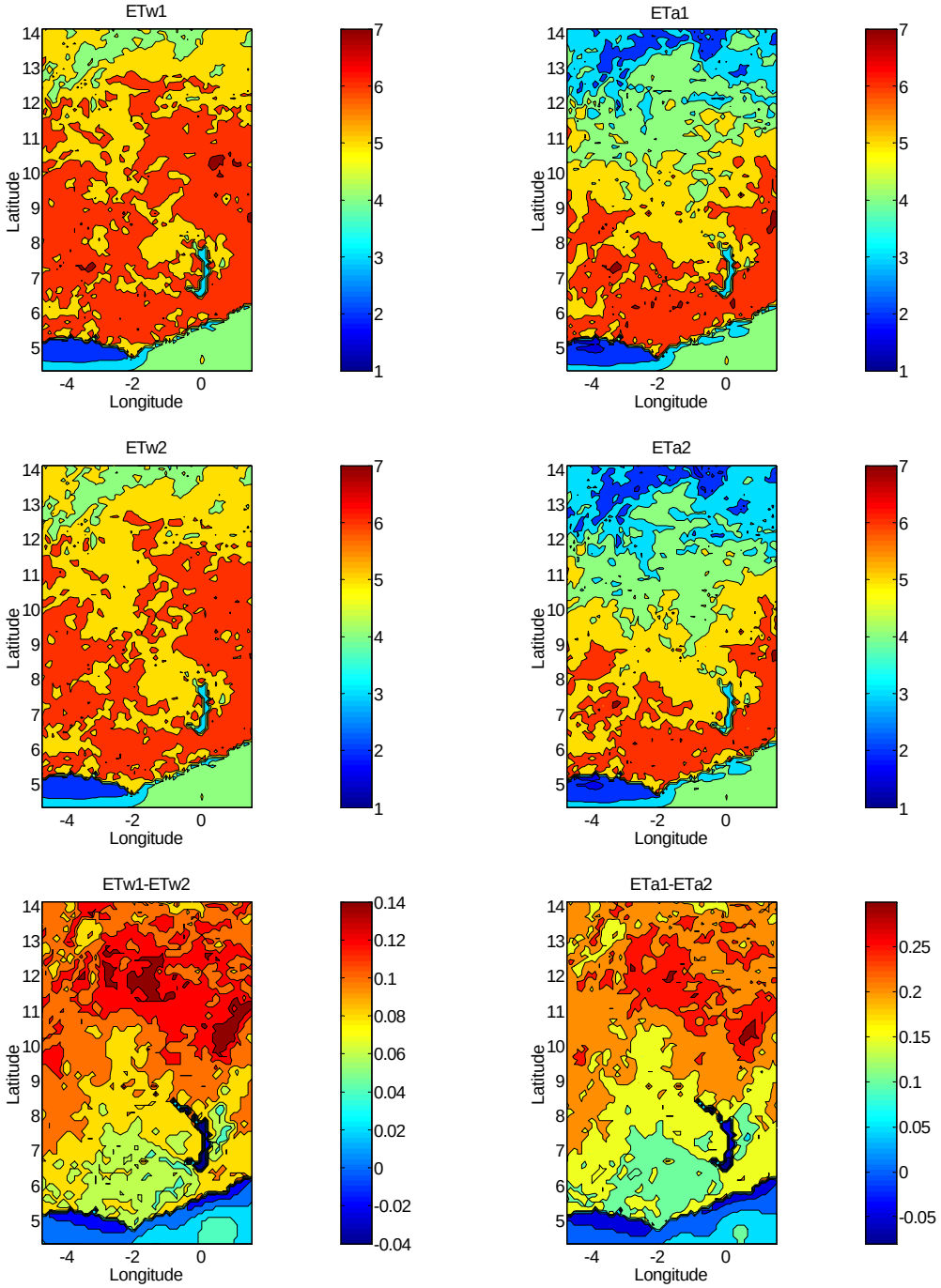

Figure 6.6a: April 2002 wet environment and actual evapotranspiration computed using AA1 and AA2. Estimated differences are presented as the third map of each column.

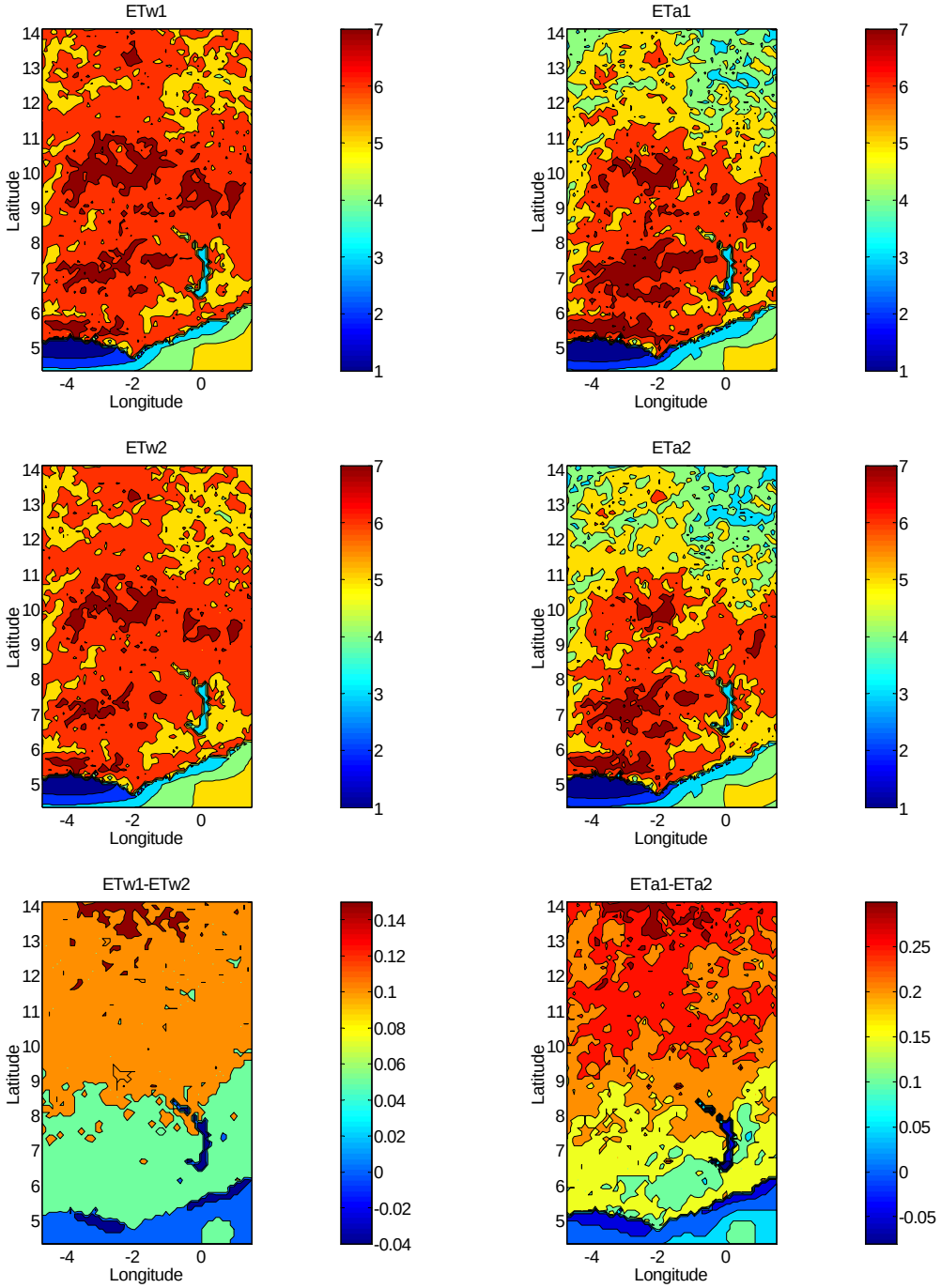

Figure 6.6b: May 2002 wet environment and actual evapotranspiration computed using AA1 and AA2. Estimated differences are presented as the third map of each column.

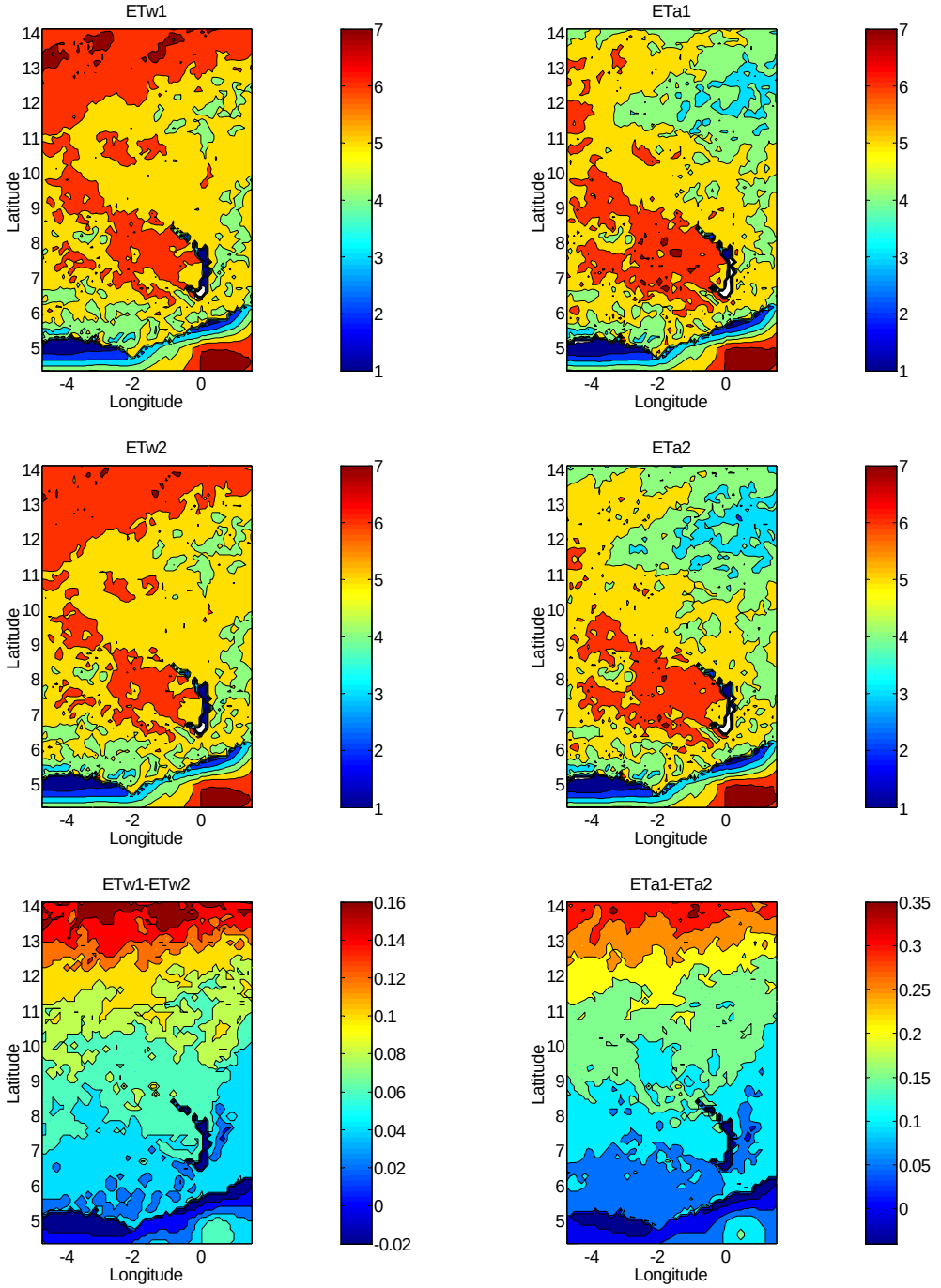

Figure 6.6c: June 2002 wet environment and actual evapotranspiration computed using AA1 and AA2. Estimated differences are presented as the third map of each column.

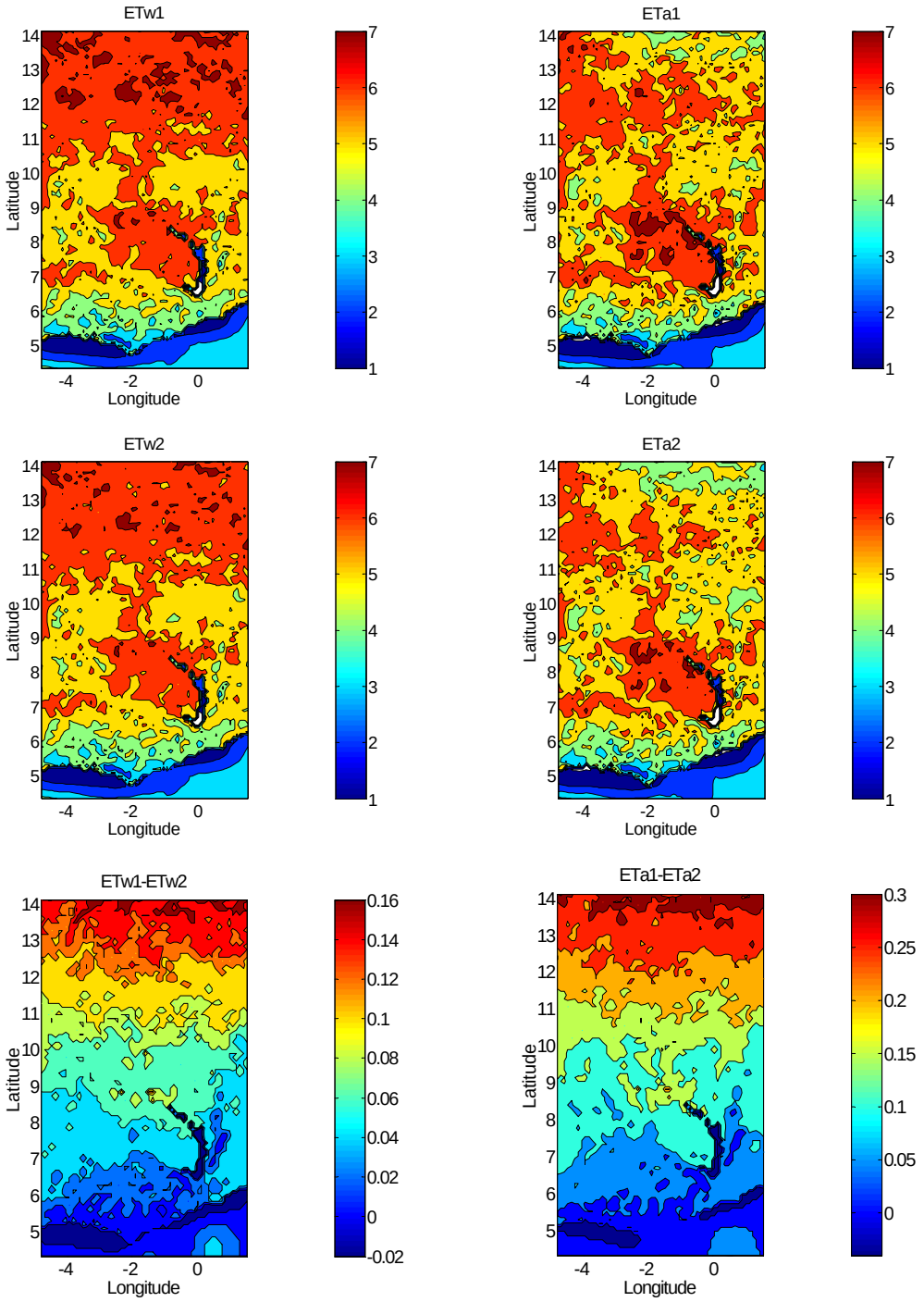

Figure 6.6d: July 2002 wet environment and actual evapotranspiration computed using AA1 and AA2. Estimated differences are presented as the third map of each column.

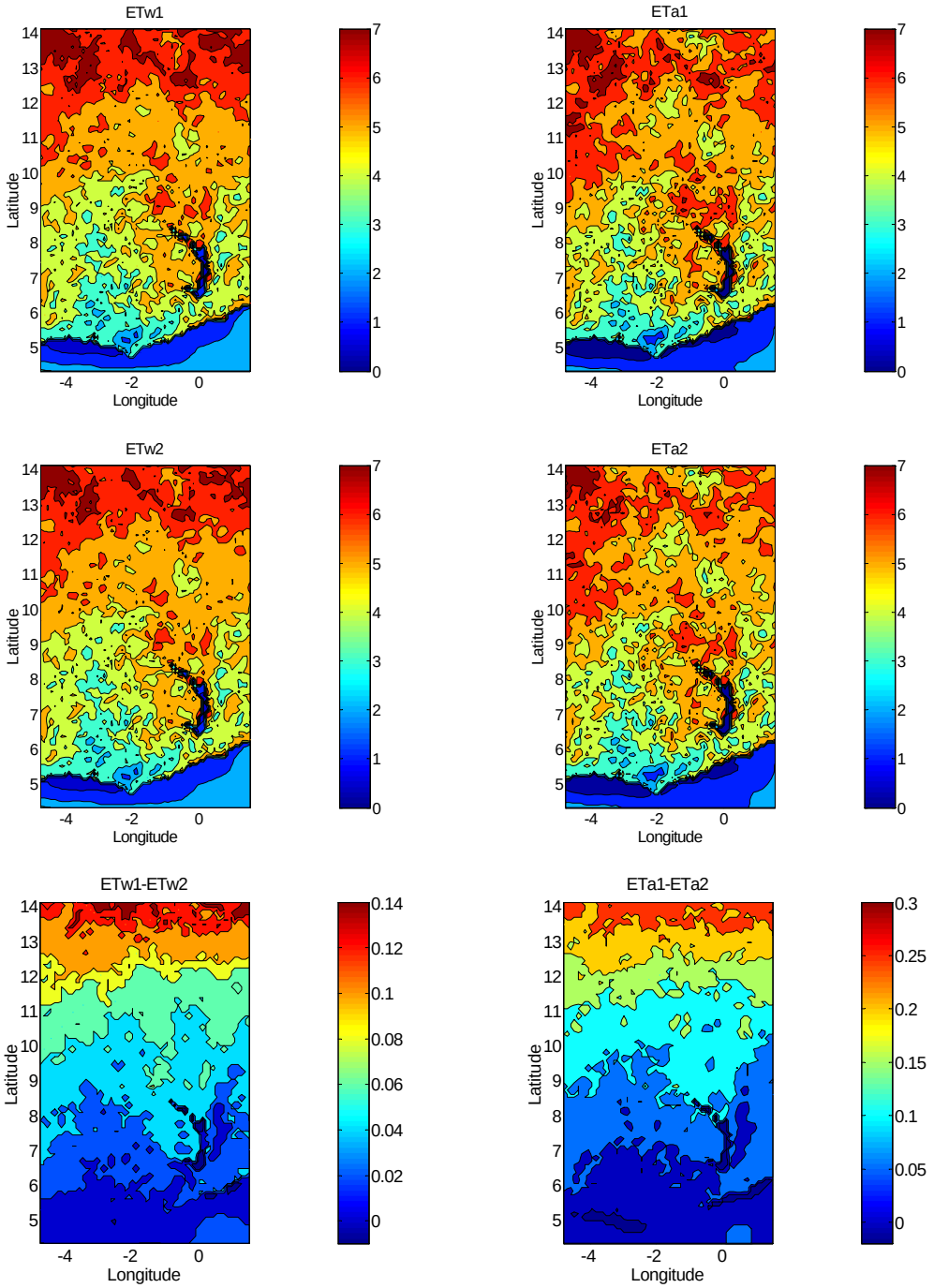

Figure 6.6e: August 2002 wet environment and actual evapotranspiration computed using AA1 and AA2. Estimated differences are presented as the third map of each column.

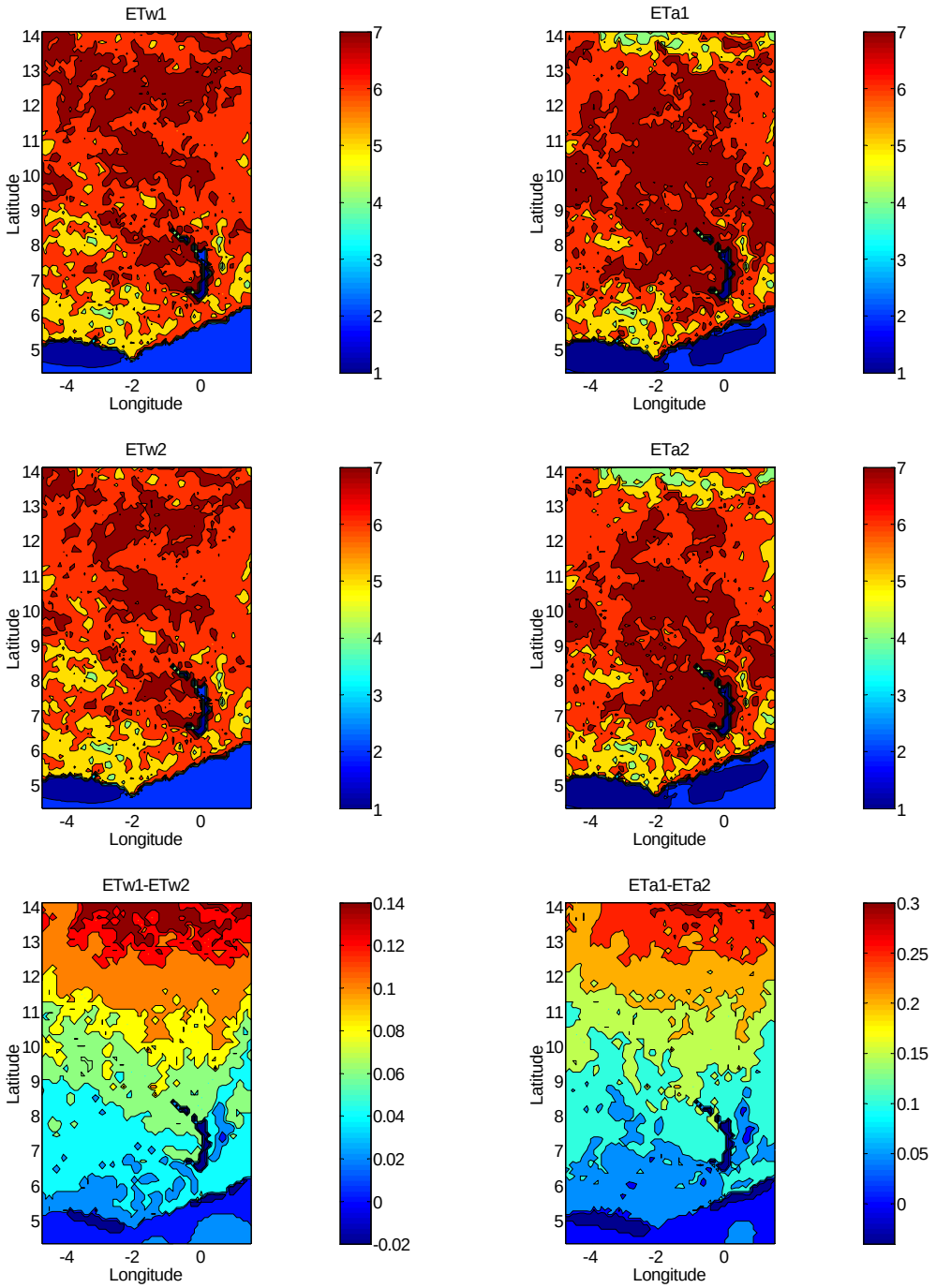

Figure 6.6f: September 2002 wet environment and actual evapotranspiration computed using AA1 and AA2. Estimated differences are presented as the third map of each column.

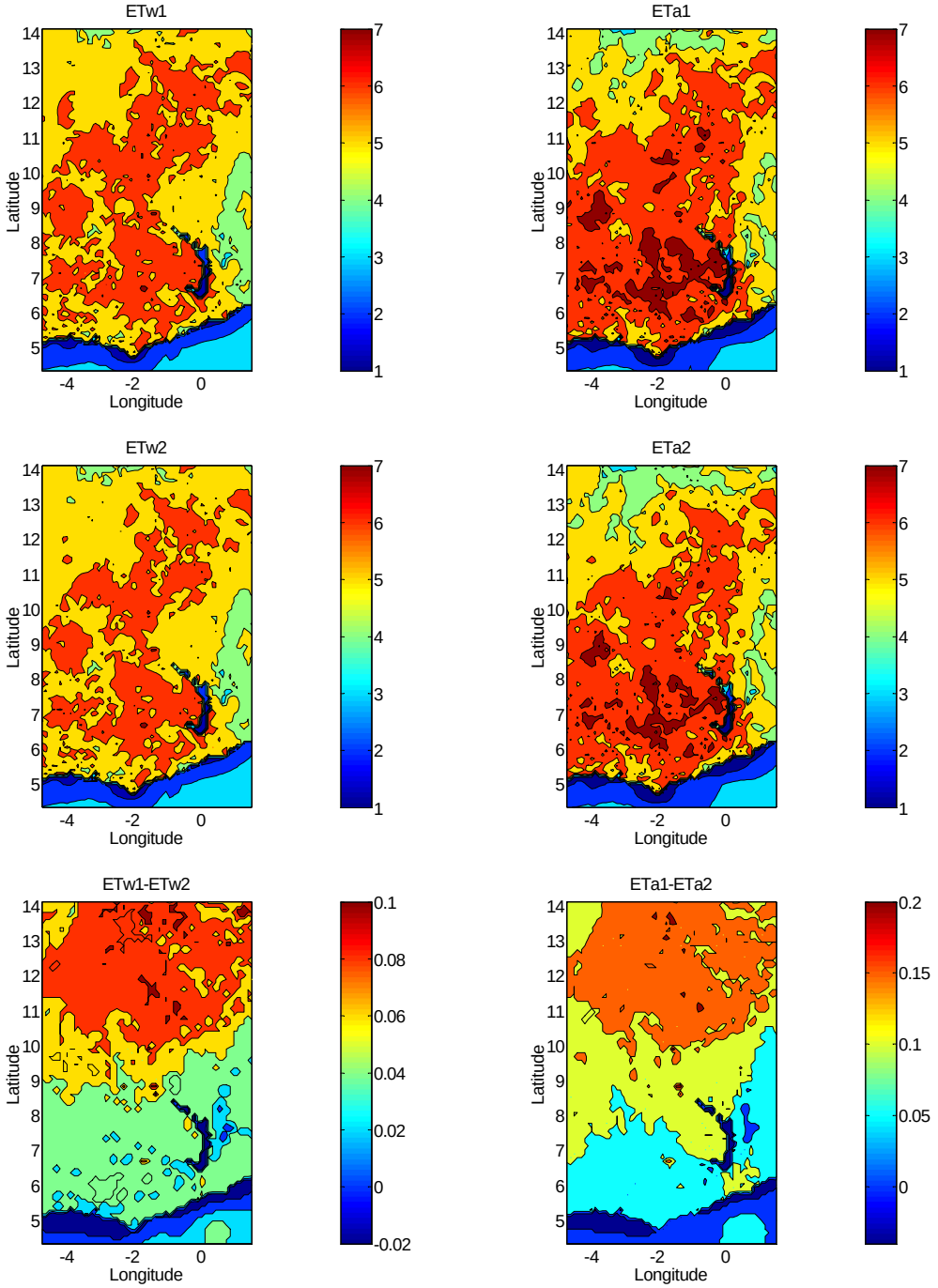

Figure 6.6g: October 2002 wet environment and actual evapotranspiration computed using AA1 and AA2. Estimated differences are presented as the third map of each column.

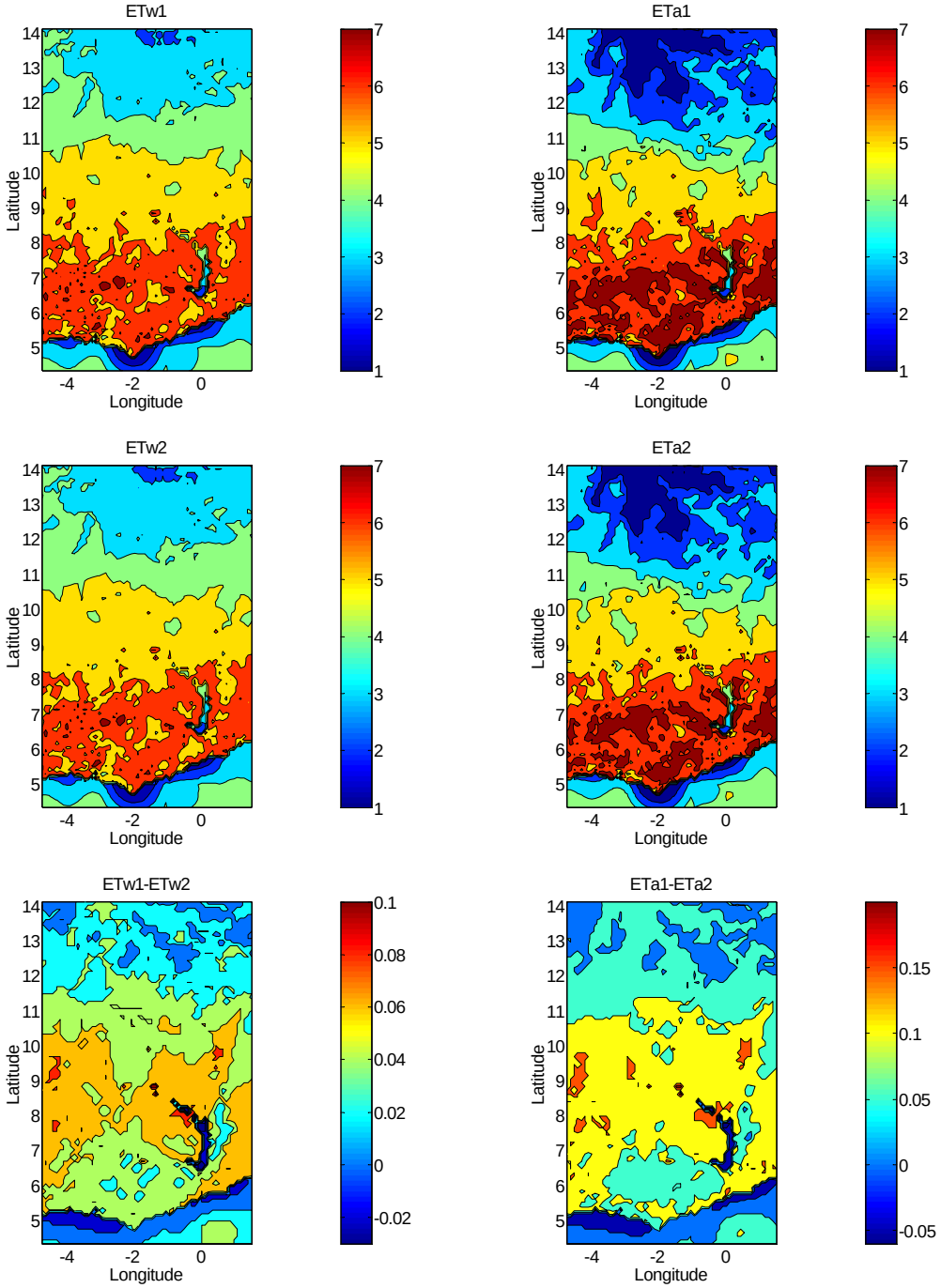

Figure 6.6h: November 2002 wet environment and actual evapotranspiration computed using AA1 and AA2. Estimated differences are presented as the third map of each column.

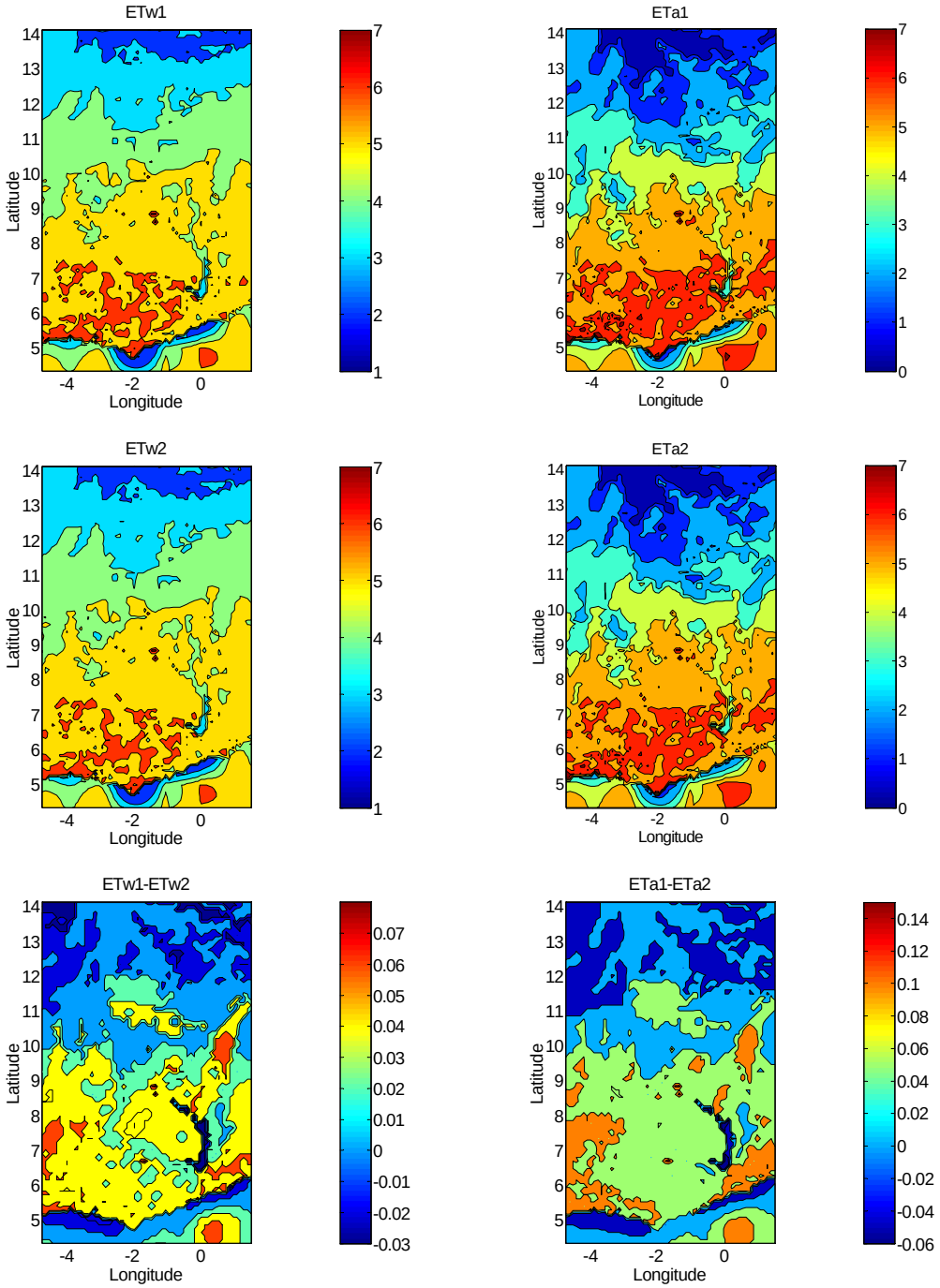

Figure 6.6i: December 2002 wet environment and actual evapotranspiration computed using AA1 and AA2. Estimated differences are presented as the third map of each column.

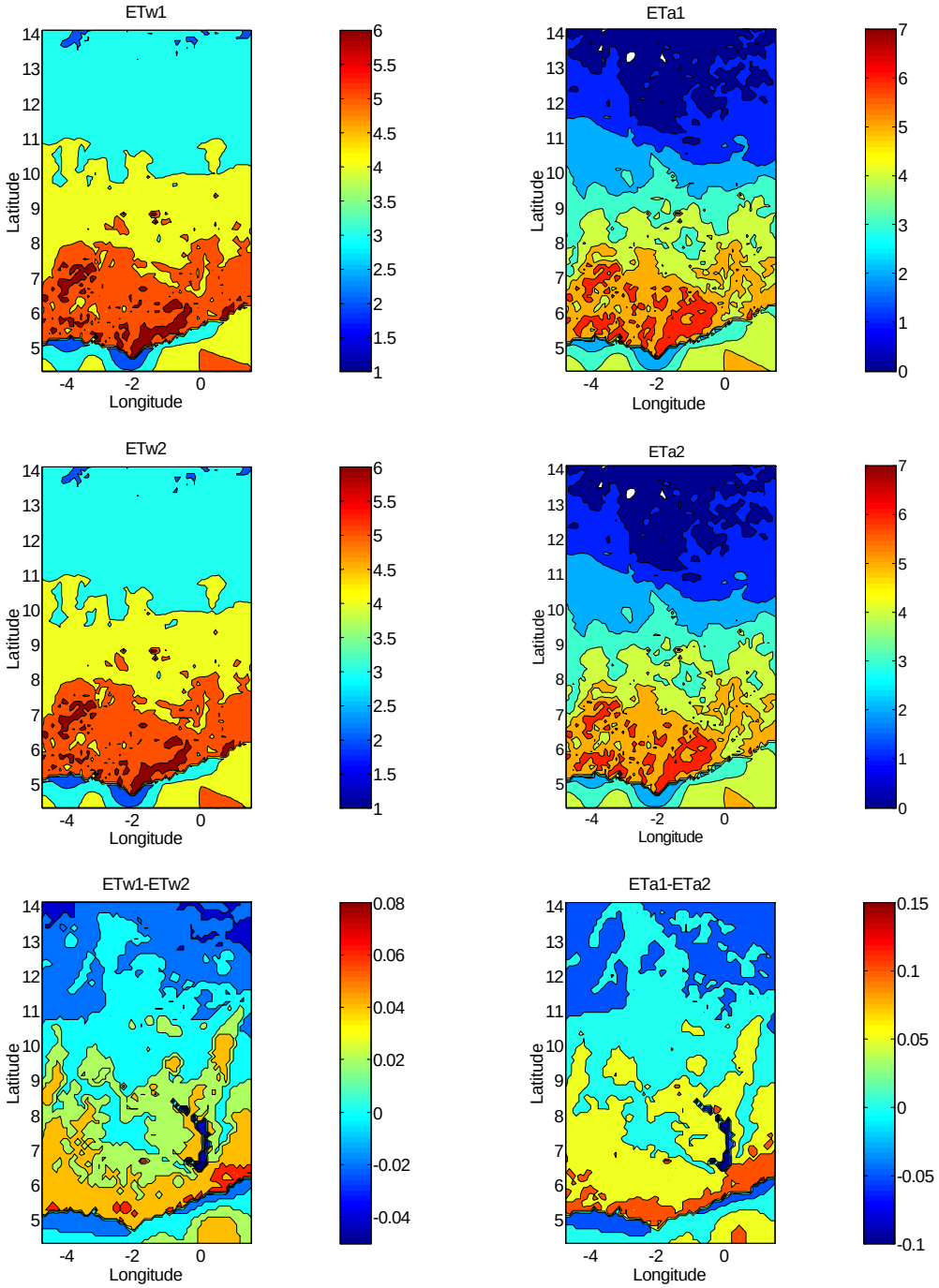

Figure 6.6j: January 2003 wet environment and actual evapotranspiration computed using AA1 and AA2. Estimated differences are presented as the third map of each column.

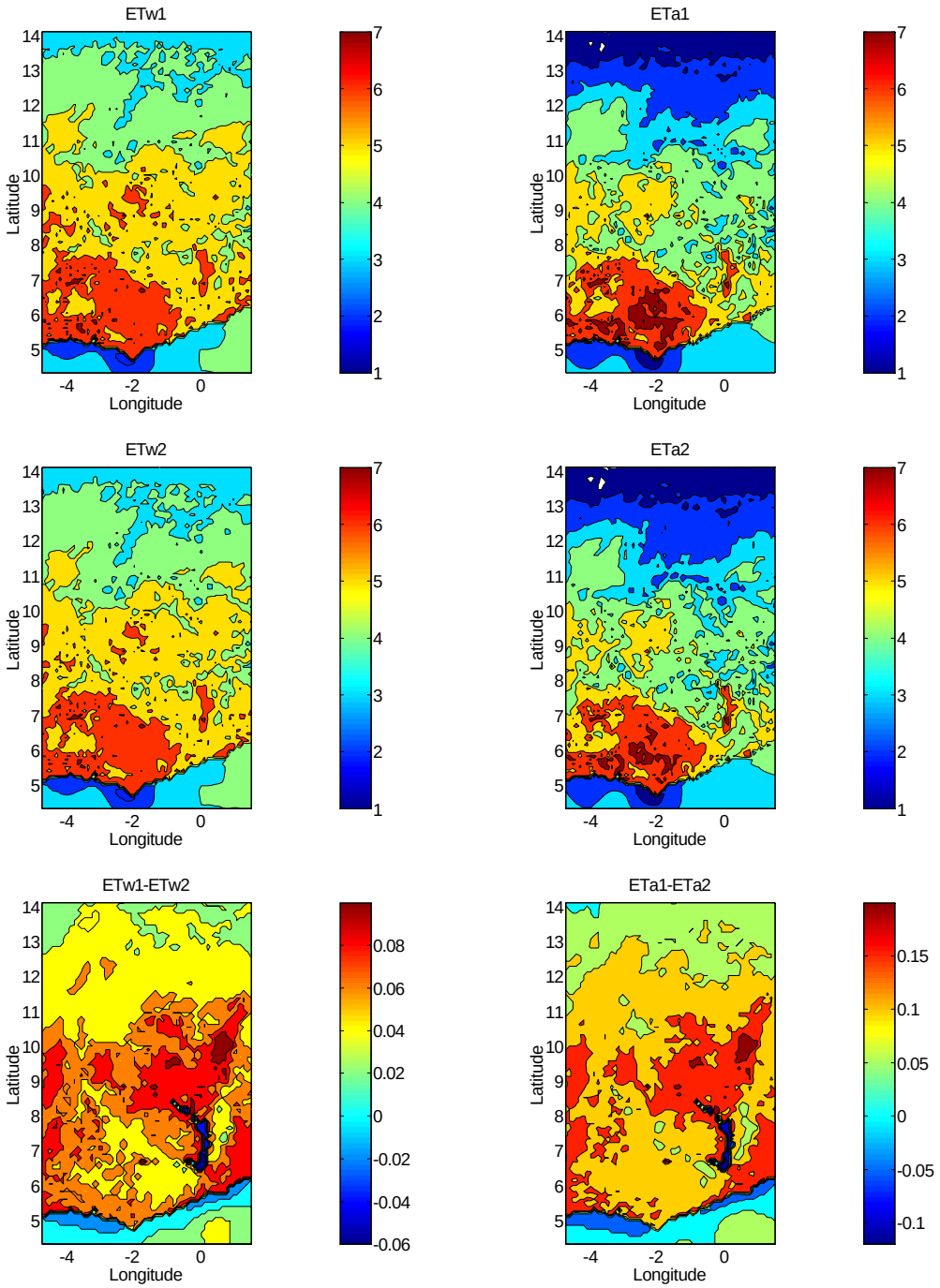

Figure 6.6k: February 2003 wet environment and actual evapotranspiration computed using the two forms of the Advection-Aridity model. Estimated differences are presented as the third map of each column.

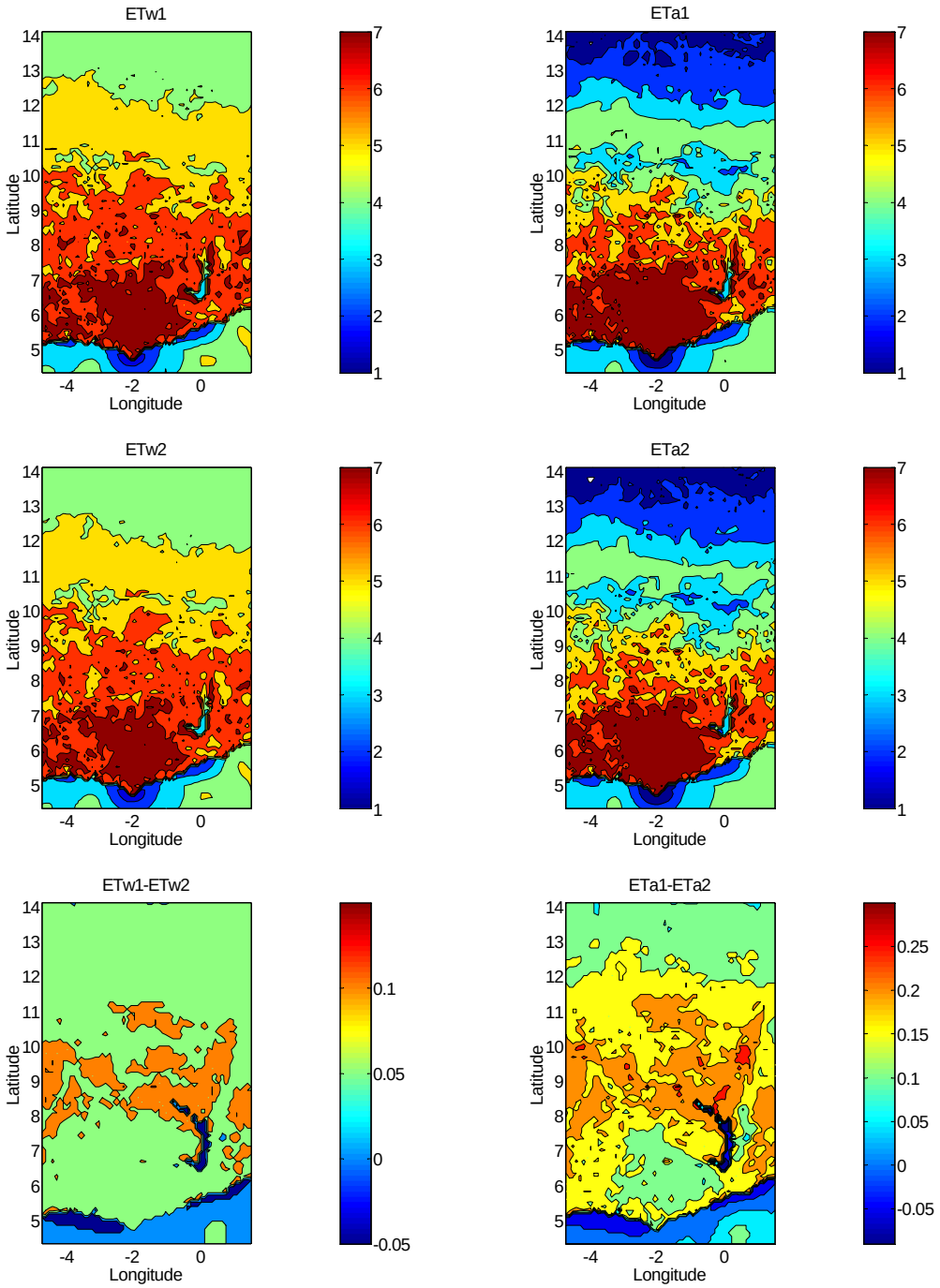

Figure 6.6l: March 2003 wet environment and actual evapotranspiration computed using AA1 and AA2. Estimated differences are presented as the third map of each column.

6.4 Comparison of actual ET estimates with independent measures

Comparisons are presented between ETa estimates and the corresponding actual evapotranspiration values denoted by ETmm5, which were obtained by the energy balance approach as simulated in the MM5 regional circulation model. Figure 6.7 shows the 1:1 relationship between the ETa(s) and the ETmm5 for two representative months (February and August) and annually. The outliers are values from the water bodies.

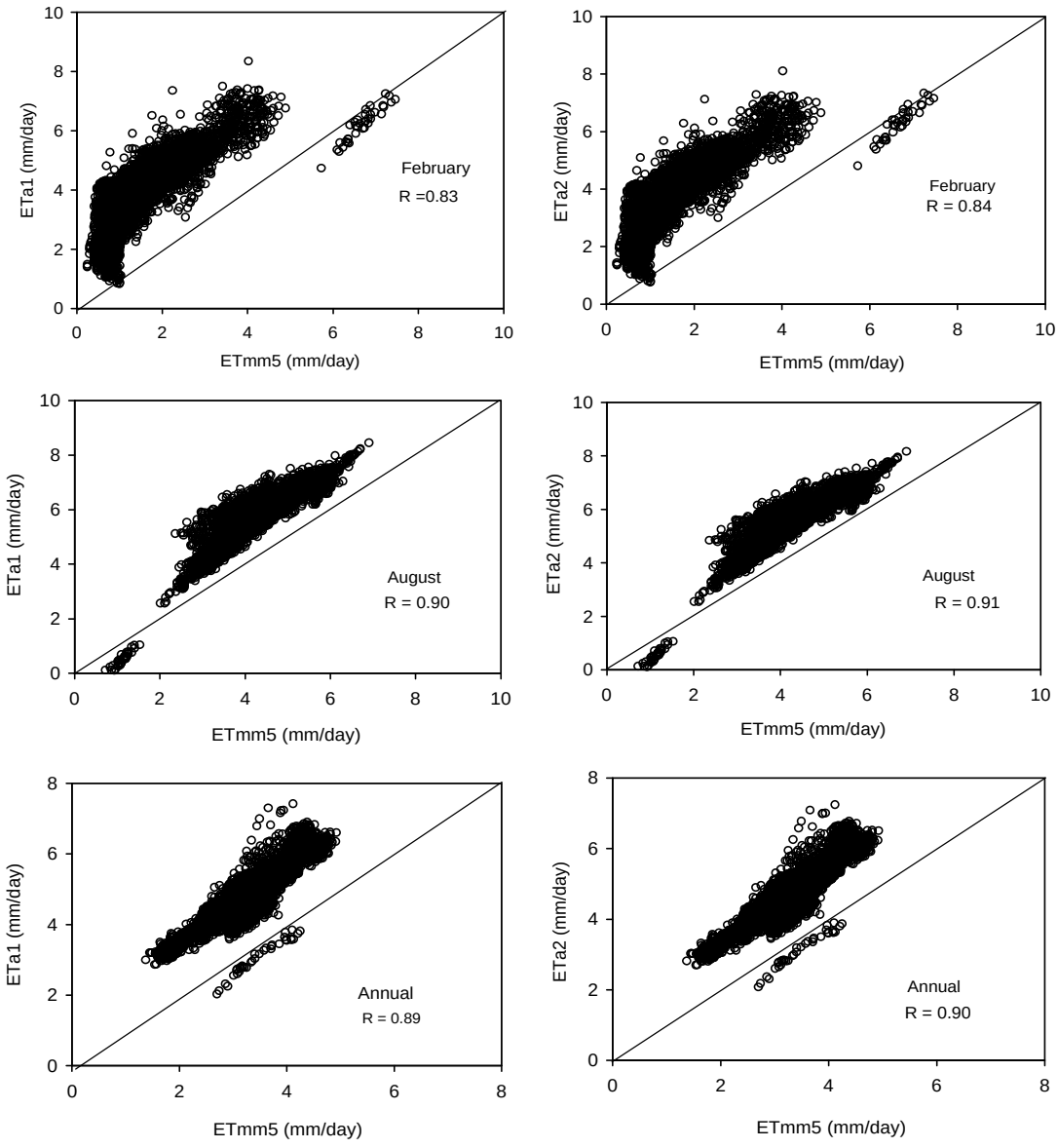

Figure 6.7: Graph of 1:1 line to compare the estimated ETa with ETmm5.

Both ETa1 and ETa2 are significantly ($p < 0.05$, $n > 4000$) related to ETmm5 with R = 0.82 and 0.83 in February, R = 0.90 and 0.91 in August, and R = 0.89 and 0.90, for the whole year. Ideally, all the points should lie on the 1:1 line shown on the graphs or be normally distributed around the line with a low variance. But the observed pattern here shows that the two version of the AA model consistently overestimate the ETmm5, as 99% of the data lie above the 1:1 line. Monthly averages of all the pixels for 2 years are presented as bar charts in Figure 6.8.

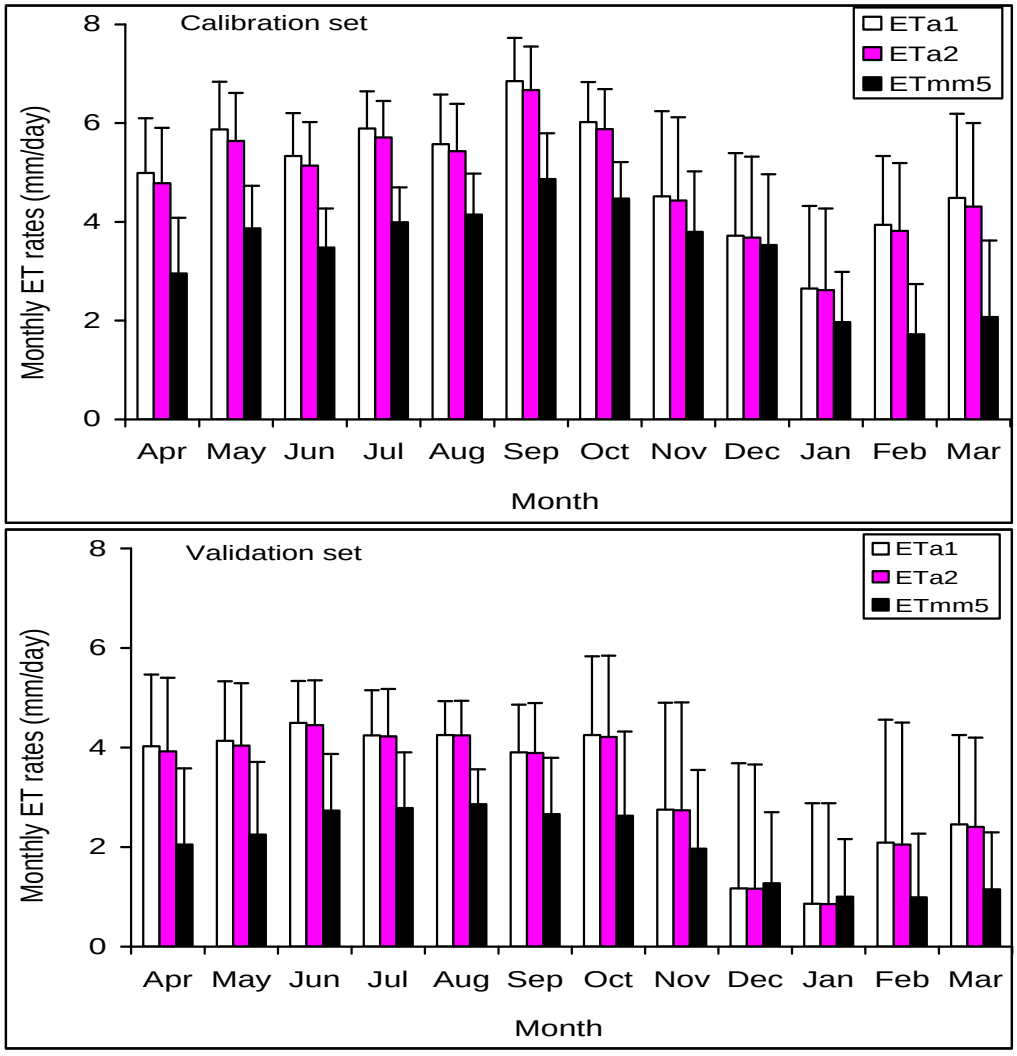

Figure 6.8: Monthly average ETa by AA1 and AA2 compared with ETmm5. Vertical spikes show one standard deviation.

Although the overestimation occurred throughout the season, the rate was reduced during the period of November to January. This observation was consistent for

the two years. Computed standard deviations are presented together with the bar as vertical spikes. As clearly indicated, rainy months are characterized with lower standard deviations compared to dry months. This may be because increased moisture availability tends to reduce the heterogeneity of the ET rates, which is then governed by available energy. In addition, the monthly Root-Mean-Square-Error (RMSE) of ETa estimates range from 1.05 mm to 2.03 mm for AA1 as compared to 1.05 mm to 1.93mm for AA2. This shows a slightly better performance of the AA2 tested herein.

6.5 Reformulation of the Advection-Aridity models

The recorded positive bias and overestimations for ETa indicate a necessity for improvement of the AA model. By examining the simple expression of the complementarity hypothesis, i.e., ETa = 2ETw-ETp, the first point of call is to examine and recalibrate if necessary models used in estimating the wet environment evapotranspiration. Thereafter the ETp parameterization can be examined. Before commencing the refinement of the AA model, the residuals of ETa(s) and ETmm5 (Res1 = ETa1-ETmm5, Res2 = ETa2-ETmm5) were related to a few basin-wide parameters: basin elevation, vapor pressure deficit, and wind speed. Both residuals exhibit a negative correlation with elevation (R^2 = 0.03 and $p < 0.05$). Similarly, Res1 and Res2 show a negative relationship with the basin vapor pressure deficit (R^2 = 0.10, 0.13, respectively and $p < 0.05$). The effect of wind speed on the performance of the AA model was evident as Res1 and Res2 show (Figure 6.9) a strong negative correlation with wind speed (R^2 = 0.34, 0.37 and $p < 0.05$). Thus, one of the refinements considered for improving the AA model is reparameterization of the wind function.

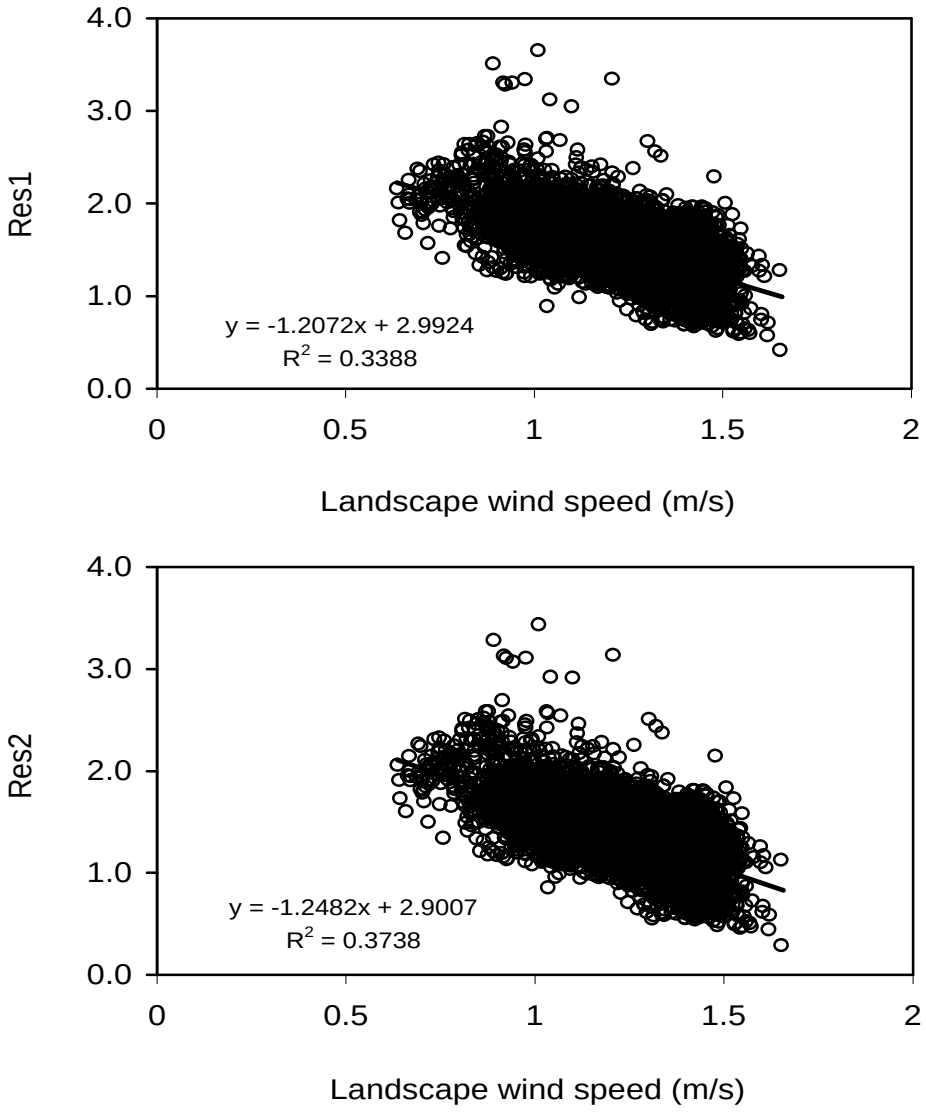

Figure 6.9: ETa residuals versus mean annual landscape wind speed (Res1= ETa1-ETmm5 and Res2 = ETa2-ETmm5).

6.5.1 ETw recalibration

On the basis of the high overestimation shown in Figures 6.7 and 6.8, it seems that the ETw models have over-prediction tendencies, and hence the need to recalibrate the Priestley-Taylor coefficient (α_{PT}) and parameters a_e and b_e in order to remove the positive bias. Decreasing ETw will consequently reduce ETa. Using a Levenberg-Marquardt least-square parameter estimation algorithm, and substituting ETmm5 in place of ETa1 and ETa2, α_{PT}, a_e and b_e were optimized. The algorithm iterates with the initial guess (taken as the original values in the AA model) and continues until the best feasible solution that corresponds to the minimum sum of the square error (SSE) is

attained. The first year data set (April 2002 to March 2003) was used for the calibration and is thereafter referred to as the calibration set.

The regional seasonally optimized parameters are presented in Table 6.1. The values of α_{PT} varied seasonally and ranged from 1.00 - 1.22 compared to 1.26 - 1.28 suggested in the literature (Brutsaert and Stricker, 1979). Lowest values were obtained for the months of February and March and the highest for the harmattan months – November, December and January. In contrast, November – January has lowest values of a_e and b_e, with b_e having negative values in 9 out of the 12 months.

Table 6.1: Seasonal optimal parameters for ETw equations used in AA1 and AA2 models

Month	AA1 (1)	AA2 (1)		AA1 (3)	AA2 (3)	
	α_{PT}	a_e	b_e	α_{PT}	a_e	b_e
April	1.042	-0.071	-0.203	1.271	2.755	0.676
May	1.063	0.668	-0.005	1.264	1.894	0.467
June	1.058	0.585	-0.033	1.258	0.774	0.200
July	1.065	0.255	-0.111	1.266	1.405	0.364
August	1.099	0.723	0.041	1.275	1.863	0.498
September	1.074	0.846	0.047	1.266	1.487	0.392
October	1.092	1.080	0.128	1.282	3.194	0.869
November	1.154	-2.187	-0.739	1.266	-1.112	-0.333
December	1.219	-2.896	-0.981	1.252	-1.358	-0.471
January	1.137	-3.369	-1.247	1.256	-0.306	-0.149
February	1.000	-1.880	-0.808	1.265	-0.882	-0.241
March	1.001	-1.703	-0.691	1.280	0.285	0.094

Figure 6.10 shows seasonal variations in ET rates for the two models and the ETmm5 (used as ET reference) for the calibration and validation sets. Both models reproduced the ETmm5 very well except for a slightly insignificant under-estimation during the months of November to February. Similarly, the two versions of the AA model properly reproduced the ETmm5 with the validation data. AA1 under-predicted ET from December to March whereas AA2 slightly overpredicted ET in all the months.

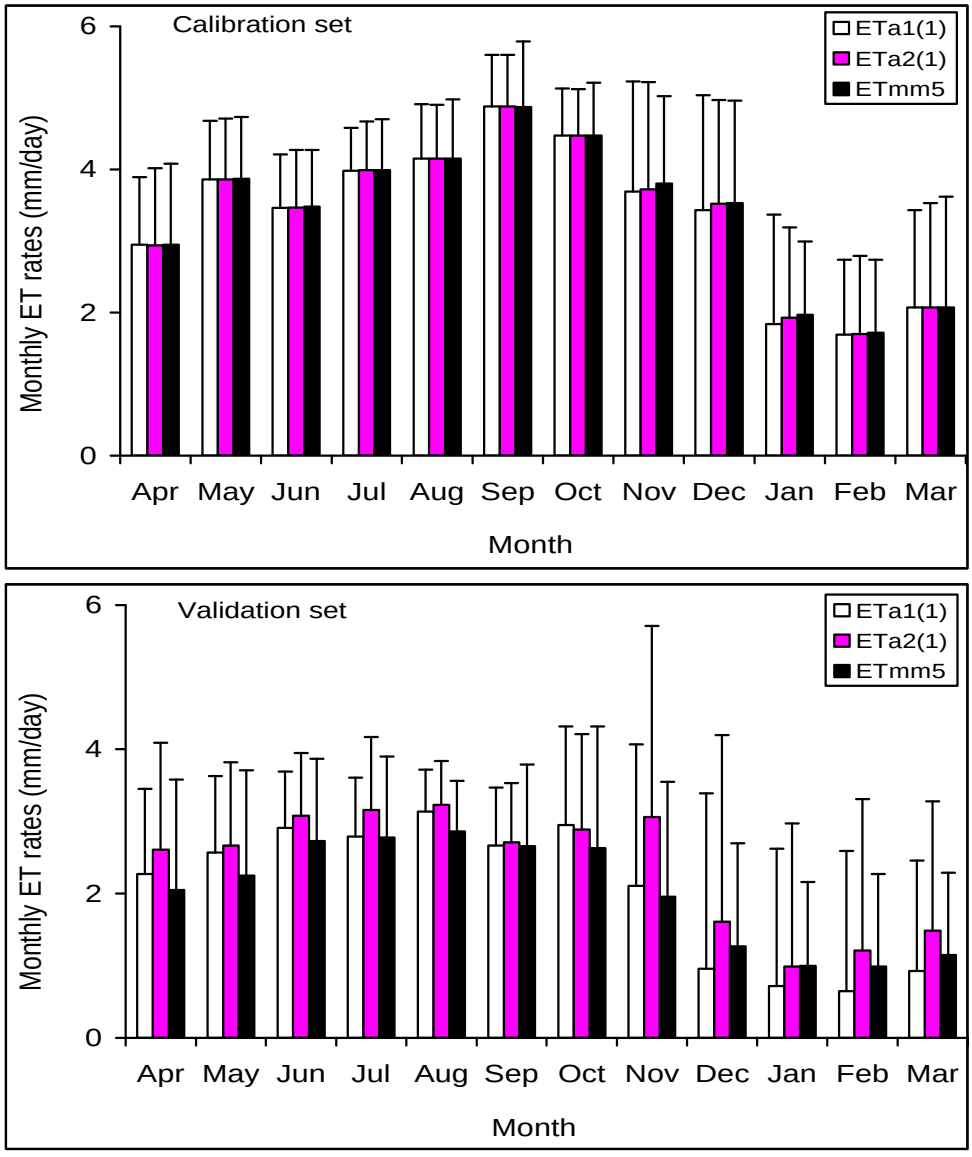

Figure 6.10: Monthly average ETa by AA1 (1) and AA2 (1) compared with ETmm5. Vertical spikes show one standard deviation.

The two measures of accuracy used are coefficient of correlation (R) and root mean square error (RMSE). These values are presented in Table 6.2.

Table 6.2: RMSE and R values to show the seasonal bias of prediction and the degree of association between the modeled ETa and Etmm5 for the first refinement of AA1 and AA2.

Month	Calibration set				Validation set			
	AA1 (1)		AA2 (1)		AA1 (1)		AA2 (1)	
	RMSE	R	RMSE	R	RMSE	R	RMSE	R
April	0.44	0.93	0.40	0.93	0.55	0.96	0.68	0.97
May	0.44	0.86	0.44	0.87	0.66	0.95	0.67	0.95
June	0.37	0.89	0.36	0.90	0.54	0.93	0.57	0.93
July	0.36	0.86	0.31	0.90	0.44	0.95	0.53	0.95
August	0.34	0.91	0.34	0.91	0.51	0.80	0.55	0.82
September	0.52	0.83	0.52	0.83	0.44	0.95	0.43	0.95
October	0.44	0.81	0.44	0.81	0.60	0.97	0.60	0.97
November	0.83	0.85	0.68	0.90	0.65	0.96	1.64	0.96
December	1.00	0.79	0.45	0.95	1.23	0.94	1.38	0.94
January	0.94	0.81	0.55	0.91	1.23	0.92	1.14	0.92
February	0.61	0.83	0.47	0.90	1.45	0.78	1.43	0.75
March	0.76	0.87	0.65	0.91	0.97	0.79	1.21	0.78

For AA1, R ranged from 0.79 - 0.93 and RMSE varied from 0.34 mm - 0.99 mm using the calibration set. For the validation set, R ranged from 0.78 – 0.97 and RMSE ranged from 0.44 – 1.44 mm. For AA2, R varied between: 0.809 and 0.951 (calibration set), 0.750 and 0.969 (validation set) while RMSE ranged between 0.311 mm and 0.684 mm (calibration set), and 0.43 mm and 1.43 mm (validation set), respectively. The standard deviation was comparably not different from the reference ET with the calibrated set. Rainy months had relatively lower standard deviations compared to dry months and AA2 showed significantly higher values especially during the dry season. The two versions of the AA model predicted ETa adequately. Nevertheless, using the listed criteria and the absolute value of the ET rates, in 7 out of 12 months, AA1 with the recalibrated ETw performed better than AA2.

6.5.2 Wind function reparameterization

Based on the strong positive correlation between AA model and the wind speed, the second form of modification made was to retain ETw in the original model and reparameterized the wind function of the advection component of the AA model. By re-arranging Equation 4.35 and substituting ETa = ETmm5 and α_{PT} = 1.26, the wind function $f(u_2)$ can be inversely calculated. The values of the $f(u_2)$ are then regressed to the observed wind speed (u_2) to create a new set of seasonal wind functions. The result of monthly the $f(u_2)$ - u_2 relationship is shown in Figure 6.11. The dashed lines represent the least squares linear regression fit; the solid lines indicate the original Penman wind function, which is non-seasonal.

From the regression equations in Figure 6.11, it can be seen that a positive gradient characterizes the months of February, March and October with the latter having a steeper slope compared to the original Penman wind function (PWF). The remaining months show a negative correlation with wind speed but in absolute terms, and the slope of the relationship is higher than that predicted by the Penman wind function for most of the months. More specifically, for 50% of all the months, the slope of the $f(u_2)$ - u_2 relationship is higher than that estimated by the PWF, indicating that the effects of increasing wind speed on the value of ETp are more pronounced than that for Penman wind function during those months. In 75% of all the months with negative gradients, the derived regional wind function leads to higher estimates of ETp for lower values of wind speeds and lower values of ETp for higher u_2. These observation deviates from the behavior of the PWF as used in the original AA model. The PWF tends to predict higher f (u_2) with increasing u_2 leading to increasing ETp. Generally all the data, except those for November to January, lie mainly above the line predicted by the PWF, leading to higher estimates of ETp than those predicted by the PWF and, hence, decreasing the estimates of ETa. For November to January, the Penman lines lie within the data but with a negative slope; this make the ETp prediction highly dependent on the wind speed.

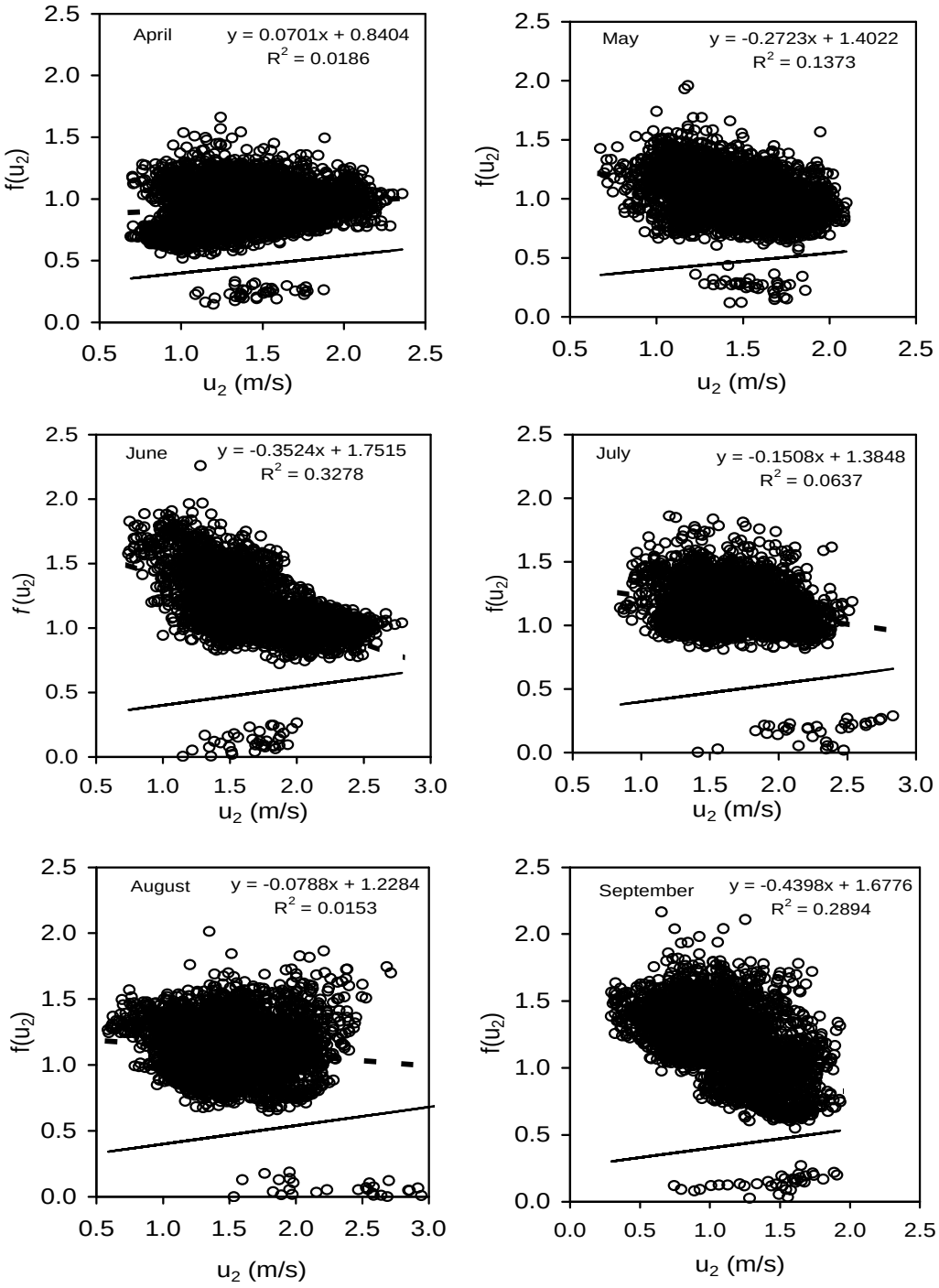

Figure 6.11a: Regional monthly $f(u_2)$–u_2 relationships for : April, May, June, July, August, and September. Solid line is the original Penman wind function.

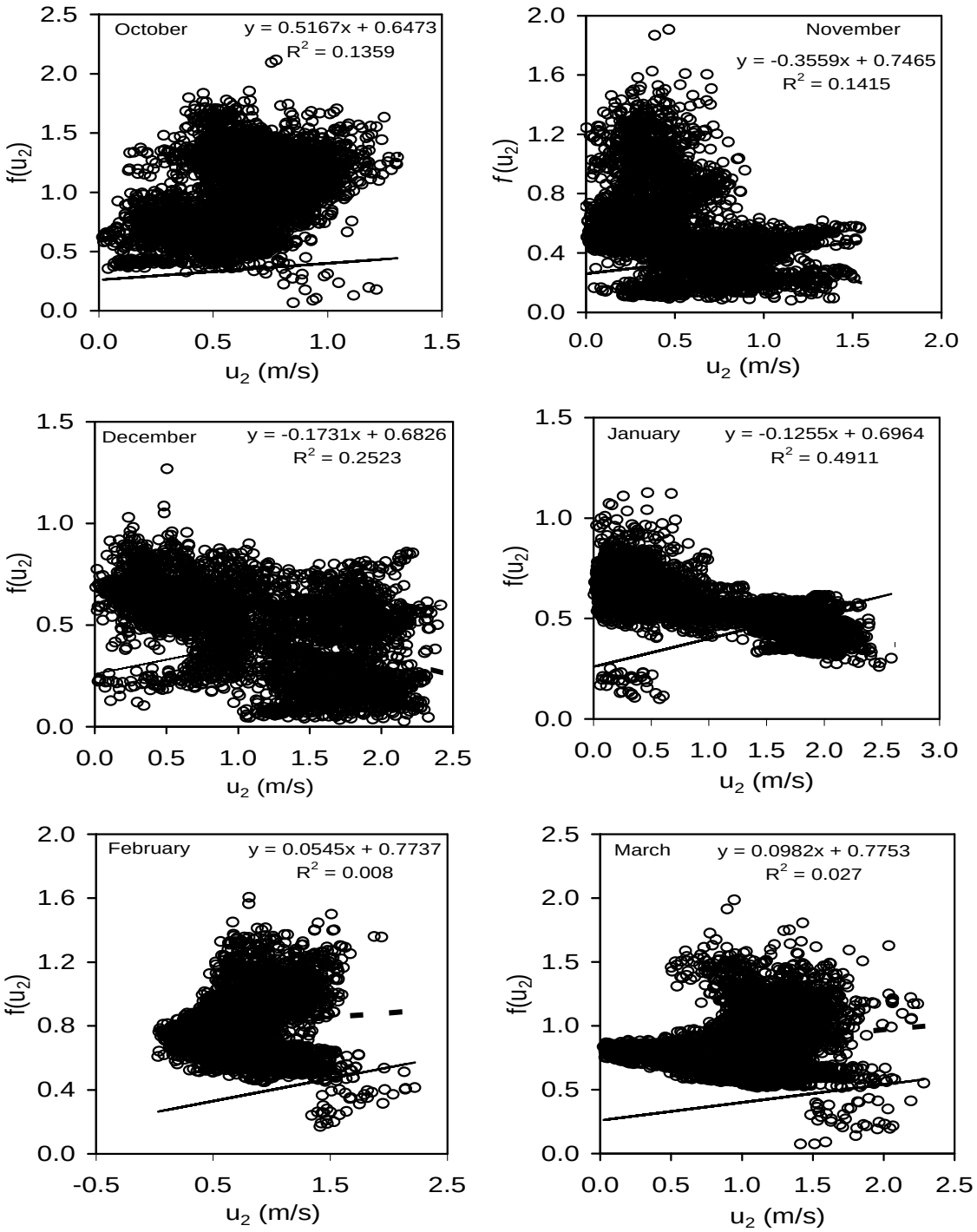

Figure 6.11b: Regional monthly $f(u_2)$–u_2 relationships for : October, November, December, January, February, March. Solid line is the original Penman wind function.

Figure 6.12 presents the seasonal variation in the predicted ETa for both the calibration and the validation set. As is clearly shown on this graph, all the months with data above the PWF line tend to slightly underestimate the ETa, but the reverse was the case for November to January, when the AA models slightly over-predict the ETa. Thus, using the newly derived wind function, ETp was overestimated during the earlier months and underpredicted during the later months, leading to the observed effect on the ETa. It should also be noted that the standard deviation followed a seasonal trend and increased with the general decrease in moisture availability during the year.

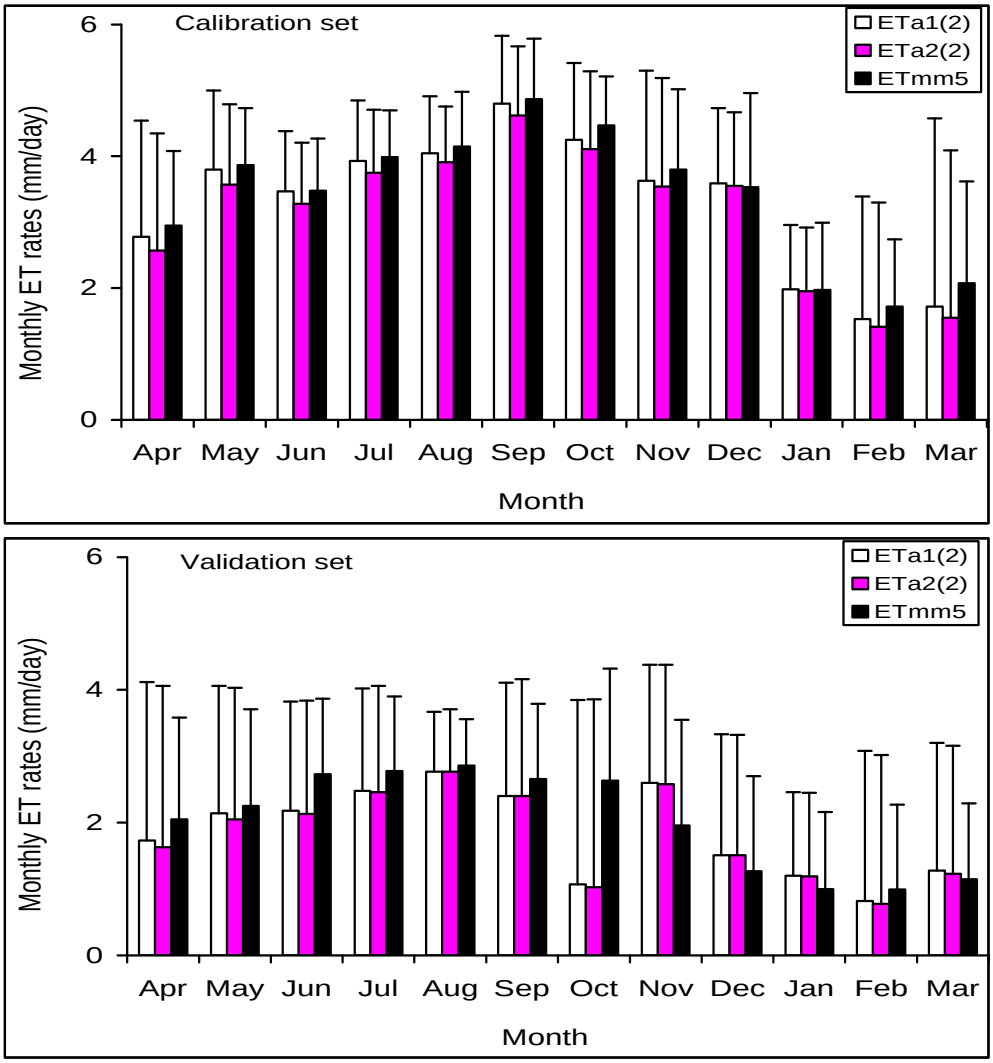

Figure 6.12: Monthly average ETa by AA1 (2) and AA2 (2) compared with ETmm5. Vertical spikes are the standard deviation.

The estimated RMSE and the R are shown in Table 6.3. The correlation between the reformed AA1 varies from 0.70-0.95 (calibration set) and 0.84 and 0.96 (validated set) whereas for the AA2 it ranged from: 0.70-0.95 (calibration set), and 0.843-0.961 (validated set). Similarly, the RMSE for the reformed AA1 varies between: 0.43 mm/day and 1.29 mm/day (calibration set), 0.41 mm/day - 1.97 mm/day (validated set) whereas it ranged from: 0.41 mm-1. 32 mm (calibration set), and 0.43 mm/day - 1.21 mm/day (validated set) for the AA2. It is notable that the new models have similar seasonal trends in the RMSE variations with lower values always during the rainy months. The correlations are quite high with a little or slight improvement over the calibrated set making the reparameterization of the wind function a worthwhile exercise.

Table 6.3: RMSE and R values to show the seasonal bias of prediction and the degree of association between the modeled ETa and Etmm5 for the second refinement of AA1 and AA2.

	Calibration set				Validation set			
	AA1 (2)		AA2 (2)		AA1 (2)		AA2 (2)	
Month	RMSE	R	RMSE	R	RMSE	R	RMSE	R
April	0.79	0.95	0.87	0.95	1.06	0.96	1.12	0.96
May	0.62	0.88	0.69	0.88	0.70	0.95	0.77	0.95
June	0.47	0.86	0.50	0.87	0.92	0.93	0.99	0.93
July	0.44	0.89	0.54	0.88	0.66	0.95	0.72	0.95
August	0.50	0.83	0.59	0.80	0.40	0.91	0.44	0.91
September	0.58	0.83	0.65	0.82	0.83	0.93	0.87	0.93
October	0.86	0.70	0.93	0.70	1.98	0.97	2.03	0.97
November	0.97	0.83	0.97	0.83	0.83	0.96	0.82	0.96
December	0.79	0.84	0.77	0.85	0.63	0.97	0.62	0.97
January	0.43	0.91	0.41	0.91	0.71	0.84	0.71	0.84
February	1.12	0.87	1.12	0.87	1.23	0.91	1.22	0.91
March	1.30	0.93	1.33	0.94	0.95	0.94	0.94	0.94

6.5.3 ETw recalibration using new wind functions

Due to the slight tendency to underpredict ETa as presented above, the same procedure used in section 6.5.1 was repeated but with the use of the newly derived monthly wind functions. The optimized $a_{PT,}$ a_e and b_e parameters are presented in Table 6.1. The a_{PT} range between 1.252 and 1.282, a_e vary from -1.358 to 2.755, and b_e varies from -0.333 to 0.869. The values of a_e and b_e are positive during the period between March and October. The estimated RMSE and R-values for the calibration and validation of the AA1 (3) and AA2 (3) are shown in Table 6.4.

Table 6.4: RMSE and R-values to show the seasonal bias of prediction and the degree of association between the modeled ETa and Etmm5 for the third refinement of AA1 and AA2.

Month	Calibration set				Validation set			
	AA1 (3)		AA2 (3)		AA1 (3)		AA2 (3)	
	RMSE	R	RMSE	R	RMSE	R	RMSE	R
April	0.78	0.95	0.63	0.91	1.05	0.96	1.20	0.95
May	0.62	0.88	0.55	0.85	0.70	0.95	0.78	0.95
June	0.47	0.86	0.47	0.86	0.93	0.93	0.92	0.93
July	0.44	0.89	0.38	0.88	0.64	0.95	0.80	0.95
August	0.49	0.84	0.38	0.91	0.40	0.91	0.69	0.90
September	0.58	0.83	0.53	0.84	0.82	0.93	0.91	0.92
October	0.84	0.71	0.66	0.70	1.86	0.97	2.47	0.96
November	0.96	0.83	0.91	0.85	0.86	0.96	1.62	0.96
December	0.79	0.84	0.60	0.92	0.60	0.96	0.95	0.95
January	0.43	0.91	0.37	0.93	0.71	0.84	0.75	0.84
February	1.12	0.87	1.05	0.92	1.23	0.91	2.24	0.88
March	1.28	0.93	1.28	0.94	0.99	0.94	1.13	0.94

The seasonal variation in the predicted ETa together with the expected value is shown in Figure 6.13. Whereas the two AA models predicted the ETa with insignificant discrepancies with the calibration set, the outlook is quite different with the validation set. The refined models underestimated the ETa during the rainy months (April to October) and overpredicted ETa between November and March. The RMSE values are

generally higher, ranging from 0.69 mm/day - 2.24 mm/day with R varying from 0.84 - 0.96 (validation set). The high values of R notwithstanding, the error level and the seasonal comparison with the expected values show that this formulation might not be worthwhile. More comparisons of the three forms of refinement presented above are further discussed in the following section.

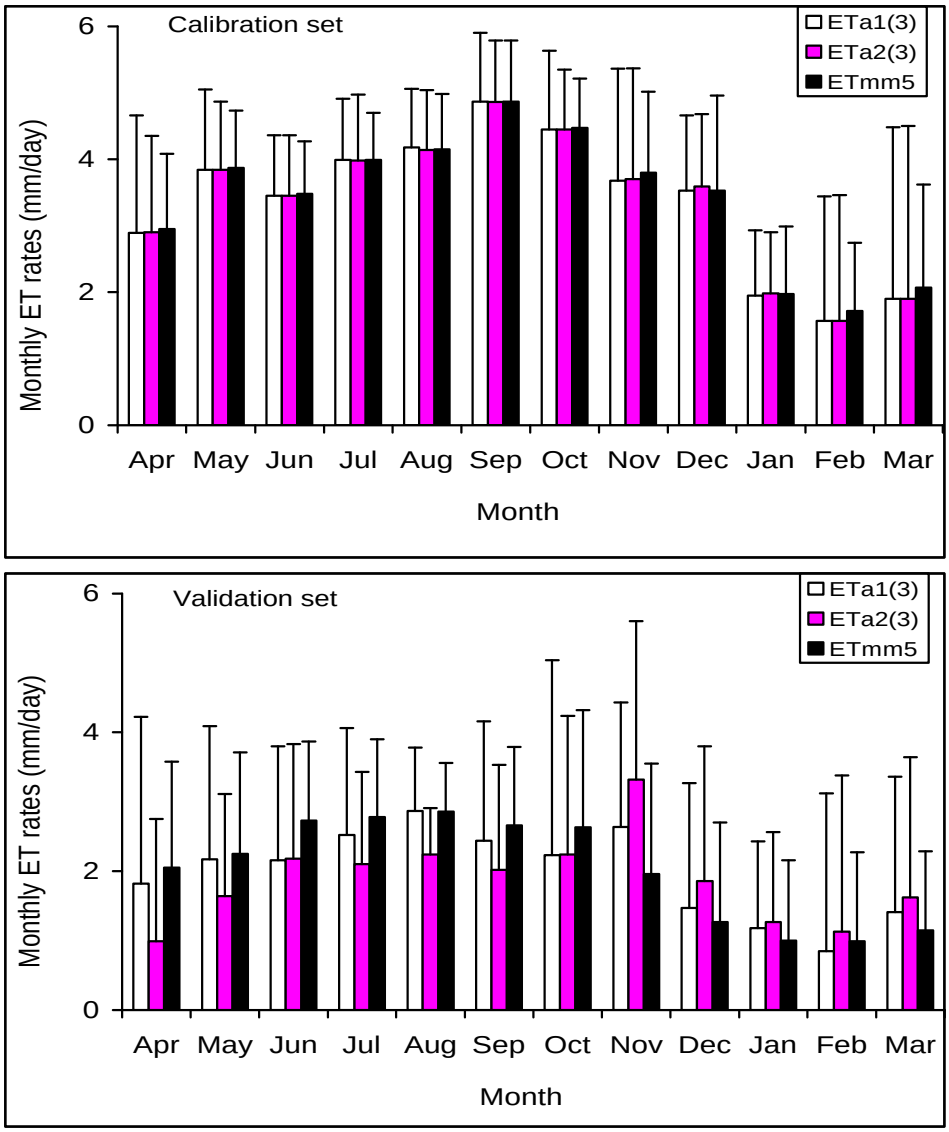

Figure 6.13: Monthly average ETa by AA1 (3) and AA2 (3) compared with ETmm5. Vertical spikes show one standard deviation.

6.5.4 All-at-once optimization of the AA models

The general form of models AA1 and AA2 can be written as:

$$ETa1 = (2a_{PT} - 1)\frac{\Delta}{\Delta + g}(Rn - G) - \frac{g}{\Delta + g}(b_0 + b_1 u_2)(e_s - e_a) \qquad (6.1)$$

and

$$ETa2 = \left[\frac{2\Delta}{(1 - b_e)\Delta + a_e g} - \frac{\Delta}{\Delta + g}\right](Rn - G) - \frac{g}{\Delta + g}(b_0 + b_1 u_2)(e_s - e_a) \qquad (6.2)$$

where a_{PT}, a_e, b_e, $ß_0$, and $ß_1$ are model constants and other variables have their usual notations. These 3 parameters for AA1 and 4 parameters for AA2 were optimized by replacing ETa1 and ETa2 with ETmm5 in Equations 6.1 and 6.2, respectively. The resulting new models are denoted AA1 (4) and AA2 (4) and the results of the seasonal estimated parameters are presented in Table 6.5.

Table 6.5: Seasonal optimal parameters for wind function and ETw equations used in AA models for all-at-once optimizations.

Month	AA1 (4)			AA2 (4)			
	a_{PT}	$ß_0$	$ß_1$	a_e	b_e	$ß_0$	$ß_1$
April	1.078	0.445	0.065	-0.770	-0.412	0.391	-0.002
May	1.084	0.539	-0.009	-0.177	-0.245	0.399	-0.016
June	1.103	0.547	0.056	-0.137	-0.236	0.398	0.034
July	1.139	0.654	0.045	0.258	-0.095	0.462	0.048
August	1.124	0.517	0.031	1.000	0.149	0.557	0.028
September	1.141	0.869	-0.157	1.072	0.188	0.915	-0.152
October	1.054	0.216	0.007	-0.192	-0.303	0.107	-0.018
November	1.067	0.172	-0.032	-2.261	-0.856	0.121	0.045
December	1.335	0.868	-0.198	-2.308	-0.764	0.462	0.025
January	1.227	0.647	-0.114	-1.194	-0.473	0.551	-0.042
February	0.941	0.341	-0.021	-1.774	-0.825	0.319	0.008
March	1.008	0.501	-0.074	-1.171	-0.552	0.465	-0.060

The Priestley-Taylor coefficient, ranging from 0.941-1.335, is significantly different from the value of 1.26 used in the original AA model. Whereas the lowest

value of a_{PT} was estimated for February, the highest value (1.335) was obtained for December. All the other 10 months show values significantly lower than 1.26. Similar to the result obtained in section 6.5.3, the wind function showed a negative correlation for 7 out of the 12 months. For the AA2 (4) model, the parameters a_e and $b_{e,}$ also showed significant variations from the 0.63 and 0.15 earlier suggested by Brutsaert and Stricker (1979). However, the value of b_e (0.149) estimated for August was not different from 0.15.

The estimated RMSE and R-values for the calibration and validation of the AA1 (4) and AA2 (4) are given in Table 6.6. Seasonal RMSE for AA1 (4) range from 0.31-0.77 mm/day (calibration set) and 0.35-1.14 mm/day (validation set). For the same model, R varies between 0.82 and 0.96 for the complete data set. Similarly for AA2 (4), RMSE varies from 0.30-0.53 mm/day (calibration set), and 0.40-1.64 mm/day (validation set) but generally with higher R-values.

Table 6.6: RMSE and R values showing the seasonal bias of prediction and the degree of association between the modeled ETa and Etmm5 for the fourth refinement of AA1 and AA2.

Month	Calibration set				Validation set			
	AA1 (4)		AA2 (4)		AA1 (4)		AA2 (4)	
	RMSE	R	RMSE	R	RMSE	R	RMSE	R
April	0.39	0.94	0.35	0.95	0.44	0.96	1.14	0.90
May	0.42	0.88	0.40	0.88	0.59	0.95	0.98	0.96
June	0.36	0.89	0.35	0.90	0.39	0.95	0.72	0.94
July	0.31	0.91	0.30	0.91	0.35	0.95	0.51	0.95
August	0.33	0.92	0.33	0.92	0.43	0.85	0.40	0.85
September	0.48	0.85	0.48	0.85	0.37	0.95	0.40	0.95
October	0.42	0.82	0.41	0.83	1.14	0.92	1.60	0.92
November	0.67	0.84	0.53	0.90	0.94	0.97	1.64	0.96
December	0.77	0.85	0.41	0.96	0.86	0.97	1.15	0.96
January	0.43	0.91	0.31	0.95	0.67	0.85	0.74	0.87
February	0.52	0.86	0.39	0.93	0.54	0.91	0.98	0.80
March	0.49	0.95	0.39	0.97	0.44	0.94	1.51	0.64

The seasonal variation in the predicted ETa together with the expected value of ETamm5 is shown in Figure 6.14. Both AA1 (4) and AA2 (4) performed well throughout the season with the exception of July, when AA2 (4) showed a slight overestimation (calibration data). The pattern is different with the validation set, as AA1 (4) shows a better fit with slight overprediction with the exception of October and November. AA2 (4) shows higher positive bias all through the season with corresponding higher values of standard deviations.

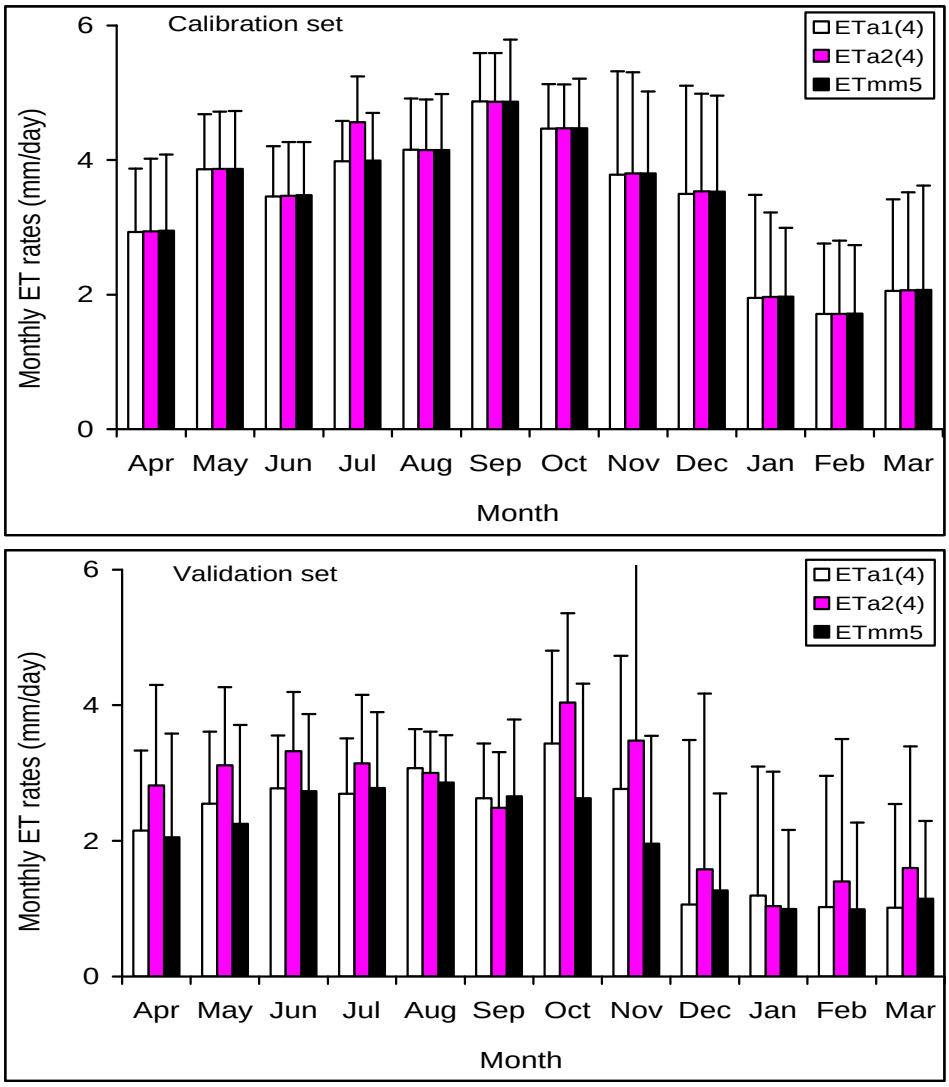

Figure 6.14: Monthly average ETa by AA1 (4) and AA2 (4) compared with ETmm5. Vertical spikes show one standard deviation.

6.6 Discussion

The components of the AA model with a coarser dataset (50 km resolution) clearly reveal well-delineated zones of ETp, ETw and ETa. However, information on the spatial variability of ET rates has been eroded under the influence of the coarse data resolution. The spatial variability of ETp, ETw and ETa monthly surfaces is more distinct with a higher resolution dataset (12 km resolution). These seasonal maps clearly identify the transitions from energy-controlled evapotranspiration to soil-controlled evapotranspiration. Climate or soil control in this context refers to energy-limited or water-limited evapotranspiration.

The observed pattern and association between the modeled ETa(s) and the actual evapotranspiration used as the reference point (ETmm5) is very remarkable, though with positive bias (Figures 6.7 and 6.8). The annual cdf of ETmm5 was significantly different from the cdfs of AA1 and AA2 ($p < 0.001$). In view of this overestimation, the AA models were refined to improve their performances. The first modification was based on the assumption that the Penman (1948) model predicts ETp satisfactorily, especially under low to medium wind run conditions (Doorenbos and Pruitt, 1977). The seasonally derived Priestley-Taylor parameter (a_{PT} = 1.00 to 1.22) is within the range already published in the literature. However, this range is lower than the 1.26–1.28 suggested by Brutsaert and Stricker (1979), and the 1.32 value suggested by Morton (1983), which was recently confirmed by Hobbins et al. (2001b) over selected basins in the USA. Other variations are also reported, e.g., a_{PT} = 1.05 for short, well watered Douglas fir (McNaughton and Black, 1973); deBruin and Keijman (1979) found diurnal variation of a_{PT} from 1.15 to 1.42 as well as a seasonal range of 1.20 to 1.50 over a shallow lake. Furthermore, Qualls and Gultekin (1997) suggested the value of a_{PT} = 1.13, which is similar to values derived over the Volta Basin. It can be concluded that regional wet environment evapotranspiration under conditions of minimal advection is smaller than the literature suggests (Priestley and Taylor, 1972) especially in the studied region.

The second refinement assumes that Penman methods require calibration of the wind function (Smith et al., 1996; Hobbins et al., 2001b) particularly in the arid regions where the aerodynamic term is relatively important (Doorenbos and Pruitt, 1977), and that α_{PT} is a universal parameter. The reparameterized seasonal wind function generally

increased the role of the aerodynamic or advective energy, leading to higher values of ETp monthly surfaces for most of the months. The resulting ETa values are lower as compared to those of the ETmm5 (Figure 6.12). This kind of underestimation was reported by Hobbins et al. (2001b) over selected basins in the USA. However, in the present study, between November and January, the predicted ETp was lower than the original Penman equation, resulting in slight overestimation of the ETa. A contrary result could have been expected, as this is a strong harmattan period with the characteristic hot, dry, dusty and windy conditions that tend to favor higher advective energy. It appears that the role of the northeasterly wind in attenuating the solar radiation, which is by far the most important energy source for evapotranspiration in the region, seems to be greater than its role of making extra energy available at the evaporating surface.

The monthly, regionally reparameterized wind function actually led to a detrended ETp equation, but with some degree of bias in modeled ETa. In order to remove this bias, the ETw equations were again recalibrated. The range of a_{PT} optimally derived is also within the established values, but the ranges of a_e and b_e are significantly different from the values of 0.15 and 0.63 suggested by Brutsaert and Stricker (1979). Furthermore, the all-at-once reformulation produced a_{PT} lower than 1.00 in March and 1.34 in December, and a_e and b_e are also significantly different from the values suggested in the literature.

The two AA models with four respective modifications resulted in a total of eight (8) new AA models. The mean bias (*MB*), mean absolute error (*MAE*), root mean square error (*RMSE)*, and correlation coefficient (*R)* values in Table 6.7 are used to compare the overall relative performance of the modifications made to both AA1 and AA2 using the combined 2-year data set. *MB* quantifies the bias of the prediction, and the closer to zero the better; *MAE* measures the total error of prediction and should be zero for correct estimation; *RMSE* combines both the precision and the bias of the prediction and the smaller the better; *R* measures the degree of association and the higher the better. Using the criteria stated above, these goodness-of-fit statistics (parameters) were ranked with the average ranking showing the order of better performance. Generally, the refined AA1 models are better than the corresponding AA2 models. The best new model is AA1 (4) followed by AA1 (1), while AA2 (3) showed

the poorest performance. Interestingly, the first four out of the eight new models are refinements to AA1, this demonstrates the possible supremacy of AA1 over AA2 and justifies why AA1 is frequently used in the literature.

Table 6.7: Statistical indices for cross-validation of AA models. Ranking is in parenthesis (1=highest, 8=lowest). The average ranking is given in the last column.

Model	MB	MAE	RMSE	R	Ranking#
AA1 (1)	-0.002 (1)	0.128 (1)	0.679 (2)	0.880 (8)	(3.0) [2]
AA2 (1)	0.175 (6)	0.191 (3)	0.685 (4)	0.900 (4)	(4.3) [3]
AA 1 (2)	-0.145(5)	0.252 (5)	0.823 (6)	0.897 (6)	(5.5) [6]
AA 2 (2)	-0.235 (7)	0.330 (7)	0.858 (7)	0.896 (7)	(7.0) [8]
AA 1 (3)	-0.089 (3)	0.203 (4)	0.815 (5)	0.898 (5)	(4.3) [3]
AA 2 (3)	-0.135 (4)	0.376 (8)	0.927 (8)	0.901 (3)	(5.8) [7]
AA 1 (4)	0.079 (2)	0.129 (2)	0.530 (1)	0.908 (1)	(1.5) [1]
AA 2 (4)	0.302 (8)	0.320 (6)	0.684 (3)	0.902 (2)	(4.8) [5]

superscripts show the order of relative performance of each model.

More specifically, the results show that the Priestley-Taylor (ETw) model is more stable, amenable to modifications and performed better than the second ETw model tested in this study. This observation is further buttressed using the annual data, which is shown as the cumulative probability distribution function in Figure 6.14. ETa estimates of all AA models except AA1 (2), AA2 (2), and AA2 (3) are not significantly different ($p>0.05$) from the ETmm5. However, the significant differences in ETa estimates from the modification based on the reparameterization of the wind function implies that the original PWF could be retained for this region, while it is highly important to recalibrate the ETw equations. A closer look at the monthly performances reveals that it might be worthwhile to use the new wind function during the harmattan or dry period. During this period, their respective *RMSE* and R are lower than the AA1 (1) and AA2 (1) as AA1 (1) and AA2 (1) yielded a slight over-estimation of ETa.

The seasonal trends in optimal parameters of the best model (AA1 (4)) shown in Table 6.5 can be combined with the results of the field measurements (Chapter 5) to further elucidate on the role of surface albedo, cloudiness (clearness index), and harmattan in evapotranspiration process in this region. An implicit assumption in the

Brutsaert and Parlange (1998) argument is that ETw does not vary appreciably with time so that changes in ETa are primarily due to changes in ETp (Szilagyi et al., 2001).

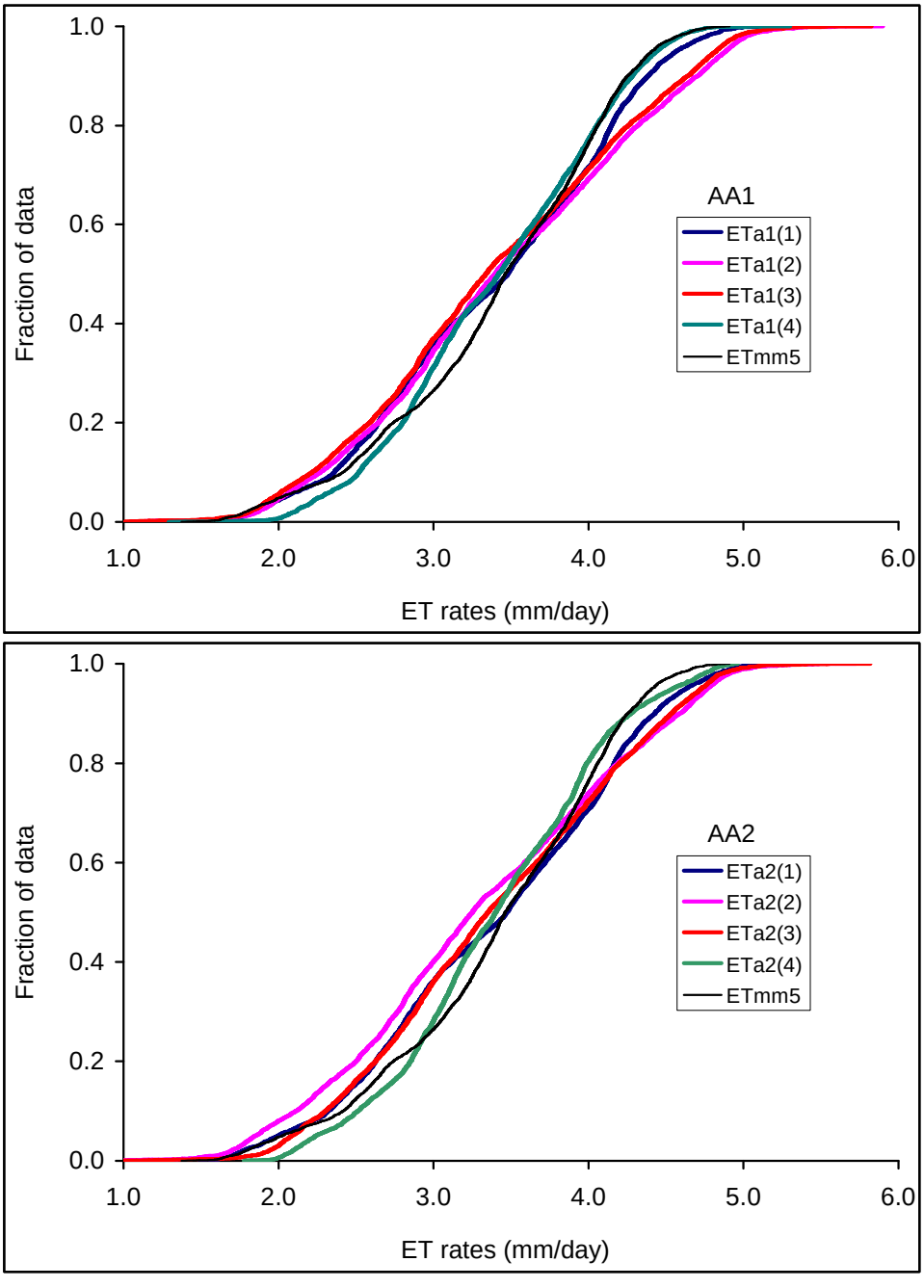

Figure 6.15: Cumulative probability distribution functions (cdfs) for ETa under different modifications of AA1 and AA2 compared to ETmm5

The values of the optimized Priestley-Taylor constant (a_{PT}) for AA1 (4) appear to support this assumption. These values varied monthly as to make the ETw near constant during the season.

Albedo was reported to increase with soil dryness and crop/vegetation phenology (LAI and CH). Low albedo during the months of January, February and/or March due to the effect of bush fires, coupled with clearer skies in February/March translates to higher available energy. This energy gradually decreased from the onset of rains (April to June), though with clear skies but the green-up increases the albedo values. The effect of convective clouds (Jegede, 1997) during the monsoon months (July to September) coupled with a slight increase in vegetation albedo further reduces the available energy at the evaporating surface. A large part of the basin starts to experience a dry down in vegetation (reduced LAI), as well as a higher clearness index during the months of October and November, leading to available energy comparable in magnitude to that of the onset of the rainy season. However, in December and January, although dry vegetation should lead to lower albedo, the role of very dry background soil dominantly increased the surface albedo; this is coupled to the harmattan effect of obscuring the sun during this period leading to a decrease in net radiation. Hence, higher a_{PT} was obtained for months with lower available energy and vise-visa for months with higher available energy, making the symmetry between ETa and ETp clearer.

Another alternative to generate input forcing parameters for the above estimation methods is the use of geostatistical techniques (Clastiansen, 1996). These involve the use of a semi-variogram model to interpolate variables that correlate in space. However, a good quality hydroclimatological data of a spatial extent are almost non-existent in the Volta Basin. The poor quality and discontinuity lapses characterizing the available meteorological records hindered the construction of semi-variogram models, which could have been used to interpolate the atmospheric surfaces needed as input in the AA model. This justifies the use of simulated surfaces from the regional climate model (MM5 community model version 3.5). Results from these models are usually internally consistent, and the hindcasting-simulated results have shown to satisfactorily reproduce the meteorological variable (van de Giesen et al., 2002; Kunstmann, 2002). Related studies, e.g. Koster and Suarez (1999), have used simulated data from Global

Circulation Models (GCM) to extend the use of aridity index to determine evaporation deviation ratio. Similarly, Arora (2002) used annual evapotranspiration and precipitation data from GCM simulations to estimate evaporation ratio and inter-annual variability of evapotranspiration and precipitation in assessing the effect of climate change on runoff.

6.7 Evapotranspiration and land use

As already stated, a change in potential evapotranspiration will cause a corresponding change in actual evapotranspiration. The change may be due to a change in available energy (net radiation) associated with a change in surface albedo, which may largely be due to land use change. One of the five focal points that emerged from a preliminary study of the Volta Basin water balance (Andreini et al., 2000) has to do with the proper examination of the critical role played by land use and cover in the partitioning of water within the basin. Differences in water use from different land use categories are statistically compared (Table 6.8a). The land use groups are based on classification from the USGS (www.mmm.ucar.edu/mm5/documents/MM5_tut_webnotes/TutTOC.html).

The results show that all 12 land-use classes found within the study area can be reclassified into five homogeneous water-use classes as shown in columns 1-5 (to the right) of Table 6.8a. The ETa values in the individual columns are not significantly different ($p > 0.05$) from one another, but are significantly different from those in the other columns with the exception of the repeated values. The probability values are shown at the bottom row of each column. The water requirement for *¨mixed shrubs/grasses¨* is lowest, while *¨mixed dry/irrigated crop and pasture¨* shows the highest. Both extremes cover a relatively low portion of the landscape, i.e., 0.09% and 0.05%, respectively. *Savannah* (55.4%), followed by *crop/grass mosaic* (24.4%), *crop/wood mosaic* (8.89%) and *grassland* (6.09%), are the dominant land-use groups in descending order of proportion of the landscape covered.

Table 6.8a: Annual mean water use by different land use/cover types

Land use/cover type (LUC)	Proportion of landscape (%)	Annual mean water use group at 5% level of significance (mm)				
		1	2	3	4	5
Mixed shrubs/grasses	0.09	929				
Grassland	6.09	1006	1006			
Savannah	55.39		1172	1172		
Water bodies	0.86			1270		
Dryland cropping/pasture	0.23			1281		
Crop/grass mosaic	24.42			1334		
No data on land use	0.19			1374	1374	1374
Crop/wood mosaic	8.89				1462	1462
Evergreen broadleaf	1.25					1546
Mixed forest	0.58					1560
Deciduous broadleaf	1.94					1569
Mixed dry/irrigated Crop and pasture	0.05					1579
Probability		**0.424**	**0.084**	**0.061**	**0.075**	**0.062**

The five water-use groups could be reduced to three by retaining each ETa value in only one group. Then the weighted average was computed based on proportion of the landscape covered (Table 6.8b). An average annual total of 1000 mm of water evaporated from water-use group1 covering about 6.2% of the total land area, group2 evaporated about 1220 mm and group3 evaporated about 1490 mm from 81.1% and 12.7% of the landscape area, respectively. The results imply that: (1) a non-linear relationship exists between land use/cover type and the partitioning of water within the basin; (2) a change in land use/cover within the LUC subgroup, leading to a particular water-use group, may not lead to any significant change in water use pattern in the Volta Basin. However, for a more detailed interaction between land use and actual evapotranspiration, integration of seasonal albedo into a numerical study of the impact of land use on water use is suggested. This could be implemented with the complementarity relationship models presented in this study.

Table 6.8b: Weighted annual water use by different LUC subgroup

LUC subgroup	PLC (%)	AWU (mm)	WAWU (mm)
Mixed shrubs/grasses	0.09	929	
Grassland	6.09	1006	1004
Savannah	55.39	1172	
Water bodies	0.86	1270	
Dry land cropping/pasture	0.23	1281	
Crop/grass mosaic	24.42	1334	
No data on land use type	0.19	1374	1223
Crop/wood mosaic	8.89	1462	
Evergreen broadleaf	1.25	1546	
Mixed forest	0.58	1560	
Deciduous broadleaf	1.94	1569	
Mixed dry/irrigated crop and pasture	0.05	1579	1492

LUC = land use/cover type; PLC = proportion of landscape covered (%); AWU = average water use (mm per annum); WAWU = weighted average water use by each sub-group

7 SUMMARY AND CONCLUSIONS

This Chapter presents the summary, conclusions and recommendations with respect to the research aims and objectives.

7.1 Surface albedo

Values of albedo increase with increasing zenith angle. The rate of increase of albedo with respect to zenith angle is higher on dry surfaces than on wet surfaces. The highest percentage decrease in mean albedo occurred for the moldboard plow treatment, while the lowest occurred for the conventional tillage system. The range of surface roughness commonly found with commercial grain production as well as with yam and root crop cropping is likely to cause between 20 and 25% change in surface albedo for wet conditions, and less than 12% for dry soil surfaces. Significant changes in mean albedo with soil wetness were observed. The bare-soil albedo increased rapidly ($p<0.01$) from wet to dry surface conditions in all the tillage treatments. The type of albedometer sensor also produced some degree of bias in the absolute values of measured shortwave albedo. A simple multiple linear regression model relating shortwave albedo (a) to surface roughness (d) and soil moisture (q_m) can be used to estimate the values of the albedo of tilled bare soil, which is similar to the tropical loamy sand reported in this study.

Growth and development stages as well as sun angle influence surface albedo of a vegetated surface. The albedo variations caused by the phenological stages were examined in relation to two reference surfaces, tilled bare soil and short grass. Relative differences in albedo values of maize were found to increase from seedling (3%) to physiological maturity (45%) in response to increases in LAI and CH. For the cowpea fields, albedo increased up to the flowering stage (37%) and decreased thereafter. For maize, cowpea and other crops with similar growth patterns, canopy structures and management practices, the expected increase in the average values of surface albedo during seedling, vegetative, flowering and maturity stages, could be estimated based on these results, especially if the bare soil albedo after soil preparation is known.

With respect to the short-grass reference surface, it was observed that albedo values exist somewhere between the vegetated and flowering stages, which have about

the same albedo values as the corresponding short-grass. The generally assumed reference albedo of 0.23 may be more valid within this period. This could be of importance in the study of radiative transfer in plant communities. The composed simple model could be used to generate albedo values for maize and cowpea fields.

7.2 Tree water use

Sap flow was highly related to the tree sapwood and generally decreased over the dry season. Water use during the phenological stage of flowering and fruit development was relatively high during the dry period. A simple model relating a parabolic response of tree sap flow to solar radiation was fitted and adequately captured the diurnal course of water use by cashew trees. The canopy scale processes showed that tree crown conductance generally decreased over the dry season in response to declining soil moisture and increasing atmospheric demand. Canopy conductance had little control on the transpiration as the tree canopy was moderately coupled to the atmosphere as indicated by the decoupling coefficient (0.46). The radiative energy had a dominant influence on transpiration processes as compared to the advective energy.

The results during the rainy season show that the clearness index, a measure of the sky condition, is useful in explaining the variations in evaporative demand and tree transpiration rates. Rainfall interception and solar radiation were found to influence tree water use more than to stomatal conductance. The coupling of tree canopy to the atmosphere was moderate (Ω = 0.40*)* and a plateau-type response to high evaporative demand was observed. The diurnal trend of tree water use could be predicted from the meteorological variables, i.e., air temperature, ambient relative humidity and incoming solar radiation. The estimated measure of accuracy revealed that the non-linear combinations of the weather variables could predict transpiration better than the corresponding linear combinations. The effects of tree crops on soil water resources and stream flow will vary depending on rainfall variability and other land-use alternatives within the watershed. This result could form the basis of further studies on the effects of the conversion of annual croplands to tree crop plantations on watershed hydrology. According to Calder (1998), a humid rain forest is able to convert virtually all the net radiation into evaporation; hence changing forested areas to annual crops has implications for increased annual stream flows. In the *Kotokosu* watershed, tree crops (especially

cashew trees) cover more than 60% of the catchment area and are still on the increase. This may likely lead to declining stream flows especially in the future when the trees are well established.

Temporal dynamics of water fluxes and relative contributions from stand components were examined in a young, widely spaced, cashew orchard in the Volta Basin of Ghana. Using cross-correlation and simple differential calculus, time lags were estimated between tree sap flow and above-canopy evapotranspiration. Similarly, lags between fluxes and atmospheric variables (incoming solar radiation and vapor pressure deficit) were determined. Water fluxes were highly related to solar radiation and decoupled from the course of the vapor pressure deficit and hence the atmosphere. Average daily evaporation during this drying-transition period gradually declined, while the proportion of total available energy consumed in evaporation was less than 50%. A decreasing trend in evaporative fraction (from 0.66 to 0.36) was observed, suggesting an increase in surface resistance. Due to the low stem density of the plantation, the contribution from the understory was indirectly estimated to be greater than 60% of the total evaporation. In addition to other outlined sources of uncertainties in the measurement systems, ways and means of on-line processing of eddy correlation fluxes may also contribute some degree of uncertainty to the eddy fluxes. In the on-going field campaign, understory and bare-soil evaporation should be directly measured so as to allow for a more accurate partitioning of evapotranspiration in this orchard.

7.3 Regional evapotranspiration

The primary aim of this part of the study was to test the validity of the complementarity relationship hypothesis in the Volta Basin and thereafter model evapotranspiration at regional scale. Average monthly and annual surfaces of ETp and ETw followed the gradients of available energy and moisture availability, respectively. The two input scales (12 km and 50 km) showed a reduction in spatial details with increasing scale of input surfaces. The ETw value generated by the AA1 model slightly exceeds those of the AA2, leading to corresponding differences between ETa1 and ETa2. ETa surfaces show a negative latitudinal gradient. Soil-controlled evapotranspiration processes dominated during the drier months, while the energy-controlled evapotranspiration processes

dominated during the rainy months. Wind speed, among other climatological parameters of the basin, significantly correlates with the actual evapotranspiration in this study.

However, ETa by both AA1 and AA2 were found to consistently exceed the ETa values by the regional circulation model (MM5). The AA models were therefore evaluated and improved in four ways: (1) by including a monthly, regionally recalibrated Priestley-Taylor coefficient (α_{PT}); (2) by including a monthly, regionally reparameterized wind function in the ETp formulation to remove wind speed dependence; (3) by using the reparameterized wind function and then recalibrating the Priestley-Taylor coefficient; and (4) by completely estimating all the AA models parameters in one go (*all-at-once*).

The original AA1 and AA2 models overpredicted the ETa, generating an average root mean square error of 1.58 mm/day and 1.54 mm/day, respectively. AA1 (4) followed by AA1 (1), were the first two new models that performed significantly better than the original AA models as shown by the computed statistical indices. The derived values of α_{PT} are generally within the values published in other related studies. The reparameterized wind function resulted in a higher ETp, leading to underprediction of ETa during most of the months, but especially during the rainy months. However, the better performances of refinements made to AA1 show the supremacy of AA1 over AA2 and explain while the Priestley-Taylor equation has been frequently used to approximate ETw in the literature.

In this region, runoff is expected to be a smaller fraction of the precipitation since the available energy is very high, resulting in high evapotranspiration. The role played by monsoon clouds and harmattan in attenuating solar radiation, as well as seasonal changes in surface albedo on evapotranspiration process, were discussed. The satisfactory performances of the improved AA models documented here indicate the utility of models based on the Bouchet complementarity relationship hypothesis in regional/large-scale evapotranspiration for providing independent estimates of ETa. However, it is suggested that the insight gained through the reformulation of AA models be incorporated and used with the CRU data set, and the output be compared to the annual ETa estimated with the water balance model. The author hopes to undertake this task in the nearest future.

7.4 Evapotranspiration and land use

The role played by land use and land cover in the partitioning of water within the basin was examined. Differences in water use in different land-use categories (LUC) were

compared. *Savannah* is the largest land use/cover type in the study area, covering about 55.4% of the total landscape with a water requirement of 1170 mm per annum. *Mixed dry/irrigated crop and pasture* is the highest water user (1579 mm per annum) of all the LUC, but occupying by far the smallest portion of the landscape (0.05%). The 12 LUC categories could be re-grouped into 3 distinct water-use sub-groups. The first LUC subgroup (*mixed shrubs/grasses, and grassland*) evaporates about 1000 mm of water per year, the second subgroup (*savannah, water bodies, dry land cropping/pasture, crop/grass mosaic*) evaporates about 1220 mm of water per annum, while the third subgroup (*crop/wood mosaic, evergreen broadleaf, mixed forest, deciduous broadleaf, and mixed dry/irrigated crop and pasture*) evaporates 1490 mm of water per year. Changes in land use between these 3 categories will have significant effects on water use, e.g., *savannah to mixed dry/irrigated crop and pasture*.

7.5 Conclusions and recommendations

Based on the analyses of the evapotranspiration and related investigation reported in this study, the following research and policy recommendations are given:

- There is need for more research on the effect of crop/vegetation phenology on seasonal evapotranspiration. One possibility would be to incorporate seasonal changes in vegetal albedo into the ETa models. In addition, information on albedo presented can be examined vis-à-vis the remotely sensed albedos in order to improve the algorithms used in deriving the satellite albedo.
- Tree water use, albedo, soil moisture and other tree allometric data could be used to validate the OSU SLM, which is included in the setup of the regional circulation model (MM5), for a better understanding of the existing feedback mechanisms in the biosphere-atmosphere interactions.
- The ETa information from the AA models may be used in conjunction with estimates of biomass from each land-use category to estimate water-use efficiency, which policy makers can use in selecting the appropriate tree species for use in regional afforestation programmes. Furthermore, application of geostatistical techniques to downscale or upscale the surfaces of ET rates to the scale of interest for decision-making should be looked into in future research.

- The empirical evidence of the validity of the complementarity relationship hypothesis in the Volta Basin makes it suitable for inclusion in the decision support system envisaged for the Volta Basin. The simple but robust algorithm used for AA models could be coded as a sub-routine in the DSS package, which can be called at any point when ET data is needed. Also, the complementarity relationship model presented in this study may be suitable for investigating long-term climate change effects on regional ET and other hydroclimatological parameters such as aridity index, evaporation ratio and runoff in the basin. It is suggested that the insight gained through the reformulation of AA models be incorporated and used with the CRU data set, and the output be compared to the annual ETa estimated with water balance model.
- Lastly, there is an urgent need for the six riparian countries of the Volta River Basin to form an Inter-governmental Basin Development Authority (IBDA), which sees to the overall management of the basin resources and puts in place a network of hydro-meteorological stations, where quality data required for the water balance studies could be monitored.

Evapotranspiration and the related variables investigated in this research provide relevant information towards the understanding of the biosphere-atmosphere interactions such as the effects of phenology and season on albedo, which in-turn have implications for consumptive water use/requirements. Data presented are expected to be a valuable input in agricultural water management, environmental monitoring, crop production models, the study of climate effects of agricultural intensification and the parameterization of land-surface schemes in regional weather and climate models. Furthermore, this information also serves as input to a decision support system that will enhance the effectiveness of water resources management in the Volta Basin of West Africa.

8 REFERENCES

Alatise MO (2002) Growth, yield and water use pattern of maize under limited water supply. PhD Dissertation, Federal University of Technology, Akure, Nigeria

Allen RG, Pereira LS, Raes D and Smith M (1998) Crop Evapotranspiration. FAO Irrigation and Drainage Paper 56. Food and Agricultural Organization of the United Nations, Rome, Italy, 300pp

Allen SJ and Grime VL (1995) Measurements of transpiration from savannah shrubs using sap flow gauges. Agric For Meteorol 75: 23-41

Allen SJ, Hall RL and Rosier PTW (1999) Transpiration by two poplar varieties grown as coppice for biomass production. Tree physiol. 19: 493-501

Andreini M, van de Giesen N, van Edig A, Fosu M and Andah W (2000) Volta Basin water balance. ZEF Discussion papers Nr 21, Bonn, Germany

Arnfield AJ (1975) A note on the diurnal, latitudinal and seasonal variation of the surface reflection coefficient. J Appl Meteorol 14: 1603-1608

Arora VK (2002) The use of the aridity index to assess climate change effect on annual runoff. J. Hydrol. 188-189: 482-493

Aubinet M, Grelle A, Ibrom A, Rannik Ü, Moncrieff J, Foken T, Kowalski AS, Martin PH, Berbigier P, Bernhofefer Ch, Clement R, Elbers JA, Granier A, Grünwald T, Morgenstern K, Pilegaard K, Rebmann C, Snijders W, Valentini R and Vesala T (2000) Estimates of the Annual Net Carbon and Water Exchanges of Forests: the EUROFLUX Methodology. Adv. Ecol. Research. 30: 113-175

Barrett DJ, Hatton TJ, Ash JE and Ball MC (1996) Transpiration by trees from contrasting forest types. Aust. J. Bot. 44: 249-263

Bastiaanssen WGM, Menenti M, Feddes RA and Holtslag AAM (1998) A remote Surface energy balance algorithm for land (SEBAL): 1. Formulation. Journal of Hydrology, 212/213: 198-212

Bates DA (1962) Geology of Ghana. In: Wills JB (ed) Agriculture and land use in Ghana. Ministry of Food and Agriculture, Ghana. Oxford University Press, pp7-50

Bauerle WL, Post CJ, McLeod MF, Dudley JB and Toler JE (2002) Measurement and modeling of the transpiration of a temperate red maple container nursery. Agric. For. Meteorology. 114: 45-57

Ben-Asher J (1981) Estimating evapotranspiration from the Sonoita Creek watershed near Patagonia, Arizona. Water Resour. Res., 17(4): 901-906

Ben-Gai T, Bitan A, Manes A, Albert P and Israeli A (1998) Aircraft measurements of surface albedo in relation to climatic changes in southern Israel. Theor. Appl. Climatol. 61: 207-215

Bond BJ, Jones JA, Moore G, Phillips N, Post D and McDonnell JJ. (2002) The zone of vegetation influence on base flow and vegetation water use in a headwater basin. Hydrological Processes. 16: 1671-1677

Bosveld FC and Bouten W. (2001) Evaluation of transpiration models with observations over a Douglas-fir forest. Agric For Meteorol. 108: 247-264

Bouchet, R.J (1963) Evapotranspiration réelle evapotranspiration potentielle, signification climatique. Int. Assoc. Sci. Hydrol., Proceedings, Berkeley, Calif., Symp. Publ. 62:134-142

Brotzge JA and Crawford KC (2003) Examination of the surface energy budget: A comparison of eddy correlation and Bowen ratio measurement systems. Journal of Hydrometeorology. 4: 160-178

Bruijnzeel LA (1996) Predicting the hydrological impact of land cover transformation in the humid: the need for integrated research. In: Amazonia Deforestation and Climate, Gash JHC, Nobre CA, Roberts JM, Victoria RL. (eds). Wiley, Chichester; pp15-55

Brutsaert W (1982) Evaporation into the Atmosphere: Theory, History, and Applications, D Riedel, MA 299 pp

Brutsaert W and Parlange MB (1998) Hydrologic cycle explains the evaporation paradox. Science 396, 30

Brutsaert W and Stricker H (1979) An advection-aridity approach to estimate actual regional evapotranspiration. *Water Resour.Res.*, 15(2): 443-450

Bugbee B, Klassen S and Tanner B (2001) Long-term stability of five types of pyranometers in continous field use. Am. Soc. Agron. Oct 20-25, Charlotte, NC

Burose D, Moene AF, Holtslag AAM, de Bruin HAR and van de Giesen N. 2004. Surface fluxes and characteristics of drying semi-arid terrain in West Africa. Boundary Layer Meteorology (submitted).

Calder IR (1992) A model of transpiration and growth of *Eucalyptus* plantation in water-limited conditions. J. Hydrol. 130: 1-15

Calder IR (1998) Water use by forests, limits and controls. Tree physiol. 18: 625-631

Calder IR Rosier PTW, Prasanna KT and Parameswarappa S (1997) Eucalyptus water use greater than rainfall input- a possible explanation from southern india. Earth Sys. Sci. 1: 249-256

Chehbouni A, Lo Seen D, Njoku EG, Lhomme J -P, Monteny B and Kerr YH, (1997) Estimation of sensible heat flux over sparsely vegetated surfaces, J. Hydrology (188-189) 1-4: 855-868

Cienciala E and Lindroth A (1995) Gas-exchange and sap flow measurements of Salix viminalis trees in short-rotation forest I Transpiration and sap flow. Trees 9 289-294

Cienciala E, Kucera J and Malmer A (2000) Tree sap flow and stand transpiration of two *Acacia mangium* plantations in sabah Borneo. J. Hydrol. 236 109-120

Claessens L (1996) The complementary relationship in regional evapotranspiration and long-term large-scale water budgets, MS thesis, Hydrologic Science and EngineeringProgram, Civil Engineering Department, Colorado State University, Fort Collins,Colorado, U.S.A., 159 pp

Coulson KE and Reynolds DW (1971) The spectral reflectance of natural surfaces. J Appl. Meteorol. 10: 1285-1295

Cresswell HP, Painter DJ and Cameron KC (1993) Tillage and water content effects on soil hydraulic properties and shortwave albedo. Soil Sci. Soc. Am. J. 57: 816-824

Cuf AD, Fisch G and Hodnett MG (1995) The albedo of Amazonian forest and rangeland. J Clim 8:1544-1554

Cutis WR and Cole WD (1972) Micro topographic profile gage. Agric. Eng. 53: 17

DeBruin HAR and Keijman JQ (1979) The Priestley-Taylor evaporation model applied to large, shallow lake in the Netherlands. J. Appl. Meteorol. 18, 898-903

Diawara A, Loustau D and Berbigier P. 1991. Comparison of two methods for estimatingthe evaporation of a Pinus pinaster (Ait.) stand: sap flow and energy balance with sensible heat flux measurements by eddy covariance method. Agric. For. Meteorol. 54: 49-66

Dickson KB and Benneh, G (1995) A New Geography of Ghana. Longman, Malaysia

Dolman AJ, Allen SJ and Lean J (1993) Climate simulation of the shahel a comparison with surface energy balance observations. IAHS Publ 212 513-519

Doorenbos J and Pruitt WO (1997) Guidelines for Predicting Crop Water Requirements. FAO Irrigation and Drainage Paper No. 24, Rome, Italy

Dykes AP (1997) Rainfall interception from a lowland tropical rainforest in Brunei. J. Hydrol. 200: 260-279

Eagleson P.S (1978) Climate, Soil and Vegetation. 1. Introduction to water balance dynamics, Water Resour. Res., 14(5): 705-712

Eastham J, Rose CW, Cameron DM Rance SJ and Talsma T (1988) The effect of tree spacing on evaporation from an agroforestry experiment. Agric. For. Meteorol. 42: 355-368

Elbers JA (2002) Eddy correlation system Alterra; User manual. Wageningen, Alterra.

Geo-EAS (2000) Geostatistical Environment Assessment Software Documentation. http://xerxes.sph.umich.edu: 2000/public_html/geoeas/doc/geoeas.html

Giambelluca TW, Fox J, Yarnasarn S, Onibutr P and Nullet MA (1999) Dry season radiation balance of land covers replacing forest in northern Thailand. Agric. For. Meteorol. 95: 53-63

Godstein G, Andrade JL, Meinzer FC, Holbrook NM, Cavelier J, Jackson P and Celis A (1998) Stem water storage and diurnal patterns of water use in tropical forest canopy trees. Plant Cell Environ. 21: 397-406

Golberg V and Bernhofer Ch (2001) Quantifying the coupling degree between land surface and the atmospheric boundary layer with the coupled vegetation-atmosphere model HIRVAC. Annales Geophysicae. 19 581-587

Granier A (1985) Une Nouvelle Methode pour la mesure du Flux de seve Brute dans le Tronc des Arbres Ann. Sci. For. 42(2) 193-200

Granier A (1987) Evaluation of transpiration in a Douglas fir stand by means of sap flow measurements. Tree Physiol 3 309-320

Granier A and Loustau D (1994) Measuring and modelling the transpiration of a maritime pine canopy from sap flow data. Agrc. For. Meteorol. 71: 61-81

Granier A, Biron P and Lemoine D (2000) Water balance transpiration and canopy conductance in two beech stands. Agric. For. Meteorol. 100: 291-308

Granier A, Bobay V, Gash JHC, Gelpe J,Saugier B and Shuttleworth WJ (1990) Vapor flux density and transpiration rate comparisons in a stand of Maritime pine (*pinus pinaster Ait.*) in Les Landes forest. Agric. For. Meteorol. 51: 309-319

Granier A, Huc R and Barigah ST (1996) Transpiration of natural rain forest and and its dependence on climatic factors. Agrc For Meteorol 78: 19-29

Grip H, Halldin S and Lindroth A. (1989) Water-use by intensively cultivated willow using estimated stomata parameter values. Hydrological Processes 3: 51-63

Hall FC, Huemmrich KF, Goetz SJ, Sellers PJ and Nickerson (1992) Satellite Remote Sensing of surface energy balance: successes, failures and unresolved issues in FIFE. J. Geophys. Res., 97 (D17): 19061 - 19089

Hall RL, Allen SJ, Rosier PTW and Hopkins R. (1998) Transpiration from coppiced poplar and willow measured using sap-flow methods. Agric. For. Meteorol. 90 275-290

Hinckley TM, Brooks JR, Cermak J, Ceulemans R, Kucera J, Meinzer FC and Roberts DA (1994) Water flux in a hybrid poplar stand. Tree Physiol 14 1005-1018

Hobbins MT and Ramirez JA and Brown TC (2001a) The Complimentary relationship in estimation of regional evapotranspiration: An enhanced Advetion-Aridity model. Water Resour. Research. 37 (5): 1389-1403

Hobins MT, Ramirez JA, Brown TC and Claessens LHJM (2001b) The Complementary relationship in estimation of regional evapotranspiration: The CRAE and Advection-Aridity models, Water Resour. Research. 37 (5): 1367-1388

Hogg EH, Black TA, Denhartog G, Neumann HH, Zimmermann R, Hurdle PA, Blanken PD, Nesic Z, Yang PC, Staebler RM, McDonald KC and Oren R (1997) A comparison of sap flow and eddy fluxes of water vapor from a boreal deciduous forest. J. Geophy. Res. Atmosph. 102: 28927-28937.

Howell, T.A.(1996) Irrigation scheduling research and its impact on water use. Evapotranspiration and Irrigation Scheduling In: Camp CR, Sadler EJ and Yoder RE (eds). The Proceedings of the International Conference of ASAE, San Antonio, Texas. 21-33.

Idso SB, Jackson RD, Reginato RJ, Kimbal BA and Nakayama FS (1975) The dependence of bare soil albedo on soil water content. J. Appl. Meteorol. 14: 109-113

Itier B and Brunet Y (1996) Recent Developments and Present Trends in Evaporation Research: A Partial Survey: Evapotranspiration and Irrigation Scheduling In: Camp CR, Sadler EJ and Yoder RE (eds). The Proceedings of the International Conference of ASAE, San Antonio, Texas. 3-6

Iziomon MG and Mayer H (2002) On the variability and modelling of surface albedo and long-wave radiation components. Agric For Meteorol 111: 141-152

Jacobs AFG and van Pul WAJ (1990) Seasonal changes in the albedo of a maize crop during two seasons. Agric For Meteorol 49: 351-360

Javis PG and McNaughton KG (1986) Stomata control of transpiration: scaling up from leaf to region. Adv. Ecol. Res. 15: 1-49

Jegede OO (1997) Diurnal variation of net radiation at a tropical station of Osu Nigeria Theor. Appl. Climatol. 58: 161-169

Jensen (1990) Evapotranspiration and irrigation water requirements, ASCE Manual. Reports on Engineering Practice No. 70 New York: ASCE

Jensen JR and Rahman Md M (1987) A semi-empirical model for calculating evaporation and transpiration from wetland rice. Agric. For. Meteorol. 41: 289-306

Jensen ME, Burman RD and Allen RG (1990) Evapotranspiration and irrigation water requirements. ASCE Manuals and reports on Engineering practice No. 70. 332 pp

Kaimal JC and Finnigan JJ (1994) Atmospheric Boundary Layer Flows: Their Structure and Measurement, Oxford University Press, Oxford, 289pp

Kaufmann MR and Kelliher FM. (1991) Estimating tree transpiration rates in forest stands. In: Techniques and Approaches in forest tree ecophysiology. Lassoie and Hinckley TM (Eds). CRC Press, boca Raton, Florida, pp 117-140

Kelliher FM, Leuning R, Raupach MR and Schulze ED (1995) Maximum conductances for evaporation from global vegetation types. Agric. For. Meteorol. 73: 1-16

Kelliher FM, Whitehead D, Mcaneney KJ and Judd MJ (1990) Partitioning evapotranspiration into tree and understorey components in two young *Pinus radiata D. don* stands. Agric. For. Meteorol. 50: 211-227

Kim CP and Entenkhabi D (1997) Examination of two methods for estimating regional evaporation using a coupled mixed layer and land surface model, Water Resources. Res., 33(9), 2109 – 2116

Kite GW and Droogers P (2000) Comparing evapotranspiration estimates from satellites, hydrological models and field data. Journal of Hydrology 229: 3-18

Koster RD and Suarez MJ (1999) A simple framework for examining the interannual variability of land surface moisture fluxes J. Clim. 12, 1911 - 1917

Köstiner BMM, Schullze ED, Kelliher FM, Hollinger DY, Byers JN, Hunt JE, McSeveny TM, Merserth R and Weir PL (1992) Transpiration and canopy conductance in a pristine broad-leaved forest of Nothofagus: an analysis of xylem sap flow and eddy correlation measurements. Oecologia 91: 350-359

Kunstmann, H (2002) Modellierung und Validierung des Niederschlags in Westafrika. Jahresbericht, Fraunhofer Institut für Atmosphärische Umweltforschung: 42-45.

Lagergren F and Lindroth A (2002) Transpiration response to soil moisture in pine and spruce trees in Sweden. Agric. For. Meteorol. 112: 67-85

Lhomme JP (1997) A theoretical basis for the Priestley-Taylor coefficient. Boundary Layer Meteorol., 82: 179-191

Liang S, Strahler AH and Walthall CW (1999) Retrieval of land surface albedo from Satellite observations: A simulation study. Journal of Applied Meteorology

Linacre E (1992) Climate data and resources, a reference and a guide, New York, Routledge Press, pp366

Lobell DB and Asner GP (2002) Moisture effects on Soil Reflectance. Soil Sci. Soc. Am. J. 66:722-727

Loustau D, Berbigier P, Roumagnac P, Arruda-Pacheco C, David JS, Ferreira MJ, Pereira JS and Tavares R (1996) Transpiration of a 64-year old maritime pine stand in Portugal I Seasonal course of water flux through maritime pine. Oecologia 107: 33-42

Magnani F, Leonardi S, Tognetti R, Grace J and Borghetti M (1998) Modelling the surface conductance of a broad-leaf canopy effects of partial decoupling from the atmosphere. Plant Cell Environ. 21: 867-879

Margolis HA and Ryan MG (1997) A physiological basis for biosphere-atmosphere interactions in the boreal forest an overview. Tree Physiol. 17: 491-499

Marquardt DW (1963) An algorithm for least square estimation of non-linear parameters. J. Appl. Math. 11: 441-443

Matthias AD, Fimbres A, Sano EE, Post DF, Accioly L, Batchily AK and Ferreira LG (2000) Surface roughness effects on soil albedo. Soil Sci Soc Am J 64:1035-1041

Maurer J (2002) Retrieval of surface albedo from space. Cited on 30th October 2003 http://cires.colorado.edu/~maurerj/albedo/albedo.htm,

Mauser W and Schädlich S (1998) Modeling the spatial distribution of evapotranspiration on different scales using remote sensing data. Journal of Hydrology 212-213: 250-267pp

McCaughey JH (1987) The albedo of a mature mixed forest and a clear-cut site at Petawawa, Ontario. Agric. For. Meteorol. 40: 251-263

McNaughton KG and Black TA (1973) Study of evapotranspiration from a Douglas-fir forest using energy-balance approach. Water Resour. Res. 9 (6): 1579-1590

McNaughton KG and Spriggs TW (1989) An evaluation of the Priestley-Taylor equation and the complementary relationship using results from a mixed-layer model of the convective boundary layer. Estimation of areal evapotranspiration. IAHS, Publ. No. 177: 89-104

Meinzer FC, Andrade JL, Goldstein G, Holbrook NM, Cavelier J and Jackson P (1997) Control of transpiration from the upper canopy of a tropical forest: the role of stomatal boundary layer and hydraulic architecture components. Plant Cell Environ. 16: 429-436

Meinzer FC, Goldstein G, Holbrook NM, Jackson P and Cavelier J (1993) Stomata and environmental control of transpiration in a lowland tropical forest tree. Plant Cell Environ. 16: 429-436

Minnis P, Mayor S, Smith WL, and Young DF (1997) Asymmetry in the diurnal variation surface albedo. IEEE Trans Geosci Romote Sensing 35: 879-891

Mitchell TD, Carter, TR, Jones PD, Hulme, M and New M (2003) A comprehensive set of high-resolution grids of monthly climate for Europe and the globe: the observed record (1901-2000) and 16 scenarios (2001-2100). Journal of Climate: submitted.

Moehrlen CG Kiely and M Pahlow (1999) Long Term Water budget in a grassland catchment in Ireland. Physics and Chemistry of the Earth, part B: Hydrology and, Oceans & Atmoshere, Special Issue: European Water Resources and Climate Change Processes-part2, 24:1-2

Monteith JL (1965)‘‘Evaporation and environment.’’The state andmovement of water in living organisms,19th Symp.of Soc.Exp.Biol., Cambridge University Press, Cambridge

Monteith JL and Unsworth MH (1990) Principles of environmental physics. Arnold, New York

Moran MS, Clarke TR, Inoue Y and Vidal A (1994) Estimating crop water deficit Using the relations between surface-air temperature and spectral vegetation index Remote Sensing of the Environment, 49(2): 246-263

Morton FI (1976) Climatological estimates of evapotranspiration. J. Hydraul. Div., ASCE, 102(HY3): 275-291

Morton FI (1983) Operational estimates of areal evapotranspiration and their significance to the science and practice of hydrology, J.Hydrol. 66: 1-76

Ogilvy JA (1991) Theory of wave scattering from random rough surfaces. Bristol, England: Adam Hilger

Ogunjobi KO, Kim YJ, Adedokun JA, Ryu SY and Kim JE. (2002) Analysis of sky condition using solar radiation data at Kwangju and Seoul South Korea and Ile-Ife Nigeria. Theor. Appl. Climatol. 72: 265-272

Overseas Development Institute, 1999. Rethinking natural resource degradation in sub-Saharan Africa: Policies to support sustainable soil fertility management, soil and water conservation, among resource-poor farmers in semi-arid areas. http://www.odi.org.uk/RPEG/soil_degradation/index.html

Parlange MB and Katul GG (1992a) An advection-aridity evaporation model. Water Resour. Res., 28(1): 127-132

Parlange MB and Katul GG (1992b) Estimation of the diurnal variation of potential evaporation from a wet bare soil surface. J.Hydrol. 132: 71-89

Penman HL (1948) Natural evaporation from open water bare soil and grass Proc. Roy. Soc. SerA 193: 120-146

Pereira LS, Perrier A, Allen RG and Alves I (1999) Evapotranspiration: Concepts and Future Trends, Journal of Irr and Dran Engineering. 125(2): 45-51

Perrier A (1977) ‘‘Evapotranspiration et bilan hydrique.’’*La Me´te´orol-ogi*e, Paris, 6(11), 7–16

Phillips N, Nagchaudhuri A and Oren RG (1997) Time constant for water transport in loblolly pine trees estimated from time series of evaporative demand and tem sap flow Trees 11: 412-419

Phillips N, Oren R, Zimmermann R and Wright SJ (1999) Temporal patterns of water flux in trees and lianas in a Panamanian moist forest. Trees. 14: 116-123

Pinker RT, Thompson OE and Eck TF (1980) The albedo of a tropical evergreen forest. QJR Meteorol. Soc. 106:551-558

Pitman AJ and Henderson-Sellers A (1998) Recent progress and results from the project for the intercomparison of land surface parameterization schemes, Journal of Hydrology 212-213: 128-135

Post DA and Jones JA (2001) Hydrologic regimes of forested, mountainous, headwater basins in New Hampshire, North Carolina, Oregon, and Puerto Rico Advances in Water Resources. 24: 1195-1210

Potter KN, Horton R and Cruse RM (1987) Soil surface roughness effects on radiation reflectance and soil heat flux. Soil Sci. Soc. Am. J. 51: 855-860

Priestley CHB and Taylor RJ (1972) On the assessment of surface heat flux and evaporation using large-scale parameters. Monthly Weather Rev 100: 81-92

Qualls RJ and Gultekin H (1997) Influence of components of the advection-aridity approach on evapotranspiration estimation. Journal of Hydrology, 199, 3-12

Rehm S and Espig G (1991) The cultivated plants of the tropics and subtropics. Verlag Josef Margraf; Germany; 243-247

Reifsnyder WE (1967) Radiation geometry in the measurement and interpretation of radiation balance. Agric. Meteorol. 4: 255-265

Ross J (1975) Radiative transfer in plant communities. In: Monteith, JL (ed) Vegetation and the atmosphere, vol 1. Principles. Academic press, London, pp13-55

Sakuratani T (1981) A heat balance method for measuring water flow in the strem of intact plant J. Agric. Met (Japan) 37, 9-17

San Jose JJ, Bracho R, Montes R and Nikonova N (2003) Comparative energy exchange from cowpeas (Vigna unguiculata L.) walpcvs. TC-9-6 and M-28-6-6) with differences in canopy architectures and growth durations at the Orinoco llanos. Agric. For. Meteorol. 116: 197-219

Saugier B, Granier A, Potailler JY, Dufrene E and Baldocchi DD (1997) Transpiration of a boreal pine forest measured by branch bag, sap flow and micrometeorological methods. Tree Physiology 17: 511-519

Schaeffer SM, Williams DG and Goodrich DC (2000) Transpiration of Cottonwood /willow forest estimated from sap flux. Agric. For. Meteorol. 105: 257-270

Scott RL, Watts C, Payan JG, Edwards E, Goodrich DC, Williams D and Shuttleworth WJ (2003) The understory and overstory partitioning of energy and water fluxes in an open canopy, semiarid woodland. Agric. For. Meteorol. 127: 211-139

Sellers PJ, Randall DA, Collatz GJ, Berr JA, Field CB, Dazlich DA, Zhang C, Collelo GD and Bounoua L (1996) A revised Land surface parameterization (SIB2) for atmospheric GCMs, part I. Model formulation. J Clim 9:676-705

Shuttleworth WJ and Wallance, JS (1985) Evaporation from sparse crops- an energy combination theory. Q. J. R. Meteorol. Soc. 111, 839-855

Siegel R and Howell JR (1972) Thermal radiation heat transfer. New York: McGraw-Hill Book Co

Slatyer, RO and IC McIloy (1961) Practical Microclimatology, CSIRO, Melbourne, Australia, 310pp

Smith M (2000) The application of climatic data for planning and management of Sustainable rainfed and irrigated crop production, Agric. For. Meteorol.103, 99-108

Smith M, Allen R And Pereira L (1996) Revised FAO Methodology for crop water requirements. In: Camp CR, Sadler EJ and Yoder RE (eds). Evapotranspiration and Irrigation Scheduling, the Proceedings of the International Conference of ASAE, San Antonio, Texas, pp 116-123

Sommer R, de Abreu Sa TD, Vielhauer K, de Araujo AC, Fölster HA and Vlek PLG (2002) Transpiration and canopy conductance of secondary vegetation in the eastern Amazon. Agric. For. Meteorol. 112: 103-121

Song J (1998) Diurnal asymmetry in surface albedo. Agric. For. Meteorol. 92: 181-189

Song J (1999) Phenological influences on the albedo of prairie grassland and crop fields. Int. J. Biometeorol. 42:153-157

Standhill G (1970) Some results of helicopter measurements of the albedo of different land surfaces. Solar Energy 13: 59-66

Stanhill G (1965) Observations of the reduction of soil temperatures Agric. Meteorol. 2: 197-203

Stannard DI (1993) Comparison of Penman-Monteith, Shuttleworth-walance and modified Priestly-Taylor evapotranspiration models for wildland vegetation in semiarid rangeland. Water Resour. Res. 29: 1379-1392

Stroeve J, Box JE, Fowler C, Haran T and Key J (2001) Intercomparison between in situ and AVHRR polar pathfinder-derived surface albedo over Greenland. Remote Sens. Environ. 75: 360-374

Szilagyi J (2001) Modeled Areal Evaporation Trends over the Conterminous United States, Journal of Irrigation and Drainage Engineering 127(4): 196-200

Szilagyi J, Katul GG and Parlange MB (2001) Evapotranspiration Intensifies over the Conterminous United States. Journal of Water Resources Planning and Management. 127(6), 354-362

Teskey RO and Sheriff DW (1996) Water use by Pinus radiata trees in a plantation. Tree Physiol. 16: 273-279

Tooming H (2002) Dependence of global radiation on cloudiness and surface albedo in Tatu, Estonia. Theoret. Appl. Climatol. 72: 165-172

Tuzet A, Castell JF, Perrier A and Zurfluh O (1997) Flux heterogeneity and evapotranspiration partitioning in a sparse canopy the fallow savannah. J. Hydrol. 188-189: 482-493

Twine TE, Kustas WP, Norman JM, Cook DR, Houser PR, Meyers TP, Prueger JH and Starks PJ (2000) Correcting eddy covariance flux underestimates over a grassland. Agric. For. Meteorol. 103: 279-300

Twomey SA, Bohren CF and Mergenthaler JL (1986) Reflectance and albedo differences between wet and dry surfaces. Appl. Optics 25: 431-437

Uchijima Z (1976) Maize and rice. In: Monteith, JL (ed) Vegetation and the atmosphere, vol 2. Principles. Academic press, London, pp33-64

UPGmbH (2001) UP Sap flow-system user's manual Version 20UP Umweltanalytische Produckte GmbH München Germany

Van de Giesen N, Kunstmann H, Jung G, Liebe J, Andreini M and Vlek PLG (2002) The GLOWA-Volta project: Integrated assessment of feedback mechanisms between climate, landuse, and hydrology. Advances in Global Change Research, 10: 151-170

van de Giesen NC, Stomph TJ and De Ridder N (2000) Scale effects of Hortonian overland flow and rainfall-runoff dynamics in a West African cantena landscape, Hydrological Process 14: 165-175

Villalobolos FJ, Mateos L and Orgaz F (1995) Non-destructive measurement of leaf area in olive (Olea europaea L.) trees using a gap inversion method

Walker HO (1962) Weather and Climate. In: Wills JG (ed) Agriculture and land-use in Ghana, Oxford University Press, London pp 51-61

Wallace JS and Batchelor CH (1997) Managing water resources for crop production, Phil. Trans. R. Soc., B5352: 937-947

Wallace JS and Holwell CJ (1997) Soil evaporation from tiger-bush in south-west Niger, J. Hydrology 188-189(1-4): 426-442

Webb EK, Pearman GI and Leuning R (1980) Correction of flux measurements for density effects due to heat and water vapor transfer. Quart J. Roy. Meteor. Soc., 106: 85-100

Whitehead D and Hinckley TM (1991) Models of water flux through forest stands: critical leaf and stand parameters. Tree Physiology 9: 35-57

Wright IR, Manzi AO and da Rocha HR. (1995) Surface conductance of Amazonian pasture: model application and calibration for canopy climate. Agric. For. Meteorol 75 51-70

Wullschleger SD, Meinzer FC and Vertessy RA (1998) A review of whole-plant water use studies in trees. Tree Physiol 18 499-512

Wullschleger SD, Wilson KB and Hanson PJ (2000) Environmental control of whole-plant transpiration, canopy conductance and estimates of the decoupling coefficient for large red maples trees. Agric. For. Meteorol. 104: 157-168

Wythers KR, Lauenroth WK and Paruelo JM (1999) Bare-soil evaporation under semiarid field conditions. Soil Sci. Soc. Am. J. 63: 1341-1349

Xia Y, Winterhalter M and Fabian P (1991) A model to Interpolate Monthly Mean Climatolohical Data at bavarian forest climate station. Theor. Appl. Climatol. 64: 27-38

Yidana JA (1996) The smallholder cashew estate management: Ghana/USAID human resources development assistance project-workshop on cashew management November 6-13th Ghana 11pp

Yin X (1998) The albedo of vegetated land surfaces: Systems analysis and mathematical modeling. Theoret Appl Climatol 60: 121-140

ACKNOWLEDGEMENTS

I am most grateful to God for his grace saw me through this study. I thank Prof. Helmut Eggers for his fatherly approach to the supervision of this work. The support, openness and encouragement from Prof. Paul Vlek are gratefully acknowledged. I sincerely appreciate the excellent guardians provided by Prof. Nick van de Giesen, he actually gave me a new direction in hydrological studies (eco-hydrology). My profound gratitude goes to the German government who, through the German Academic Exchange Services (DAAD) and its Ministry of Education, Science and Technology (BMBF), provided stipend and research grant for this study. I appreciate the efforts of Dr Günther Manske, the gracious doctoral and ZEFc staff for their administrative and technical assistances. Regards to Drs Marc Andreini and Matthias Fosu, the project co-coordinators in Ghana, for their support during the field campaign. I am grateful to the field staff at Ejura. I acknowledge the efforts of Mr Kofi Campion, Mr Sanmi Acqua, Pastor and Dr (Mrs) Mark for making my stay in Ghana enjoyable.

Many thanks to the management of the Federal university of Technology, Akure for granting the study leave. I thank all the staff of the Department of Agricultural Engineering for their moral support. To mention a few: Profs. O.C.Ademosun, A.S.Ogunlowo, A.A. Olufayo, Drs M.O. Alatise, L.A.S. Agbetoye, Wale Olukunle, B.A. Adewumi, Engrs N.O.A. Ajayi, J.T. Fasinminrin, R.A. Falayi, Mr A. Adesina and Akinpelumi. Special regards to my friends: Dr B.J.Abiodun, Dr. – Ing A.E. Ajayi and Dr A.K. Braimoh for their inspirations and encouragements.

The warmth and fellowship enjoyed from members of the Redeemed Christian Church of God, Bonn is highly appreciated. Special thanks to Mrs Ibidun Ajayi, Mama Okantey, Mrs Olanike Nist, Pastor (Dr) and Mrs Oyetade, Pastor Chinedum Ezebugbum, Dr Pius Tamangi, Engr. Opeyemi Amusan. I acknowledge the prayers and support of Mr and Mrs A.S. Ayodele, O.J. Ezekiel, J. F. Ogunbunmi and Pastor and Mrs A.O. Odesola. Best regards to the Alatises, the ijatuyis, the Oyerindes, the Adeduntans, the Adekolas and the Olukunles; you are all dare to me.

Finally, my profound gratitude goes to my family. To my parent Solomon and Ruth Oguntunde who have always been my financiers from my basic to first-degree education. To my sisters Deborah, Maria, and Dupe and my brothers Dare and Sola: thanks for your prayers. To my children Mercy Oluwapelumi and David Ayomide-you are the great two. My deepest gratitude and regards to my dare wife-Victoria Gbolahan, for her understanding and support/encouragement at all time.